Millennial-scale variations of the intermediate water circulation in the Indian Ocean since the last glacial period inferred from assemblages and geochemistry of benthic foraminifera.

Ruifang Ma

NNT : 2019SACLS159

Millennial-scale Variations of the Intermediate Water Circulation in the Indian Ocean since the Last Glacial Period Inferred from Assemblages and Geochemistry of Benthic Foraminifera

Thèse de doctorat de l'Université Paris-Saclay
préparée à l'Université Paris-Sud

École doctorale n°579 : sciences mécaniques et énergétiques, matériaux et géosciences (SMEMAG)
Spécialité de doctorat: Terre solide : géodynamique des enveloppes supérieures, paléobiosphère

Thèse présentée et soutenue à Orsay, le 10 juillet 2019 par

Ruifang Ma

Composition du Jury :

Valérie Daux Professeur, CEA/CNRS/UVSQ, LSCE	Présidente
Claire Lazareth Chargée de Recherche, BOREA, IRD	Rapporteur
Bruno Malaizé Maître de Conférences, Université de Bordeaux, OASU	Rapporteur
Damien Cardinal Professeur, Sorbonne Université, LOCEAN	Examinateur
Franck Bassinot Chercheur au CEA, LSCE/IPSL	Examinateur
Laetitia Licari Maître de Conférences, Aix-Marseille Université, CEREGE	Examinatrice
Christophe Colin Professeur, Université de Paris-Sud, GEOPS	Directeur de thèse
Sophie Sépulcre Maître de Conférences, Université de Paris-Sud, GEOPS	Co-Directrice de thèse

Thèse de doctorat

Acknowledgements

For the moment, it is almost at the end of my thesis and my doctoral research in Laboratoire de Geosciences Paris-Sud (GEOPS) is going to finish. My thesis can't be completed without earnest instructions and inspiring helps from my supervisors, cooperators, colleagues, friends and family. Here, I would like to express my sincerely thanks to them for their contributions and participation for my research and my thesis.

First of all, I would like to sincerely thank my advisors, Prof. Christophe COLIN and Sophie SEPULCRE. Their abundant knowledge, scientific training and helpful suggestions let me find the directions of my research and master various useful skills for doctoral research. I also would like to express my sincere appreciate for their patience and hard work on my thesis. Their preciseness and kindness enables me to overcome difficulties in my research.

I am particularly grateful to Laetitia LICARI, with her kindly help for learning foraminiferal identification of MD77-176 in CEREGE, Aix-Marseille Université–Europole. Despite her busy schedules, she is always taking the time to solve each problem I encountered. Particular thanks also go to Prof. Franck BASSINOT and Nadine TISNERAT-LABORDE for organizing my work in the geochemical lab at the Laboratoire des Sciences du Climat et de l'Environnement (LSCE) and for their constructive comments during the preparation of the manuscripts. I also particularly thank Prof. Zhifei Liu of Tongji University for his organizing of foraminiferal stable isotopes analyses.

Many people have helped me carry out essential laboratory work for this thesis. It has been a great pleasure to work with them. Special thanks go to Frédéric HAURINE for his invaluable assistance with the elemental ratios analysis using the HP-ICP-MS instrument whenever needed. I also thank Xiaolei Pang, Qiong Wu, Zhaojie Yu, and Maxence DUHAMEL for their assistance of work carried out in the clean lab.

I'm grateful to the members of jury for their willingness to review this thesis and for helping me to improve it.

My sincere thanks go to my colleagues Margaux BRANDON and Alexis DERYCKE for their kindly help in translation. I would like to thank also my numerous friends: Jinjin Zhao, Qiong Wu, Yating Lin, Junqin Jiang, Xiaolei Pang, Zhaojie Yu, Xinquan Zhou, and Wei Shu… for all the fun we had since our first encounter.

I would like also thank the China Scholarship Council for the full scholarship support of my four-year stay in France.

Last but not least, I particular thanks to my loving parents for their supports and encouragements. I would also thank my husband Zhenpeng Cui for his endless love, meticulous care and companionship.

Contents

General Introduction

Natural and human-induced climate changes are major concerns for this century, as it induces an increase of 0.8°C in average global temperature since 1951 due to the human activity (IPCC, 2013). The changes caused by the warming of the climate system are now observable, such as the risen sea level and decreasing snow and ice cover. Indeed, these changes may finally affect all aspects of human lives and extending to all biospheres. Thus, understanding natural changes in the climate system by paleoclimate reconstructions is a key to improve the climate models to better estimate the future climate changes. As shown by the last decades of IPCC work, fully unraveling the dynamics of climate changes requires quality observational datasets with extensive spatial and time coverage to meet the most recent standards in climate modeling. Because instrumental records of environmental changes are short (<150 yrs), it is only through the study of natural environmental archives (i.e., ice cores, lake and ocean sediments, speleothems…) that one can address pre-anthropic climate changes and environmental variability at centennial to geological timescales. For such studies, we have to work with qualitative and quantitative "proxies" determined in geological archives (e.g., marine sediments, ice cores, speleothems…) to reconstruct paleo-environmental changes.

Paleoclimate records from ice cores, marine sediments and continental archives indicate that the Earth's climate system experienced climate changes and gave evidence for large climate instability from decadal to orbital timescales. For instance, when looking at ice cores, a series of variations can be observed, from around 1 to 100 kyr (the so-called glacial-interglacial cycles) (Figure 1). In the ocean, the last glacial period and deglaciation were also systematically punctuated by abrupt changes in the north Atlantic freshwater budget related to iceberg discharges (e.g. Dansgaard-Oeschger cycles and Heinrich events) (e.g., Taylor et al., 1993; Bond et al., 1993; McManus et al., 1994). When comparing both ocean and ice-cores records of the northern and southern hemispheres, large bipolar seesaw shifts detected in the Greenland and Antarctic ice cores can be associated through the major reorganization in ocean heat advection (e.g., Dansgaard et al., 1993; Bond et al., 1997; Andrew, 1998; IPCC, 2013; Figure 1).

The thermohaline ocean circulation (THC) is a part of the large-scale ocean circulation which is driven by global density gradients created by surface heat and freshwater fluxes (Rahmstorf, 2006; Figure 2). THC could transport energy (heat) and material (solids, dissolved substances and gases) around the world through the mixing water masses between the ocean basins (Rahmstorf, 2006; Wunsch, 2002). In addition, the Atlantic meridional overturning circulation (AMOC) is an important part of thermohaline ocean circulation. The AMOC is characterized by a northward flow

of warm, salty water in the upper layers of the Atlantic, along with a southward flow of colder,

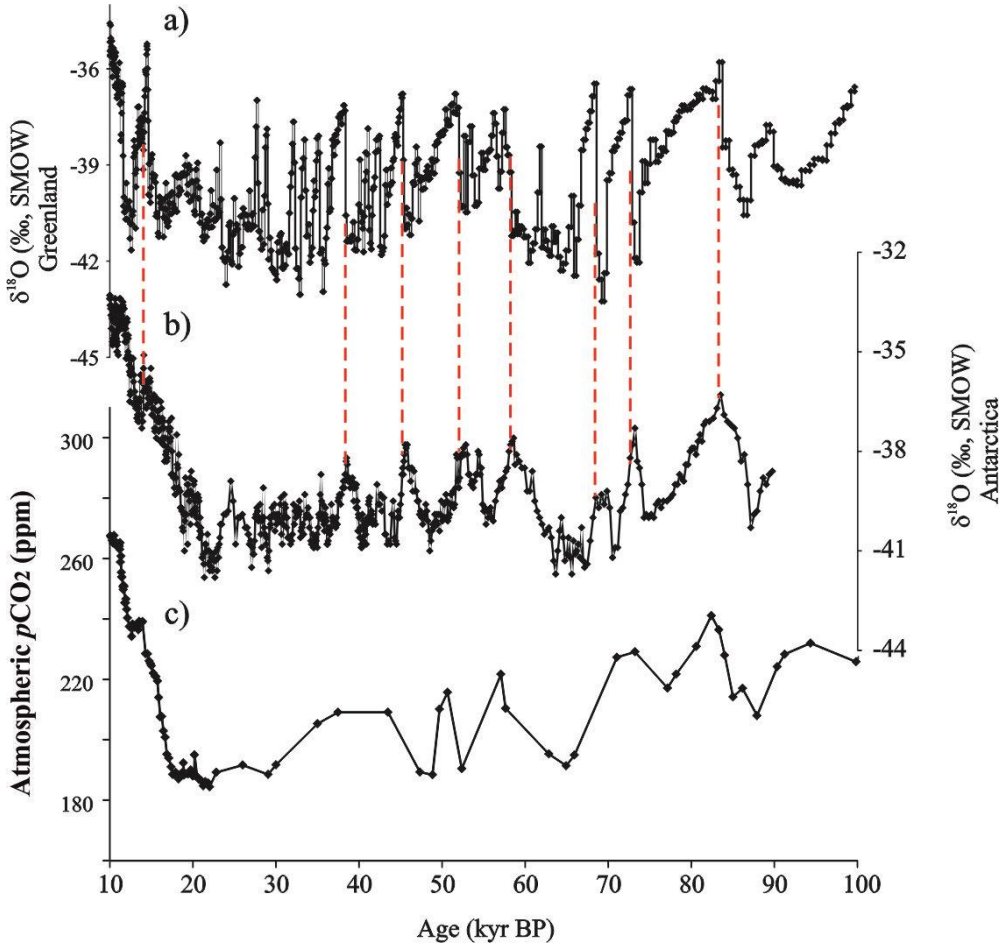

Figure 1. *Records of (a)Greenland ice core GISP2 $\delta^{18}O$ (Grootes and Stuiver, 1997) compared with (b) Antarctic ice core $\delta^{18}O$ from Byrd station (Johnsen et al., 1972), and (c) atmospheric pCO_2 (Lüthi et al., 2008). The red lines show that Antarctic trends to be warm when Greenland is cold.*

deep waters. The surface limb of the AMOC plays an important role in regulating the global climate changes through heat redistribution from the tropical region to the high latitudes by surface and intermediate-deep water masses and carbon cycling, as ocean is the largest external carbon reservoir (e.g., Rahmstorf, 1995; Stocker and Wright, 1996; Tomczak and Godfrey, 2003; Bryan et al., 2010; Talley et al., 2011; Figure 2).

A large amount of previous studies have worked on the links between ocean circulation changes and climate changes in the past (e.g., Barker et al., 2011; Skinner et al., 2010). It has recently been shown that vigorous AMOC may have persisted in the North Atlantic throughout most of the last glacial period, only disrupted by episodes of sluggish circulation associated with the catastrophic iceberg discharges of the coldest Heinrich stadials (HS), the Dansgaard-Oeschger stadials (D-O

stadials) and the Younger Dryas cold event of the last termination (Böhm et al., 2015). These major perturbations in Atlantic circulation have been related to the reduced North Atlantic Deep Water (NADW) flow (e.g., Mcmanus et al., 2004; Böhm et al., 2015) and the advection of southern-sourced waters filling a large part of the deep Atlantic ocean (e.g., Duplessy et al., 1988; Lynch-Stieglitz et al., 2007; Roberts et al., 2010; Böhm et al., 2015), affecting the circulation in all ocean basins (e.g., Lynch-Stieglitz et al., 2007; Roberts et al., 2010; Böhm et al., 2015). Thus, many previous works have documented past changes in deep ocean circulation (e.g., Mix and Fairbanks, 1985; Corliss et al., 1986; Oppo and Fairbanks, 1987; Kallel et al., 1988; Waelbroeck et al., 2006).

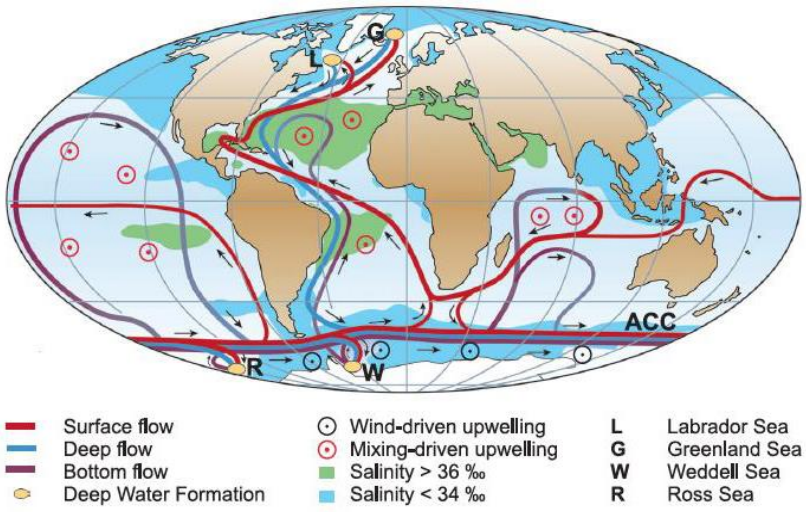

Figure 2. *The map of world ocean thermohaline circulation. According to Rahmstorf (2006).*

In modern time, intermediate water masses play a key role as heat and carbon storage reservoirs, which can exchange with the atmosphere on a millennial timescale through changes in water mass stratification (Sigman and Boyle, 2000). However, the evolution of intermediate waters circulation is less documented than those of deep water masses. In addition, studies of the intermediate water circulation since the LGM mainly focused on the Atlantic Ocean (e.g., Oppo and Fairbanks, 1987; Tsuchiya et al., 1992; Pérez et al., 2001; Lynch-Stieglitz et al., 2007; Pahnke et al., 2008; Barbero et al., 2010; Bashmachnikov et al., 2015; Dubois-Dauphin et al., 2016) and the Pacific Ocean (e.g., Kallel et al., 1988; Mix et al., 1991; Yasuda, 2004; Pahnke and Zahn, 2005; Bostock et al., 2010). These studies suggest an increased northward penetration of Antarctic Intermediate Water (AAIW) into the Pacific and Atlantic Oceans during glacial periods, as well as at millennial time scale during the Heinrich events and stadials (e.g., Pahnke and Zahn, 2005; Cao et al., 2007; Pahnke et al., 2008; Dubois-Dauphin et al., 2016; Figure 3). However, the role of AAIW is still controversial in the

Atlantic Ocean, where several studies suggest a reduced northward flux of AAIW into the tropical Atlantic (e.g. Came et al., 2008; Xie et al., 2012; Howe et al., 2016; Gu et al., 2017; Figure 3).

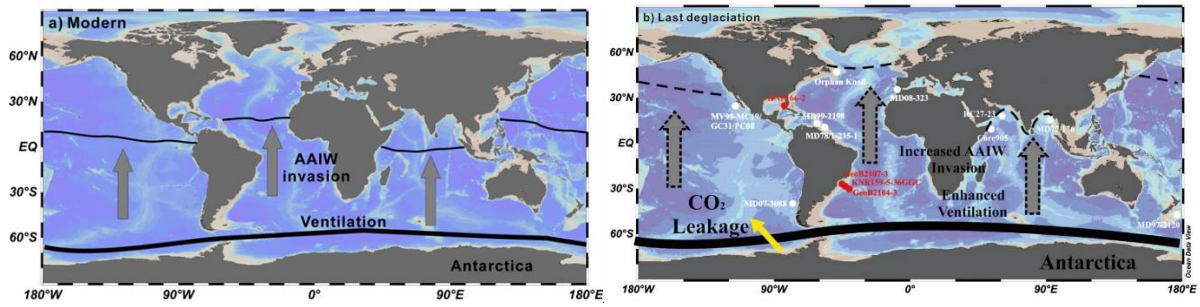

Figure 3. *Schematic map showing the northward flow of AAIW at present and during the last deglaciation. a) The northward flow invasion of AAIW at the present time; b) the northward flow of AAIW during the last deglaciation. The white dots suggest strong invasion of AAIW during the last deglaciation (Cao et al., 2005; Pahnke et al., 2008; Marchitto et al., 2007; Bryan et al., 2010; Yu et al., 2018), by contrast, the red circles indicate reduced northward flux of AAIW (Xie et al., 2012; Howe et al., 2016).Corrected based on Yu et al. (2018).*

Moreover, during the last deglaciation, a two-step rapid increase of atmospheric CO_2 occurred in the 18-14.7 and 12.8-11.7 cal kyr BP time intervals (Monnin et al., 2001). Decades of paleoceanographic research suggest that the variation of Southern Ocean circulation played a key role in transferring the deep ocean carbon to the upper ocean and atmosphere during the last deglaciation, by enhancing the upwelling and increasing the northward penetration of the Antarctic Intermediate Water (AAIW) (e.g., Anderson et al., 2009; Marchitto et al., 2007; Skinner et al., 2014). The formation and advection of AAIW in the Southern Ocean, plays an important role in understanding the deglacial circulation variation, as it is sensitive to changes in the Southern Ocean dynamics and the strength of the westerly wind (Ribbe, 2001). The Southern Ocean is thus also a crucial area in the global carbon cycle through strong air-sea exchanges as well as interactions between the ocean surface, intermediate and deep waters (e.g., Lynch-Stieglitz et al., 1994; Ribbe, 2001). Thus, the extension of AAIW and the relationships with the atmospheric CO_2 variations still need to be constrained, as well as the relationships with enhanced upwelling in the Southern Ocean during the last deglaciation at millennial scales.

The Indian Ocean plays an important role in global ocean circulation in terms of affecting the carbon storage capacity of the ocean and climate (e.g., Ahmad et al., 2008, 2012; Bryan et al., 2010; Raza et al., 2014; Talley et al., 2011). In addition, due to the land-sea configuration in the northern Indian Ocean, much of the intermediate and deep waters of the northern Indian Ocean

originate from the south, with only small contributions of intermediate waters from the Red Sea and of Pacific water through the Indonesian sea (Talley et al., 2011). Consequently, studying intermediate waters in the north Indian Ocean will allow us to better constrain past changes in the production of intermediate and deep water and in circulation from the Southern Ocean. In addition, it will help us to understand their potential role in global climate changes. Finally, through its connections with the Southern Ocean via the AAIW, the Indian Ocean could also have played a key role in past changes in the C storage.

Carbon in the ocean exists in different chemical forms expressed as the seawater carbonate system, and mainly consists of six parameters [CO_2], [HCO_3^-], [CO_3^{2-}], pH, DIC (total dissolved inorganic carbon) and total alkalinity. The solubility of CO_2 in seawater increases with the pressure of the gas and decreases as the temperature and salinity of the seawater increase. The dissolution equilibrium reaction is:

$$CO_2(g) \Leftrightarrow CO_2(aq)$$

Compared with the dissolution of a non-reactive gas, after the CO_2 dissolved in seawater, the reactions of $CO_{2(aq)}$ with seawater, acid-base reactions as well as ionic solubility reactions are more complex.

$$CO_2(aq) + H_2O \overset{k_{a1}}{\Leftrightarrow} HCO_3^-(aq) + H^+(aq)$$

$$HCO_3^-(aq) \overset{k_{a2}}{\Leftrightarrow} CO_3^{2-}(aq) + H^+(aq)$$

The ocean's carbonate system can be affected by variations in atmospheric CO_2 and ocean circulation. It thus plays a crucial role in the global carbon cycle (e.g., Sigman and Boyle, 2000; Ridgwell and Zeebe, 2005; Anderson et al., 2009). The deep-water carbonate ion concentration especially determines the seawater carbonate saturation, controlling the preservation state of solid Calcium carbonate $CaCO_3$ and affects the carbon reorganization in the climate system, through exchanges with intermediate and surface water, the later being in equilibrium with the atmospheric CO_2. Thus, reconstruction of past deep-ocean seawater variations in the global Carbon content and forms could help to better constrain the processes and mechanisms controlling the past global carbon cycle.

In order to obtain information about the ocean characteristics such as carbon cycle, ocean circulation or productivity, it is necessary to use multiple proxies that play a vital role in

paleoceanographic and paleoclimate studies. Among these proxies, a lot of our knowledge about past changes of ocean conditions can be obtained from the foraminifera. They live in many environmental conditions of the surface and the sub-surface of the ocean and the seafloor, and their shells can be preserved inside marine sediments. Thus, foraminifera are a reliable archive to reconstruct several physical parameters of the ocean in the past.

Foraminifera can be used as proxies for paleoenvironmental conditions through their abundance and diversity, the so-called assemblages. Moreover, their tests may record the geochemical signature of the water in which they lived and calcified their tests. For instance, Oxygen and Carbon stable isotopes $\delta^{18}O$ and $\delta^{13}C$ are widely used foraminiferal proxies, that can record the bottom water temperature, paleo-nutrient and deep-water circulation. The ^{14}C obtained from foraminifera could also be a reliable tracer of water masses circulation and ventilation, and the raw difference between benthic and planktonic radiocarbon ages can help to reconstruct past circulation strenght (e.g. Broecker and Peng, 1984; De Pol-Holz et al., 2010; Wan and Jian, 2014; Siani et al., 2013). In addition, the reconstruction of bottom water temperature, carbonate system parameters and paleo-nutrient over geological time from benthic foraminifera elemental/Ca ratios has received increasing attention (e.g. Boyle and Keigwin, 1982; Boyle et al., 1995; Yu et al., 2008; Raitzsch et al., 2011; Marchitto et al., 2018).

Thus, decades of paleoceanography research using benthic foraminifera geochemical proxies have helped to better understand past changes in intermediate and deep water masses circulation in the Atlantic Ocean (e.g., Lynch-Stieglitz et al., 2007; Pahnke et al., 2008; Barbero et al., 2010; Bashmachnikov et al., 2015), the Pacific Ocean (e.g., Pahnke and Zahn, 2005; Bostock et al., 2010) and the north Indian Ocean (Bryan et al., 2010; Raza et al., 2014; Yu et al., 2018; Ma et al., 2019). However, there are few continuous and high-resolution benthic foraminiferal records that have been reported in the north Indian Ocean at intermediate water depths (e.g., Ahmad et al., 2008, 2012; Bryan et al., 2010; Raza et al., 2014; Yu et al., 2018; Ma et al., 2019).

To sum up, as much of the intermediate and deep waters of Indian Ocean originate from the south, the mainly intermediate water masses (500-1200m) in the Indian Ocean are Antarctic Intermediate Water (AAIW), Red Sea Intermediate Water (RSIW) and Indonesian Intermediate Water (IIW). Thus, the north Indian Ocean could be a key area to better constrain past changes in intermediate circulation in the Northern Indian Ocean, and the relationships with the other ocean basins as well as their influence on the global Carbon cycle. Therefore, in this study, we have investigated three sediment cores at intermediate water depth:

- from the Bay of Bengal, in the high latitude of the Indian Ocean, where the different intermediate water masses can be mixed;

- from the Arabian Sea, in the southern tip of India, to better constrain the temporal evolution of

RSOW and the connexion between the BoB and the Arabian Sea;

- in the Eastern Equatorial Indian Ocean, to track the contribution of IIW and the northward penetration of AAIW.

In addition, these three cores have high sedimentation rates and could provide high-resolution records to reconstruct past changes in the intermediate circulation at a high temporal scale.

To reach these objectives, we have investigated benthic foraminiferal assemblages together with stable isotopes ($\delta^{13}C$, $\delta^{18}O$) and ^{14}C of benthic foraminifera in order to reconstruct past hydrological changes at intermediate water depth and a high temporal resolution since the LGM. Our goal is to better understand the relationships between ocean circulation (and, especially, the role of AAIW), Southern Ocean upwelling intensity and changes in the atmospheric CO_2.

We have developed an instrumental protocol on a newly installed single collector sector field high-resolution inductively coupled plasma mass spectrometer (HR-ICP-MS) Thermo Element XR to measure benthic foraminiferal elemental/Ca ratios. The Mg/Ca, Sr/Ca, Cd/Ca, Ba/Ca, Li/Ca and U/Ca of benthic foraminifera were used to reconstruct the intermediate water properties (especially, the seawater [CO_3^{2-}] content and paleo-nutrient) from the northern and equatorial Indian Ocean to better understand the temporal evolution of the source and ventilation of intermediate water mass in the northern Indian Ocean and their relationships with the other ocean basins and the global C cycle.

The results of all investigations performed are presented in five chapters.

The hydrological settings at modern time and in the past of the studied areas (Bay of Bengal, Arabian Sea and eastern equatorial Indian Ocean) constitute Chapter 1.

The material used as well as the background of the multiple proxies that have been used in this work -benthic foraminiferal assemblages, stable isotopes, ^{14}C and benthic elemental ratios analysis-, are detailed in Chapter 2.

Chapter 3 presents results of benthic foraminiferal assemblage analysis, benthic stable isotopes and ^{14}C from one core located in the northern Bay of Bengal at intermediate depth (core MD77-176) in order to constrain the temporal evolution of the source, ventilation and structure of intermediate and deep-water masses of the Bay of Bengal and the northward penetration of AAIW.

The chapter 4 focused on benthic foraminifera elemental ratios obtained from one core of the Arabian Sea (southern tip of India) (core MD77-191) and core from one core of the northern Bay of Bengal (core MD77-176). Benthic foraminiferal $\delta^{13}C$ and seawater carbonate ion concentration estimated from trace element ratios (Mg/Ca, Sr/Ca, Li/Ca and U/Ca) of aragonite benthic *Hoeglandina elegans* were used to trace the evolution of past intermediate-deep water masses and constrain ocean-atmosphere exchanges during the two-stage increase in atmospheric CO_2 across

the last deglaciation.

The Chapter 5 represents the first continuous and high-resolution benthic foraminifera Cd/Ca and Ba/Ca records in the northern Indian Ocean, displayed as a manuscript. These new results help to improve our knowledge on the paleo-nutrient reconstruction by benthic Cd/Ca and Ba/Ca. In addition, the results of benthic assemblage analysis of core MD77-191 (Arabian Sea) to estimate the changes in bottom water conditions (oxygen concentration and organic matter flux) are also presented.

Chapter 6 contains the geochemical results (benthic foraminiferal $\delta^{13}C$, $\delta^{18}O$ and elemental ratios) obtained from one core of the eastern equatorial Indian Ocean (core SHI9001).

Finally, conclusions and perspectives of this work are the last part of this PhD dissertation.

Chapter 1: Physiography and hydrological settings

In this first chapter, I present the general background information of the study area. Firstly, I illustrate the physiography and environmental settings of the Bay of Bengal, Arabian Sea and eastern equatorial Indian Ocean. In addition, I introduce the hydrological settings of the Indian Ocean in the modern time and in the past.

1.1 Physiography and environmental settings

The Indian Ocean is bounded by Asia in the north, the Indonesia and Australia in the east, Antarctica in the south and Africa in the west. The Indian Ocean does not have high northern latitudes, as it is only extending to 25°N, which differs from the Atlantic and Pacific Oceans. The Indian Ocean is connected with the Atlantic and Pacific Oceans through the Antarctic Circumpolar Current in the southern Ocean, and with the Pacific Ocean through the Indonesian archipelago.

The Indian Ocean has several marginal seas. The northern part has two large embayment: Bay of Bengal (BoB) and Arabian Sea, separated by the Indian peninsula. The Red Sea and the Persian Gulf are the inland seas in the north. Other marginal seas are the Andaman Sea located in the northeast, gulfs of Aden and Oman in the northwest, and the Great Australian Bight off the southern coast of Australia. The geographical settings of northern Indian Ocean are shown in Figure 1.1.

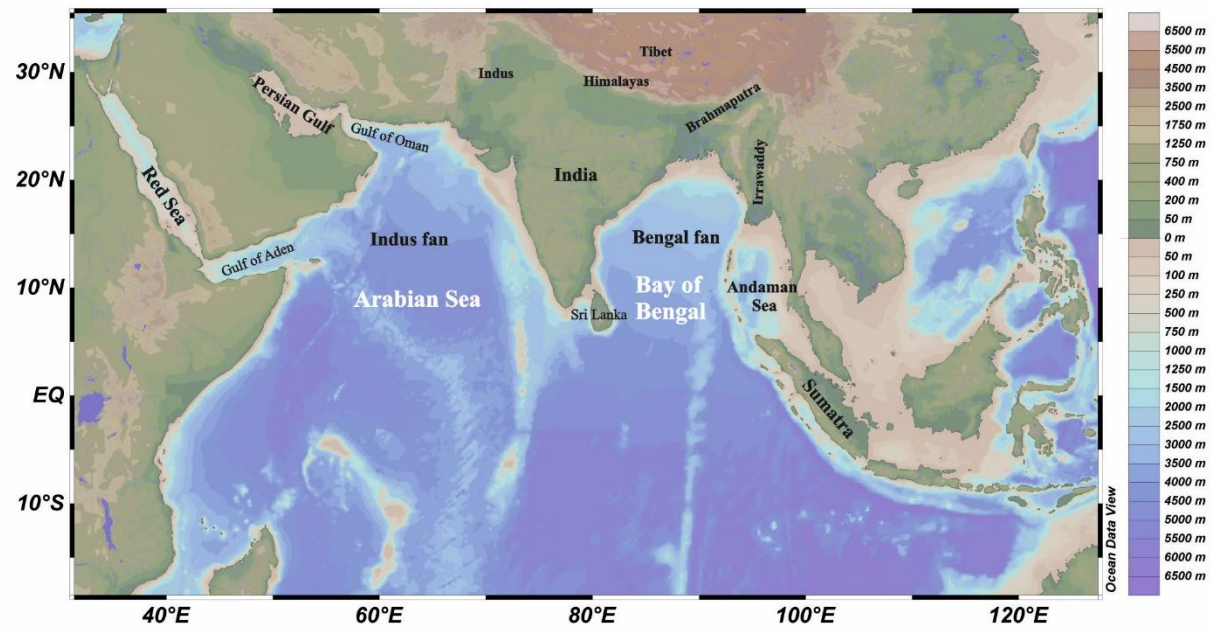

Figure 1.1. *Map of the main topographical features of the northern Indian Ocean. The marginal seas of Arabian Sea and Bay of Bengal investigated in this study have reported.*

The BoB is a shallow embayment of the northeastern Indian Ocean, occupying a total area of ~ 2,173,000 km^2 (Figure 1.1). It is bounded to the west by the Sri Lanka and India, to the north by the Bangladesh, to the east by Burma and the northern Malay Peninsula. The large amount sediment discharge of Ganges-Brahmaputra river system (1.1×10^9 t/yr), the Indo-Burman rivers, the Irrawaddy river (2.3 to 3.3×10^8 t/yr) and several Indian peninsular rivers (2.4×10^8 t/yr) make a

huge contribution for the BoB (Curray and Moore, 1971; Robinson et al., 2007; Tripathy et al., 2011). In addition, the Ganges-Brahmaputra river discharges huge amounts of sediments onto the BoB, which dominate the river input budget to the BoB (Milliman and Meade, 1983; Sarin and Krishnaswami, 1984; Sengupta et al., 2006).

The Arabian Sea is located in the northwestern Indian Ocean, covering an area of ~ 3,862,000 km^2. It is bordered by the Horn of Africa and the Arabian Peninsula to the west, Iran and Pakistan to the north and the Indian Peninsula to the east (Figure 1.1). The Arabian Sea is mainly fed by the Indus River system with around 400×10^6 t/yr of suspended load from the Himalayas and Transhimalaya (Milliman and Meade, 1983), and by Narmada River, Tapi River and Western Ghats rivers ($\sim100\times10^6$ t/yr) (Alagarsamy and Zhang, 2005; Chandramohan and Balchand, 2007). In addition, the aeolian dust from the deserts of Oman, Africa and western India also contribute around 100×10^6 t/yr in the Arabian Sea (Sirocko and Sarnthein, 1989; Ramaswamy and Nair, 1994).

The eastern equatorial Indian Ocean is limited to the East by Sumatra Island (Figure 1.1). The subduction of the Indian oceanic plate beneath the Eurasian continental plate formed the volcanic arc in western Indonesia, one of the most seismically active areas on the planet with a long history of powerful eruptions and earthquakes. This chain of active volcanoes formed Sumatra, Java, Bali, and Nusa Tenggara islands. The sediments of eastern equatorial Indian Ocean are mainly volcanogenic derived from the Indonesian Archipelago in the northeast, from submarine volcanic of the Mid-Indian Ocean Ridge (Venkatarathnam and Biscaye, 1973).

1.2 Hydrological settings

1.2.1. Surface circulation

The surface mixed layer and the boundary currents in the tropics and northern Indian Ocean (Arabian Sea and Bay of Bengal) are dominated by the seasonal reversing Indian monsoon wind (Figure 1.2). Monsoons are the seasonal changes of the large-scale winds. The summer monsoon (from May to September) in the northern Indian Ocean blow from the southwest to northeast, and the winter monsoon (during November to January) occur from the northeast. Therefore, the surface circulation in the northern Indian Ocean is characterized by cyclonic flow in the winter monsoon period, and displays an anticyclonic direction during the summer monsoon period.

The surface circulation of tropical and northern Indian Ocean is dominated by the monsoonal wind forcing (Figure 1.2) (Talley et al., 2011). Today, the surface water masses above 150m in the

Arabian Sea are Arabian Sea high Salinity Water (ASHS; 36.5 psu) (Talley et al., 2011). In contrast, the surface water shallower than 100m in the Bay of Bengal is much fresh Bay of Bengal surface waters (BoBSW; 31 psu), due to the high river input (Talley et al., 2011). In addition, the surface mixed layer and the boundary currents in the Arabian Sea and the Bay of Bengal are directly forced by the seasonal reversal of the Indian monsoon wind. Thus, by the influence of Indian monsoon, the surface water of Arabian Sea and Bay of Bengal forms from a mix of high saline ASHS and low saline BoBSW, respectively (Tomczak and Godfrey, 2003; Talley et al., 2011). In addition, low salinity surface water from BoB could also enter in the Arabian Sea from the south tip of Indian by the East India Coastal Current (EICC) (Figure 1.2).

The surface water of the eastern equatorial Indian Ocean represents a westward extension of the Pacific's warm pool. Compared with lower salinity of the northeastern Indian Ocean (BoBSW), the eastern equatorial Indian Ocean is characterized by high temperature and high salinity due to the influence of West Pacific Warm Pool. However, this area has complex dynamic currents and wave systems. The dominant current is the Indonesian Through Flow, which is outflow from the Pacific Ocean to the Indian Ocean.

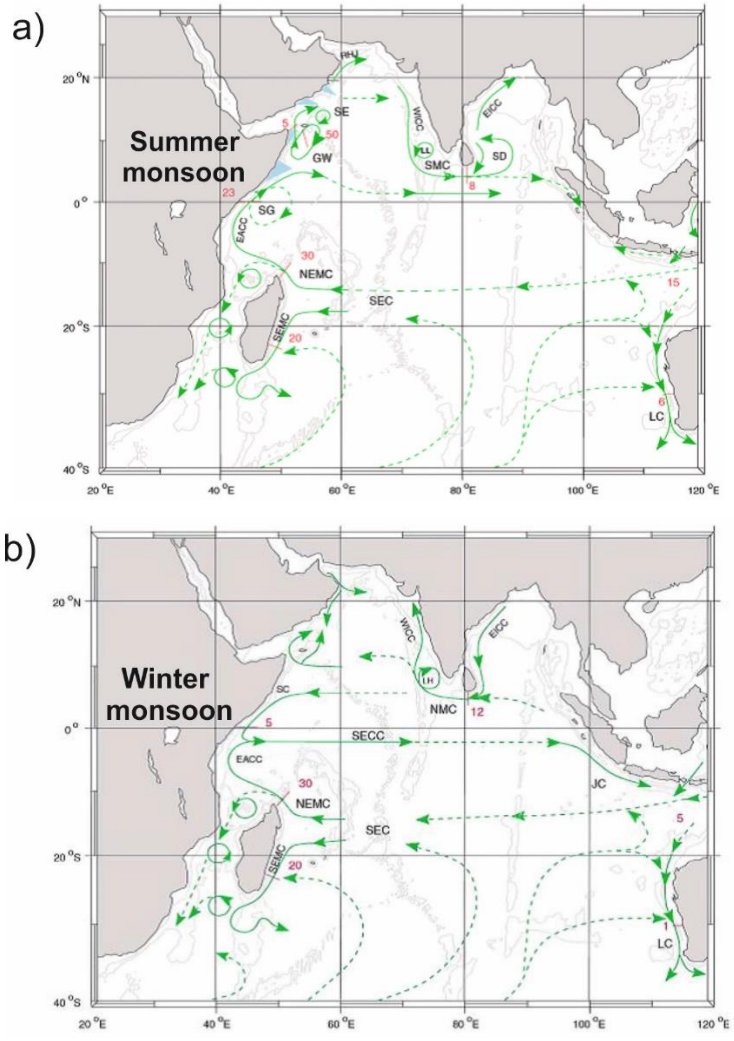

Figure 1.2. *A schematic representation of identified current branches during the Southwest Monsoon (a) and Northeast Monsoon (b), including some choke point transport numbers (Sv=$10^6 m^3.s^1$). Current branches indicated are the South Equatorial Current (SEC), South Equatorial Countercurrent (SECC), Northeast and Southeast Madagascar Current (NEMC and SEMC), East African Coast Current (EACC), Somali Current (SC), Southern Gyre (SG) and Great Whirl (GW) and associated upwelling wedges, Socotra Eddy (SE), Ras al Hadd Jet (RHJ) and upwelling wedges off Oman, West Indian Coast Current (WICC), Laccadive High and Low (LH and LL), East Indian Coast Current (EICC), Southwest and Northeast Monsoon Current (SMC and NMC), South Java Current (JC) and Leeuwin Current (LC). According to Schott and McCreary (2001).*

1.2.2. Intermediate and deep-water circulations

The main intermediate water masses found at around 500-1200 m water depths in the Indian Ocean are Antarctic Intermediate Water (AAIW), Red Sea Intermediate Water (RSIW) and Indonesian Intermediate Water (IIW) (Figures 1.3 and 1.4) (You, 1998; Talley et al., 2011).

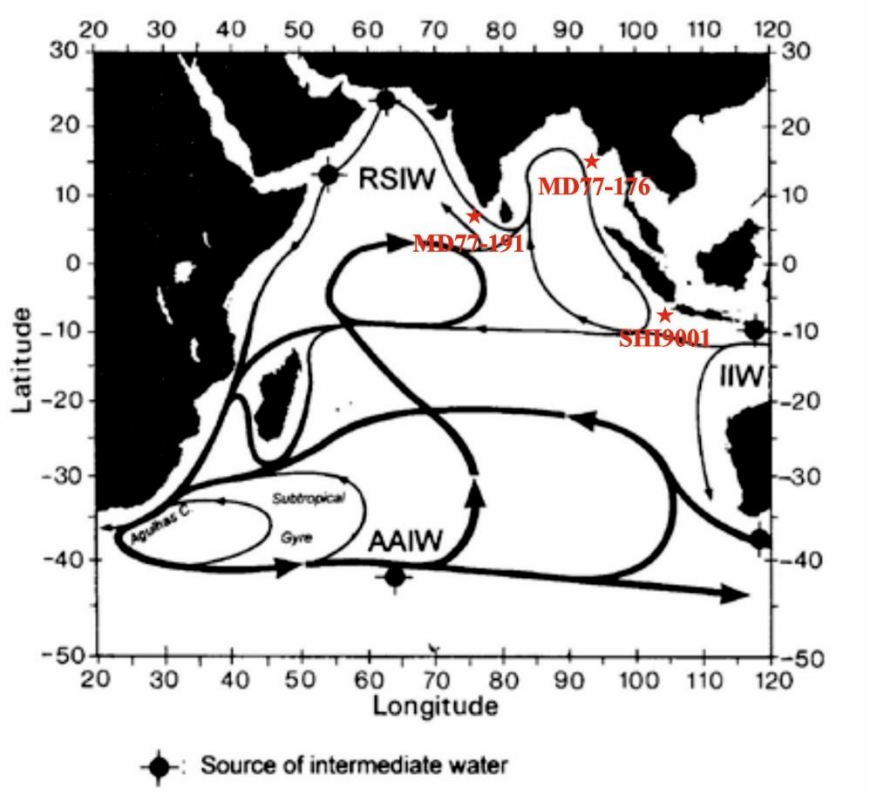

Figure 1.3. *Schematic map showing the intermediate water circulation of the Indian Ocean (You,*

1998). Locations of the studied cores are represented by red stars.

AAIW is a global intermediate water mass that is found in all three major oceans, characterized by a very low salinity (~ 34.39 psu). AAIW is considered to be important water mass at thermocline depths in the southern hemisphere, thus, it may potentially affect the global circulation through affecting the temperature gradients and nutrient (Olson et al., 1993; Sarmiento et al., 2004; Hendry et al., 2012). Modern AAIW in the Indian Ocean originates mainly from the southwestern Atlantic Ocean (Talley et al., 2011). It extends to the tropics through East African Coast Current (EACC) and Somali Current at about 1000-1500m water depth in the south Indian Ocean, just above the North Atlantic Deep Water (NADW) (Talley et al., 2011). In addition, part of AAIW sourced from the south of Australia, and flows northward along the Australian coast in the Western Australian Current and Leeuwin Undercurrents (e.g., You, 1998; Smith et al., 1991). In the South Indian Ocean, AAIW lies between 1000 and 1500 m, just above the Indian NADW (Tomczak and Godfrey, 2003). The northward extension of AAIW in the Indian Ocean rarely reaches beyond 10°S in the modern Indian Ocean (Lynch-Stieglitz et al., 1994).

The Red Sea Intermediate Water (RSIW) results from the outflow of high salinity Red Sea Water (density ~ 27.6 kg/m^3). Thus, it is the salinity maximum intermediate water filling the Arabian Sea between 400 and 1400m (Beal et al., 2000; Talley et al., 2011). RSIW spreads eastward to the eastern boundary at 5°N, in addition, intensification and rapid RSIW flows southward along the western boundary towards the Agulhas (You, 1998; Beal et al., 2000; Talley et al., 2011). In addition, RSIW represents only a small contribution to the BoB as its main flow is along the western margin of the Indian Ocean (You, 1998; Talley et al., 2011).

IIW is an intermediate-depth water mass originating from the Pacific Central Water. It passes through the Australasian Mediterranean Sea as Indonesian Through Flow, which remains relatively low salinity at 34.8 psu (Tomczak and Godfrey, 2003). IIW flows zonally westward and bifurcates into a northward and a southward flow in the western Indian Ocean (You, 1998). Around 50–60% of IIW water flows into the Bay of Bengal through the south of Sri Lanka. IIW flows clockwise at thermocline levels in the BoB, and returns along the Sumatra and Java Islands (You, 1998).

The deep-water masses of the northern Indian Ocean are characterized by a mixture of water masses from Atlantic (North Atlantic Deep Water, NADW) and Antarctic oceans (Antarctic Bottom Water, AABW), without any surface contribution to deep or bottom water masses in the Indian Ocean (Figure 1.4 and Figure 1.5) (Reid, 2003; Talley et al., 2011). Between 1200 and 3800m, the dominant deep water in the North Indian Ocean is Indian Deep Water (IDW), originating from the Circumpolar Deep Water and NADW (You and Tomczak, 1993; Tomczak and Godfrey, 2003). However, in the eastern Indian Ocean, IDW originates from the mixture of Circumpolar Deep Water

(CPDW) and NADW (Warren, 1981).

Below 3800m of water depth, the abyssal basins are dominated by the AABW, which is formed in the Weddell Sea and Ross Sea (Wyrtki, 1973; Kolla et al., 1976; Reid, 2003; Tomczak and Godfrey, 2003). However, AABW only reaches the southern part of the BoB as most of the BoB is shallower than 4000m (Tomczak and Godfrey, 2003). In the BoB, the bottom water upwells when it moves northward, so the deep waters can eventually return to shallower depths (Talley et al., 2011). Thus, changes in the bottom waters can also affect shallower-depth water masses in the northern BoB.

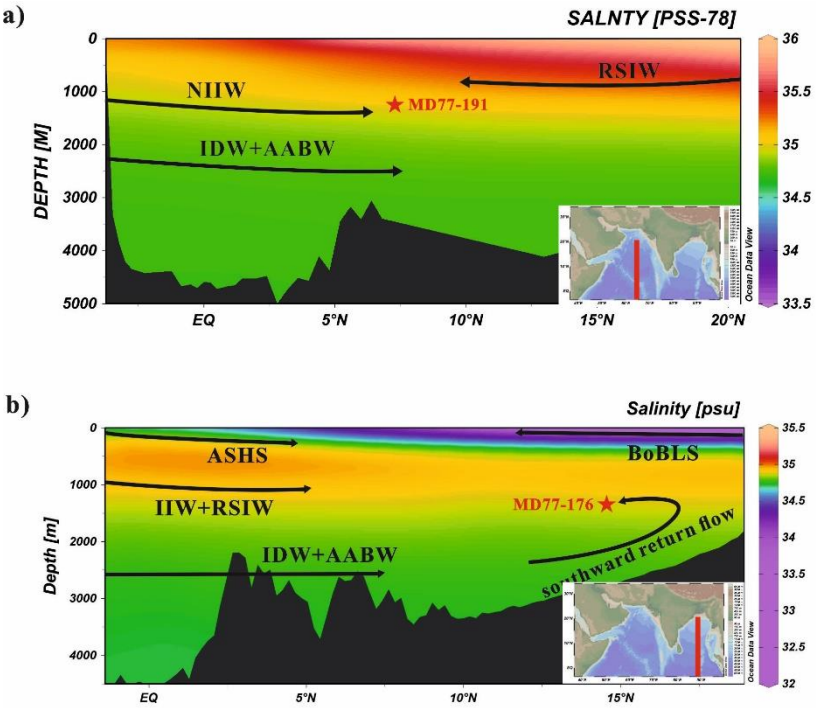

Figure 1.4. *(a) and (b) Salinity (psu, coloured shading) depth-latitude section using the Ocean Data View (ODV) software (Schlitzer, 2015) and vertical distribution of water masses in the Arabian Sea and Bay of Bengal (N-S cross section). BoBLS: Bay of Bengal low salinity Water, ASHS: Arabian Sea High Salinity Water, RSIW: Red Sea Intermediate Water, IIW: Indonesian Intermediate Water, AABW: Antarctic Bottom Water, IDW: Indian Deep Water.*

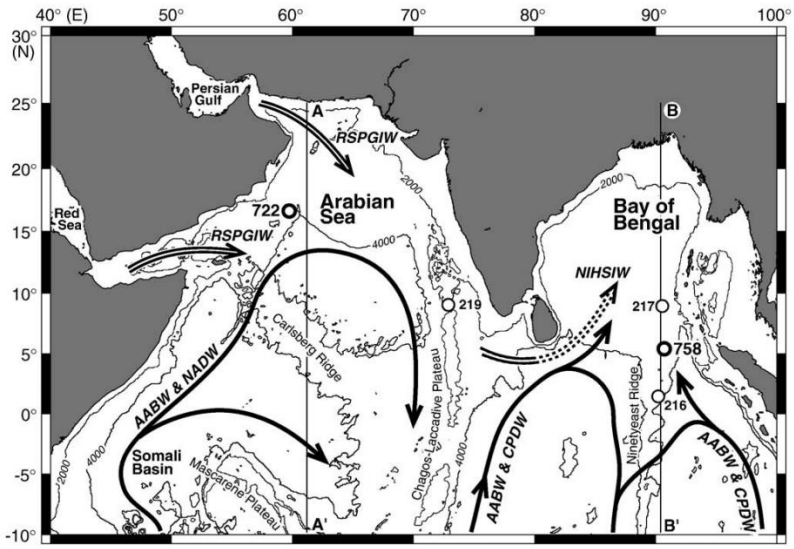

Figure 1.5. *Schematic map showing the deep-water masses circulations of the northern Indian Ocean. The black arrows represent deep circulation. Figure from (Kolla et al., 1976).*

1.2.3. Modern primary productivity and nutrient content of water masses

The northern Indian Ocean, especially the Arabian Sea, is characterized by seasonal highly productive (Shankar et al., 2002). During the summer monsoon, the southwest wind blows more salinity water from the northern to the southeastern Arabian Sea. By contrast, during the winter monsoon, the northeastern winds bring low salinity water (BoBSW) from the BoB. In addition, enhanced upwelling occurs in the western Arabian Sea during the summer monsoon, resulting in a strong Ekman pumping, and thus leading to an increased surface productivity (Lévy et al., 2007; Bassinot et al., 2011; Figure 1.6).

However, the surface productivity in the BoB is generally weak compared with the Arabian Sea (e.g., Prasanna Kumar et al., 2002; Thushara and Vinayachandran, 2016; O'malley, 2017; Figure 1.6). In the BoB, seasonally large river input could lead to a more stable stratification in the upper ocean (Vinayachandran et al., 2002), and hence the vertical mixing of nutrients from the subsurface to the euphotic zone is generally limited (Gomes et al., 2000). In addition, the primary productivity of the western BoB suggests a slight increase during the winter monsoon, as indicated by the distribution of chlorophyll in the surface water (Thushara and Vinayachandran, 2016; O'malley, 2017; Figure 1.6).

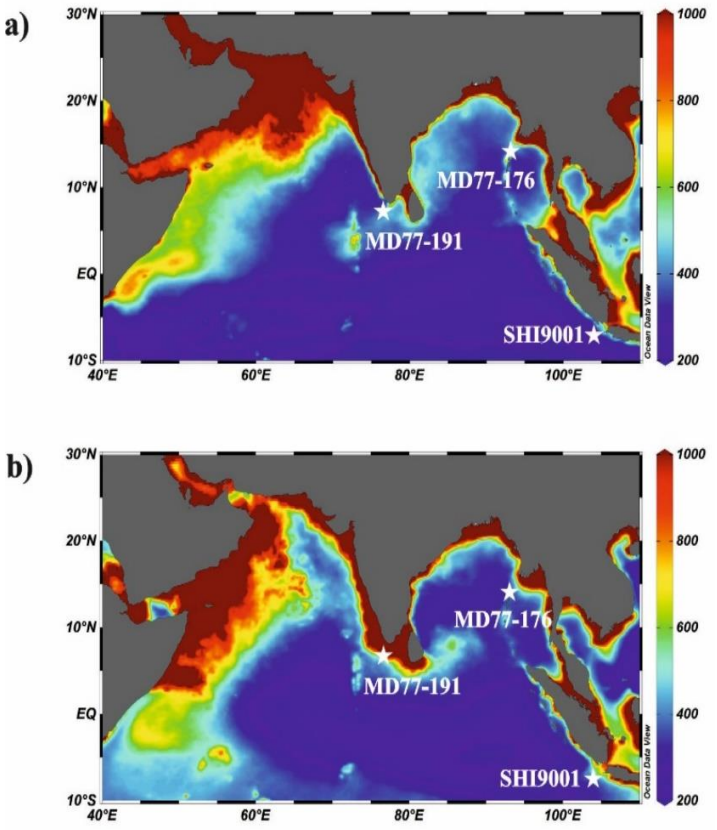

Figure 1.6. *a) – b) the Net primary productivity distribution in Northern Indian Ocean during January and July, respectively. Maps based on MODIS chlorophyll-a, SST, PAR satellite data, using the standard vertically Generalized Production Model (VGPM) (Behrenfeld and Falkowski, 1997) as the standard algorithm.*

In the modern Indian Ocean, surface water is characterized by a relatively depleted nutrient content, with ~ 1.5 µmol/kg phosphate concentration (Fig 1.7). For the intermediate water masses in the northern Indian Sea (BoB and Arabian Sea), the phosphate concentration is at around 2.5-3 µmol/kg. In addition, the modern data indicate that the southern sourced intermediate water (AAIW) in the south Indian Ocean shows a lower phosphate concentration at about 2-2.5 µmol/kg (Fig 1.7). Moreover, the phosphate concentration of deep-water masses (~2-2.5 µmol/kg) is slightly lower than the intermediate water masses in the northern Indian Ocean.

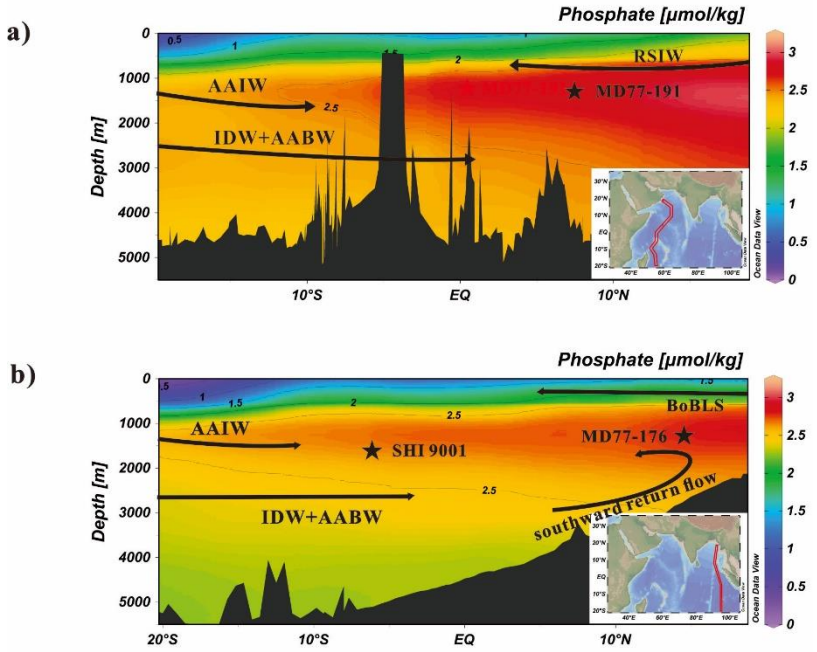

Figure 1.7. *Phosphate (µmol/kg, coloured shading) depth-latitude section using the Ocean Data View (ODV) software (Schlitzer, 2015) and vertical distribution of water masses in the (N-S cross-section) (a) the Western and (b) the Eastern Indian Ocean. BoBLS: Bay of Bengal low salinity Water, AIIW: Antactic Intermediate Water, RSIW: Red Sea Intermediate Water, AABW: Antarctic Bottom Water, IDW: Indian Deep Water.*

1.2.4. The past hydrology of the Indian Ocean since the last glacial times

The thermohaline ocean circulation plays a key role in regulating climate changes at different time-scales through heat redistribution and carbon cycling (e.g., Rahmstorf, 1995; Stocker and Wright, 1996; Tomczak and Godfrey, 2003; Bryan et al., 2010; Talley et al., 2011). In the modern ocean, as shown in Figure 1.8 A, North Atlantic Deep Water (NADW) enters the Southern Ocean through the South Atlantic, and joins in the deep waters flowing through the Drake Passage. The combination of deep waters from Pacific, Indian, and Atlantic is transported eastward as Circumpolar Deep Water (CDW). CDW upwells to intermediate water in the Pacific sector around Antarctica, which forms an important component of the upward limb of the thermohaline overturning circulation (Talley, 2013; Sikes et al., 2017). Then, these waters flow northward through the Polar Front (PF) and sink as Antarctic Intermediate Water (AAIW) and Subantarctic Mode Water (SAMW) (Talley, 2013). Furthermore, AAIW (800–1500 m) and SAMW (400–800 m) move northward beneath warmer and saltier subtropical surface waters. Thus, in the modern thermohaline circulation, the oceans are connected by NADW transport and converted by the upwelling in the Southern, Indian, and Pacific Oceans (Sikes et al., 2017).

A large amount of previous studies have worked on the links between ocean circulation variations and climate changes in the past (e.g., Barker et al., 2011; Skinner et al., 2010). Based on the previous studies, the Atlantic Meridional Overturning (AMOC) circulation was slowdown during most of the last glacial periods and associated with the formation of shallower Glacial North Atlantic Intermediate Water (e.g., McManus et al., 2004; Böhm et al., 2015). The AMOC has only been disrupted during episodes of sluggish circulation associated with the catastrophic iceberg discharges of the coldest Heinrich stadials (HS), the Dansgaard-Oeschger stadials (D-O stadials) and the Younger Dryas cold event (YD) of the last termination (Böhm et al., 2015) (Figure 1.8B). These slowdowns of the AMOC have been related to the reduced North Atlantic Deep Water (NADW) flow (e.g., Mcmanus et al., 2004; Böhm et al., 2015) and an increased advection of southern-sourced waters, filling a large part of the deep Atlantic ocean (e.g., Lynch-Stieglitz et al., 2007; Roberts et al., 2010; Böhm et al., 2015; Duplessy et al., 1988) and affecting the circulation in all ocean basins (e.g., Lynch-Stieglitz et al., 2007; Roberts et al., 2010; Böhm et al., 2015).

The Indian Ocean plays an important role in the global overturning circulation, as it is an upwelling region, like the Pacific Ocean (Talley et al., 2011). In addition, as the northern Indian Ocean is in the land-sea configuration, the deep-water masses of the Northern Indian Ocean are characterized by a mixture of water masses from Atlantic (North Atlantic Deep Water, NADW) and Antarctic oceans (Antarctic Bottom Water, AABW), without surface contribution to deep or bottom water masses in the Indian Ocean; furthermore, much of the intermediate waters of the northern Indian Ocean originate from the south, with only small contributions of intermediate waters from the Red Sea and of Pacific water through the Indonesian sea (Talley et al., 2011). In addition, the Eastern Equatorial Indian Ocean is a key area to study the connections between the Pacific Ocean and the Indian Ocean through the Indonesian Throughflow (ITF). Thus, reconstruction of Indian Ocean circulation will allow us to better constrain past changes in the production of intermediate and deep water and in circulation from the global ocean.

In the Indian Ocean, most of previous works have documented past changes in deep ocean circulation (e.g., Kallel et al., 1988; Naqvi et al., 1994; Ahmad et al., 2008, 2012; Raza et al., 2014). They all suggested that during the glacial, the reduction in the NADW flux into the Indian Ocean allowed for a higher contribution from the Southern Ocean. By contrast, the Holocene is mainly influenced by better-ventilated NADW (Ahmad et al., 2008, 2012; Raza et al., 2014), in agreement with the past variations of AMOC in the Atlantic Ocean.

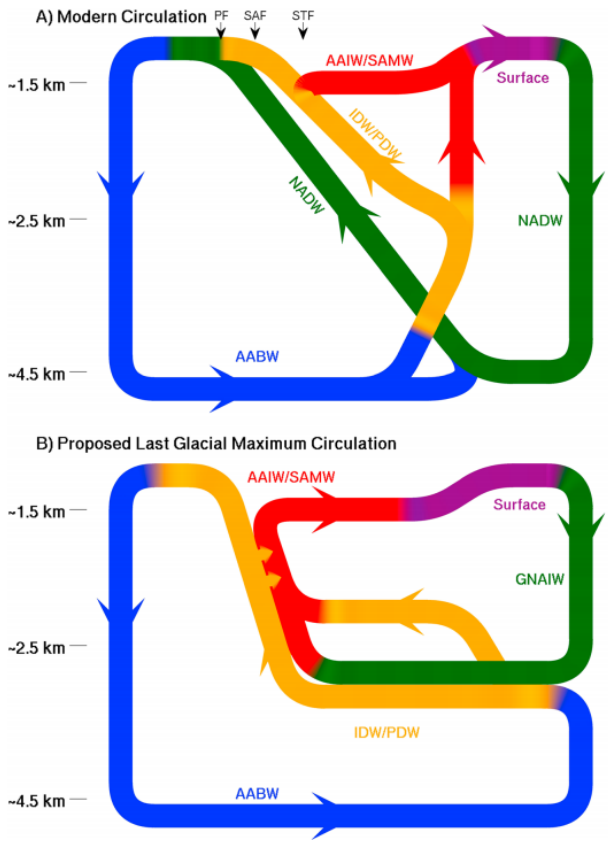

Figure 1.8. *View of overturning circulation schematics. (a) Modern circulation and (b) Hypothesized overturning circulation during the LGM (Sikes et al., 2017). Polar Front (PF), Subantarctic Front (SAF), and Subtropical Front (STF), which are major fronts separate the interior water formation zones. Colors represent the water masses as follows: blue = AABW, green = NADW/GNAIW, orange = PDW/IDW, red = AAIW/SAMW, and purple = surface low-latitude and mainly in the Atlantic Ocean.*

As mentioned before, from the Last Glacial Maximum (LGM) to the Holocene, the AMOC was likely experienced major changes (e.g. McManus et al., 2004; Böhm et al., 2015). During the HS1 and YD, which are abrupt deglacial climate cooling events recorded in the northern hemisphere, a weak or even a collapse of AMOC occurred (Böhm et al., 2015). Synchronously, the Southern Hemisphere increased the heat fluxes and reduced sea ice cover in the Southern Ocean. Thus, strong winds enhanced the upwelling and increased the northward penetration of the northward flow of AAIW/ SAMW, which could increase northward transport of nutrient and heat at intermediate waters depth (Anderson et al., 2009; Skinner et al., 2014; Poggemann et al., 2017; 2018). The role of AAIW is still controversial during the last deglaciation in the Atlantic Ocean: several previous studies indicated a reduced influence of northward AAIW into the tropical Atlantic (e.g. Came et al., 2008; Xie et al., 2012; Howe et al., 2016; Gu et al., 2017), whereas others suggested an

increased penetration (e,g., Pahnke et al., 2008; Dubois-Dauphin et al., 2016; Poggemann et al., 2017; 2018). In addition, the enhanced northward transport is also strongly supported by the intermediate records of benthic carbon isotope, ε_{Nd} and B-P age offsets from the North Indian (Jung et al., 2009; Bryan et al., 2010; Yu et al., 2018; Ma et al., 2019), and Pacific Ocean (e.g., Mix et al., 1991; Pahnke and Zahn, 2005; Bostock et al., 2010).

To sum up, a large amount of previous studies have worked on the seasaw relationship between the AMOC and the Southern Ocean circulation during the transition from the Last Glacial Maximum to the Holocene (e.g., McManus et al., 2004; Böhm et al., 2015; Came et al., 2008; Anderson et al., 2009). However, the role of AAIW in rapid climate changes resulting from major AMOC are controversial, especially in the Atlantic Ocean (e.g., Pahnke et al., 2008; Dubois-Dauphin et al., 2016; Came et al., 2008; Xie et al., 2012; Jung et al., 2009; Pahnke and Zahn, 2005). Thus, studying intermediate waters in the Indian Ocean will allow us to better constrain past changes in the production of intermediate and deep water and in circulation from the Southern Ocean; in addition, it will help us to understand their potential role in global climate changes.

Chapter 2: Materials and Methods

In order to reconstruct variations of intermediate water circulation of the Bay of Bengal, the Arabian Sea and the Eastern Equatorial Indian Ocean since the LGM, we selected three cores to constrain the northward penetration of the AAIW, the intermediate waters of the Red Sea and of the Pacific through the Indonesian sea. It was necessary to use a multi-proxy approach (stable isotopes, ^{14}C ages, elemental ratios and assemblages on benthic foraminifera) to constrain past water masses conditions, ventilation as well as the sources of water masses. In this chapter, I present the material used, as well as the different methods. The development needed to measure the element/Ca ratios is also displayed.

2.1. Material

The samples used in this study are foraminifera obtained from marine cores collected at intermediate water depth from the Bay of Bengal (BoB), Arabian Sea and eastern equatorial Indian Ocean.

2.1.1. Northern Bay of Bengal: core MD77-176

Core MD77-176 (14°30'5N-93°07'6E, 1375m) was collected from the northeastern BoB during the OSIRIS III cruise of the N.0. Marion Dufresne in 1977 (Figure 1.3). The sediment consists of intercalated olive grey terrigenous clay and silty clay layers with foraminifer- or nannofossil-bearing ooze. In addition, several turbidite layers were identified. The age model of core MD77-176 was previously established by using 31 planktonic foraminifer (*Globigerinoides ruber*) AMS ^{14}C dates combined with the MD77-176 oxygen isotope record obtained on planktonic foraminifera *G. ruber*, which were correlated to the GISP2 Greenland ice core record (Marzin et al., 2013). Core MD77-176 displays high accumulation rates (average ~25 cm/kyr and up to 40 cm/kyr for the Holocene), and could thus provide high-resolution records since 40 cal kyr BP. The samples were collected outside from the identified turbidite levels (429-432 cm, 460-463 cm, 470-472 cm, 485-493 cm, 508-514 cm, 577-582 cm, 732-738 cm, 918-921 cm, 950-951 cm and 962-963 cm) (Marzin et al., 2013).

2.1.2. Arabian Sea: core MD77-191

Core MD77-191 (07°30'N-76°43'E, 1254m) located in the southern tip of India in the Arabian Sea was collected during the OSIRIS III cruise of the N.0. Marion Dufresne in 1977 (Figure 1.3). The age model of core MD77-191 was established in this work by using 9 monospecific planktonic foraminifer *Globigerinoides bulloides* accelerator mass spectrometry (AMS) ^{14}C dating (Bassinot et al., 2011), one ^{14}C date made on pteropods (Mléneck et al., 1997), and three ^{14}C dates obtained on planktonic foraminifera *Globigerinoides ruber* measured with the ECHoMICADAS at the LSCE, France (see details in section 2.3.2. below). The ^{14}C ages were converted to calendar ages by using the CALIB Rev. 7.1 software (Stuiver and Braziunas, 1993). Core MD77-191 provides a continuous record since the last 17 kyr BP with an average sedimentation rate of about 53 cm/kyr and up to 90 cm/kyr for the Holocene.

Samples of these two cores (MD77-191 and MD77-176) were available from previous studies

(Kallel et al., 1988; Marzin et al., 2013; Bassinot et al., 2011) and were sieved in the 63-150 and >150 μm fractions. A total of 75 samples (MD77-191) and 217 samples (MD77-176) were collected for benthic foraminiferal analysis.

2.1.3. Eastern Equatorial Indian Ocean: core SHI9001

Core SHI9001 (6°11.57' S 103°11.80' E, 1348m) is located in the Eastern Equatorial Indian Ocean EEIO and was collected during the SHIVA cruise (Figure 1.3). The lithology of core SHI9001 is dominated by olive grey terrigenous clay and nanno-fossil carbonate ooze. The sampling interval is every 10 cm and a total of 88 samples were sieved for benthic foraminiferal analysis. Each ~20 g of bulk sediments were dried at 60 °C and weighed. Dried samples were soaked in water for 2 days, and a few drops of hydrogen peroxide were added to adequately disaggregate the samples, if necessary. Samples were washed through a 63 μm mesh-size sieve. The residue on the sieve was transferred to the filter paper in the 63-150 and >150 μm fractions, dried at 60 °C and weighed.

The age model of core SHI9001 was based on the stratigraphical correlation between the benthic $\delta^{18}O$ record with a reference record (LR04 benthic stack, Lisieki and Raymo, 2005; see details in section 6.5.1. from Chapter 6). Core SHI9001 spans the last 685 kyr, reaching Marine Isotope Stage MIS 17. Sedimentation rates are on average 2.5 and 1 cm/ka for interglacial and glacial periods, respectively.

2.2. Methods

2.2.1. General information on foraminifera

Foraminifera are single-celled, protists with exo-skeletal tests (Mortyn and Martinez-Boti, 2007). They existed and diversified as part of the burst in development of the Kingdom Protista since Cambrian times (Escalante and Ayala, 1996). Base on their marine habitat, foraminifera could be recognized as planktonic and benthic foraminifera. The majority of modern foraminifera are benthic, and only about 40–50 are planktonic species (Gupta, 1999; Mortyn and Martinez-Boti, 2007).

The foraminifera distribute in a wide range of ocean environments and could be a good fossil recorder due to the well-preserved, calcite or aragonite shells. The foraminiferal tests are a common component of marine sediments, which assemblages can be used as a proxy for paleo-environment, such as organic carbon flux, bottom water oxygen concentration and ventilation (e.g., Corliss, 1985;

Fontanier et al., 2002).

In addition, the shells of foraminifera can powerfully record the chemical and physical properties of the ocean through their isotopic (e.g., Oxygen, Carbon, Boron… stable isotopes) and minor or trace element composition (e.g., Mg/Ca, Sr/Ca, U/Ca, Li/Ca, B/Ca, Cd/Ca, Ba/Ca, B/Ca…) (e.g., Katz et al., 2010). Therefore, the foraminifera can be used to reconstruct the paleo-ecological and past global environmental evolution.

We especially used three benthic foraminifera species commonly used in paleoceanography for geochemical analysis during this PhD work, thanks to their abundance in the studied cores (see also details in the sections dedicated to assemblage results in Chapter 3 and 5). Two of the used benthic foraminiferal are made of calcite (*Cibicidoides wuellerstorfi* and *Uvigerina peregrina*) and one of aragonite (*Hoeglundina elegans*) (Figure 2.1). *Cibicidoides wuellerstorfi* and *Hoeglundina elegans* belong to epifaunal species, and *U. peregrina* is an endobenthic species (Fontanier et al., 2002).

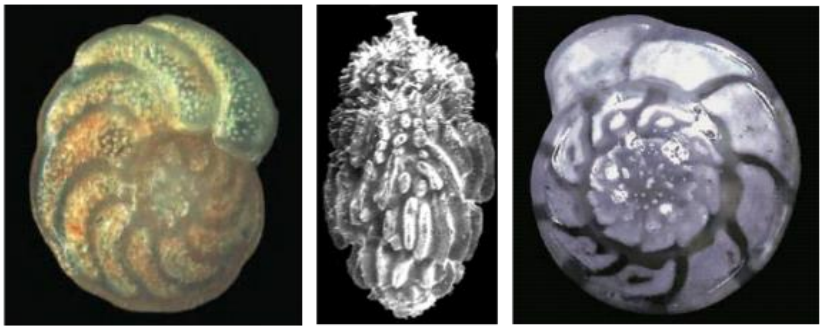

Figure 2.1. *Benthic foraminiferal species used for geochemical analysis in this work. Cibicidoides wuellerstorfi (left), Uvigerina peregrina (middle), and Hoeglundina elegans (right). Figures from (Holbourn et al., 2013).*

In this study, we investigated the stable isotopes $\delta^{13}C$, $\delta^{18}O$, the radiocarbon ages ^{14}C and elemental ratios (Mg/Ca, Sr/Ca, U/Ca, Li/Ca, Cd/Ca and Ba/Ca) of these three benthic foraminifera, together with benthic foraminiferal assemblages from marine cores MD77-176, MD77-191 and SHI9001 located in the Indian Ocean, as described in greater detail below.

Table 2.1. *Summarize of all analytical investigations.*

Species / Core	$\delta^{13}C$, $\delta^{18}O$	^{14}C	Elemental /Ca	Assemblages
MD77-176	*Cibicidoides wuellerstorfi*, *Cibicidoides pachyderma*, *Uvigerina peregrina*	*Cibicidoides wuellerstorfi*, *Cibicidoides pachyderma*, *Hoeglundina elegans*	*Hoeglundina elegans*, *Uvigerina peregrina*	X
MD77-191	*Cibicidoides wuellerstorfi*, *Cibicidoides pachyderma*, *Uvigerina peregrina*, *Globigerinoides ruber*	*Globigerinoides ruber*	*Hoeglundina elegans*, *Cibicidoides pachyderma*, *Uvigerina peregrina*, *Globobulimina* spp.	X
SHI9001	*Cibicidoides wuellerstorfi*		*Hoeglundina elegans*, *Uvigerina peregrina*	

2.2.1.1 Oxygen and Carbon stable isotopes

Oxygen and carbon are naturally present in abundance on Earth, such as in the Calcium Carbonate ($CaCO_3$) of which is the material of benthic and planktonic foraminiferal shells. Oxygen is made of three stable isotopes whose respective relative abundances are: ^{16}O 99.76%, ^{17}O 0.04% and ^{18}O 0.2%. Individual measurements of $^{18}O/^{16}O$ obtained from nature are reported as departures in parts per thousand (‰) from a laboratory standard:

$$\delta^{18}O\ (‰) = \frac{(^{18}O/^{16}O)_{sample} - (^{18}O/^{16}O)_{standard}}{(^{18}O/^{16}O)_{standard}} \times 1000$$

Carbon (C) has mainly two stable isotopes: ^{13}C and ^{12}C. The abundance of ^{12}C isotope is around 98.9%, and the ^{13}C isotope accounts for about 1.1%. As similar with the oxygen, the carbon isotopic composition is expressed in the δ notation:

$$\delta^{13}C\ (‰) = \frac{(^{13}C/^{12}C)_{sample} - (^{13}C/^{12}C)_{standard}}{(^{13}C/^{12}C)_{standard}} \times 1000$$

The standard material for carbonate samples is the Pee Dee Belemnite (PDB). In addition, $\delta^{18}O$ and $\delta^{13}C$ values are calibrated versus PDB by using National Bureau of Standards (NBS) standards.

The ocean and ice sheet are the major oxygen reservoir. During the glacial period, the ^{16}O is more enriched in the icecaps and shows a light $\delta^{18}O$ values. By contrast, the ocean shows heavier $\delta^{18}O$. Thus, benthic foraminiferal $\delta^{18}O$ that reflect the ocean geochemical signature is thus affected by the global ice volume, the source of deep-water masses, and bottom water temperature (Shackleton and Opdyke, 1973; Figure 2.2 a). As a salty water mass will have a high $\delta^{18}O$ signal because both of them have a positive relationships with evaporation, changes in the salinity are also recorded by the $\delta^{18}O$.

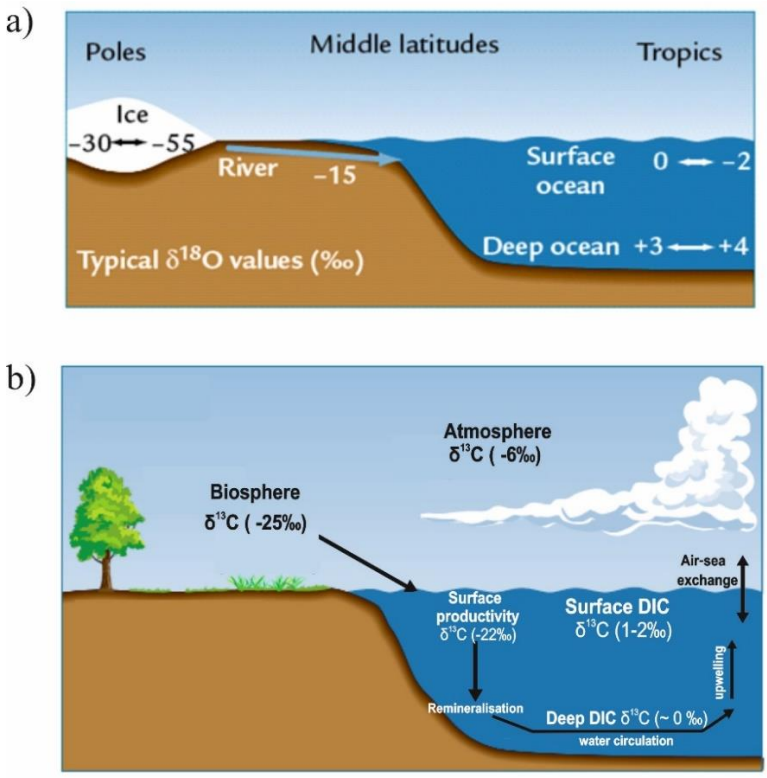

***Figure 2.2**. Modern simplified oxygen and carbon cycle by Ruddiman, (2014).*

According to studies in the modern ocean with living foraminifera (e.g., McCorkle et al., 1990 and 1997), the epifaunal benthic foraminiferal $\delta^{13}C$ can reflect the dissolved inorganic carbon $\delta^{13}C$ in bottom water (e.g., Duplessy et al., 1984; Curry et al., 1988). During the glacial times, ^{12}C enriched organic carbon transferred from the land to the ocean, the $\delta^{13}C$ of inorganic carbon in the

ocean should be more negative due to the remineralization of ^{12}C-rich organic carbon. In addition, the photosynthesis and carbon isotope fractionation lead to higher values of the surface water compared with the deep water masses (Ruddiman, 2014) (Figure 2.2 b and Figure 2.3). Changes in $\delta^{13}C$ values of epifaunal benthic foraminifera can be influenced by different processes such as surface productivity, changes of the water mass sources and/or mixing and air-sea exchanges (Lynch-Stieglitz et al., 1995) (Figure 2.2 b and Figure 2.3). Infaunal benthic foraminiferal $\delta^{13}C$ (such as *U. peregrina*) is mainly affected by the pore water, thus carrying a signal influenced by the remineralization of organic matter in the ocean floor (e.g., Mackensen et al., 2000; Mackensen and Licari, 2004).

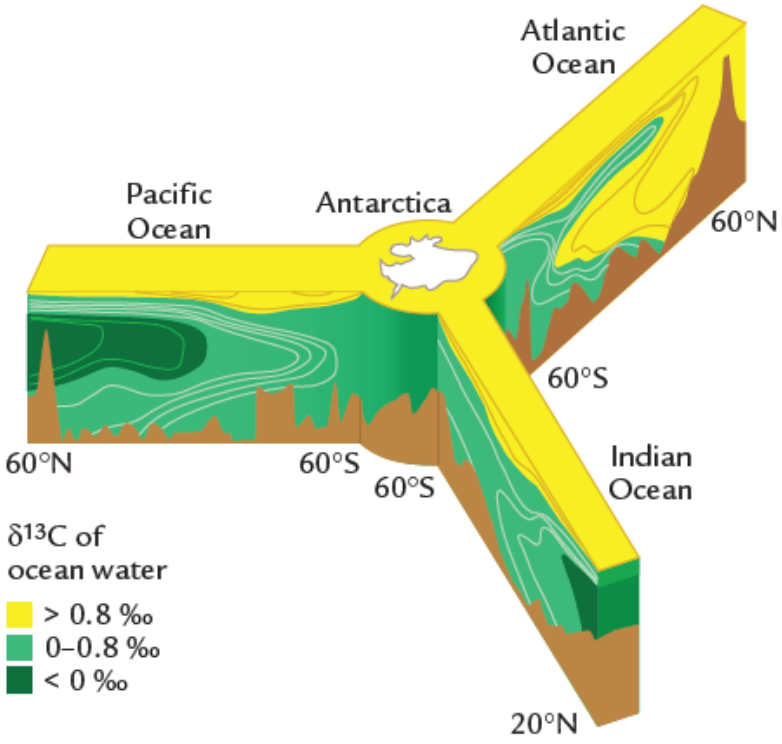

Figure 2.3. *Modern deep-ocean GEOSECS $\delta^{13}C$ data patterns, figure from Ruddiman, (2014).*

2.2.2. Benthic radiocarbon content as a tracer for water ventilation

The carbon exchanges of surface waters in the ocean mainly occur at the ocean-atmosphere interface. The surface waters have the highest $^{14}C/^{12}C$ ratio compared with deep water masses. However, the exchanges between ocean and atmosphere are not instantly, the radioactive ^{14}C atoms are continuously decaying during this process. Thus, the radiocarbon age is different between surface water and atmosphere, and the average difference age is around 400 years (Key et al., 2004).

In the ocean, the ^{14}C content stops to renew due to the isolation from the surface water layer, and ^{14}C begins to decrease by radioactive decay and deeper water masses get aging. The ^{14}C of deep-water masses in different oceans are in good agreement with the modern circulation scheme (e.g., Matsumoto, 2007; Khatiwala et al., 2012). For instance, the deep-water masses of Atlantic Ocean have the younger ^{14}C age compared to other oceans, as the surface water sinks as deep waters and fill the ocean interior (Figure 2.4). Thus, the ^{14}C could be a useful tracer of water masses ventilation and circulation. The ^{14}C of water masses could be obtained from foraminifera measurements. The benthic and planktonic species could provide the intermediate-deep and surface water signals, respectively. The ^{14}C age difference between benthic and planktonic foraminiferal species is useful to reconstruct the ventilation of the water masses (e.g., Broecker et al., 1984; De Pol-Holz et al., 2010; Wan and Jian, 2014; Siani et al., 2013). The ventilation recorded in foraminifera depends on (i) ^{14}C of surface water related to atmospheric ^{14}C through air-sea gas exchange and timing of equilibrium between the atmosphere and water masses; (ii) the time elapsed since water masses reaching the studied sites have become isolated from the atmosphere, and (iii) vertical and horizontal mixing processes involving water masses with different ^{14}C signatures.

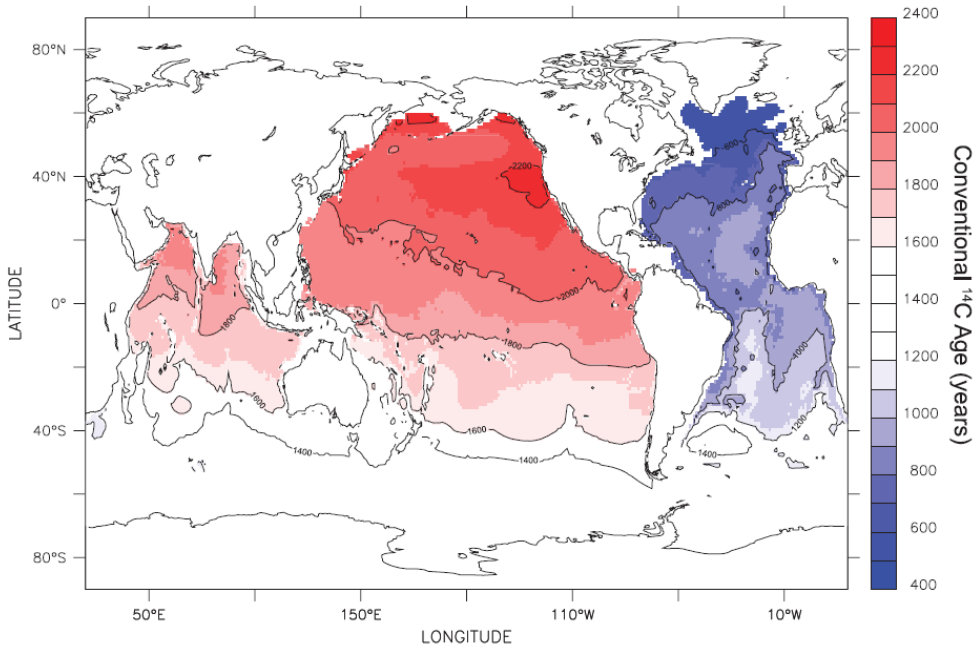

Figure 2.4. *An objectively mapped conventional ^{14}C age of natural radiocarbon below 1500 m of the ocean. Figure from Matsumoto, (2007).*

2.2.3. Benthic foraminiferal assemblages

Benthic foraminifera exist in all marine environments, which consist of above, at, or below the water-sediment interface (e.g., Corliss, 1980; Holbourn et al., 2013; Jorissen, 1999) (Figure 2.5). In the deep water depth, benthic foraminiferal distribution could be used to estimate the bottom water condition changes (e.g., Corliss et al., 1986; Schmiedl et al., 1998; Almogi-Labin et al., 2000), especially indicating a strong relationship with the organic matter flux to the seafloor (e.g., Altenbach et al., 1999; Caulle et al., 2015; Fontanier et al., 2002; Van der Zwaan et al., 1999).. Both the depth of the principle redox fronts and the microhabitat of deep infaunal species show important increases with depth. Therefore, the exported flux of organic matter appears to be the main parameter controlling the composition and the vertical distribution of benthic foraminiferal faunas below the sediment-water interface.

The benthic foraminiferal microhabitat could be a function of organic flux and benthic ecosystem oxygenation, thus, by comparing benthic foraminiferal assemblages to modern ones, changes of food supply and oxygen concentrations of the bottom water can be reconstructed (e.g., Peterson, 1984; Corliss, 1979; Murgese and De Deckker, 2005). For example, as shown in the Figure 2.5, at the deepest oligotrophic stations, deep infaunal faunas (*G. affinis*) become relatively poor and the benthic faunas are dominated by *H. elegans*, *Q. seminula* and *C. pachydermus* (Fontanier et al., 2002). Combining the benthic foraminiferal fauna analysis with the measurements of the geochemistry ($\delta^{18}O$, $\delta^{13}C$, ^{14}C, trace and minor elemental ratios) allows to constrain the paleoceanographic evolution (like oxygen, nutrient, …).

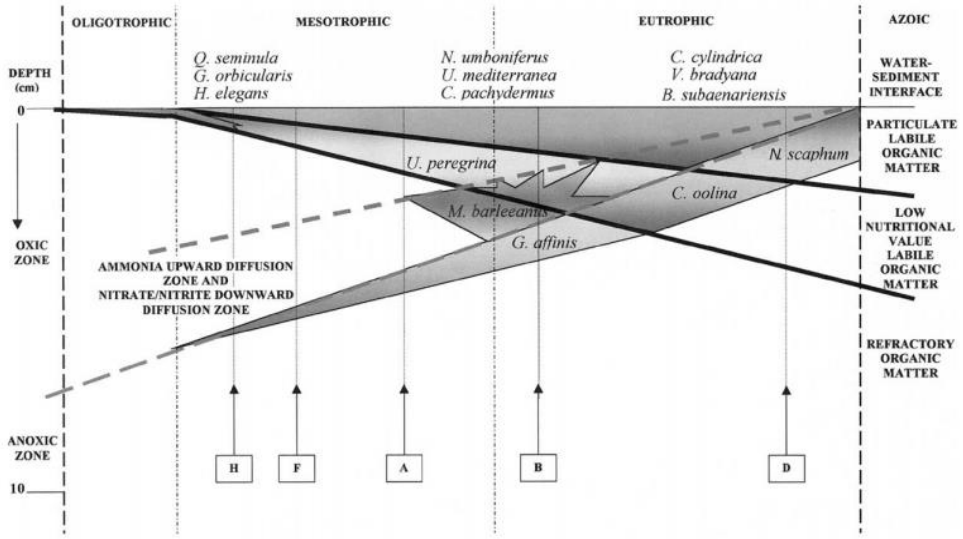

Figure 2.5. *Microhabitat distribution and specific foraminiferal composition along the bathymetric transect in the Bay of Biscay, figure from Fontanier et al. (2002).*

2.2.4. Benthic foraminiferal elemental ratios

Past variations in the hydrography and circulation of intermediate/deep water masses are reconstructed using benthic foraminiferal elements/Ca (Mg/Ca, Sr/Ca, Li/Ca, B/Ca, Cd/Ca, Ba/Ca, U/Ca…), which are commonly used as water mass tracers (e.g., Boyle and Keigwin, 1985; Boyle et al., 1995; Ahmad et al., 2008; Lear et al., 2010; Katz et al., 2010). Among the various existing proxies, Mg/Ca in benthic foraminifera has been used for a long time to reconstruct bottom water temperature changes (e.g., Rosenthal et al., 1997; Lear et al., 2002; Martin et al., 2002; Marchitto et al., 2007; Barrientos et al., 2018). The reconstruction of bottom water temperature based on the benthic foraminiferal Mg/Ca, is calculated by comparing core-top samples with bottom water temperatures (Figure 2.6). However, there is also another possible influence on benthic Mg/Ca, and these previous studies especially indicate the influence of carbonate ion concentration on the Mg/Ca (e.g., Rosenthal et al., 2006; Bryan and Marchitto, 2008; Yu and Elderfield, 2008; Marchitto et al., 2018).

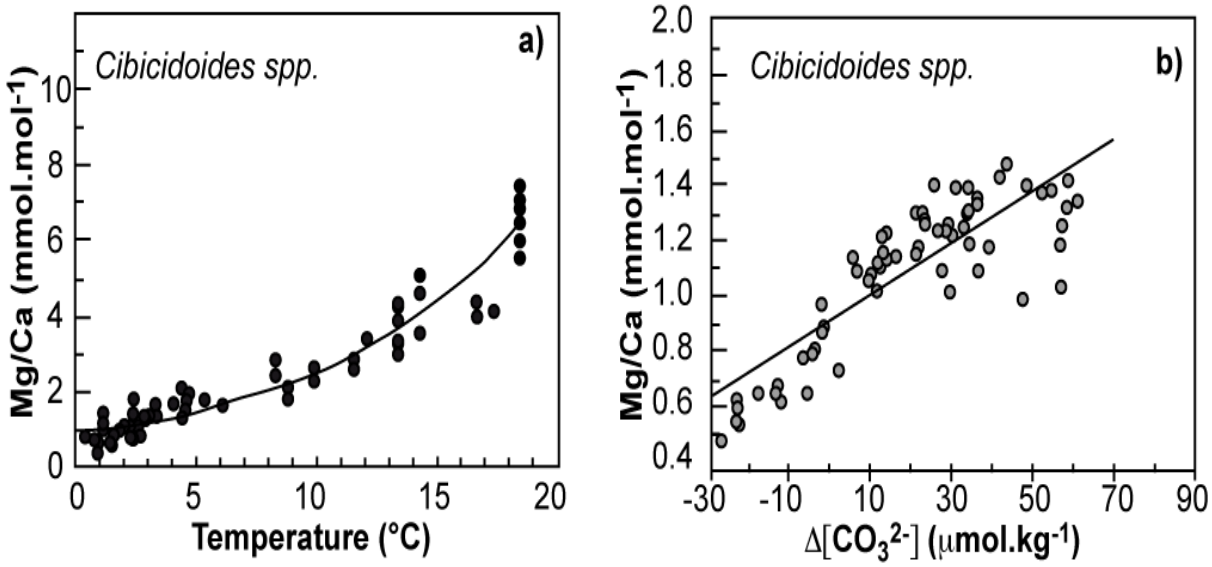

Figure 2.6*. Relationships between the Mg/Ca measured in Cibicidoides and a) bottom water temperature (adapted from Lear et al., 2002) and b) seawater [CO_3^{2-}] (adapted from Yu and Elderfield, 2008).*

Other elemental/Ca ratios have been explored to reconstruct past bottom temperatures, such as benthic foraminifera (*H. elegans*, *Uvigerina peregrina*, *Planulina ariminensis*, and *Planulina foveolata*) Li/Ca and Sr/Ca ratios (Rosenthal et al., 2006; Bryan and Marchitto, 2008; Marchitto et al., 2018). But for other species, previous works suggest that benthic Li/Ca and Sr/Ca in *H. elegans* for instance could be used as paleo-proxies for both carbonate ion concentration and temperature

(Rosenthal et al., 2006; Hall and Chan, 2004; Marchitto et al., 2018; Doss et al., 2018). Other works have tested empirical calibration exercises and have shown that the B/Ca ratio is directly linked to bottom water carbonate ion concentration (e.g., Yu and Elderfield, 2007; Brown et al., 2011; Yu et al., 2010), but emerging proxies are also explored such as U/Ca, Li/Ca and Sr/Ca (e.g., Rosenthal et al., 2006; Raitzsch et al., 2011; Yu et al., 2014b). Indeed, previous works conducted on deep-sea benthic species seem to show that benthic foraminiferal U/Ca, Li/Ca, Sr/Ca are promising marine dissolved carbon/carbonate system proxies (Hall and Chan, 2004; Bryan and Marchitto, 2008; Raitzsch et al., 2011; Keul et al., 2013; Yu et al., 2014a), impacting our ability to fully reconstruct intermediate and deep-water circulation and C content associated to global carbon cycle (Came et al., 2003; Yu et al., 2008; Makou et al., 2010; Poggemann et al., 2017). However, most of these studies were devoted to calcitic foraminifera, and only a few works have focused on the benthic foraminifera *H. elegans*. Indeed, this aragonitic specie is not widely found in the sediment due to its higher sensitivity to dissolution compared to calcitic foraminifera (Rosenthal et al., 2006; Hall and Chan, 2004; Marchitto et al., 2018).

Despite bottom water temperature and seawater [CO_3^{2-}], other deep-water properties can be reconstructed from element/Ca ratios. For instance, the benthic foraminifera Cd/Ca can be a robust proxy to reconstruct the paleo-nutrient, as the labile nutrient (phosphate and nitrate) shows a positive correlation with the seawater Cd (Boyle et al., 1976; Boyle, 1988; Elderfield and Rickaby, 2000; Figure 2.7; equation 1).

$$Cd = 1.2/\left(\alpha_{Cd/P}(3.3/P - 1)\right) + 1 \qquad \text{(Eq. 1)}$$

In the modern sediments, Cd/Ca ratios measured in the tests of benthic foraminifera are strongly correlated with seawater dissolved Cd concentrations, and the distribution of seawater Cd is highly correlated with the nutrient PO_4^{3-}. Benthic foraminifera Ba/Ca have also been explored to reconstruct paleo-nutrient (e.g., Lea and Boyle, 1989, 1990; Hall and Chen, 2004; Martin and Lea, 1998), because the dissolved barium exhibits a positive correlation with the ocean alkalinity and silica (refractory nutrients), which both seems to mainly regenerate at deep depth (Chan et al., 1977; Lea and Boyle, 1989; Hall and Chan, 2004).

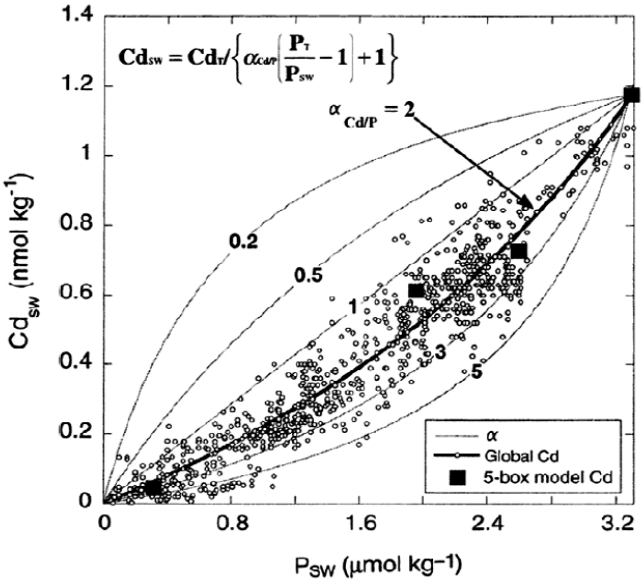

Figure 2.7. *Dissolved Cd versus dissolved phosphate in the global ocean, figures from Elderfield and Rickaby (2000). Curves show different solutions to the inset equation (equation (1) with Cd_T = 1.2 and P_T = 3.3) that can explain regional relationships between the two nutrients. Bold line is the best fit to the global data set, with $\alpha_{Cd/P}$=2.*

2.3. Analytical Methods

2.3.1. The preservation state of foraminifera

The benthic foraminiferal trace elemental (e.g., Cd/Ca, Ba/Ca, Sr/Ca…) and stable isotop values may could be influenced by the calcite dissolution, which may be induced by highly carbonate corrosive bottom water and/or the seasonal high productivity, thus, they could not correctly reflect bottom water values under the dissolution contidions (e.g., McCorkle et al., 1995; Zarriess and Mackensen, 2011). Then, for our study, well-preserved benthic foraminifera samples were handpicked and carefully checked under a binocular microscope to ensure that the samples have no dissolusion.

2.3.2. Benthic foraminiferal $\delta^{18}O$ and $\delta^{13}C$ analyses

Picking of the foraminiferal samples was performed on the washed, dry samples by a series of sieves in order to separate special size fractions. The size fraction (250-315 µm) was then sprinkled into a tray, and species identification and picking were done using the binocular lens. Stable oxygen ($\delta^{18}O$) and carbon ($\delta^{13}C$) isotope measurements were performed on well-preserved (clean, intact and without dissolution) samples.

On core MD77-176 located in the northeastern BoB, measurements of $\delta^{18}O$ and $\delta^{13}C$ were performed on 191 samples of benthic foraminiferal species. The $\delta^{18}O$ and $\delta^{13}C$ records covering the period over the last 14 cal kyr BP had been previously analysed on benthic foraminifera *Cibicidoides wuellerstorfi* at the Laboratoire des Sciences du Climat et de l'Environnement (LSCE, France). These analyses were carried out on a Finnigan MAT 251 mass spectrometer, and the mean external reproducibility of carbonate standards is ±0.05‰ for $\delta^{18}O$ and ±0.03‰ for $\delta^{13}C$. In order to obtain a higher resolution of the $\delta^{18}O$ and $\delta^{13}C$ records spanning the last 40 cal kyr BP, benthic foraminifera *C. wuellerstorfi*, *C. pachyderma,* and *U. peregrina* were also analyzed at the State Key Laboratory of Marine Geology of Tongji University (Shanghai, People's Republic of China). Approximately 4-8 clean and well-preserved specimens (>250 μm) were selected per sample. Stable isotope analyses were performed using a Finnigan MAT 253 mass spectrometer, with a mean external reproducibility better than ±0.07‰ for $\delta^{18}O$ and ±0.04‰ for $\delta^{13}C$. In addition, $\delta^{18}O$ and $\delta^{13}C$ values were calibrated versus PDB by using National Bureau of Standards (NBS) standards.

The stable isotopes records for cores MD77-191 (Arabian Sea) were also performed on 83 of planktonic foraminifera *Globigerinoides rub*er from the 250-315 μm size fractions, respectively. 167 samples of benthic species *C. pachyderma*, *C. wuellerstorfi*, and *U. peregrina* from >250 μm were selected for the $\delta^{18}O$ and $\delta^{13}C$ analyses for MD77-191. These stable isotopes analyses have been performed on approximately 4 to 8 clean and well-preserved specimens on a Finnigan MAT 251 mass spectrometer hosted at the Laboratoire des Sciences du Climat et de l'Environnement (LSCE, France). The mean external reproducibility of carbonate standards is ±0.05‰ for $\delta^{18}O$ and ±0.03‰ for $\delta^{13}C$. Both $\delta^{18}O$ and $\delta^{13}C$ values are presented relative to the Pee Dee Belemnite (PDB) scale by comparison with the National Bureau of Standards (NBS).

In addition, the benthic stable isotopes ($\delta^{18}O$ and $\delta^{13}C$) were only analysed on 70 samples of benthic foraminiferal *C. wuellerstorfi* from core SHI9001 to build the age model. These measurements were performed at the State Key Laboratory of Marine Geology of Tongji University (Shanghai, People's Republic of China). Around 2 to 4 clean and well-preserved samples (>250 μm) were selected. Stable isotope analyses were performed using a Finnigan MAT 253 mass spectrometer, with a mean external reproducibility better than ±0.07‰ for $\delta^{18}O$ and ±0.04‰ for $\delta^{13}C$.

2.3.3. Radiocarbon dating of foraminifera

Benthic radiocarbon analyses were performed on epifaunal species *Cibicidoides* spp. and *Hoeglundina elegans* (size >150μm) of core MD77-176 (BoB). Approximately 400 to 1000 μg of benthic foraminiferal shells were picked. They were leached with HNO_3 (10^{-2} M), rinsed with Milli-

Q^{TM} water, converted to CO_2 by reacting with anhydrous phosphoric acid (Tisnérat-Laborde et al., 2001) and collected in small glass tubes (Wacker et al., 2013). Samples were analyzed with the ECHoMICADAS at the LSCE, France. Measurements were taken using the gas handling system and cracker system (Wacker et al., 2013). Radiocarbon results are reported as conventional ^{14}C ages in yr BP and the benthic-planktonic ^{14}C age offsets.

In addition, for core MD77-191, three ^{14}C dates obtained on planktonic foraminifera *Globigerinoides ruber* measured with the ECHoMICADAS at the LSCE, France. Combined with 9 monospecific planktonic foraminifer *G. bulloides* accelerator mass spectrometry (AMS) ^{14}C dating and one ^{14}C date made on pteropods (Mléneck et al., 1997), we could establish the age model of MD77-191.

2.3.4. Benthic foraminiferal assemblage analyses

Benthic foraminifera are an important component of faunal communities in many benthic environments, and distribute from intertidal to greater depths. Due to high densities of the benthic foraminifera, small sediment volumes provide large numbers of specimens, making them very useful for the paleo-ecological reconstructions. Based on previous studies, the benthic foraminiferal assemblages display strong relationships to the quantity and nutritive quality of the organic detritus reaching the ocean floor, and to the oxygenation of the interstitial waters (e.g., Jorissen et al., 1998, 2007; Gooday, 2003).

For each sample in this study, benthic foraminifera (>150 μm) were extracted, counted and identified to species level following the taxonomical descriptions of various authors (e.g., Jones, 1994; Holbourn et al., 2013; Loeblich and Tappan, 1988). Around 102, and 75 samples from MD77-176 and MD77-191 were selected, respectively. As bulk samples of core MD77-176 and MD77-191 were not weighed, we could not calculate absolute abundance of foraminifera or accumulation rates. All specimens were counted, and individual census counts were expressed as the percentage of total benthic foraminifera present in each sample.

To describe major faunal variations, we performed principal component analysis (PCA) using PAST software (Version 3.0, Hammer et al., 2001). Species with a percentage presence of >1% in at least 1 sample were used for statistical analysis and diversity calculation.

2.3.5. Benthic foraminiferal elemental ratios

2.3.5.1. Pre-experiments for the HR-ICP-MS

Trace and minor elemental compositions of foraminiferal tests are widely used to reconstruct paleoceanography conditions. Mg/Ca (0.5-5 mmol/mol), Sr/Ca (1-2.5 mmol/mol), Fe/Ca (<1 mmol/mol), Al/Ca (<1 mmol/mol) and Mn/Ca (<100 µmol/mol) are present in foraminifera $CaCO_3$ at relatively high concentrations, it could be measured by ICP atomic emission spectrometry (AES) or ICP optical emission spectrometry (OES) techniques (e.g., Schrag, 1999; Green et al., 2003). Cd/Ca (0.004-0.2 µmol/mol), Ba/Ca (1-120 µmol/mol), Li/Ca (10-24 µmol/mol), and U/Ca (3-22 nmol/mol), are trace elements, thus their concentrations are below the detection limits of these techniques. However, a single collector sector field high resolution inductively coupled plasma mass spectrometer (HR-ICP-MS) Thermo Element XR provides higher sensitivity than AES and OES, allowing the measurement of many trace and minor elements with small samples. Methods presented here allow the simultaneous determination of Mg/Ca, Sr/Ca, Fe/Ca, Mn/Ca, Al/Ca, Cd/Ca, Ba/Ca, Li/Ca and U/Ca by HR-ICP-MS (Figure 2.8). In order to develop the best measurement method, we did pre-test by using modern samples of benthic foraminiferal *Ammonia tepida* from the Bay of Biscay. Therefore, we will present these pre-experiment in detail below.

Figure 2.8. *Photos showing the instrument of HR-ICP-MS*

Firstly, we prepared two series of mother standard solutions for the elemental ratios analyses. First six standard solutions are Mn, Al and Fe mixtures with linear Ca concentration (0.5-7 ppm) to get more precise Ca concentration dilutions for the second run, and could also avoid quite long time for the all element ratios measurement in one time. Then, seven multi-element stock standard

solutions (J0-J6) were prepared gravimetrically by spiking a 1000 µg/ml Ca standard with appropriate amounts of Mg, Sr, Cd, Li, B, Ba and U mono-elemental 1000 µg/ml certified ICP-MS grade stock solutions (Table 2.2). The ratios of stock solutions were spaced linearly to contain the natural ratio ranges expected in both planktonic and benthic foraminifera. Working mother standards were made by diluting the stock standard solutions with 0.1N HNO_3 to get calcium concentrations of ~1 ppm and 50 ppm separately, as we performed analyses in two time (the first run is diluted in ~1 ppm Ca to get real calcium concentration of the sample; the second run is diluted in ~50 ppm to measure the elemental ratios at the same calcium concentration). In addition, we did the pre-analysis of the standard solutions and the coefficients (r^2) of standard curves used to calculate elemental/Ca ratios are >0.9999 for all elemental ratios (Figure 2.9).

Table 2.2. *Elements concentrations of two series of mother standard solutions*

Label	[Ca]	[Fe]	[Mn]	[Al]
	ppm	ppm	ppm	ppm
Solution 1	0.51	3.7×10^{-4}	5×10^{-5}	5.1×10^{-5}
Solution 2	0.97	9.4×10^{-4}	1.4×10^{-4}	1.4×10^{-4}
Solution 3	3.05	4.1×10^{-3}	2×10^{-4}	6.1×10^{-4}
Solution 4	4.06	7×10^{-3}	2.9×10^{-4}	1.2×10^{-3}
Solution 5	5.07	0.01	5×10^{-4}	1.7×10^{-3}
Solution 6	7.05	0.02	9.8×10^{-4}	2.5×10^{-3}

Label	[Ca]	[Mg]	[Sr]	[B]	[Li]	[Cd]	[Ba]	[U]
	ppm	ppm	ppm	ppb	ppb	ppb	ppb	ppb
J0	51.51	0.004	0.005	0.008	0.056	0.005	1.01	0.005
J1	51.9	0.02	0.06	0.28	0.10	0.012	1.10	0.094
J2	51.66	0.05	0.096	0.7	0.15	0.015	1.19	0.19
J3	49.62	0.08	0.11	0.94	0.18	0.019	1.23	0.30
J4	52.10	0.12	0.18	1.42	0.24	0.027	1.47	0.47
J5	50.54	0.16	0.23	2.06	0.31	0.033	1.6	0.61
J6	51.38	0.24	0.28	2.76	0.5	0.04	1.89	0.79

The instrument used during this work has been set up in November 2015, and the first tests have begun in May 2016. However, as this instrument is shared with different colleagues with other kinds of analysis, it was not possible to work on long time periods to set up the method, but rather like one or two weeks every 8 weeks. Thus, the development of the method occurred from May 2016, July 2016, March-April 2017, June 2017 and the first sample measurements were made on July 2017, when we were sure that the instrumental settings as well as the measurement method

were optimized.

The first point to test was the introduction of the sample. Indeed, the HR-ICP-MS has 2 injection systems that can be used, the FAST and the direct (with a normal or a micro-nebulizer) injection. For the FAST analysis system, the required volume of sample is 4ml. As the trace elements in the foraminifera are at levels of about µmol/mol to nmol/mol, this system would require tens of specimens to get the sufficient sensitivity to be measured on the ICP-MS-HR. Thus, we decided to use the direct injection. Moreover, the minimum volume with the micro- system is 500 µl.

The target elements to measure were from the ppm (Ca) (Mg, Sr, Al, Fe and Mn) to the ppt (Cd, U, Li and Ba), so we decided to measure them in two different series. First, the minor elements are measured at Ca concentration of around 1ppm, calculated from the weight of the shells. Then, knowing the real Ca concentration, we can thus adjust all concentrations of Ca first to minimize the matrix effect (de Villiers et al., 2002) and secondly to measure the trace elements.

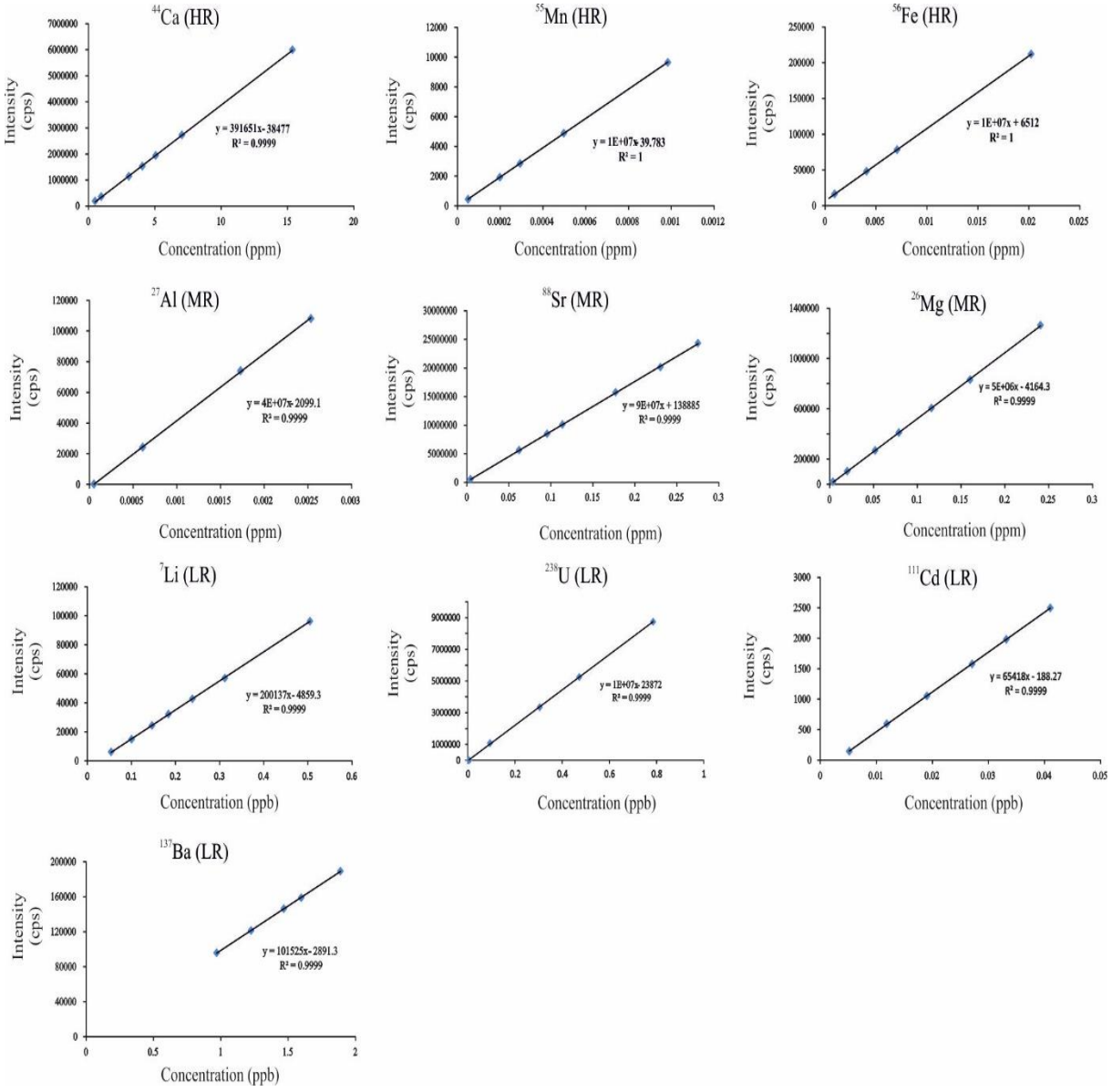

Figure 2.9. *The correlation ships of standard solution for each element*

The sequence of analysis was constructed as illustrated in Table 2.3. Based on the previous studies, when measuring high-calcium samples such as foraminifera (100 ppm), data quality could be affected by decreasing sensitivity caused by Ca deposition on sampling cones (Yu et al., 2005). Yu et al. (2005) suggest that it is possible to perform the drift correction standards by every 3 samples to check the instrument performance and achieve optimal correction quality in case of sudden changes in drift. As the drift correction monitored every 3 samples strongly extends the time of analysis, and as the maximum Ca concentration of our measurements is around 50 ppm, thus, we decided to perform every 4 samples to correct the drift.

Table 2.3. An example of analysis sequence

No.	Analysis sequence
1	Blank-1
2	Check-std4
3	STD-0
4	STD-1
5	STD-2
6	STD-3
7	Check-std4
8	STD-4
9	STD-5
10	STD-6
11	Check-std4
12	Blank-2
13	Sample 1
14	Sample 2
15	Sample 3
16	Check-std4
17	Sample 4
18	Sample 5
19	Sample 6
20	Sample 7
21	Check-std4

For the instrument settings, a multitude of spectral interferences may combine with analyzed

isotope peaks in low resolution, and these interferences could be constrained by moving to medium or high resolution. We checked the most recurrent interferences and their occurrence for each element to be measured to choose the resolution from the Thermo software. We tested the sensitivity and the accuracy of the different resolution especially for the following elements:

-Fe: medium/high resolution: the reproducibility vary from 3-7% to <2%, respectively;

-Mn: medium/high resolution: the reproducibility decreases from 2-4% to <2.8%, respectively;

-Ca: medium/high resolution: the reproducibility decreases from 2-2.5% to <2%, respectively;

-Sr: low/medium resolution: for the 2 isotopes tested (see below), the reproducibility is quite similar between the different resolutions (<2%) but slightly better at medium resolution.

We also tested different isotopes for some elements, to select the best analytical method:

- ^{24}Mg and ^{26}Mg;
- ^{86}Sr and ^{88}Sr;
- ^{44}Ca and ^{48}Ca.

This methodology for Ca was chosen because for the first series of analysis, the Ca concentration is low enough to allow for the measurement of ^{44}Ca, but in order to get a higher concentration to measure trace elements, the concentration of Ca is to high to be measured by ICP-MS-HR except if choosing a very low abundant isotope, such as the ^{48}Ca. Measuring both isotopes during the first series allow to check for the same results obtained on both isotopes, whereas ^{48}Ca is the only isotope that can be measured during the second series at the same time than trace elements thanks to its low abundance. For Mg and Sr, the results are quite similar for both isotopes of the same element, but we decided to keep both isotopes for each of them to ensure that if a problem occurs on one isotope we could use the other one.

For trace elements, the loss of sensitivity by changing the resolution was too important to work at another template than low resolution. Moreover, there is no frequent interference with these isotopes, so we decided to stay in low resolution.

Finally, we selected the following template:

- ^{7}Li, ^{11}B, ^{111}Cd, ^{137}Ba, ^{238}U in low resolution;
- ^{24}Mg, ^{26}Mg, ^{27}Al, ^{86}Sr, ^{88}Sr in medium resolution;
- ^{44}Ca, ^{48}Ca, ^{55}Mn, ^{56}Fe in high resolution.

Then, to ensure for the cleanness of the analysis, blanks were measured using the same acid as used for sample dissolution and dilution. In order to minimize the memory effect, we tested different rinse times with the blank values to have a sufficient cleaning and a reasonable time of analysis, and a value of 40s was chosen. To avoid cross-contamination, the rinse acid was made of 50ml 0.1N HNO_3 in 50µl HF.

In order to find the minimum weight of samples needed, we did the pre-test of trace elements

analysis in 10 ppm, 30 ppm, 50 ppm and 90 ppm (the maximum concentration) for the micro-system. We found that the measurements performed on the trace elemental RSD% were decrease with the increased calcium concentration. And for 50 ppm and 90 ppm Ca all have a very low RSD% <3%. With the consideration of the instrument sensitivity, 90 ppm Ca is the maximum concentration to be measured, thus we choose to analysis the trace element in 50 ppm calcium (Table 2.4).

Table 2.4. Comparision of RSD % in different Ca concentration

Ca con.	RSD (%)						
	Mg	Sr	Li	U	Cd	Ba	Ca
10 ppm	1.06	2.24	1.39	3.7	9.43	1.51	4.61
30 ppm	1.01	2.04	0.97	1.67	11.5	1.52	2.61
50 ppm	0.53	0.88	0.75	1.44	3.65	0.64	1.99
90 ppm	0.65	0.67	0.78	1.35	3.37	0.88	1.59

2.3.5.2. Cleaning procedures for benthic foraminifera

Approximately 8-15 well-preserved (clean, intact and without dissolution) benthic foraminifera samples were handpicked by the binocular microscope. The foraminiferal tests were gently crushed between two glass plates to open all the chambers. Then the fragments were cleaned to remove clay. The steps consist of cleaning by Milli-Q^{TM} water for around four times until the overlying water became clean and then methanol for further clay removal in two times. In every time, the fragments with liquid should be sonicated in an ultrasonic bath for 1 minute and pipetted most of overlying liquid carefully without risk of sample loss.

The clay-free samples were treated for oxidative and reductive cleaning to remove the organic matter and elemental oxides. The benthic foraminifera cleaning procedure followed published methods (Boyle and Keigwin, 1985; Barker et al., 2003). For the reductive cleaning step, each sample was injected by 100 µl reductive solutions, heated in the water for 30 minutes, and performed an ultrasonic cleaning for 10s every 5-10 minutes (Table 2.5). In addition, the procedure of oxidative cleaning consist of adding 250 µl oxidative solutions, heating in water bath for 10 minutes and also performing on ultrasonic bath for 10s every 2.5 minutes (Table 2). Thereafter, the samples were transferred to a new 500 µl Teflon tuber, cleaned with weak acid 0.001N HNO_3 for one time and Milli-Q^{TM} water for 2 times with an ultrasonic bath. Then, samples were dissolved in 0.075N HNO_3 and diluted with 0.1N HNO_3 for the analysis.

Table 2.5. *Chemical composition of oxidative and reductive cleaning solutions (Boyle and Keigwin, 1985; Barker et al., 2003)*

Cleaning solutions	compositions
Oxidative	15ml 0.1N NaOH + 50 µl 30 % H_2O_2
Reductive	250 µl 31M hydrous hydrazine +2 ml 16M $NH_4.NH_2.H_2O$ +2ml 0.25M citric acid

2.3.5.3. Analytical protocols of elemental ratios

We analyzed multiply elemental ratios (Mg/Ca, Sr/Ca, U/Ca, Cd/Ca, Ba/Ca, Li/Ca, Fe/Ca, Mn/Ca, and Al/Ca) in benthic foraminifera obtained from cores MD77-191 (Arabian Sea), MD77-176 (Bay of Bengal) and SHI9001 (Eastern Equatorial Indian Ocean). For core MD77-191, we performed measurements on three calcite (*C. pachyderma*, *Globobulimina* spp., and *U. peregrina*) and one aragonite (*H. elegans*) benthic foraminiferal species. For cores MD77-176 and SHI 9001, due to the limitation of the benthic foraminifers' quantities, we only measured the elemental ratios in shells of *H. elegans* and *U. peregrina*. Each sample contained approximately 8-15 individual foraminifera larger than 250µm.

Instrumental settings for trace element analyses are listed in Table 2.6. The instrument sensitivity was optimized daily using 100 ppt Tune standard solutions. Given the limited foraminiferal sample size, we used a high efficiency PFA MicroFlow Nebulizer (ES-2000-3503-080), producing an uptake rate of 50 µl/min. One measurement of eight element ratios over 8 min requires 1ml solution at a calcium concentration of 50 ppm.

Sample and standard solutions were then systematically adjusted at 50 ppm Ca through dilution using 0.1N HNO_3. A blank consisting of the same 0.1N HNO_3 used to dilute the standards and samples is also analyzed. On HR-ICP-MS, the elemental blanks are better than 4.5% for Al/Ca, 0.05% for Mn/Ca, 0.8% for Fe/Ca, 6.5% for Li/Ca, 0.05% for U/Ca, 0.03% for Mg/Ca, 0.01% for Sr/Ca, 6.5% for Cd and 1.8% for Ba/Ca. All raw intensities (including standards) are minus blank intensities, raw data are calculated by correcting the drift by using two-point linear standard curves interspersed between every four samples with a same standard. Standard curves are used to calculate elemental/Ca ratios, coefficients of determination (r^2) are always >0.9999 for all elemental ratios (Figure 2.8).

Table 2.6. *ICP-MS settings for elemental ratios determinations.*

Parameter	Trace element mode
Plasma RF power	1200
Nebulizer	ES-2000-3503-080
Spray chamber	Twister Spray Chamber with Helix
Injector	2.0 mm QUARTZ INJECTOR
Sample cone	Ni
Skimmer cone	Ni "H" high performance
Sample matrix	0.1N HNO_3
Uptake time	50s
Analysis time	490s
Washout time	40s
Mass resolution	Low (Li, B, Cd, Ba, U), Medium (Mg, Al, Sr) and High (Ca, Mn, Fe)
Runs	10
Passes	6
Detection mode	Tripple (analog, counting, faraday)

Chapter 3: Changes in intermediate circulation in the Bay of Bengal since the Last Glacial Maximum as inferred from benthic foraminifera assemblages and geochemical proxies

.

The Bay of Bengal (BoB) is a key area to study past intermediate water circulation on the Indian Ocean. Indeed, the BoB is landlocked to the north by Asia, and this land - sea configuration implies that much of the intermediate and deep waters of the northern Indian Ocean originate from the south, with only small contributions of intermediate waters from the Red Sea and of Pacific water through the Indonesian sea (Talley et al., 2011). Thus, studying intermediate waters in the northeastern Indian Ocean will allow us to better constrain past changes in of the hydrology of intermediate and deep-water masses from the Southern Ocean. It will help us to understand their potential role in global climate changes (Kallel et al., 1988; Jung et al., 2009; Yu et al., 2018).

In this chapter, I present high resolution records of benthic foraminiferal assemblages, $\delta^{13}C$, $\delta^{18}O$, and ^{14}C since the Last Glacial Maximum (LGM) at intermediate water depths in the BoB from core MD77-176 (14°30'5N-93°07'6E, 1375 m water depth). This multi-proxy approach combining micro-paleontological (benthic assemblages) and geochemical ($\delta^{13}C$, $\delta^{18}O$, and ^{14}C) proxies allowed to reconstruct past hydrological changes of the Intermediate waters, and to interpret the observed changes in terms of variations in the water mass sources and changes in the ventilation rate since the last 40 kyr. Then, combining results with previous foraminifera ε_{Nd} obtained on the same core and on several deeper cores of the BoB allowed to constrain the temporal evolution of the source, ventilation and structure of intermediate and deep-water masses of the northern Indian Ocean and the northward penetration of AAIW.

AGU100 ADVANCING EARTH AND SPACE SCIENCE

Geochemistry, Geophysics, Geosystems

RESEARCH ARTICLE
10.1029/2018GC008179

Key Points:
- We produced high-resolution records of benthic foraminiferal assemblages, ^{14}C ages, oxygen, and carbon stable isotopes since 40 kyr BP
- Hydrological changes of the intermediate water in Bay of Bengal since LGM, were influenced by SSW during the LGM and NADW during the Holocene
- During the last deglaciation, geochemical records indicate increased northward flow of AAIW and enhanced upwelling in the Southern Ocean

Supporting Information:
- Supporting Information S1
- Table S1
- Table S2
- Figure S1

Correspondence to:
R. Ma,
rui-fang.ma@u-psud.fr

Citation:
Ma, R., Sépulcre, S., Licari, L., Bassinot, F., Liu, Z., Tisnérat-Laborde, N., et al (2019). Changes in intermediate circulation in the Bay of Bengal since the Last Glacial Maximum as inferred from benthic foraminifera assemblages and geochemical proxies. *Geochemistry, Geophysics, Geosystems*, *20*. https://doi.org/10.1029/2018GC008179

Received 4 JAN 2019
Accepted 1 MAR 2019
Accepted article online 5 MAR 2019

Changes in Intermediate Circulation in the Bay of Bengal Since the Last Glacial Maximum as Inferred From Benthic Foraminifera Assemblages and Geochemical Proxies

Ruifang Ma[1], Sophie Sépulcre[1], Laetitia Licari[2], Franck Bassinot[3], Zhifei Liu[4], Nadine Tisnérat-Laborde[3], Nejib Kallel[5], Zhaojie Yu[6], and Christophe Colin[1]

[1]GEOPS, Université Paris-Sud, CNRS, Université Paris-Saclay, Orsay, France, [2]CEREGE, Aix-Marseille Université-Europole de l'Arbois-BP80, Aix-en-Provence, France, [3]LSCE/IPSL, CEA CNRS UVSQ, UMR 8212, Gif Sur Yvette, France, [4]State Key Laboratory of Marine Geology, Tongji University, Shanghai, China, [5]Laboratoire Georessources, Matériaux, Environnements et Changements Globaux, LR13ES23, Faculté des Sciences de Sfax, Université de Sfax, Sfax, Tunisia, [6]Key Laboratory of Marine Geology and Environment Institute of Oceanology, Chinese Academy of Sciences, Qingdao, China

Abstract Benthic foraminiferal assemblages and geochemical tracers ($\delta^{18}O$, $\delta^{13}C$ and ^{14}C) have been analyzed on benthic and planktonic foraminifera from core MD77-176, located in the northern Bay of Bengal, in order to reconstruct the evolution of intermediate circulation in the northern Indian Ocean since the last glaciation. Results indicate that during the Last Glacial Maximum (LGM), Southern Sourced Water masses were dominant at the core site. A high relative abundance of intermediate and deep infaunal species during the LGM reflects low oxygen concentration and/or mesotropic to eutrophic deep water conditions, associated with depleted benthic $\delta^{13}C$ values. During the Holocene, benthic foraminiferal assemblages indicate an oligotropic to mesotrophic environment with well-ventilated bottom water conditions compared with LGM. Higher values for benthic foraminifera $\delta^{13}C$ and B-P ^{14}C age offsets suggest an increased contribution of North Atlantic Deep Water to the northern Bay of Bengal during the Late Holocene compared to the LGM. Millennial-scale events punctuated the last deglaciation, with a shift in the $\delta^{13}C$ and the ε_{Nd} values coincident with low B-P ^{14}C age offsets, providing strong evidence for an increased contribution of Antarctic Intermediate Water at the studied site. This was associated with enhanced upwelling in the Southern Ocean, reflecting a strong sea-atmospheric CO_2 exchange through Southern Ocean ventilation during the last deglaciation.

1. Introduction

The thermohaline ocean circulation plays a key role in regulating climate changes at different time scales through heat redistribution and carbon cycling (e.g., Bryan et al., 2010; Rahmstorf, 1995; Stocker & Wright, 1996; Talley et al., 2011; Tomczak & Godfrey, 2003). It has recently been shown that a deep and vigorous overturning circulation may have persisted in the North Atlantic throughout most of the glacial period, only disrupted by episodes of sluggish circulation associated with the catastrophic iceberg discharge of the coldest Heinrich stadials (HS), the Dansgaard-Oeschger stadials, and the Younger Dryas cold event of the last termination (Böhm et al., 2015). These major perturbations in Atlantic circulation have been related to the reduced North Atlantic Deep Water (NADW) flow (e.g., Böhm et al., 2015; Mcmanus et al., 2004) and the advection of southern sourced waters (SSWs) filling a large part of the deep Atlantic ocean (e.g., Böhm et al., 2015; Lynch-Stieglitz et al., 2007; Roberts et al., 2010).

Past changes in intermediate circulation are less well-documented than those of deep water (e.g., Kallel et al., 1988; Mix & Fairbanks, 1985; Oppo & Fairbanks, 1987; Waelbroeck et al., 2006). Previous studies of the intermediate water circulation during the last glaciation have mainly focused on the Atlantic Ocean (e.g., Lynch-Stieglitz et al., 2007; Oppo & Fairbanks, 1987; Pahnke et al., 2008) and the Pacific Ocean (e.g., Bostock et al., 2010; Mix et al., 1991; Pahnke & Zahn, 2005). These studies suggest an increased northward penetration of Antarctic Intermediate Water (AAIW) into the Pacific and Atlantic Oceans during glacial periods, as well as at a millennial time scale during the Heinrich events and stadials (e.g., Cao et al., 2007; Dubois-Dauphin et al., 2016; Pahnke et al., 2008; Pahnke & Zahn, 2005). In contrast, several studies based

Geochemistry, Geophysics, Geosystems 10.1029/2018GC008179

on ε_{Nd} and Cd/Ca records (e.g., Came et al., 2008; Gu et al., 2017; Howe et al., 2016; Xie et al., 2012) suggest that no changes occurred or even that there was decreased northward penetration of AAIW during HS1 and the Younger Dryas. For the Southern Ocean, previous studies based on opal flux records (Anderson et al., 2009) and ^{14}C data (Skinner et al., 2010) have suggested an increase in the production and advection of AAIW during the LGM and the deglaciation, relative to the modern ocean, associated with more pronounced Southern Ocean upwelling. Thus, evidence for changes in the AAIW circulation through the last glacial period remains scarce and controversial, whereas changes in intermediate water masses need to be accurately constrained as they play a major role in regulating heat and salt distribution in the ocean and also affect the global climate through their influence on ventilation changes and atmosphere-ocean CO_2 exchange (e.g., Anderson et al., 2009; Skinner et al., 2010).

The Northern Indian Ocean is characterized by only weak vertical contrasts in physical properties of the water column due to a progressive vertical mixing of deep-water masses with intermediate ones. It plays an important role in global ocean circulation in terms of affecting the carbon storage capacity of the ocean and climate (e.g., Ahmad et al., 2008, 2012; Bryan et al., 2010; Raza et al., 2014; Talley et al., 2011). Compared to the Atlantic Ocean, only limited hydrographical observations have been carried out in the Indian Ocean due to its less distinguishable water mass characteristics, and little is known about the circulation below a depth of 1,000 m. Even though it has received increasing attention over recent decades (e.g., Bryan et al., 2010; Jung et al., 2009; Yu et al., 2018), the evolution through time of North Indian Intermediate and Deep Water (NIIW and NIDW, respectively) and the penetration of SSW into the North Indian Ocean, associated with changes of the large-scale thermohaline ocean circulation observed in the North Atlantic, are still poorly constrained for the period since the last glaciation and remain controversial (Naqvi et al., 1994; Ahmad et al., 2008, 2012; Bryan et al., 2010; Raza et al., 2014; Yu et al., 2018).

The Arabian Sea and the Bay of Bengal (BoB) are landlocked to the north by Asia. This land-sea configuration implies that much of the intermediate and deep waters of the northern Indian Ocean originate from the south, with only small contributions of intermediate waters from the Red Sea and of Pacific water to the Indonesian sea (Talley et al., 2011). Consequently, studying intermediate waters in the northeastern Indian Ocean will allow us to better constrain past changes in the production of intermediate and deep water and in circulation from the Southern Ocean; in addition, it will help us to understand their potential role in global climate changes (Jung et al., 2009; Kallel et al., 1988; Yu et al., 2018).

In this study, we have investigated benthic foraminiferal assemblages together with $\delta^{13}C$, $\delta^{18}O$, and ^{14}C of benthic foraminifera from core MD77-176, located in the BoB, in order to reconstruct hydrological changes in the intermediate waters at high temporal resolution over the last 40 cal kyr. Our results, combined with previous foraminifera ε_{Nd} obtained on the same core (Yu et al., 2018) and on several deeper cores in the BoB, allow us to constrain the temporal evolution of the source, ventilation and structure of intermediate and deep-water masses of the northern Indian Ocean and the northward penetration of AAIW.

2. Modern Hydrological Settings

Today, surface water above 100 m in the BoB results from a mix of Arabian Sea Surface Water and Bay of Bengal Water (Figure 1; Talley et al., 2011; Tomczak & Godfrey, 2003). Thermocline and intermediate-depth water masses are Indonesian Intermediate Water (IIW) and Red Sea Intermediate Water (RSIW). IIW originates from the Pacific Central Water and enters the BoB via the Indonesian through flow. IIW flows clockwise at thermocline levels in the BoB (You, 1998). RSIW is created by the outflow of water from the Red Sea and Persian Gulf into the Arabian Sea, where it can sink to depths of 400–1,400 m due to its high salinity (Talley et al., 2011). RSIW enters the BoB around the southern tip of India and also circulates in a clockwise direction (You, 1998). In the South Indian Ocean, Antarctic Intermediate Water (AAIW) is found at 1,000- to 1,500-m depth, just above Indian NADW (Tomczak & Godfrey, 2003). Today, the northward extension of AAIW in the Indian Ocean rarely reaches beyond 10°S (Lynch-Stieglitz et al., 1994).

The Indian Deep Water (IDW) lies between 1,500 and 3,800 m. It forms when the Circumpolar Deep Water admixes with NADW (Tomczak & Godfrey, 2003; You & Tomczak, 1993). At depths below 3,800 m, the Antarctic Bottom Water (AABW) only reaches the southern part of the BoB as most of the BoB is shallower than 4,000 m (Tomczak & Godfrey, 2003). However, AABW can also mix with the IDW and thus contributes

Geochemistry, Geophysics, Geosystems 10.1029/2018GC008179

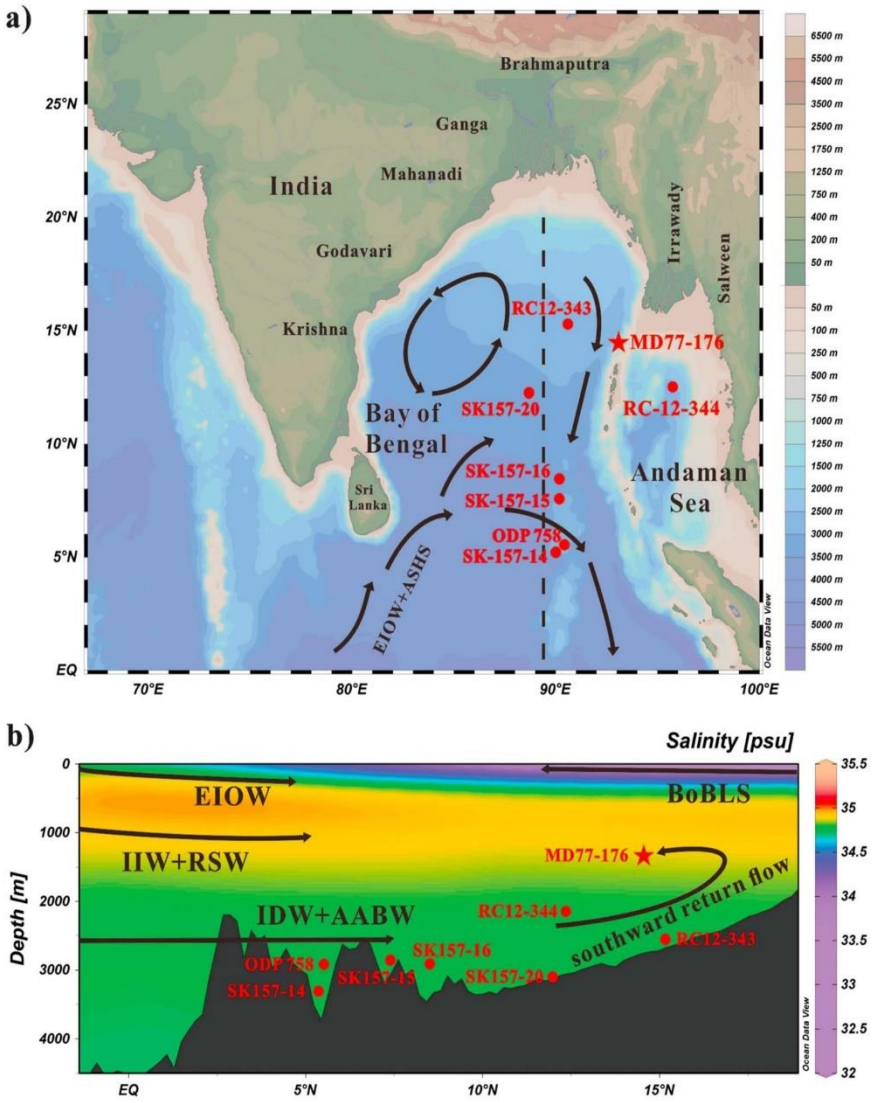

Figure 1. (a) Geographical setting and locations of reference sites (red circles) and MD77-176 (red star) in the Bay of Bengal. The black arrows show the general direction of surface circulation in the Bay of Bengal from June to September (Shankar et al., 2002). (b) Salinity (psu, colored shading) depth-latitude section using Ocean Data View (ODV) software (Schlitzer, 2015) and vertical distribution of water masses in the Bay of Bengal (N-S cross-section). EIOW = Eastern Indian Ocean Water; BoBLS = Bay of Bengal low salinity Water; IIW = Indonesian Intermediate Water; RSW = Red Sea Intermediate Water; AABW = Antarctic Bottom Water; IDW = Indian Deep Water.

significantly to the deep-water masses in the BoB. As the bottom water upwells when it moves northward, the deep waters can eventually return to shallower depths (Talley et al., 2011). Thus, changes in the bottom waters can also affect shallower-depth water masses in the northern BoB.

3. Material and Methods

3.1. Sediment Core and Age Model

Core MD77-176 was collected from 1,375-m water depth in the northeastern BoB (14°30′5N–93°07′6E; Figure 1). The sediment consists of intercalated olive gray terrigenous clay and silty clay layers with foraminifer- or nannofossil-bearing ooze. The age model of core MD77-176 was previously established by

Geochemistry, Geophysics, Geosystems 10.1029/2018GC008179

using 31 planktonic foraminifer (*Globigerinoides ruber*) AMS ^{14}C dates combined with the MD77-176 oxygen isotope record obtained on planktonic foraminifera *G. ruber*, which were correlated to the GISP2 Greenland ice core record (Marzin et al., 2013). Core MD77-176 displays high accumulation rates (average ~25 cm/kyr and up to 40 cm/kyr for the Holocene) and could provide high-resolution records for the period since 40 cal kyr BP.

3.2. Methods

Samples were available from previous studies (Kallel et al., 1988; Marzin et al., 2013) and were sieved in the 63- to 150- and >150-μm fractions. A total of 217 samples were collected for benthic foraminiferal analysis.

3.2.1. δ^{18}O and δ^{13}C Analyses

Measurements of δ^{18}O and δ^{13}C were performed on 191 samples of benthic foraminiferal species (supporting information Table S1). The δ^{18}O and δ^{13}C records covering the period since 14 cal kyr BP had previously been analyzed on benthic foraminifera *Cibicidoides wuellerstorfi* at the Laboratoire des Sciences du Climat et de l'Environnement (LSCE, France). These analyses were carried out on a Finnigan MAT 251 mass spectrometer, and the mean external reproducibility of carbonate standards is ±0.05‰ for δ^{18}O and ±0.03‰ for δ^{13}C. In order to obtain high-resolution δ^{18}O and δ^{13}C records spanning the last 40 cal kyr BP, benthic foraminifera *Cibicidoides wuellerstorfi*, *C. pachyderma*, and *Uvigerina peregrina* were also analyzed at the State Key Laboratory of Marine Geology of Tongji University (Shanghai, People's Republic of China). Approximately four to eight clean and well-preserved specimens (>250 μm) were selected per sample. Stable isotope analyses were performed using a Finnigan MAT 253 mass spectrometer, with a mean external reproducibility better than ±0.07‰ for δ^{18}O and ±0.04‰ for δ^{13}C. δ^{18}O and δ^{13}C values were calibrated versus Pee Dee Belemnite (PDB) by using National Bureau of Standards. The average time resolution of δ^{18}O and δ^{13}C obtained on benthic foraminifera is about 160 years for the Holocene and 1,100 years for the deglacial and the last glacial period.

3.2.2. Radiocarbon Dating of Benthic Foraminifera

Radiocarbon analyses were performed on epifaunal species *Cibicidoides* spp. and *Hoeglundina elegans* (size >150 μm). Approximately 400 to 1,000 μg of benthic foraminiferal shells were picked. They were leached with HNO_3 (10^{-2} M), rinsed with Milli-Q™ water, converted to CO_2 by reacting with anhydrous phosphoric acid (Tisnérat-Laborde et al., 2001) and collected in small glass tubes (Wacker et al., 2013). Fourteen samples were analyzed with the *ECHo*MICADAS at the LSCE, France. Measurements were taken using the gas handling system and cracker system (Wacker et al., 2013). Radiocarbon results are reported as conventional ^{14}C ages in yr BP and the benthic-planktonic ^{14}C age offsets.

3.2.3. Faunal Analysis

For each sample, benthic foraminifera (>150 μm) were extracted, counted, and identified to species level following the taxonomical descriptions of various authors (e.g., Holbourn et al., 2013; Jones, 1994; Loeblich & Tappan, 1988). As bulk samples of core MD77-176 were not weighed, we could not calculate absolute abundance of foraminifera or accumulation rates. All specimens were counted, and individual census counts were expressed as the percentage of total benthic foraminifera present in each sample.

To describe major faunal variations, we performed principal component analysis using PAST software (Version 3.0, Hammer et al., 2001). Species with a percentage presence of >1% in at least one sample were used for statistical analysis and diversity calculation.

4. Results

4.1. Stable Isotope Results

We combined stable isotope analyses performed on *C. pachyderma*, *C. wuellerstorfi*, and *U. peregrina* in order to produce the most complete record possible. Vital effects on δ^{18}O and δ^{13}C of selected species have been extensively documented in several previous studies. *U. peregrina* is known to record the calcite δ^{18}O at equilibrium (e.g., Shackleton, 1974), whereas *C. wuellerstorfi* exhibits a vital effect ranging from 0.64‰ to 0.82‰ (Ahmad et al., 2012; Duplessy et al., 1984; Mackensen et al., 1993; Naqvi et al., 1994; Raza et al., 2014). As *U. peregrina* is an endobenthic species, its δ^{13}C cannot be used to reconstruct changes in the bottom water δ^{13}C, whereas *C. wuellerstorfi* is known to record the δ^{13}C of bottom water (Duplessy et al., 1984; Zahn

Geochemistry, Geophysics, Geosystems 10.1029/2018GC008179

Table 1
Stable Isotope Data (Per Mil Versus PDB) From the Core MD77-176 of Cibicidoides pachyderma, Cibicidoides wuellerstorfi, and Uvigerina peregrina in the Same Levels to Assess the Vital Effect and Microhabitat Effect for $\delta^{18}O$ and $\delta^{13}C$, Respectively

	$\delta^{13}C$ (‰ versus PDB)		$\delta^{18}O$ (‰ versus PDB)	
Depth (cm)	*Cibicidoides pachyderma*	*Cibicidoides wuellerstorfi*	*Cibicidoides wuellerstorfi*	*Uvigerina peregrina*
30–33	0.30	0.42	1.80	2.61
35–38	0.07	0.39	1.91	2.88
40–43			1.88	2.69
45–48	0.12	0.42	1.97	2.97
50–53			2.00	2.72
55–58	0.09	0.42	2.00	2.94
65–68	0.26	0.47	2.09	
70	0.24	0.25	2.00	
80–83	0.20	0.44	2.09	
85–88	0.17	0.36	1.96	2.87
90	0.12	0.22	1.84	
170	0.33	0.28	1.89	
180	0.35	0.43	2.01	
185	0.25	0.24	1.72	
200	0.19	0.37	1.93	2.69
220	0.21	0.46	1.92	
230			1.94	2.78
280			2.01	2.84
300			2.02	2.85
585			3.23	3.75
930	−0.37	−0.29	2.88	3.74
940	−0.27	−0.36	2.87	3.87
970	−0.11	0.01	3.07	
980	−0.16	−0.09	3.12	3.66

et al., 1986) without any microhabitat effect (except in some particular areas, such as the Southern Ocean, Mackensen et al., 1993).

Most of the benthic $\delta^{13}C$ records were obtained from *C. wuellerstorfi*. In order to correct the $\delta^{13}C$ results from *C. pachyderma* to *C. wuellerstorfi*, we produced 18 pairs of measurements for certain levels where the two species coexisted (Table 1). Results indicate a slight difference in the stable isotopic composition (0.13‰ for $\delta^{13}C$). In addition, the results of 15 pairs of *C. wuellerstorfi* and *U. peregrina* measurements (Table 1) indicate a mean offset of about 0.82‰ in the $\delta^{18}O$ values. We corrected *C. wuellerstorfi* $\delta^{18}O$ values for this vital effect of 0.82‰ to establish a composite record combining results obtained on both species.

For core MD77-176, downcore benthic $\delta^{18}O$ values range between 2.48‰ and 4.23‰ (Figure 2). The most enriched $\delta^{18}O$ value (4.23‰) occurred in the last glacial maximum and the most depleted (2.48‰) in the late Holocene (3.5 cal kyr BP). In addition, during the later part of the deglaciation, the $\delta^{18}O$ showed a marked decrease at 11.5 kyr (2.51‰) followed by higher values during the early Holocene (mean value of 3.15‰ between 10.5 and 8 cal kyr BP), and then a decrease from 9.9 cal kyr BP to the core top (mean value of 2.83‰).

The $\delta^{13}C$ values range from −0.46‰ to 0.49‰ (Figure 2). Compared with the lower values (−0.13‰) for the LGM, a rapid increase in the $\delta^{13}C$ begins at 17 cal kyr BP, highlighting the end of the LGM. From 17 to about 10 cal kyr BP, the $\delta^{13}C$ record exhibits a succession of large oscillations with a first wide peak (0.1‰) occurring between 17 and 14 cal kyr BP, and a second shorter maximum (0.15‰) between 13 and 10.5 cal kyr BP. During the Holocene, the mean value of $\delta^{13}C$ was 0.19‰, which is higher than in the LGM (mean value of −0.14‰). However, significant decreases of about ~0.31 ‰ occurred at 3.8–3.1, 5.4–4.9, and 10.5–9 cal kyr BP.

4.2. Radiocarbon Dating of Benthic Foraminifera

^{14}C ages of one planktonic (*G. ruber*) and two benthic (*Cibicidoides* spp. and *H. elegans*) foraminiferal species from 11 different sample horizons of core MD 77-176 have been analyzed. Radiocarbon ages for Core MD 77-176 are given in Table 2. ^{14}C ages obtained on benthic *Cibicidoides* spp. and *H. elegans* from samples at 65-, 220-, and 400-cm depth give similar ages within the analytical error bar (1σ; Table 2). This suggests that correction of age is not useful for the mixed benthic sample (*Cibicidoides* spp. and *H. elegans*) analyzed at 558-cm depth. Downcore benthic ^{14}C ages range between 4.18 and 23.55 kyr.

The benthic-planktonic ^{14}C offset (B-P age) is the difference between coexisting benthic and planktonic foraminifera ^{14}C ages. In core MD 77-176, the B-P age offset drops from ~1290 to ~380 years between ~19.6 and 16.9 cal kyr BP (Table 2). The B-P age offset shows a higher value (770 years) around 14 cal kyr BP and then decreases to reach a minimum value of 200 years at 12.3 cal kyr BP. Then, in the upper part of the record, B-P age offset steadily increases to reach a maximum value of ~1210 years over the late Holocene (2.6 cal kyr BP).

4.3. Foraminiferal Assemblages

The diversity of benthic foraminiferal assemblages ranges from 18 to 41 species, with specimen abundance fluctuating between 82 and 648 individuals (supplementary Table S2). The hyaline benthic foraminifera are the dominant constituents (>80%), mainly composed of *Bulimina aculeata*, *H. elegans*, *C. wuellerstorfi*, and *U. peregrina* (in decreasing order of relative average abundance). The mean agglutinated benthic foraminifera relative abundance is only 1.2%, including *Textularia* sp., *Martinottiella communis*, and *Eggerella bradyi*, while the average percentage of porcelaneous forms is about 4.1%, characterized by *Pyrgo lucernula*, *Pyrgo murrhina*, *Pyrgoella osloensis*, *Quinqueloculina* spp., *Sigmoilopsis schlumbergeri*, and *Spiroloculina* spp.

Geochemistry, Geophysics, Geosystems 10.1029/2018GC008179

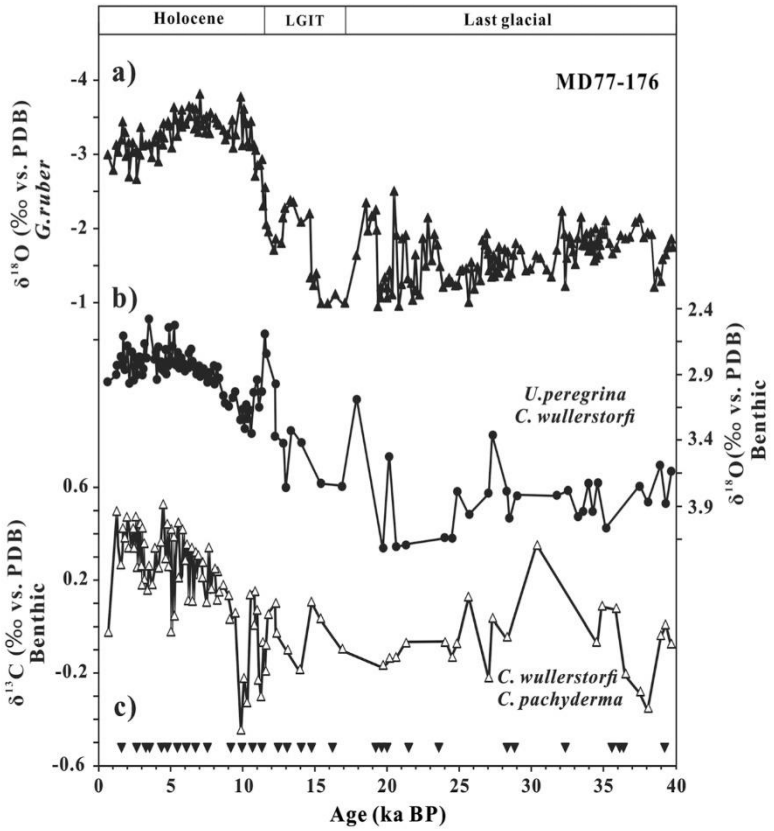

Figure 2. Stable isotopes of oxygen and carbon plotted against age in Core MD77-176. (a) $\delta^{18}O$ record of the planktonic foraminifera (*G. ruber*, Marzin et al., 2013), (b) benthic $\delta^{18}O$, and (c) $\delta^{13}C$ records for MD77-176. The black inverted triangles represent the ^{14}C calculated calendar age points (Marzin et al., 2013). LGIT = last glacial-interglacial transition.

We merged species that show ecological similarities, such as *Globobulimina affinis*, *Globobulimina pacifica*, *Praeglobobulimina spinescens*, and *Praeglobobulimina pupoides*, into *Globobulimina* spp. Species with a relative abundance of >1% in at least one sample were subjected to statistical analysis.

A total of 102 samples and 56 groups/species were selected for principal component analysis (supplementary Table S2). This analysis suggests that benthic foraminiferal faunas can be grouped into two main assemblages that represent about 37% of the total variance (Table 3 and Figure 3). *B. aculeata* and *H. elegans* dominate assemblage 1, which corresponds to the benthic foraminiferal fauna from the late deglaciation to the Holocene (between 14 and 0.7 kyr; Figure 3). The main associated species of assemblage 1 are *C. wuellerstorfi* and *Globocassidulina subglobsa*. In contrast, *C. robertsonianus* and *Bolivina robusta* dominate assemblage 2, which is more important during the LGM and the early deglaciation. Other quantitatively important contributors are *C. pachydermus*, *Pullenia bulloides*, and *Globobulimina* spp.

5. Discussion

Results obtained from core MD77-176 reveal (i) a clear glacial-interglacial variability, as already described in the area and at different water depths and (ii) millennial-scale events that punctuated the Last Termination and the Early Holocene. We will discuss the significance of these variations at the core site and also compare the results with records for other water depths in the studied area. Then, we will compare the MD77-176 records with other areas in the ocean, particularly in order to discuss the role of the Southern Ocean in the BoB hydrological variations at intermediate depths.

Geochemistry, Geophysics, Geosystems 10.1029/2018GC008179

Table 2
Calibrated AMS ^{14}C Age Determined on Planktonic (Data Taken From Marzin et al., 2013) and Benthic (This Study) Foraminifera Sampled in core MD77-176

Depth (cm)	Calendar age (yr B.P.)	1 sigma error (±yr)	Taxa	^{14}C age (year)	1 sigma error (±year)	B-P age offsets years	1 sigma error (±year)
65	2620	40	*G.ruber*	3060	60		
65			*Cibicidoides* spp.	4180	60	1120	120
65			*Hoeglundina elegans*	4270	55	1210	115
220	5520	100	*G.ruber*	5120	70		
220			*Cibicidoides* spp.	5870	60	750	130
220			*Hoeglundina elegans*	6110	70	990	140
305	7290	70	*G.ruber*	6960	80		
305			*Hoeglundina elegans*	7890	90	930	170
400	9985	180	*G.ruber*	9350	45		
400			*Cibicidoides* spp.	9730	100	380	145
400			*Hoeglundina elegans*	9700	90	350	135
445	11000	110	*G.ruber*	10950	90		
445			*Hoeglundina elegans*	11080	100	130	190
496	12280	120	*G.ruber*	11450	90		
496			*Hoeglundina elegans*	11650	90	200	180
535	14000	230	*G.ruber*	12910	110		
535			*Hoeglundina elegans*	13680	110	770	220
565	15405	180	*G.ruber*	14880	70		
565			*Hoeglundina elegans*	15260	80	380	150
585	16890	100	*G.ruber*	16420	70		
585			Mixed two benthic species	17250	280	830	350
617	19580	100	*G.ruber*	16660	120		
617			*Hoeglundina elegans*	17950	130	1290	250
740	27060	240	*G.ruber*	23420	140		
740			*Cibicidoides* spp.	23550	360	130	500

Note. ^{14}C ages were converted into calendar years (cal. yr BP, BP = AD 1950) BY USING THE AGE MODEL ESTABLISHED BY MARZIN ET AL. (2013). SPECIES USED FOR THE RADIOCARBON DATING ARE ALSO REPORTED.

Table 3
Species Composition of Benthic Foraminiferal Assemblages From Core MD77-176

Principal component number	Dominant species		Important associated species		Variance (%)
PC1					37
Negative loadings	*Bulimina aculeata*	−0.78	*Cibicidoides wuellerstorfi*	−0.05	
	Hoeglundina elegans	−0.45	*Globocassidulina subglobsa*	−0.14	
Positive loadings	*Cibicidoides robertsonianus*	0.24	*Cibicidoides pachyderma*	0.1	
	Bolivina robusta	0.12	*Pullenia bulloides*	0.1	
			Globobulimina spp.	0.04	
PC2					20
Negative loadings	*Globocassidulina subglobsa*	−0.86	*Cibicidoides wuellerstorfi*	−0.06	
	Cibicidoides pachyderma	−0.06	*Bulimina aculeata*	−0.02	
Positive loadings	*Hoeglundina elegans*	0.44	*Uvigerina peregrina*	0.12	
	Bolivina robusta	0.1	*Pullenia bulloides*	0.03	
	Sphaeroidina bulloides	0.09			

Geochemistry, Geophysics, Geosystems 10.1029/2018GC008179

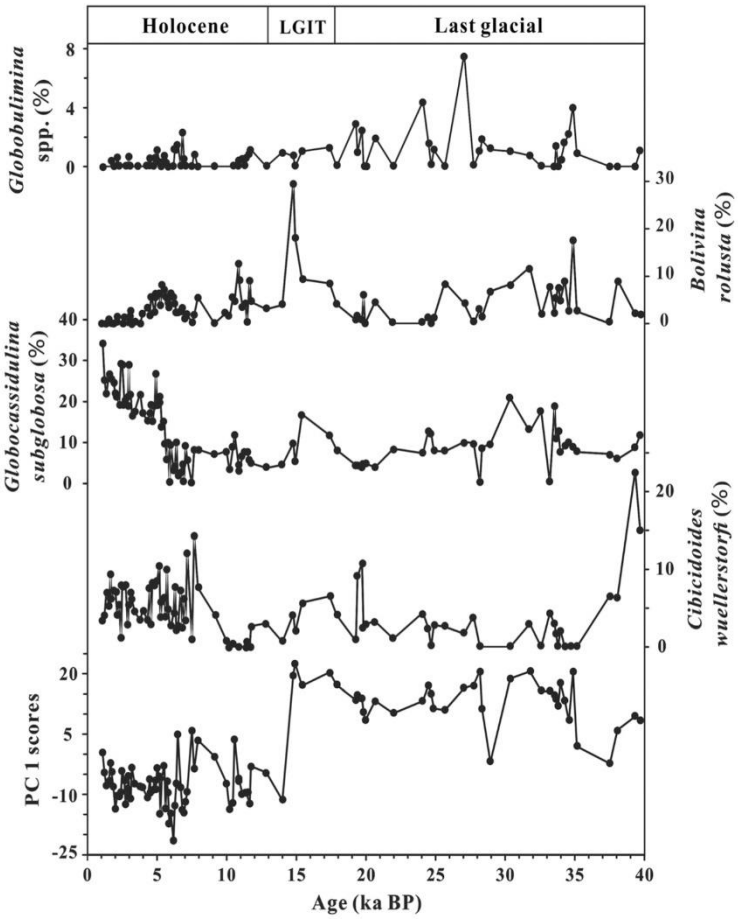

Figure 3. Downcore variations of PC 1 scores and the percentages of major species. LGIT = last glacial-interglacial transition.

5.1. Glacial and Interglacial Variations

Results from core MD77-176 indicate an average value for *Cibicidoides* $\delta^{13}C$ of −0.13‰ during the LGM, which is close to the $\delta^{13}C$ records collected at a deeper water depth, Sk157–14 (3,306 m, $\delta^{13}C$: −0.05‰), Sk157–15 (2,855 m, $\delta^{13}C$: −0.11‰), and Sk157–16 (2,920 m, $\delta^{13}C$: −0.12‰) in the southern BoB (Ahmad et al., 2008; Raza et al., 2014; Figure 1 for core locations) and core RC12344 (2,140 m, −0,12 ‰) in the Andaman Sea (Naqvi et al., 1994). Glacial to Holocene $\delta^{13}C$ shift is about 0.35‰, consistent with previous studies in the northern Indian Ocean (e.g., Curry et al., 1988; Duplessy et al., 1984; Naqvi et al., 1994) and an increased benthic $\delta^{13}C$ of 0.38 ± 0.08‰ from LGM to Holocene for 0.5–5 km in the global ocean corresponded to the changes in the terrestrial carbon reservoir (Peterson et al., 2014). This increase from the LGM to the Holocene reflects more invigorated circulation associated with better ventilated waters at intermediate depth in the Northern BoB during the Holocene (Duplessy et al., 1984; Waelbroeck et al., 2006).

During the LGM, the outflow from the Red Sea, Persian Gulf, and the ITF was greatly reduced, or ceased altogether, due to sea-level lowstand (Locke & Thunell, 1988; Naqvi et al., 1994; Siddall et al., 2003). Lower values of $\delta^{13}C$ during the LGM in the BoB have been interpreted as reflecting a reduction in the NADW flux into the southern BoB, and an increased contribution from the SSW (Ahmad et al., 2008, 2012; Raza et al., 2014). Such results are also consistent with the radiogenic ε_{Nd} values (from −6.5 to −8) observed on several cores collected at different water depths of the BoB which indicate a higher contribution of SSW before 18 cal kyr BP (Figure 4; Yu et al., 2018).

Geochemistry, Geophysics, Geosystems 10.1029/2018GC008179

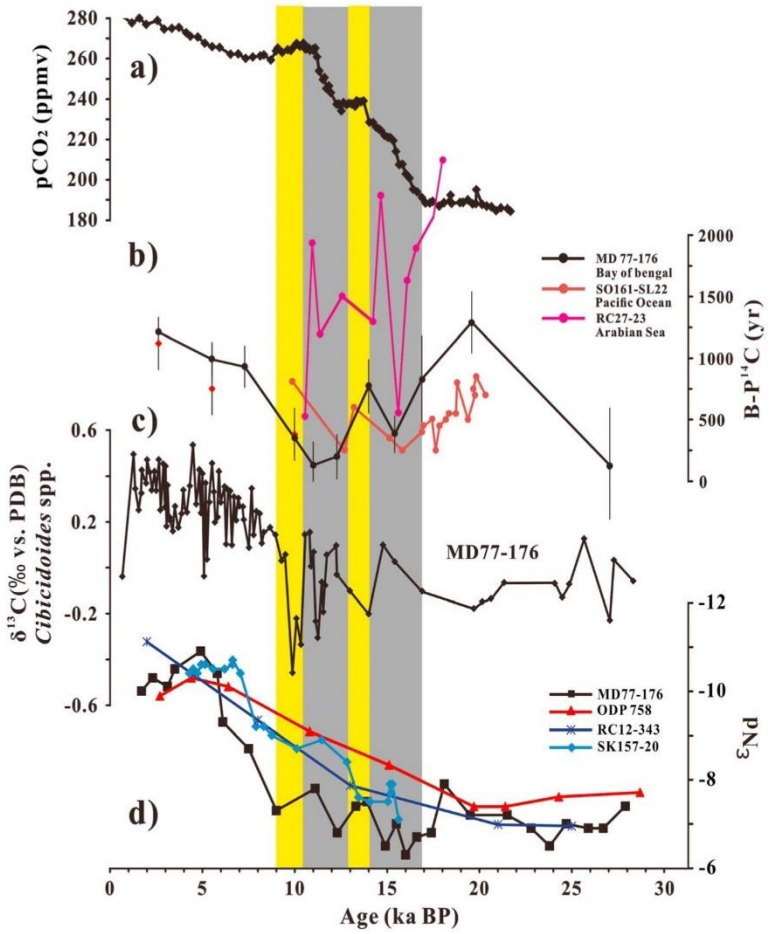

Figure 4. (a) Ice core atmospheric CO_2 from Antarctic Dome C (Monnin et al., 2001), (b) comparison of the intermediate water B-P ^{14}C age offset: Arabian Sea records, shown in pink (RC 27-23; Bryan et al., 2010), dark red (SO161-SL22; De Pol-Holz et al., 2010) and MD 77-176 (black, B-P ^{14}C age offset calculated by benthic *H. elegans* age, red diamond, calculated by benthic *Cibicidoides* spp.), (c) benthic $\delta^{13}C$ records for MD77-176, (d) comparison of seawater ε_{Nd} records in BoB obtained from planktonic foraminifera in core MD77-176 (Yu et al., 2018), core RC12-343 (Stoll et al., 2007), SK157-20 (Naik et al., 2019), and ODP site 758 (Burton & Vance, 2000). The gray-shaded intervals mark the two-step increase in atmospheric CO_2; the yellow-shaded interval marks the 14–13 cal kyr BP interval and the early Holocene (10.5–9 cal kyr BP), respectively.

This is also supported by a $\delta^{18}O$ shift of 1.8‰ from the LGM to the Holocene in core MD 77-176, in agreement with other benthic $\delta^{18}O$ records from the BoB (Ahmad et al., 2008, 2012; Naqvi et al., 1994; Raza et al., 2014). If we assume a limited deep local salinity change at the studied site during the LGM, and an ice-volume effect of about 1 to 1.2‰, the higher values of benthic $\delta^{18}O$ during the LGM indicate that temperature of the intermediate water in the northern BoB was about 3–4 °C lower than those of the Holocene. Such colder intermediate water in the BoB can be linked to a higher proportion of cold deep water masses.

The $\delta^{13}C$ and $\delta^{18}O$ records obtained on benthic foraminifera and the foraminiferal ε_{Nd} record accord closely with the faunal record, which is dominated during the LGM by assemblage 2 (Figure 3 and Figure S1), of which *B. robusta*, *P. bulloides* and *Globobulimina* spp. are major components. The distribution of living *B. robusta* ranges from 700 to 2,000 m and is associated with low dissolved oxygen conditions (Murgese & De Deckker, 2007; Szarek et al., 2009). *P. bulloides* and *Globobulimina* spp. prefer an intermediate to deep infaunal microhabitat, associated with a meso-eutrotrophic environment in poorly ventilated deep waters (e.g., Corliss, 1985; Fontanier et al., 2002). Thus, assemblage 2 could indicate relatively low-oxygen and mesotropic to eutrophic bottom water conditions during the LGM. This environment may be linked to the higher

Geochemistry, Geophysics, Geosystems 10.1029/2018GC008179

contribution of the SSW, which is known to present a higher trophic condition and a lower oxygen concentration than waters from the North Atlantic.

By contrast, assemblage 1 dominates during the Holocene. The major species are *B. aculeata*, *H. elegans*, *C. wuellerstorfi*, and *G. subglobsa*. Previous studies on *B. aculeata* indicate that this species has a widespread distribution and shows adaptability with respect to food (e.g., Altenbach et al., 1999; Caulle et al., 2015). However, *H. elegans*, *C. wuellerstorfi*, and *G. subglobsa* were observed in areas with low organic carbon flux rates and in high-oxygen content water masses (e.g., Altenbach et al., 1999; De & Gupta, 2010; Fontanier et al., 2002, and references therein). Periods dominated by these taxa probably correspond to high oxygen levels and oligotrophic environments. All of those elements suggest that intermediate water masses during the Holocene were characterized by oligotropic to mesotrophic conditions and/or well-ventilated conditions.

Today, the deep water in the BoB is filled with a mixture of NADW and Circumpolar Deep Water (Talley et al., 2011). In the northern BoB, the bottom water could contribute to shallower-depth water masses, because bottom water can upwell when it flows northward (Naqvi et al., 1994; Talley et al., 2011). The Glacial to Holocene *Cibicidoides* $\delta^{13}C$ shift is around 0.35‰ at core MD77-176 site, consistent with the average $\delta^{13}C$ shift (~0.4‰) obtained from RC12-344 (2,140 m, intermediate water depth) in the Andaman Sea (Naqvi et al., 1994). However, at deeper water depth from the southern BoB (Sk157-14, 3,306 m; Sk157-15, 2,855 m; Sk157-16, 2,920 m), the average Glacial to Holocene *Cibicidoides* $\delta^{13}C$ shift is around 0.6‰–0.65‰. This benthic $\delta^{13}C$ shift is interpreted as reflecting the enhanced influence of better-ventilated deep water NADW (Ahmad et al., 2008; Raza et al., 2014). Thus, the increased benthic $\delta^{13}C$ at intermediate water at the studied site may also reflect the enhanced contribution of NADW during the Holocene. Compared with deeper records of *Cibicidoides* $\delta^{13}C$, the benthic $\delta^{13}C$ at intermediate water depth may also be affected by the larger river input during the Holocene (Marzin et al., 2013), discharging lighter ^{13}C terrigenous organic matter into the ocean margin. However, in the modern situation, the percentage of terrigenous organic carbon from the Irrawaddy River decreases gradually offshore. On the outer Irrawaddy continental shelf, the contribution of terrigenous organic carbon is reduced and does not seem to a large contribution at the core site (Ramaswamy et al., 2008). In addition, benthic foraminifera assemblage 1 is also consistent with the higher values of *Cibicidoides* $\delta^{13}C$, reflecting better-ventilated waters at the core site during the Holocene that could correspond to NADW. Thus, we suggest that benthic $\delta^{13}C$ during the Holocene is mainly influenced by the better-ventilated water masses (NADW).

In addition, B-P ^{14}C values dramatically increase from 10 cal kyr BP onward, and reach a maximum (~1,210 years) at 2.6 cal kyr BP (late Holocene). The maximum value in the late Holocene is similar to the B-P age offset of ~1,290 years at 19.6 cal kyr BP (during the LGM; Figure 4). Higher values of B-P age offset could indicate intrusions of deep old water masses and a strong stratification of the upper water column. Moreover, the decrease in ε_{Nd} at deep water depth of the BoB could be interpreted as the increased influence of NADW (−13), and/or enhanced nonradiogenic Nd inputs from Ganges-Brahmaputra river system during the Holocene (Naik et al., 2019; Yu et al., 2018). Combined with the $\delta^{13}C$, $\delta^{18}O$ and assemblage records, higher values of B-P ^{14}C age offset may also suggest the contribution of NADW and SSW, respectively, during the late Holocene and LGM.

Our results indicate that during the LGM, deep and intermediate waters in the BoB were dominated by SSW, with a lesser contribution of water mass from the North Atlantic Ocean; this is in contrast to the Holocene. Bottom conditions changed from eutrophic to oligotrophic as we move from the LGM toward the Holocene, which could indicate a reduction in the supply of organic matter and an increase in oxygen levels in the bottom water.

5.2. Millennial-Scale Variations

5.2.1. Intermediate and Deep Water Depth Evolution in the BoB during the Last Termination and the Early Holocene

Superimposed on the glacial-interglacial trends, short events have also been recorded at the Core MD77-176 site during the 17–14, 13–10.6, and 10.5–9 cal kyr BP intervals. Increases of $\delta^{13}C$ values in the 17–14 and 13–10.6 cal kyr BP intervals correspond to reductions of B-P ^{14}C age offset to around ~300 and 200 years, respectively (Figure 4). The $\delta^{13}C$ decreases at around 10.5–9 cal kyr BP are coeval with lower values of B-P ^{14}C age offset of about ~350 years. The B-P ^{14}C age offsets subsequently increase significantly from 10 kyr onward

Geochemistry, Geophysics, Geosystems 10.1029/2018GC008179

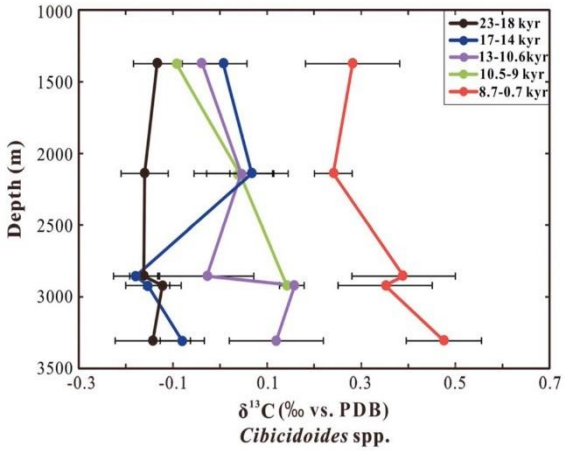

Figure 5. Benthic average $\delta^{13}C$ profiles for each of the cores in the vertical transects for selected time slices (23–18, 17–14, 13–10.6, 10.5–9, and 8.7–0.7 cal kyr BP). The $\delta^{13}C$ data are obtained from Sk157-14 (3,306 m), Sk157-15 (2,855 m), and Sk157-16 (2,920 m) in the southern BoB (Ahmad et al., 2008; Raza et al., 2014) and core RC12-344 (2,140 m) in the Andaman Sea (Naqvi et al., 1994).

and reach a maximum value of ~1,210 years at the late Holocene (2.6 kyr). In addition, even if the benthic $\delta^{18}O$ record does not exhibit a clear trend during the 17–14 cal kyr BP interval, a significant decrease in values of about 2.5‰–3‰ occurred at 13–10.6 cal kyr BP (Figure 2).

In order to examine the changes on a millennial time-scale during the last deglaciation and early Holocene at intermediate and deep water depth in the BoB, we compared the benthic $\delta^{13}C$ record of MD77-176 with the $\delta^{13}C$ record at intermediate depth from the Andaman Sea (RC12-344, 12.46°N–96.04°E, 2,140-m water depth; Naqvi et al., 1994), and at deep water depth from the southern BoB (Sk157-14, 5°11′N–90°05′E, 3,306 m; Sk157-15, 7°48′N–90°15′E, 2,855 m; Sk157-16, 8°46′N–90°18′E, 2,920 m; Ahmad et al., 2008; Raza et al., 2014). We averaged the benthic $\delta^{13}C$ of each core in different time intervals (23–18, 17–14, 13–10.6, 10.5–9, and 8.7–0.7 cal kyr BP) and plotted the results as vertical depth profiles (Figure 5). During the LGM, benthic $\delta^{13}C$ records obtained at intermediate and deep depths show similar values (~−0.15‰). Then, the $\delta^{13}C$ records show a continuous increase throughout the deglaciation until the Holocene. However, the evolution of deep and intermediate water mass $\delta^{13}C$ is quite different over the intervals 17–14, 13–10.6, and 10.5–9 cal kyr BP. After 23–18 cal kyr BP, the intermediate $\delta^{13}C$ values display an increasing trend at 17–14 and 13–10.6 cal kyr BP intervals, while during the 17–14 cal kyr BP interval the $\delta^{13}C$ records from deep water depths show similar $\delta^{13}C$ values to those of the LGM and they begin to increase from the 13–10.6 cal kyr BP interval onward. This difference suggests an increased stratification between intermediate and deeper water masses during the last deglaciation. In addition, the $\delta^{13}C$ decrease around 10.5–9 cal kyr BP (early Holocene) is also observed in the deep water depth cores from the southern BoB (Ahmad et al., 2008; Raza et al., 2014), with a clear shift from the early Holocene to late Holocene.

The last glacial period and the last deglaciation, until approximately 10.5 cal kyr, were characterized by ε_{Nd} values of between -7.9 ± 0.3 and -6.3 ± 0.2 in core MD77-176 (Figure 4). Before 18 cal kyr BP, the ε_{Nd} values of intermediate and deep-water masses are quite similar and become decoupled during the deglaciation. From 18 to 9 kyr BP, the ε_{Nd} values of deep water display a decreasing trend dropping down to ~−9. However, the ε_{Nd} record obtained on intermediate-depth core MD77-176 maintains an increasing trend at 17–14, 13–10.6, and 10.5–9 cal kyr BP intervals (ε_{Nd} values range between −8 and −6). The decoupling of ε_{Nd} values between various water depths since the LGM may reflect enhanced stratification between deep and intermediate water during the deglacial period (Yu et al., 2018). This is in agreement with the evolution of the vertical profile of *Cibicidoides* $\delta^{13}C$ collected from different water depth cores in the BoB (Figure 5). The deeper water masses could be associated with a higher contribution of unradiogenic NADW ε_{Nd} values from about 18 cal kyr BP, whereas intermediate water masses are associated with a higher contribution of AAIW implying a strong propagation of SSW (AAIW) into the Northern Indian Ocean (Yu et al., 2018).

However, changes in $\delta^{13}C$ values of benthic foraminifera can be influenced by different processes such as surface productivity, changes of the water mass sources and/or mixing and air-sea exchanges (Lynch-Stieglitz et al., 1995). The B-P ^{14}C age offset could also reflect the source of water masses and/or the renewal process of deep water masses. Therefore, we will discuss these issues in greater detail below and will combine our data to enable us to decipher these different processes.

5.2.2. Variations in Local Processes

Variations of primary productivity can impact the $\delta^{13}C$ of benthic foraminifera, but do not appear to be a major control at our core site. The distribution of chlorophyll in surface water of the western BoB suggests a slight increase in productivity during the winter monsoon period (around January) in the BoB (O'Malley, 2017; Thushara & Vinayachandran, 2016). The Indian summer monsoon intensity decreased, relatively speaking, during the 17–14 and 13–10.6 cal kyr BP intervals (Marzin et al., 2013), whereas East Asia Winter Monsoon (EAWM) strengthened during the same intervals (Wen et al., 2016). If the intensity of EAWM influenced our core site in the BoB during the 17–14 and 13–10.6 cal kyr BP intervals, we should

Geochemistry, Geophysics, Geosystems 10.1029/2018GC008179

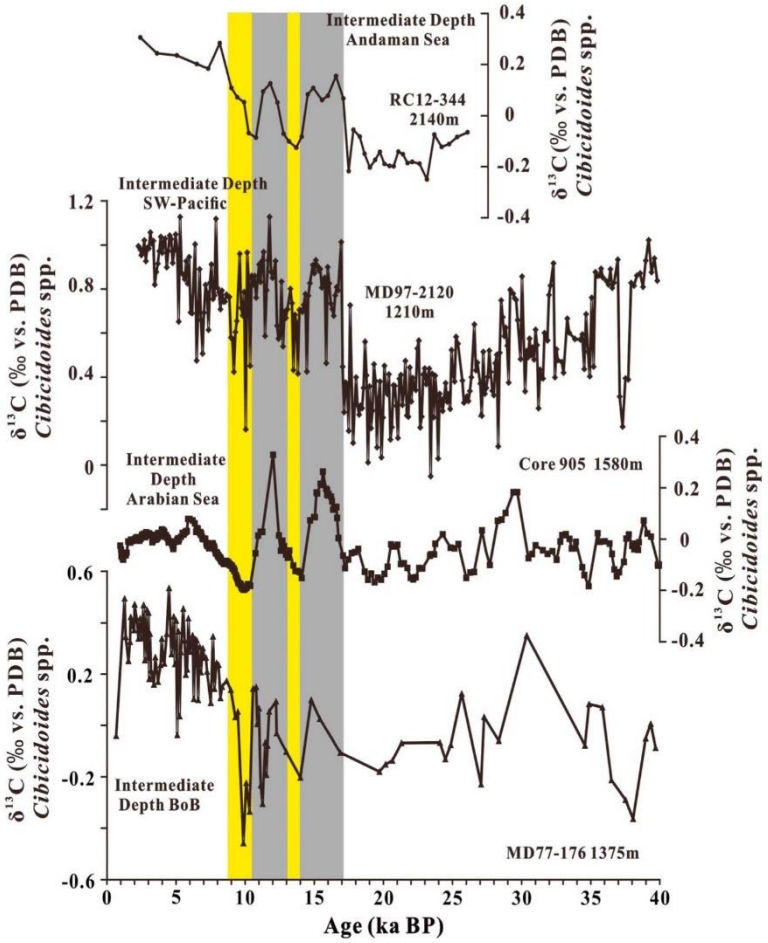

Figure 6. Compilation of benthic $\delta^{13}C$ records obtained from core MD77-176 (water depth of 1,325- m; this study), core RC12–344 (2,140-m water depth; Naqvi et al., 1994), MD97–2120 (1,210-m water depth; Pahnke & Zahn, 2005), and core 905 (1,580-m water depth; Jung et al., 2009). The color-shaded intervals are the same as in Figure 4.

expect an increased surface productivity during those intervals of intense winter monsoon and, therefore, lower *Cibicidoides* $\delta^{13}C$ values through enhanced export and decay of organic carbon at intermediate depth. This is in contradiction to what we observe in the $\delta^{13}C$ record of MD77-176. Thus, the influence of primary productivity on the benthic $\delta^{13}C$ values can be discounted.

The *G. ruber* $\delta^{18}O$ record of core MD77-176 indicates the surface salinity variations in the core site (Marzin et al., 2013), and the lower salinity during the earliest Holocene (around 10 kyr) is associated with an intensified Indian monsoon, leading to more freshwater discharge from the Ganges-Brahmaputra river system and from the Irrawaddy River. This should have led to pronounced ocean stratification of the northern BoB. During this period, however, we observe a decrease in the B-P age offsets, the opposite of what would be expected from strong upper water column stratification. Thus, we suggest that vertical mixing does not appear to play an important role in this area.

5.2.3. Changes in Intermediate Water Circulation

We compared the benthic $\delta^{13}C$ record of MD77-176 with $\delta^{13}C$ records at intermediate depth from the Arabian Sea (Core 905, 10°46′N–51°57′E, 1,580-m water depth), the Southwest Pacific Ocean (MD97-2120, 45°32.06′S–174°55.85′E, 1,210-m water depth) and the Andaman Sea (RC12-344, 12.46°N–96.04°E, 2,140-m water depth; Jung et al., 2009; Naqvi et al., 1994; Pahnke & Zahn, 2005; Figure 6). All of the benthic $\delta^{13}C$ records display an increasing trend during the 17–14 cal kyr BP and 13–10.6 cal kyr BP intervals. Furthermore, we also observed a decrease in those intermediate $\delta^{13}C$ records at the beginning of the

Geochemistry, Geophysics, Geosystems 10.1029/2018GC008179

Holocene (10.5–9 cal kyr BP; Jung et al., 2009; Naqvi et al., 1994; Pahnke & Zahn, 2005; Figure 6). This suggests that the variations during these intervals are related to global changes at intermediate water depths in the Indo-Pacific region. The similarity of the benthic $\delta^{13}C$-increases reflects the northward expansion of AAIW during these time intervals in the Arabian Sea and Pacific Ocean (Jung et al., 2009; Pahnke & Zahn, 2005). In addition, the transition in the ε_{Nd} and $\Delta^{14}C$ records during the deglaciation also indicates a strong northward penetration of AAIW within the North Atlantic (e.g., Cao et al., 2007; Pahnke et al., 2008). Combined with the ε_{Nd} record of core MD77-176, all of these signals tend to show that, during 17–14 cal kyr BP and 13–10.6 cal kyr BP intervals, BoB circulation was driven by Southern Ocean processes.

By contrast, the generally decreased trend in the presented intermediate benthic $\delta^{13}C$ records during the 14–13 cal kyr BP interval associated to a more stable ε_{Nd} may indicate the weakened formation and northward advection of AAIW (Yu et al., 2018). In addition, the decrease of intermediate benthic $\delta^{13}C$ corresponds to the rapid increase in sea-level during the ~14–14.5 cal kyr BP time interval, the so-called Melt-Water Pulse 1A (MWP-1A; Deschamps et al., 2012; Fairbanks et al., 2005; Peltier & Fairbanks, 2006). This significant sea-level fluctuation during the 14–13 cal kyr BP interval could have influenced the discharge of terrigenous organic matter into the ocean. Thus, this large input of lighter $\delta^{13}C$ terrigenous organic carbon may have contributed to the global decrease in the benthic foraminifer $\delta^{13}C$ values.

The changes in the carbon isotope record and B-P age offsets obtained on the sedimentary section from MD77-176 at the 17–14 and 13–10.6 cal kyr BP intervals correspond to warming episodes in Antarctica and the Southern Hemisphere during the deglaciation (e.g., Cuffey et al., 2016; Epica, 2006). These time intervals also correspond to a decrease of the Antarctic sea-ice (Shemesh et al., 2002; Wais, 2013) and the reduction of stratification resulting in better ventilation in the South Ocean (e.g., Anderson et al., 2009; Skinner et al., 2010). The Southern Hemisphere westerlies migrated to a southern position during those same intervals, which could have led to an increase of the northward Ekman transport (Toggweiler et al., 2006). Therefore, during the 17–14 and 13–10.6 cal kyr BP intervals, enhanced vertical ventilation in the Southern Ocean could have led to an increased production of subsurface water masses (Subantarctic Mode Water, SAMW) and intermediate water masses (AAIW; Anderson et al., 2009). These water masses could have carried a chemical signature resulting in a reduced difference between intermediate and surface water masses (e.g., $\delta^{13}C$ values, B-P offsets, temperature, and salinity) and which was transported at the same time to the north.

Strengthened upward mixing would provide a conduit for moving much younger ^{14}C age surface water to deep water masses; this in turn may lead to a greater decrease of the B-P age offsets. In addition, the intermediate benthic $\delta^{13}C$ in the Southern Ocean is dominated by the influence of air-sea exchange (Lynch-Stieglitz et al., 1994), and values of intermediate benthic $\delta^{13}C$ could increase relatively via stronger upwelling during the formation of AAIW/SAMW. Such a hypothesis is consistent with the variations of intermediate benthic $\delta^{13}C$ records and B-P age offsets from the Northern BoB, Arabian Sea, and Pacific Ocean (Figures 6 and 4b). Coinciding with the carbon isotopes and ^{14}C ages, the disconnection observed in the ε_{Nd} values between core MD77-176 and the other deeper cores of the BoB during the deglaciation could confirm the influence of glacial radiogenic AAIW (Yu et al., 2018; Figure 4d).

Increased benthic carbon isotope values and smaller B-P age offsets obtained from MD77-176 at 17–14 and 13–10.6 cal kyr BP intervals are synchronous with a two-step increase of atmospheric CO_2 (Figure 4). The changes in B-P age offset and benthic $\delta^{13}C$ records reported here indicate strong upwelling and enhanced northern flow of AAIW from the Southern Ocean during these two periods. Thus, the variations of these records could support the hypothesis that the Southern Ocean upwelling played a vital role for the CO_2 increase in the deglacial period (Anderson et al., 2009; Skinner et al., 2010; Skinner et al., 2014).

The variations of intermediate benthic $\delta^{13}C$, B-P age offsets and ε_{Nd} records during the 17–14 and 13–10.6 cal kyr BP intervals correspond to warming in South Hemisphere and increased atmospheric CO_2. These elements support the idea of more fresh water input in the North Atlantic Ocean and associated to a weakened northward transport of heat. Synchronously, the Southern Hemisphere increased the heat fluxes and reduced sea ice cover in the Southern Ocean. Thus, strong winds enhanced the upwelling and increased the northward penetration of the northward flow of AAIW/SAMW, which could increase northward transport of nutrient and heat at intermediate waters depth (Anderson et al., 2009; Poggemann et al., 2017, 2018;

Geochemistry, Geophysics, Geosystems 10.1029/2018GC008179

Skinner et al., 2014). The role of AAIW is still controversial during the last deglaciation in the Atlantic Ocean, several studies suggesting a reduced northward flux of AAIW into the tropical Atlantic (e.g., Came et al., 2008; Gu et al., 2017; Howe et al., 2016; Xie et al., 2012). However, other studies indicate an increased penetration of AAIW in the Atlantic Ocean (e.g., Dubois-Dauphin et al., 2016; Pahnke et al., 2008; Poggemann et al., 2017, 2018). This is also strongly supported by the intermediate records of benthic carbon isotope, ε_{Nd}, and B-P age offsets from the North Indian (Bryan et al., 2010; Jung et al., 2009; Yu et al., 2018), and Pacific Ocean (e.g., Bostock et al., 2010; Mix et al., 1991; Pahnke & Zahn, 2005). Therefore, we suggest that the global northern flow intermediate water was sourced from the Southern Ocean by AAIW/SAMW during the deglaciation.

$\delta^{13}C$ records subsequently display a short-term decreasing trend in the northern Indian Ocean and SW Pacific Ocean at the beginning of the Holocene (10.5–9 cal kyr BP; Jung et al., 2009; Naqvi et al., 1994; Pahnke & Zahn, 2005). The B-P ^{14}C age offsets and ε_{Nd} from core MD77-176 are close to the values obtained for the deglaciation (Figure 4). Thereafter, from the 10.5–9 cal kyr BP interval to the late Holocene, the increased benthic $\delta^{13}C$ and B-P age offsets, associated to depleted ε_{Nd} records, seem to indicate the enhanced influence of the NADW since the 9 cal kyr BP. Thus, we suggest that the BoB circulation during the 10.5–9 cal kyr BP interval was also driven by the northward expansion of AAIW, with a progressive increase in the influence of the NADW during the Holocene, as is also indicated by the $\delta^{18}O$ and benthic assemblage records.

6. Conclusions

Changes in benthic foraminiferal assemblages, together with $\delta^{13}C$, $\delta^{18}O$, and ^{14}C ages obtained from benthic foraminifera have been analyzed on core MD77-176, located in the BoB at 1,375-m water depth, in order to reconstruct the evolution of intermediate water masses in the northeast Indian Ocean from the LGM to the Holocene. Benthic $\delta^{13}C$ and $\delta^{18}O$ records suggest that the LGM was dominated by expansion of South Ocean waters with low $\delta^{13}C$ values, whereas the late Holocene is characterized by strengthened NADW flows into the BoB, with higher values of $\delta^{13}C$ and B-P age offsets. Benthic foraminiferal assemblages are consistent with the geochemical proxies, with the LGM assemblage reflecting a relatively low-oxygen level and mesotropic to eutrophic deep water conditions. The typically Holocene assemblage indicates well-ventilated conditions and/or an oligotropic to mesotrophic environment.

Furthermore, during the last deglaciation to the Early Holocene, events at 17–14, 13–10.6, and 10.5–9 cal kyr BP intervals display decreased B-P age offsets, increased benthic $\delta^{13}C$ records, and changes in the $\delta^{18}O$ values and ε_{Nd} results. All of these results are best explained by a northern Indian Ocean variation associated with changes in water masses formed in the South. Our proxy variations are consistent with enhanced upwelling in the Southern Ocean and increased northward penetration of the northward flow of AAIW/SAMW during the 17–14, 13–10.6, and 10.5–9 cal kyr BP intervals. These signals are coeval with the two-step increase of atmospheric carbon dioxide (CO_2), indicating that the enhanced Southern Ocean ventilation could have played an important role in the CO_2 increase during the last deglaciation.

Acknowledgments
This work was supported by the National Natural Science Foundation of China (41806060). R. Ma acknowledges the China Scholarship Council for providing funding for her study in France. We thank F. Thil for the ^{14}C measurements taken using the *ECHo*MICADAS and two anonymous reviewers for useful suggestions and discussions. This work has been supported by grants from the INSU-LEFE-IMAGO-CITRON GLACE program. All data are given in Tables 1–3 and S1 and S2.

References

Ahmad, S. M., Babu, A. G., Padmakumari, V. M., & Raza, W. (2008). Surface and deep water changes in the northeast Indian Ocean during the last 60 ka inferred from carbon and oxygen isotopes of planktonic and benthic foraminifera. *Palaeogeography, Palaeoclimatology, Palaeoecology*, *262*(3-4), 182–188. https://doi.org/10.1016/j.palaeo.2008.03.007

Ahmad, S. M., Zheng, H., Raza, W., Zhou, B., Lone, M. A., Raza, T., & Suseela, G. (2012). Glacial to Holocene changes in the surface and deep waters of the Northeast Indian Ocean. *Marine Geology*, *329-331*, 16–23. https://doi.org/10.1016/j.margeo.2012.10.002

Altenbach, A. V., Pflaumann, U., Thies, R. S. A., Timm, S., & Trauth, M. (1999). Scaling percentages and distributional patterns of benthic foraminifera with flux rates of organic carbon. *Journal of Foraminiferal Research*, *29*(3), 173–185.

Anderson, R. F., Ali, S., Bradtmiller, L. I., Nielsen, S. H. H., Fleisher, M. Q., Anderson, B. E., & Burckle, L. H. (2009). Wind-driven upwelling in the Southern Ocean and the deglacial rise in atmospheric CO_2. *Science*, *323*(5920), 1443–1448. https://doi.org/10.1126/science.1167441

Böhm, E., Lippold, J., Gutjahr, M., Frank, M., Blaser, P., Antz, B., et al. (2015). Strong and deep Atlantic meridional overturning circulation during the last glacial cycle. *Nature*, *517*(7532), 73–76. https://doi.org/10.1038/nature14059

Bostock, H. C., Opdyke, B. N., & Williams, M. J. M. (2010). Characterising the intermediate depth waters of the Pacific Ocean using $\delta^{13}C$ and other geochemical tracers. *Deep Sea Research Part I: Oceanographic Research Papers*, *57*(7), 847–859. https://doi.org/10.1016/j.dsr.2010.04.005

Bryan, S. P., Marchitto, T. M., & Lehman, S. J. (2010). The release of ^{14}C-depleted carbon from the deep ocean during the last deglaciation: Evidence from the Arabian Sea. *Earth and Planetary Science Letters*, *298*(1-2), 244–254. https://doi.org/10.1016/j.epsl.2010.08.025

Burton, K. W., & Vance, D. (2000). Glacial–interglacial variations in the neodymium isotope composition of seawater in the Bay of Bengal recorded by planktonic foraminifera. *Earth and Planetary Science Letters*, *176*(3-4), 425–441. https://doi.org/10.1016/S0012-821X(00)00011-X

Came, R. E., Oppo, D. W., Curry, W. B., & Lynch-Stieglitz, J. (2008). Deglacial variability in the surface return flow of the Atlantic meridional overturning circulation. *Paleoceanography*, *23*, PA1217. https://doi.org/10.1029/2007PA001450

Cao, L., Fairbanks, R., Mortlock, R., & Risk, M. (2007). Radiocarbon reservoir age of high latitude North Atlantic surface water during the last deglacial. *Quaternary Science Reviews*, *26*(5-6), 732–742. https://doi.org/10.1016/j.quascirev.2006.10.001

Caulle, C., Mojtahid, M., Gooday, A. J., Jorissen, F. J., & Kitazato, H. (2015). Living (Rose-Bengal-stained) benthic foraminiferal faunas along a strong bottom-water oxygen gradient on the Indian margin (Arabian Sea). *Biogeosciences*, *12*(16), 5005–5019. https://doi.org/10.5194/bg-12-5005-2015

Corliss, B. H. (1985). Microhabitats of benthic foraminifera within deep-sea sediments. *Nature*, *314*(6010), 435–438. https://doi.org/10.1038/314435a0

Cuffey, K. M., Clow, G. D., Steig, E. J., Buizert, C., Fudge, T. J., Koutnik, M., et al. (2016). Deglacial temperature history of West Antarctica. *Proceedings of the National Academy of Sciences*, *113*(50), 14,249–14,254. https://doi.org/10.1073/pnas.1609132113

Curry, W. B., Duplessy, J. C., Labeyrie, L. D., & Shackleton, N. J. (1988). Changes in the distribution of $\delta^{13}C$ of deep water ΣCO_2 between the Last Glaciation and the Holocene. *Paleoceanography*, *3*(3), 317–341. https://doi.org/10.1029/PA003i003p00317

De Pol-Holz, R., Keigwin, L., Southon, J., Hebbeln, D., & Mohtadi, M. (2010). No signature of abyssal carbon in intermediate waters off Chile during deglaciation. *Nature Geoscience*, *3*(3), 192–195. https://doi.org/10.1038/ngeo745

De, S., & Gupta, A. K. (2010). Deep-sea faunal provinces and their inferred environments in the Indian Ocean based on distribution of recent benthic foraminifera. *Palaeogeography, Palaeoclimatology, Palaeoecology*, *291*(3-4), 429–442. https://doi.org/10.1016/j.palaeo.2010.03.012

Deschamps, P., Durand, N., Bard, E., Hamelin, B., Camoin, G., Thomas, A. L., et al. (2012). Ice-sheet collapse and sea-level rise at the Bølling warming 14,600 years ago. *Nature*, *483*(7391), 559–564. https://doi.org/10.1038/nature10902

Dubois-Dauphin, Q., Bonneau, L., Colin, C., Montero-Serrano, J. C., Montagna, P., Blamart, D., et al. (2016). South Atlantic Intermediate Water advances into the north-east Atlantic with reduced Atlantic meridional overturning circulation during the last glacial period. *Geochemistry, Geophysics, Geosystems*, *17*, 2336–2353. https://doi.org/10.1002/2016GC006281

Duplessy, J. C., Shackleton, N. J., Matthews, R. K., Prell, W., Ruddiman, W. F., Caralp, M., & Hendy, C. H. (1984). ^{13}C record of benthic foraminifera in the last interglacial ocean: Implications for the carbon cycle and the global deep water circulation. *Quaternary Research*, *21*(02), 225–243. https://doi.org/10.1016/0033-5894(84)90099-1

EPICA, C.M (2006). One-to-one coupling of glacial climate variability in Greenland and Antarctica. *Nature*, *444*(7116), 195–198. https://doi.org/10.1038/nature05301

Fairbanks, R. G., Mortlock, R. A., Chiu, T.-Z., Cao, L., Kaplan, A., Guilderson, T. P., et al. (2005). Radiocarbon calibration curve spanning 0 to 50,000 years BP based on paired $^{230}Th/^{234}U/^{238}U$ and ^{14}C dates on pristine corals. *Quaternary Science Reviews*, *24*(16-17), 1781–1796. https://doi.org/10.1016/j.quascirev.2005.04.007

Fontanier, C., Jorissen, F. J., Licari, L., Alexandre, A., Anschutz, P., & Carbonel, P. (2002). Live benthic foraminiferal faunas from the Bay of Biscay: Faunal density, composition, and microhabitats. *Deep Sea Research Part I: Oceanographic Research Papers*, *49*(4), 751–785. https://doi.org/10.1016/S0967-0637(01)00078-4

Gu, S., Liu, Z., Zhang, J., Rempfer, J., Joos, F., & Oppo, D. W. (2017). Coherent response of Antarctic Intermediate Water and Atlantic Meridional Overturning during the last deglaciation: Reconciling contrasting neodymium isotope reconstructions from the tropical Atlantic. *Paleoceanography*, *32*, 1036–1053. https://doi.org/10.1002/2017PA003092

Hammer, Ø., Harper, D.A.T., and Ryan, P.D. (2001). Past: Paleontological statistics software package for education and data analysis.

Holbourn, A., Henderson, A. S., & Macleod, N. (2013). Front matter. In *Atlas of benthic foraminifera*, (pp. 1–641).

Howe, J. N. W., Piotrowski, A. M., Oppo, D. W., Huang, K. F., Mulitza, S., Chiessi, C. M., & Blusztajn, J. (2016). Antarctic intermediate water circulation in the South Atlantic over the past 25,000 years. *Paleoceanography*, *31*, 1302–1314. https://doi.org/10.1002/2016PA002975

Jones, R. W. (1994). *The challenger foraminifera*, (p. 149). Oxford University Press.

Jung, S. J. A., Kroon, D., Ganssen, G., Peeters, F., & Ganeshram, R. (2009). Enhanced Arabian Sea intermediate water flow during glacial North Atlantic cold phases. *Earth and Planetary Science Letters*, *280*(1-4), 220–228. https://doi.org/10.1016/j.epsl.2009.01.037

Kallel, N., Labeyrie, L. D., Juillet-Leclerc, A., & Duplessy, J. C. (1988). A deep hydrological front between intermediate and deep-water masses in the glacial Indian Ocean. *Nature*, *333*(6174), 651–655. https://doi.org/10.1038/333651a0

Locke, S., & Thunell, R. C. (1988). Paleoceanographic record of the last glacial/interglacial cycle in the Red Sea and Gulf of Aden. *Palaeogeography, Palaeoclimatology, Palaeoecology*, *64*(3-4), 163–187. https://doi.org/10.1016/0031-0182(88)90005-3

Loeblich, A. R., & Tappan, H. (1988). Generic taxa erroneously regarded as foraminifers. In A. R. Loeblich, & H. Tappan (Eds.), *Foraminiferal genera and their classification*, (pp. 726–730). Boston, MA: Springer US. https://doi.org/10.1007/978-1-4899-5760-3_10

Lynch-Stieglitz, J., Adkins, J. F., Curry, W. B., Dokken, T., Hall, I. R., Herguera, J. C., et al. (2007). Atlantic meridional overturning circulation during the Last Glacial Maximum. *Science*, *316*(5821), 66–69. https://doi.org/10.1126/science.1137127

Lynch-Stieglitz, J., Fairbanks, R. G., & Charles, C. D. (1994). Glacial-interglacial history of Antarctic Intermediate Water: Relative strengths of Antarctic versus Indian Ocean sources. *Paleoceanography*, *9*(1), 7–29. https://doi.org/10.1029/93PA02446

Lynch-Stieglitz, J., Stocker, T. F., Broecker, W. S., & Fairbanks, R. G. (1995). The influence of air-sea exchange on the isotopic composition of oceanic carbon: Observations and modeling. *Global Biogeochemical Cycles*, *9*(4), 653–665. https://doi.org/10.1029/95GB02574

Mackensen, A., Hubberten, H.-W., Bickert, T., Fischer, G., & Fütterer, D. K. (1993). The $\delta^{13}C$ in benthic foraminiferal tests of Fontbotia wuellerstorfi (Schwager) relative to the $\delta^{13}C$ of dissolved inorganic carbon in Southern Ocean Deep Water: Implications for glacial ocean circulation models. *Paleoceanography*, *8*(5), 587–610. https://doi.org/10.1029/93PA01291

Marzin, C., Kallel, N., Kageyama, M., Duplessy, J. C., & Braconnot, P. (2013). Glacial fluctuations of the Indian monsoon and their relationship with North Atlantic climate: New data and modelling experiments. *Climate of the Past*, *9*(5), 2135–2151. https://doi.org/10.5194/cp-9-2135-2013

McManus, J. F., Francois, R., Gherardi, J. M., Keigwin, L. D., & Brown-Leger, S. (2004). Collapse and rapid resumption of Atlantic meridional circulation linked to deglacial climate changes. *Nature*, *428*(6985), 834–837. https://doi.org/10.1038/nature02494

Mix, A. C., & Fairbanks, R. G. (1985). North Atlantic surface-ocean control of pleistocene deep-ocean circulation. *Earth and Planetary Science Letters*, *73*(2-4), 231–243. https://doi.org/10.1016/0012-821X(85)90072-X

Mix, A. C., Pisias, N. G., Zahn, R., Rugh, W., Lopez, C., & Nelson, K. (1991). Carbon 13 in pacific deep and intermediate waters, 0-370 ka: Implications for ocean circulation and pleistocene CO_2. *Paleoceanography*, *6*(2), 205–226. https://doi.org/10.1029/90PA02303

Monnin, E., Indermühle, A., Dällenbach, A., Flückiger, J., Stauffer, B., Stocker, T. F., et al. (2001). Atmospheric CO_2 concentrations over the last glacial termination. *Science*, *291*(5501), 112–114. https://doi.org/10.1126/science.291.5501.112

Murgese, D. S., & De Deckker, P. (2007). The Late Quaternary evolution of water masses in the eastern Indian Ocean between Australia and Indonesia, based on benthic foraminifera faunal and carbon isotopes analyses. *Palaeogeography, Palaeoclimatology, Palaeoecology*, *247*(3-4), 382–401. https://doi.org/10.1016/j.palaeo.2006.11.002

Naik, S. S., Basak, C., Goldstein, S. L., Naidu, P., & Naik, S. M. (2019). A 16-kyr record of ocean circulation and monsoon intensification from the Central Bay of Bengal. *Geochemistry, Geophysics, Geosystems*, *20*. https://doi.org/10.1029/2018GC007860

Naqvi, W. A., Charles, C. D., & Fairbanks, R. G. (1994). Carbon and oxygen isotopic records of benthic foraminifera from the northeast Indian Ocean: Implications on glacial-interglacial atmospheric CO_2 changes. *Earth and Planetary Science Letters*, *121*(1-2), 99–110. https://doi.org/10.1016/0012-821X(94)90034-5

O'Malley, R. (2017). Ocean productivity. http://www.science.oregonstate.edu/ocean.Productivity/index.php.

Oppo, D. W., & Fairbanks, R. G. (1987). Variability in the deep and intermediate water circulation of the Atlantic Ocean during the past 25,000 years: Northern hemisphere modulation of the Southern Ocean. *Earth and Planetary Science Letters*, *86*(1), 1–15. https://doi.org/10.1016/0012-821X(87)90183-X

Pahnke, K., Goldstein, S. L., & Hemming, S. R. (2008). Abrupt changes in Antarctic Intermediate Water circulation over the past 25,000 years. *Nature Geoscience*, *1*(12), 870–874. https://doi.org/10.1038/ngeo360

Pahnke, K., & Zahn, R. (2005). Southern hemisphere water mass conversion linked with North Atlantic climate variability. *Science*, *307*(5716), 1741–1746. https://doi.org/10.1126/science.1102163

Peltier, W. R., & Fairbanks, R. G. (2006). Global glacial ice volume and Last Glacial Maximum duration from an extended Barbados sea level record. *Quaternary Science Reviews*, *25*(23-24), 3322–3337. https://doi.org/10.1016/j.quascirev.2006.04.010

Peterson, C. D., Lisiecki, L. E., & Stern, J. V. (2014). Deglacial whole-ocean $\delta^{13}C$ change estimated from 480 benthic foraminiferal records. *Paleoceanography*, *29*, 549–563. https://doi.org/10.1002/2013PA002552

Poggemann, D. W., Hathorne, E. C., Nürnberg, D., Frank, M., Bruhn, I., Reißig, S., & Bahr, A. (2017). Rapid deglacial injection of nutrients into the tropical Atlantic via Antarctic Intermediate Water. *Earth and Planetary Science Letters*, *463*, 118–126. https://doi.org/10.1016/j.epsl.2017.01.030

Poggemann, D. W., Nürnberg, D., Hathorne, E. C., Frank, M., Rath, W., Reißig, S., & Bahr, A. (2018). Deglacial heat uptake by the Southern Ocean and rapid northward redistribution via Antarctic Intermediate Water. *Paleoceanography and Paleoclimatology*, *33*, 1292–1305. https://doi.org/10.1029/2017PA003284

Rahmstorf, S. (1995). Bifurcations of the Atlantic thermohaline circulation in response to changes in the hydrological cycle. *Nature*, *378*(6553), 145–149. https://doi.org/10.1038/378145a0

Ramaswamy, V., Gaye, B., Shirodkar, P. V., Rao, P. S., Chivas, A. R., Wheeler, D., & Thwin, S. (2008). Distribution and sources of organic carbon, nitrogen and their isotopic signatures in sediments from the Ayeyarwady (Irrawaddy) continental shelf, northern Andaman Sea. *Marine Chemistry*, *111*(3-4), 137–150. https://doi.org/10.1016/j.marchem.2008.04.006

Raza, T., Ahmad, S. M., Sahoo, M., Banerjee, B., Bal, I., Dash, S., et al. (2014). Hydrographic changes in the southern Bay of Bengal during the last ~65,000 y inferred from carbon and oxygen isotopes of foraminiferal fossil shells. *Quaternary International*, *333*, 77–85. https://doi.org/10.1016/j.quaint.2014.02.010

Roberts, N. L., Piotrowski, A. M., McManus, J. F., & Keigwin, L. D. (2010). Synchronous deglacial overturning and water mass source changes. *Science*, *327*(5961), 75–78. https://doi.org/10.1126/science.1178068

Schlitzer, R. (2015). Ocean data view. http://odv.awi.de.

Shackleton, N. J. (1974). Attainment of isotopic equilibrium between ocean water and benthonic foraminifera genus uvigerina: Isotopic changes in the ocean during the last glacial. Les méthodes quantitatives d'étude des variations du climat au cours du pleistocène, Gif-sur-Yvette. Colloque international du CNRS 219, 203–210.

Shankar, D., Vinayachandran, P. N., & Unnikrishnan, A. S. (2002). The monsoon currents in the north Indian Ocean. *Progress in Oceanography*, *52*(1), 63–120. https://doi.org/10.1016/S0079-6611(02)00024-1

Shemesh, A., Hodell, D., Crosta, X., Kanfoush, S., Charles, C., & Guilderson, T. (2002). Sequence of events during the last deglaciation in Southern Ocean sediments and Antarctic ice cores. *Paleoceanography*, *17*(4), 1056. https://doi.org/10.1029/2000PA000599

Siddall, M., Rohling, E. J., Almogi-Labin, A., Hemleben, C., Meischner, D., Schmelzer, I., & Smeed, D. A. (2003). Sea-level fluctuations during the last glacial cycle. *Nature*, *423*(6942), 853–858. https://doi.org/10.1038/nature01690

Skinner, L. C., Fallon, S., Waelbroeck, C., Michel, E., & Barker, S. (2010). Ventilation of the deep Southern Ocean and deglacial CO_2 rise. *Science*, *328*(5982), 1147–1151. https://doi.org/10.1126/science.1183627

Skinner, L. C., Waelbroeck, C., Scrivner, A. E., & Fallon, S. J. (2014). Radiocarbon evidence for alternating northern and southern sources of ventilation of the deep Atlantic carbon pool during the last deglaciation. *Proceedings of the National Academy of Sciences*, *111*(15), 5480–5484. https://doi.org/10.1073/pnas.1400668111

Stocker, T. F., & Wright, D. G. (1996). Rapid changes in ocean circulation and atmospheric radiocarbon. *Paleoceanography*, *11*(6), 773–795. https://doi.org/10.1029/96PA02640

Stoll, H. M., Vance, D., & Arevalos, A. (2007). Records of the Nd isotope composition of seawater from the Bay of Bengal: Implications for the impact of northern hemisphere cooling on ITCZ movement. *Earth and Planetary Science Letters*, *255*(1-2), 213–228. https://doi.org/10.1016/j.epsl.2006.12.016

Szarek, R., Kuhnt, W., Kawamura, H., & Nishi, H. (2009). Distribution of recent benthic foraminifera along continental slope of the Sunda Shelf (South China Sea). *Marine Micropaleontology*, *71*(1-2), 41–59. https://doi.org/10.1016/j.marmicro.2009.01.004

Talley, L. D., Pickard, G. L., Emery, W. J., & Swift, J. H. (2011). Preface. In *Descriptive physical oceanography*, (sixth ed.pp. 1–383). Boston: Academic Press.

Thushara, V., & Vinayachandran, P. N. (2016). Formation of summer phytoplankton bloom in the northwestern Bay of Bengal in a coupled physical-ecosystem model. *Journal of Geophysical Research: Oceans*, *121*, 8535–8550. https://doi.org/10.1002/2016JC011987

Tisnérat-Laborde, N., Poupeau, J. J., Tannau, J. F., & Paterne, M. (2001). Development of a semi-automated system for routine preparation of carbonate samples. *Radiocarbon*, *43*(2A), 299–304. https://doi.org/10.1017/S0033822200038145

Toggweiler, J. R., Russell, J. L., & Carson, S. R. (2006). Midlatitude westerlies, atmospheric CO_2, and climate change during the ice ages. *Paleoceanography*, *21*, GB3003. https://doi.org/10.1029/2005PA001154

Tomczak, M., & Godfrey, J. S. (2003). *Regional oceanography: An introduction*. Daya Publishing House.

Geochemistry, Geophysics, Geosystems 10.1029/2018GC008179

Wacker, L., Fahrni, S. M., Hajdas, I., Molnar, M., Synal, H. A., Szidat, S., & Zhang, Y. L. (2013). A versatile gas interface for routine radiocarbon analysis with a gas ion source. *Nuclear Instruments and Methods in Physics Research Section B: Beam Interactions with Materials and Atoms*, *294*, 315–319. https://doi.org/10.1016/j.nimb.2012.02.009

Waelbroeck, C., Levi, C., Duplessy, J. C., Labeyrie, L., Michel, E., Cortijo, E., et al. (2006). Distant origin of circulation changes in the Indian Ocean during the last deglaciation. *Earth and Planetary Science Letters*, *243*(1-2), 244–251. https://doi.org/10.1016/j.epsl.2005.12.031

Wais, D. P. M. (2013). Onset of deglacial warming in West Antarctica driven by local orbital forcing. *Nature*, *500*, 440.

Wen, X., Liu, Z., Wang, S., Cheng, J., & Zhu, J. (2016). Correlation and anti-correlation of the East Asian summer and winter monsoons during the last 21,000 years. *Nature Communications*, *7*(1), 11999. https://doi.org/10.1038/ncomms11999

Xie, R. C., Marcantonio, F., & Schmidt, M. W. (2012). Deglacial variability of Antarctic Intermediate Water penetration into the North Atlantic from authigenic neodymium isotope ratios. *Paleoceanography*, *27*, PA002337. https://doi.org/10.1029/2012PA002337

You, Y. (1998). Intermediate water circulation and ventilation of the Indian Ocean derived from water-mass contributions. *Journal of Marine Research*, *56*(5), 1029–1067. https://doi.org/10.1357/002224098765173455

You, Y., & Tomczak, M. (1993). Thermocline circulation and ventilation in the Indian Ocean derived from water mass analysis. *Deep Sea Research Part I: Oceanographic Research Papers*, *40*(1), 13–56. https://doi.org/10.1016/0967-0637(93)90052-5

Yu, Z., Colin, C., Ma, R., Meynadier, L., Wan, S., Wu, Q., et al. (2018). Antarctic Intermediate Water penetration into the Northern Indian Ocean during the last deglaciation. *Earth and Planetary Science Letters*, *500*, 67–75. https://doi.org/10.1016/j.epsl.2018.08.006

Zahn, R., Winn, K., & Sarnthein, M. (1986). Benthic foraminiferal $\delta^{13}C$ and accumulation rates of organic carbon: *Uvigerina peregrina* group and *Cibicidoides wuellerstorfi*. *Paleoceanography*, *1*(1), 27–42. https://doi.org/10.1029/PA001i001p00027

Chapter 4: North Indian Ocean circulation since the last deglaciation as inferred from new elemental ratios records of benthic foraminifera *Hoeglundina elegans*

As the ocean is the largest external carbon reservoir that can exchange rapidly with atmosphere (Broecker and Peng, 1982), the ocean's carbonate system can be affected by variations in atmospheric CO_2 and ocean circulation. Thus, it plays a crucial role in the global carbon cycle (e.g., Sigman and Boyle, 2000; Ridgwell and Zeebe, 2005; Anderson et al., 2009), and reconstruction of past deep-ocean seawater variations in the global Carbon content and forms could help to better constrain the processes and mechanisms controlling the past global carbon cycle.

In particular, during the last deglaciation, a two-step rapid increase of atmospheric CO_2 occurred during time intervals from 18 to 14.7 cal kyr BP and from 12.8 to 11.7 cal kyr BP (Monnin et al., 2001). Decades of paleoceanographic research suggest that variations of the Southern Ocean circulation played a key role in transferring the deep ocean carbon to the upper ocean and atmosphere during the last deglaciation, by enhancing the upwelling and increasing the northward penetration of the Antarctic Intermediate Water (AAIW) (e.g., Anderson et al., 2009; Marchitto et al., 2007; Skinner et al., 2014). However, the role of AAIW in rapid climate changes resulting from major AMOC as already described in the literature is controversial (e.g., Pahnke et al., 2008; Dubois-Dauphin et al., 2016; Came et al., 2008; Xie et al., 2012; Jung et al., 2009; Pahnke and Zahn, 2005). Thus, studying intermediate waters in the Indian Ocean will allow us to better constrain past changes in the production of intermediate and deep-water and its circulation from the Southern Ocean.

In this chapter, we have investigated two marine cores (MD77-191 and MD77-176) from the Northern Indian Ocean located at intermediate depth, and performed benthic foraminiferal oxygen and carbon isotopes combined with trace element ratios (Mg/Ca, Sr/Ca, Li/Ca and U/Ca) of aragonite benthic species H. elegans to trace the evolution of past intermediate-deep water masses and constrain ocean-atmosphere exchanges during the two-stage increase in atmospheric CO_2 across the last deglaciation.

North Indian Ocean circulation since the last deglaciation as inferred from new elemental ratios records of benthic foraminifera *Hoeglundina elegans*

Ruifang MA[1], Sophie SEPULCRE[1], Franck BASSINOT[2], Frédéric HAURINE[1], Nadine TISNERAT-LABORDE[2], Christophe COLIN[1].

1. GEOPS, Université Paris-Sud, CNRS, Université Paris-Saclay, Rue du Belvédère, 91405, Orsay, France.
2. LSCE/IPSL, CEA CNRS UVSQ, UMR 8212, F-91190 Gif Sur Yvette, France.

Abstract:

The evolution of intermediate circulation in the northern Indian Ocean since the last deglaciation has been reconstructed from two marine cores located at intermediate depths off the southern tip of India (core MD77-191) and in the northern Bay of Bengal (BoB) (MD77-176). Benthic foraminiferal $\delta^{13}C$ and seawater carbonate ion concentration ($[CO_3^{2-}]$) estimated from trace element ratios (Mg/Ca, Sr/Ca, Li/Ca and U/Ca) of aragonite benthic species *Hoeglundina elegans* were used to trace the evolution of past intermediate-deep water masses and constrain ocean-atmosphere exchanges during the two-stage increase in atmospheric CO_2 across the last deglaciation. We show that intermediate water carbonate ion concentration was mainly affected by oceanic alkalinity inventory changes and linked to the modulation of atmospheric CO_2 on glacial-interglacial time scales. Higher benthic foraminiferal $\delta^{13}C$, depleted $[CO_3^{2-}]$ and decreased Benthic-Planktonic age ^{14}C offsets at intermediate water depths suggest a release of deep-sea CO_2 to the atmosphere through the Antarctic Intermediate Water (AAIW) in the Southern Ocean during the 17-15.2 and 12.6-10.5 cal kyr BP time intervals. During the late Holocene, a decrease in the intermediate-water $[CO_3^{2-}]$ indicates the contribution to atmospheric CO_2 rise since 8 cal kyr BP, due to the depleted global ocean alkalinity.

Key words: carbonate ion concentration, benthic elemental ratios, AAIW, deglaciation, atmospheric CO_2, North Indian Ocean

1. Introduction

Atmospheric CO_2 records from ice cores in Antarctica exhibit variations at glacial-interglacial and millennial timescales over the last 800 kyr, that are correlated to global climatic changes (Lisiecki and Raymo, 2005; Luthi et al., 2008). This indicates that the climatic system and, in particular, Earth heat budget and temperature are highly sensitive to variations of greenhouse gas CO_2 (IPCC, 2013). Past variations in the global carbon cycle are, therefore, a key element to understand processes controlling atmospheric CO_2 and its relationships to climate changes. As the ocean is the largest external carbon reservoir that can exchange rapidly with atmosphere, changes in the oceanic carbon pool are strongly linked to past atmospheric CO_2 variations (Broecker and Peng, 1982), with complex feedback relationships. For instance, a decrease in atmospheric CO_2 can drive Earth cooling, and such cooling could in turn results in a further decrease in atmospheric CO_2 by enhancing the carbon solubility and thus carbon storage in ocean waters. This effect led to a net decrease of ~ 15 ppm in atmosphere CO_2 during the glacial period (Sigman and Boyle, 2000; Brovkin et al., 2007; Yu et al., 2014a). The atmospheric CO_2 increases from 180 to 265 ppm during the last deglaciation, as well as millennial abrupt events call for more complex ocean processes, involving changes in the ocean biogeochemistry and circulation. Several previous studies suggested that these atmospheric variations can be linked to processes occurring in the Southern Ocean (e.g., Sigman and Boyle, 2000; Toggweiler et al., 2006; Anderson et al., 2009; Skinner et al., 2014; Poggemann et al., 2018).

The deep ocean is the largest external carbon reservoir of the ocean and it can exchange with the atmosphere at millennial timescale through changes in water mass stratification (Sigman and Boyle, 2000). It has been suggested, for instance, that enhanced Southern Ocean ventilation released CO_2 through the strong upwelling of carbon-rich deep waters during the last deglaciation (Anderson et al., 2009; Bryan et al., 2010; Marchitto et al., 2007; Skinner et al., 2014). This mechanism could explain the two-step increase of atmospheric CO_2 during the last deglaciation (18-10 kyr BP; Monnin et al., 2001). The formation and advection of Antarctic Intermediate Water (AAIW), which is sensitive to westerly winds position and intensity (Ribbe, 2001), likely played a key role in the circulation changes of Southern Ocean during the last deglaciation. Decades of paleoceanography research using benthic foraminifera geochemical proxies have helped to better understand past changes in intermediate and deep water masses circulation in the Atlantic Ocean (e.g., Lynch-Stieglitz et al., 2007; Pahnke et al., 2008; Barbero et al., 2010; Bashmachnikov et al., 2015), the Pacific Ocean (e.g., Pahnke and Zahn, 2005; Bostock et al., 2010) and the north Indian Ocean

(Bryan et al., 2010; Raza et al., 2014; Yu et al., 2018; Ma et al., 2019). These studies all suggested a northward propagation of Antarctic Intermediate Water (AAIW) in Pacific, Atlantic and Indian Oceans at millennial time scales during Heinrich stadial periods (e.g. Mangini et al., 2010; Pahnke et al., 2008; Ma et al., 2019).

Vertical stratification and redistribution of carbon through the ocean and to/from the atmosphere result -or are linked- to changes in the dissolved inorganic carbon system (e.g., Sigman and Boyle, 2000; Ridgwell and Zeebe, 2005; Anderson et al., 2009). Among the dissolved inorganic carbon species, deep-water carbonate ion concentration ($[CO_3^{2-}]$) is a particularly important one as it determines seawater carbonate saturation with respect to the Calcium carbonates deposited in ocean surface sediments (e.g., foraminifer tests, pteropod shells, coccoliths…). Variations in deep-water carbonate ion, by driving changes in the preservation/dissolution of sedimentary carbonate make this carbonate fraction an active player of the ocean and global carbon cycle. Reconstructing past deep-ocean seawater $[CO_3^{2-}]$ variations is mandatory, therefore, to better constrain the processes and mechanisms controlling past global carbon cycle.

The reconstruction of bottom water temperature and carbonate system parameters over geological time from benthic foraminifera elemental/Ca ratios has received increasing attention over recent decades (e.g. Boyle and Keigwin, 1985; Boyle et al., 1995; Yu et al., 2008; Raitzsch et al., 2011; Marchitto et al., 2018). Mg/Ca in benthic foraminifera has been used to reconstruct bottom water temperature changes (e.g., Rosenthal et al., 1997; Lear et al., 2002; Martin et al., 2002; Marchitto et al., 2007; Barrientos et al., 2018), and/or sensitive to the bottom water carbonate ion saturation ($\Delta[CO_3^{2-}]$, defined as the difference between $[CO_3^{2-}]$ and $[CO_3^{2-}]_{sat}$; e.g., Yu and Elderfield, 2008; Rosenthal et al., 2006; Bryan and Marchitto, 2008; Marchitto et al., 2018). Other elemental/Ca ratios, benthic foraminifera Li/Ca and Sr/Ca ratios have been explored to co-vary with both past bottom temperatures and $\Delta[CO_3^{2-}]$ (e.g., Hall and Chan, 2004; Rosenthal et al., 2006; Bryan and Marchitto, 2008; Doss et al., 2018; Marchitto et al., 2018). Most of these studies were devoted to calcitic foraminifera. Only a few studies focused on the benthic foraminifera *Hoeglundina elegans*, since this aragonite specie is not widely found in the sediment due to its higher sensitivity to dissolution than calcitic foraminifera (Rosenthal et al., 2006; Marchitto et al., 2018). Previous works suggest that Mg/Ca, Li/Ca and Sr/Ca in *H. elegans* could be also used as paleo-proxies for both carbonate ion concentration and temperature (e.g., Hall and Chan, 2004; Rosenthal et al., 2006; Bryan and Marchitto, 2008; Marchitto et al., 2018).

In calcitic benthic foraminifera, empirical calibration exercises have shown that the B/Ca ratio is directly linked to bottom water carbonate ion concentration (e.g., Yu and Elderfield, 2007; Brown et al., 2011; Yu et al., 2010a). Previous works seem to show that benthic foraminiferal U/Ca, Li/Ca,

Sr/Ca are promising marine dissolved carbon/carbonate system proxies, have been conducted for deep-sea benthic species (Bryan and Marchitto, 2008; Raitzsch et al., 2011; Keul et al., 2013; Yu et al., 2014b), impacting our ability to fully reconstruct intermediate and deep-water link to global carbon cycle (Came et al., 2008; Yu et al., 2008; Makou et al., 2010; Poggemann et al., 2017). In addition, most of these applications studies of elemental ratios have focused on the Atlantic Ocean (e.g., Yu et al., 2008; Makou et al., 2010; Poggemann et al., 2017). As the Northern Indian Ocean plays an important role in global ocean circulation in terms of deep-water ventilation or stratification (e.g., Ahmad et al., 2008, 2012; Bryan et al., 2010; Raza et al., 2014), it has received increasing attention over recent decades (e.g., Bryan et al., 2010; Sijinkumar et al., 2016; Yu et al., 2018; Ma et al., 2019). However, there are no continuous and high-resolution benthic foraminiferal elemental ratios records that have been reported from this area.

In this study, we investigated benthic and planktonic foraminifera $\delta^{13}C$, $\delta^{18}O$, and elemental ratios of benthic foraminifera from two cores located at intermediate water depths off the southern tip of India and in the Northeastern BoB, to better constrain the temporal evolution of the source and ventilation of intermediate water mass in the northern Indian Ocean and, in particular, track the northward penetration of AAIW over the last 17 cal kyr BP.

2. Material and hydrological setting

Cores MD77-191 and MD77-176 were collected respectively in the southern tip of India in the edge of Arabian Sea (07°30'N-76°43'E, 1254 m water depth), and in the Northeastern BoB (14°30'5N-93°07'6E, 1375 m water depth) during the OSIRIS III cruise of the N.0 *Marion Dufresne* in 1977 (Fig.1).

Today, the surface water masses above 150m in the Arabian Sea correspond to the Arabian Sea high Salinity Water (ASHS; salinity 36.5 psu) (Talley et al., 2011). By contrast, in the Bay of Bengal, the surface water shallower than 100m, the Bay of Bengal surface water (BoBSW) is much fresher (salinity ~31 psu) because of the considerable river input (Talley et al., 2011). The surface mixed layer and the boundary currents in the Arabian Sea and in the BoB are directly controlled by wind forcing and display, therefore, changes related to the seasonal reversal of the Indian monsoon wind system (Fig. 1). The surface waters at the site of cores MD77-191 and MD77-176 are a mix of high salinity Arabian Sea Surface Water and low salinity Bay of Bengal Water, respectively (Tomczak and Godfrey, 2003; Talley et al., 2011). MD77-191 is also located in the summer

upwelling area of the Arabian Sea, and the average depth of the permanent thermocline is around 100m (Ravichandran et al., 2012).

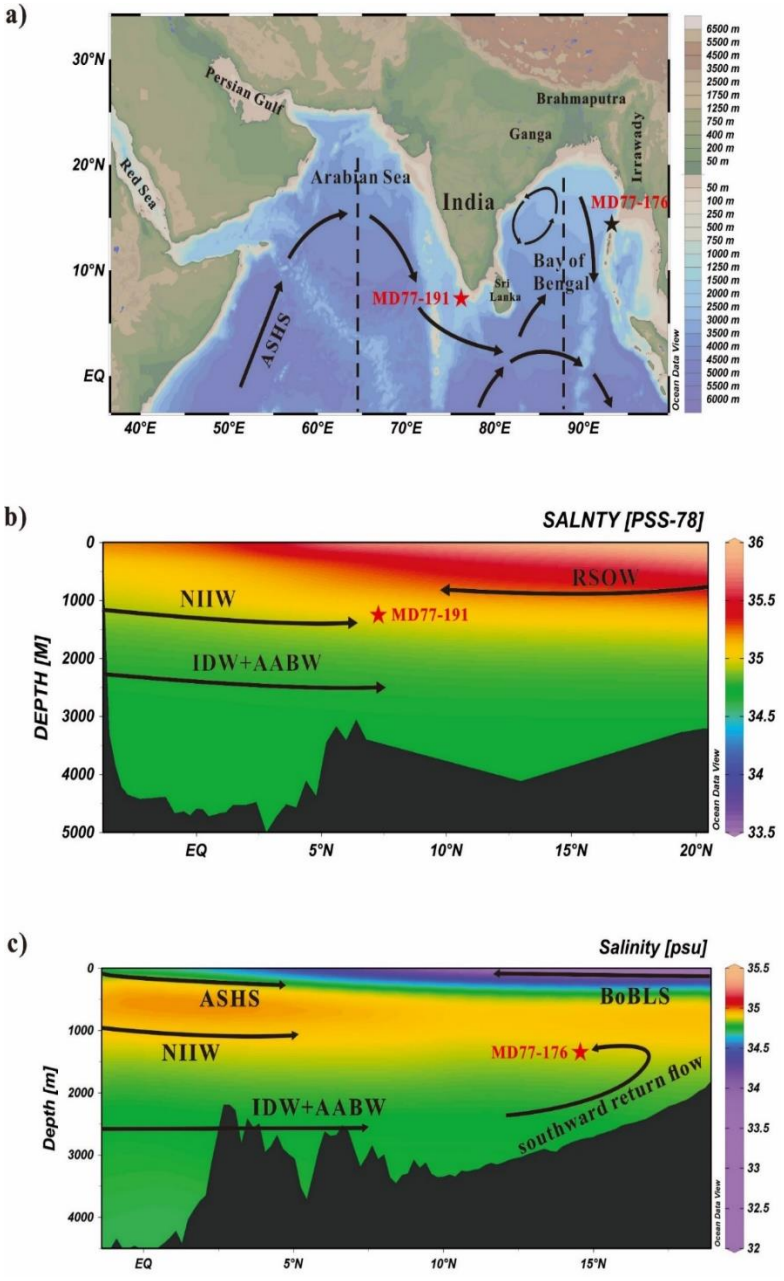

Fig. 1. *(a) Geographical setting, locations of MD77-191 (red star) in the Arabian Sea and MD77-176 (black star) in the Bay of Bengal. The black arrows are the general surface circulation direction in the Northern Indian Ocean drifted by Southwest Monsoon (Schott and McCreary, 2001). (b) and (c) Salinity (psu, coloured shading) depth-latitude section using the Ocean Data View (ODV) software (Schlitzer, 2015) and vertical distribution of water masses in the Arabian Sea and Bay of Bengal (N-S cross section). ASHS: Arabian Sea High Salinity Water, NIIW: North*

Indian Intermediate Water, RSOW: Red Sea Water, NADW: North Atlantic Deep Water, BoBLS: Bay of Bengal low salinity Water, AABW: Antarctic Bottom Water, IDW: Indian Deep Water.

The main intermediate water masses in the Indian Ocean are the Antarctic Intermediate Water (AAIW), the Red Sea Water (RSOW) and the Indonesian Intermediate Water (IIW) (You, 1998; Talley et al., 2011). The northward extension of AAIW in the Indian Ocean reaches only as far as 10°S in the modern Indian Ocean (Lynch-Stieglitz et al., 1994). The Red Sea Water is a high salinity intermediate water and fills the Arabian Sea (between 400 and 1400m) (Beal et al., 2000; Talley et al., 2011). RSOW spreads eastward to the eastern boundary at 5°N and flows through much stronger western boundary toward the Agulhas (You, 1998; Beal et al., 2000; Talley et al., 2011). Thus, RSOW could affect MD77-191 core site at the southern tip of India, but should have only a small contribution in the Bay of Bengal at core MD77-176 site. IIW originates from the Pacific Central Water and enters the BoB via the Indonesian through flow. IIW flows clockwise at thermocline levels in the BoB (You, 1998).

The deep water masses of the Northern Indian Ocean are characterized by a mixture of Atlantic and Antarctic water masses (Reid, 2003; Talley et al., 2011). Between 1200 and 3800m, the dominant deep water in the North Indian Ocean is Indian Deep Water (IDW), originating from the Circumpolar Deep Water and NADW (You and Tomczak, 1993; Tomczak and Godfrey, 2003). Below 3800m, the abyssal basins are bathed chiefly by the Antarctic Bottom Water (AABW) (Reid, 2003; Tomczak and Godfrey, 2003). However, AABW only reaches the southern part of the BoB as most the bay is shallower than 4000m (Tomczak and Godfrey, 2003). In the BoB, the bottom water upwells when it moves northward (Talley et al., 2011), thus changes in bottom waters are transferred upward to shallower water masses.

3. Methods

3.1. $\delta^{18}O$ and $\delta^{13}C$ analyses

Stable oxygen ($\delta^{18}O$) and carbon ($\delta^{13}C$) isotope measurements were performed on well-preserved (clean and intact) samples of the planktonic foraminifera *Globigerinoides ruber* (250-315 µm fraction) and the endo-benthic foraminifera *Uvigerina peregrina* (250-315 µm fraction) on core MD77-191. As *U. peregrina* is an infaunal benthic foraminiferal species, the $\delta^{13}C$ values may reflect pore water isotopic compositions rather than deep-water signature. In order to get a high-

resolution benthic $\delta^{13}C$ records that would reflect more accurately bottom water changes, epi-benthic foraminifera *Cibicidoides wuellerstorfi*, and *Cibicidoides pachyderma* were also analyzed. These stable isotopes analyses had been performed on approximately 4 to 8 clean and well-preserved specimens per sample on a Finnigan MAT 251 mass spectrometer at the Laboratoire des Sciences du Climat et de l'Environnement (LSCE, France). Both $\delta^{18}O$ and $\delta^{13}C$ values are presented relative to the Pee Dee Belemnite (PDB) scale through calibrations performed with standards from the National Bureau of Standards (NBS). The mean external reproducibility of carbonate standards is ±0.05‰ for $\delta^{18}O$ and ±0.03‰ for $\delta^{13}C$.

3.2.Analytical protocols of elemental ratios

Mg/Ca, Sr/Ca, U/Ca and Li/Ca ratios were measured in shells of the epi-faunal benthic foraminifera *H. elegans* from cores MD77-191 and MD77-176. *H. elegans* is an epi-faunal species that growths on the sediment-seawater interface, minimizing the influence of pore water composition on the elemental ratios (Lutze and Thiel, 1989). Each sample contained approximately 8-15 individual foraminifers larger than 250µm. The foraminifera tests were crushed open between two glass plates. The resulting fragments were ultrasonically cleaned to remove clays, and then submitted to oxidative and reductive protocols to remove organic matter and oxides following methods described by Boyle and Keigwin (1985) and Barker et al., (2003). Samples were dissolved in 0.075N HNO_3 and analyzed using a single collector sector field high resolution inductively coupled plasma mass spectrometer (HR-ICP-MS) Thermo Element XR hosted at the Laboratory GEOPS (University Paris-Sud, France).

Instrumental settings for trace element analyses are listed in Table 1. The instrument sensitivity was optimized daily using 100 ppt tuning standard solutions. Given the limited amount of solution obtained after dissolution of foraminifera samples, we used a high efficiency PFA MicroFlow Nebulizer (ES-2000-3503-080) resulting in an uptake rate of 50 µl/min. One measurement requires 1ml solution at a calcium concentration of both ~ 1 ppm and 50 ppm.

We prepared two series of mother standard solutions for elemental ratio analyses. First six standard solutions are Mn, Al and Fe mixtures with linear Ca concentration (0.5-7 ppm) to get more precise Ca concentration dilutions for the second run. Then, seven multi-element stock standard solutions (J0-J6) were prepared gravimetrically by spiking a 1000 µg/ml Ca standard with appropriate amounts of Mg, Sr, Cd, Li, B, Ba and U mono-elemental 1000 µg/ml certified ICP-MS grade stock solutions. The ratios of stock solutions were spaced linearly to contain the natural ratio

ranges expected in both planktonic and benthic foraminifers. Working mother standards were made by diluting the stock standard solutions with 0.1N HNO_3 to get calcium concentrations of 50 ppm.

Table 1. *ICP-MS settings for elemental ratios determinations.*

Parameter	Trace element mode
Plasma RF power	1200
Nebulizer	ES-2000-3503-080
Spray chamber	Twister Spray Chamber with Helix
Injector	2.0 mm QUARTZ INJECTOR
Sample cone	Ni
Skimmer cone	Ni "H" high performance
Sample matrix	0.1N HNO_3
Uptake time	50s
Analysis time	490s
Washout time	40s
Mass resolution	Low (Li, B, Cd, Ba, U), Medium (Mg, Al, Sr) and High (Ca, Mn, Fe)
Runs	10
Passes	6
Detection mode	Tripple (analog, counting, faraday)

Sample solutions were systematically adjusted at 50 ppm Ca through dilution using 0.1N HNO_3. A blank consisting of the same 0.1N HNO_3 used to dilute the standards and samples is also analyzed. The elemental blanks are better than ±0.14% for Mg, ±0.02% for Sr, ±5.3% for Li and ±0.05% for U. All raw intensities (including standards) are corrected by removing the specific blank intensity values. Drift corrections during the course of daily analyses were performed through bracketing and linear regression estimated using standards interspersed every four samples. Standard curves are used to calculate elemental/Ca ratios, coefficients of determination (r^2) are always >0.9999 for all elemental ratios. The mean reproducibility and accuracy is Mg/Ca 2%, Sr/Ca 0.9%, Li/Ca 0.2% and U/Ca 3.5%.

4. Chronological framework of studied cores

The age model of core MD77-191 was established by using 9 monospecific planktonic foraminifer *G. bulloides* accelerator mass spectrometry (AMS) ^{14}C dating (Bassinot et al., 2011),

one ^{14}C date made on pteropods (Mléneck et al., 1997), and three ^{14}C dates obtained on planktonic foraminifera *Globigerinoides ruber* measured with the *ECHo*MICADAS at the LSCE, France (Table 2). The ^{14}C ages were converted to calendar ages by using the CALIB Rev. 7.1 software (Stuiver and Braziunas, 1993), the marine calibration data set (Reimer et al., 2013), and correcting for a surface marine reservoir of around 400 years. Core MD77-191 provides a continuous record since the last 17 kyr BP with an average sedimentation rate of about 53 cm/kyr and up to 90 cm/kyr for the Holocene.

Table 2. *Calibrated AMS ^{14}C age determined on planktonic (10 data taken from Bassinot et al., 2011). ^{14}C ages were converted into calendar years (cal. yr BP, BP = AD 1950) by using the Calib Rev. 7.1 software (Stuiver and Braziunas, 1993).*

Depth(cm)	Calendar age (yr B.P.)	Taxa	^{14}C age (yr)	1 Sigma error (±yr)
28	1526	*G. bulloides*	1970	60
76	2226	*G. bulloides*	2560	70
127	2797	*G. bulloides*	3020	60
175	3567	*G. bulloides*.	3660	60
222	4236	*G. bulloides*	4160	60
271	5070	*G. bulloides*	4790	60
373	6582	*G. bulloides*	6150	80
425	8757	*G. bulloides*	8230	90
482	9648	*G. bulloides*	8970	80
550	11294	*G. ruber*	10300	50
580	13285	*G. ruber*	11810	50
594	14258	*Pteropods* sp.	12630	190
710	16142	*G. ruber*	13820	60

The age model of core MD77-176 was previously established by using 31 planktonic foraminifer (*G. ruber*) AMS ^{14}C dates combined with the MD77-176 oxygen isotope record obtained on planktonic foraminifera *G. ruber*, which was correlated to the GISP2 Greenland ice core record (Marzin et al., 2013). Core MD77-176 displays high accumulation rates (average ~25 cm/kyr and up to 40 cm/kyr for the Holocene), and provide a high-resolution record since 40 cal kyr BP.

5. Results

5.1. Stable isotope results

Stable isotope analyses were performed on planktonic foraminifera *G. ruber*, benthic *C. pachyderma*, *C. wuellerstorfi* and *U. peregrina* from core MD77-191 in order to produce the most complete records. Benthic $\delta^{18}O$ were obtained from *U. peregrina* which is known to record the calcite $\delta^{18}O$ at equilibrium (e.g., Shackleton, 1974). Most of the benthic $\delta^{13}C$ record was obtained from *C. wuellerstorfi*. In order to get a higher resolution, we corrected the $\delta^{13}C$ results from *C. pachyderma* to *C. wuellerstorfi* by using the average difference of 0.27‰ between both species obtained from 19 pair measurements of samples where the two species co-existed (Table 3).

Table 3. *Stable isotope data (per mil versus PDB) from the core MD77-191 of Cibicidoides pachyderma and Cibicidoides wuellerstorfi in the same levels to assess the vital effect and microhabitat effect for $\delta^{18}O$ and $\delta^{13}C$, respectively.*

Depth (cm)	$\delta^{13}C$ (‰ vs.PDB)		$\delta^{18}O$ (‰ vs.PDB)	
	Cibicidoides wuellerstorfi	*Cibicidoides pachyderma*	*Cibicidoides wuellerstorfi*	*Cibicidoides pachyderma*
40	0.28	0.07	1.87	2.02
160	0.31	0.01	1.87	1.90
170	0.15	-0.03	1.91	2.01
230	0.39	-0.03	1.84	2.00
260	0.48	0.08	2.05	2.02
270	0.34	0.05	2.01	2.20
290	0.51	0.07	1.94	2.04
300	0.51	0.05	2.11	2.05
320	0.28	0.03	1.78	1.94
330	0.37	0.03	2.10	2.04
340	0.39	0.05	2.04	2.04
350	0.39	0.05	2.07	2.06
370	0.38	-0.01	1.97	2.05
380	0.41	0.00	2.06	2.13
390	0.26	0.12	2.02	2.20
410	0.29	-0.09	2.11	2.27
720	0.22	0.06	2.48	2.64
730	0.28	0.30	2.08	2.73
750	0.11	0.36	3.54	2.92

The $\delta^{18}O$ of *G. ruber* was enriched during the last deglaciation compared with the Holocene (Fig. 2). A marked maximum in *G. ruber* $\delta^{18}O$ is evident during the early deglaciation, reaching -0.7‰ at

16 cal kyr BP. After that, the $\delta^{18}O$ displays a general decrease and reaches more depleted during the Holocene with the average ~ -2.58‰. In addition, the general trend is punctuated by higher values around ~ -1.53‰ in the interval 12.6-10.5 cal kyr BP (the late deglaciation).

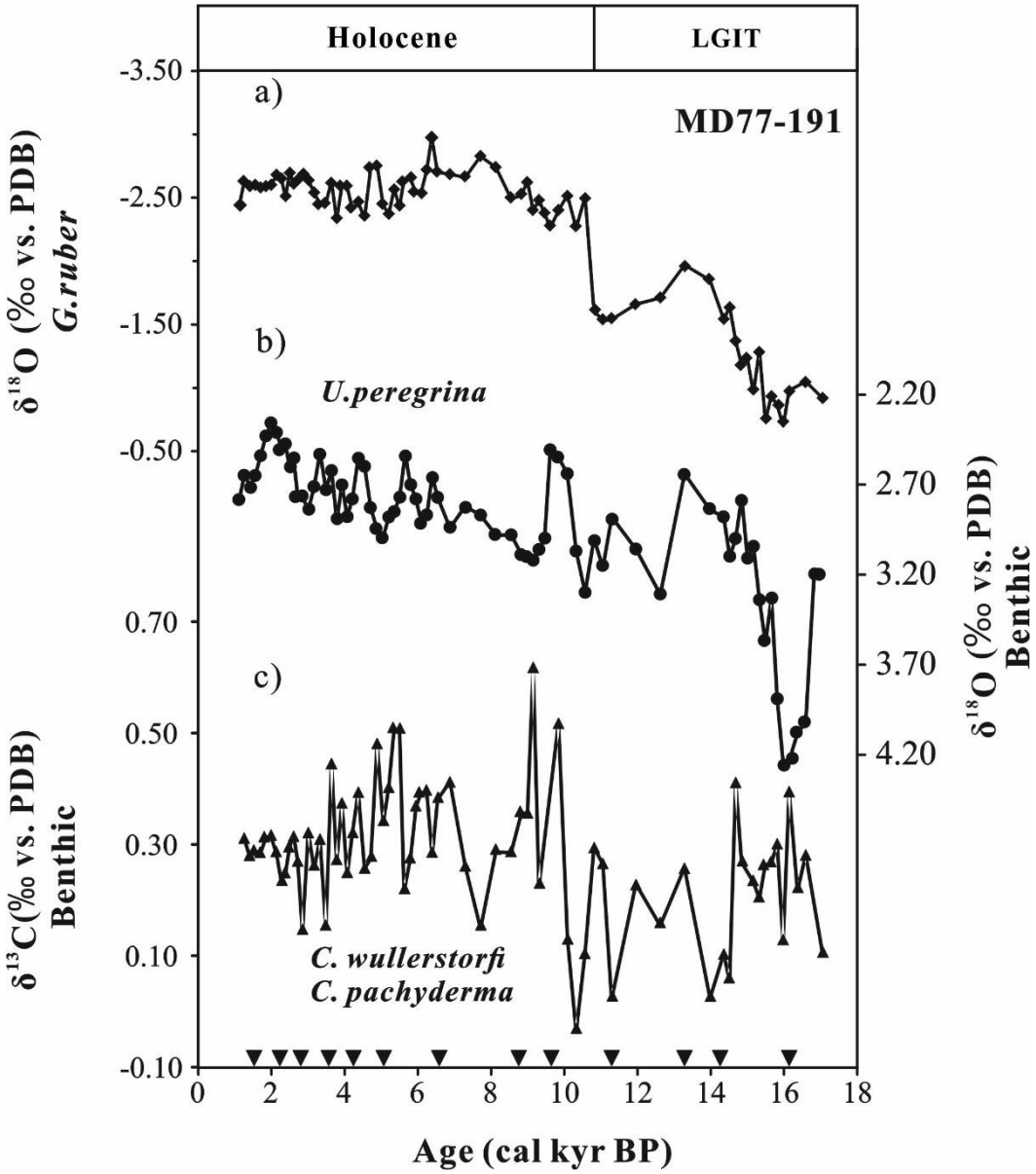

Fig. 2. *(a) $\delta^{18}O$ records of the planktonic foraminifera G. ruber, (b) benthic $\delta^{18}O$ and (c) $\delta^{13}C$ records for MD77-191. The black inverted triangles represent the ^{14}C calculated calendar age points (Bassinot et al., 2011). LGIT: Last glacial-interglacial transition.*

For core MD77-191, down-core benthic $\delta^{18}O$ values range between 2.36 to 4.25‰ (Fig. 2). The most enriched $\delta^{18}O$ value (4.25‰) was found during the last deglaciation period (16 cal kyr BP), whereas the most depleted (2.36 ‰) occurs in the late Holocene (2.36 cal kyr BP). In the late part of

the deglaciation, the $\delta^{18}O$ shows a shift towards higher values around ~3‰ in the interval 12.6-10.5 cal kyr BP. This interval is followed by a decrease of $\delta^{18}O$ from 10 cal kyr BP to the core top (mean value of 2.75‰).

The *Cibicidoides* $\delta^{13}C$ values of core MD77-191 range from -0.04 to 0.62‰ (Fig. 2). During the last deglaciation, the *Cibicidoides* $\delta^{13}C$ values increased during the time intervals 17-15.2 and 12.6-10.5 cal kyr BP and decreased (~0.03‰) at around 15-13.3 cal kyr BP. From 10.3 to about 9 cal kyr BP, the *Cibicidoides* $\delta^{13}C$ record suggests large oscillations with high peak values (0.52-0.62‰) at around 9.8-9.1 cal kyr BP. Then, the $\delta^{13}C$ records display a decrease during the middle and late Holocene, the mean value of *Cibicidoides* $\delta^{13}C$ is at ~0.31‰.

5.2. Elemental ratios

To check the robustness of our results and potential diagenetic imprint (i.e. oxides), the Mn/Ca ratio was systematically measured. It ranges between 6.5-10 µmol/mol, which is much lower values than the 100 µmol/mol threshold proposed by Boyle (1983) to sort out sample results and eliminate trace element results that chiefly reflect the presence of oxides. Barker et al. (2003) also suggested to check for potential clay contamination, with an Al/Ca <0.5 mmol/mol. All Al/Ca results are below 0.2 mmol/mol, indicating a good sample cleaning, and thus no sedimentary clay contamination.

Mg/Ca, Sr/Ca, Li/Ca and U/Ca ratios of core MD77-191 range from 0.5-1.5 mmol/mol, 0.8-2.1 mmol/mol, 2.7-6.4 µmol/mol and 7.4-34.1 nmol/mol, respectively (Figs.3a-d). All these elemental ratios display a minimum during the 17-15.2 cal kyr BP time interval, with average values of Mg/Ca (~0.8 mmol/mol), Sr/Ca (~1.4 mmol/mol), Li/Ca (~3.9 µmol/mol), and U/Ca (~15.1 µmol/mol). Elemental ratios display higher values in the 15-13.3 cal kyr BP interval, and the most enriched values of Mg/Ca (1.5 mmol/mol), Sr/Ca (2.1 mmol/mol). Li/Ca (6.4 µmol/mol), U/Ca (34.1 µmol/mol) occur during this time interval. Then, the Mg/Ca, Sr/Ca, Li/Ca and U/Ca records generally show a continuous decrease throughout the deglaciation until the late Holocene. The lowest values are found in the late Holocene with mean values of Mg/Ca, Sr/Ca, Li/Ca and U/Ca reaching 0.6 mmol/mol, 1.0 mmol/mol, 3.5 µmol/mol and 17.3 µmol/mol, respectively. However, the continuous decrease is interrupted by an increase during the early Holocene (10.3-9 cal kyr BP).

For core MD77-176 located in the BoB, *H. elegans* Mg/Ca and Sr/Ca values range between 0.35 and 0.82 mmol/mol, and from 0.55 to 1.32 mmol/mol, respectively. The *H. elegans* Mg/Ca and Sr/Ca records from core MD77-176 show a strong covariation (Figs.3e-f). The most enriched Mg/Ca (0.82 mmol/mol) and Sr/Ca (1.32 mmol/mol) values occurred during the last deglaciation

(11.7-11.5 cal kyr BP). From 17 to about 12.5 cal kyr BP, the Mg/Ca and Sr/Ca records exhibit a succession of oscillations with a first minimum (0.39 and 0.7 mmol/mol, respectively) occurring between 17 and 15.4 cal kyr BP, and a second shorter low (0.54 and 0.68 mmol/mol, respectively) between 13.4 and 12.5 cal kyr BP. During the Holocene, the values of Mg/Ca and Sr/Ca decrease continuously to reach a minimum at the end of Holocene.

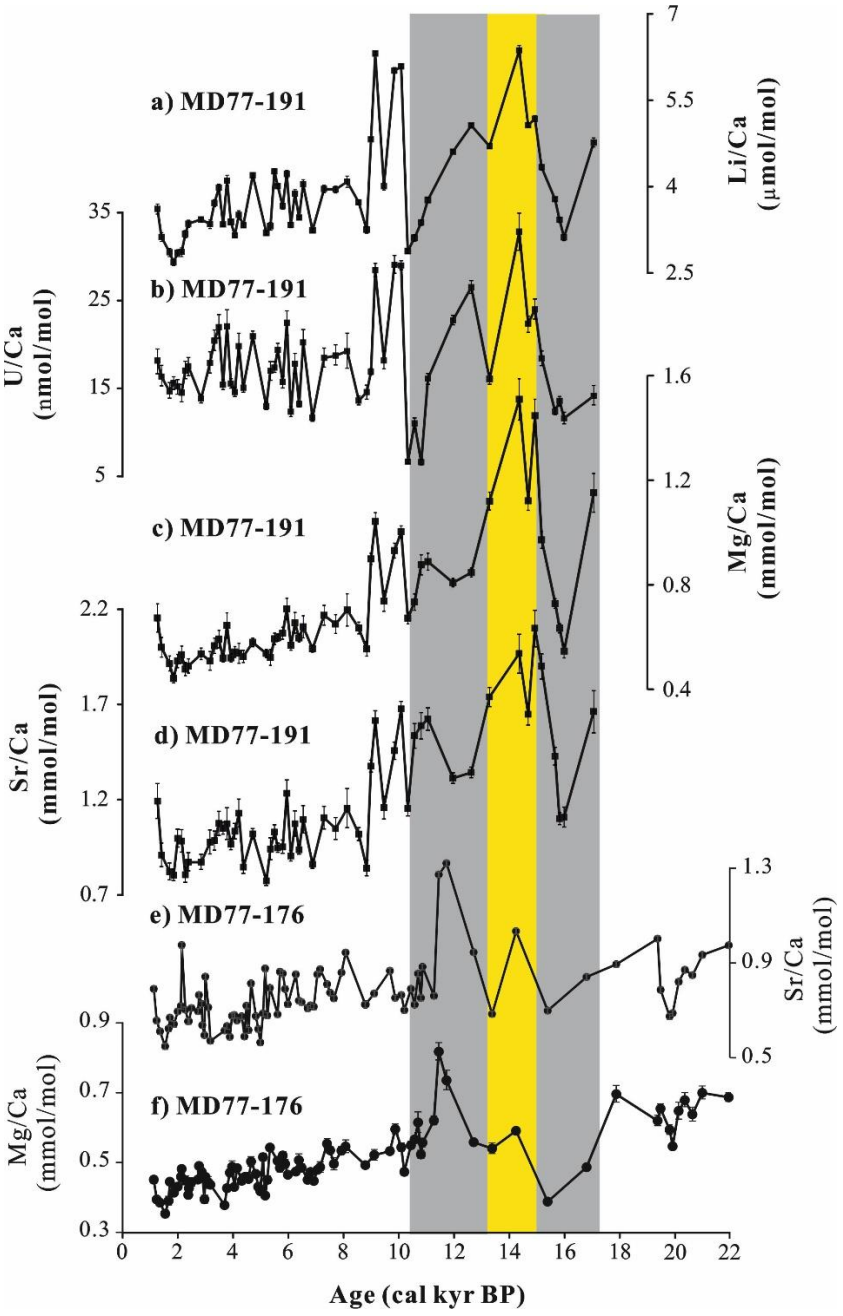

Fig. 3. *Comparison of benthic foraminifera H. elegans elemental ratios. (a)-(d) MD77-191 Mg/Ca, Sr/Ca, Li/Ca and U/Ca; (e)-(f) MD77-176 Sr/Ca and Mg/Ca. The grey-shaded intervals mark the two-step increase in atmospheric CO_2, the yellow-shaded interval marks the 15-13.3 cal kyr BP interval.*

6. Discussion

6.1. Reconstruction of past [CO_3^{2-}] variations

6.1.1. Temperature versus carbonate ion effects

Following the previous works, the influences of benthic foraminiferal elemental ratios are not well understood. Several studies obtained from aragonite benthic specie *H. elegans*, Rosenthal et al. (2006) proposed that the Mg/Ca and Sr/Ca of *H. elegans* may reflect a combination effect of [CO_3^{2-}] and bottom water temperature when the degree of $\Delta[CO_3^{2-}]$ is below 15 µmol/mol. Both calcite and Aragonite benthic species Li/Ca ratio were also suggested to reflect the changes of saturation state and bottom plaeotemperature (Hall and Chan, 2004; Marriott et al., 2004; Lear and Rosenthal, 2006; Lear et al., 2010). As already observed in previous studies (Bryan and Marchitto, 2008; Marchitto et al., 2018), by contrast to the Mg/Ca and Li/Ca ratios of *H. elegans*, Mg/Li ratio shows a better correlated to bottom-temperature. Thus, *H. elegans* Mg/Ca and Li/Ca could be used as paleo-proxies for both carbonate ion concentration and temperature (e.g., Rosenthal et al., 2006; Bryan and Marchitto, 2008; Marchitto et al., 2018).

The benthic foraminiferal $\delta^{18}O$ can record the changes in local temperature, ice-volume and salinity. We used the ice-volume related, global seawater $\delta^{18}O$ estimate of Bintanja and Wal (2008) to correct our benthic $\delta^{18}O$ record for ice volume changes. Thus, we suggest that the resulting corrected $\delta^{18}O_{sw\text{-}ivc}$ record indicates mostly deep water paleo-temperature and/or salinity variations. In the modern ocean, Red Sea Water (RSOW) flows through much stronger western boundary toward the Agulhas compared with eastward flows to the eastern boundary at 5°N (You, 1998; Beal et al., 2000; Talley et al., 2011). Thus, core MD77-191 (located in the eastern Arabian Sea) may be influenced by the RSOW, which is characterized by high salinity (Beal et al., 2000; Talley et al., 2011). However, core MD77-176 site in the northeastern BoB should have no or limited influence of RSOW (Talley et al., 2011). Thus, we compared the $\delta^{18}O_{sw\text{-}ivc}$ records obtained from core MD77-176 and MD77-191 to estimate the influence of high salinity of RSOW (Figs.4a-b). The comparison of benthic oxygen records since the 17 cal kyr BP seems not obvious clarifies the influence of high salinity and/or temperature.

H. elegans Mg/Li ratio has been suggested to be a better correlated to the bottom temperature in positive relationship (R^2=0.95) compared with the Mg/Ca or Li/Ca (Bryan and Marchitto, 2008; Marchitto et al., 2018). However, according to the equation established by Marchitto et al. (2018), there was a flat part of the exponential curve in the cold part (related to Mg/Li ~0.1-0.3 mol/mmol),

showing a less sensitivity compared with the higher temperature. In addition, the *H. elegans* Mg/Li from core MD77-191 ranges between 0.14-0.28 mol/mmol (Fig.4c), which is corresponding to the less sensitivity cold end part. Thus, we keep use the Mg/Li raw data to show the variations of intermediate water temperature from core MD77-191. In addition, we compared the trend of *H. elegans* Mg/Li results from core MD77-191 with other intermediate water paleo-temperature (IWT) record obtained from the tropical West Atlantic Ocean, which was calculated by using *Uvigerina* spp. Mg/Ca ratios (Core M78/1-235-1, 11°36.53'N-60°57.86'W, 852 m water depth; Poggemann et al., 2018; Figs.4c-d). Fore core MD77-191, *H. elegans* Mg/Li record displays higher values in the 15-13.3 cal kyr BP interval, and shows decreasing trend during 17-15.2 and 12.6-10.5 cal kyr BP intervals, which may indicate colder intermediate water temperature compared with 15-13.3 cal kyr BP interval (Fig.4c). Then, the Mg/Li record generally shows a continuous decrease during the Holocene, and shows a good in agreement with the tropical W-Atlantic Ocean ITW record at the Holocene period (Fig.4c). During the last deglaciation the tropical W-Atlantic Ocean ITW record generally displays an increased trend at the 17-15.2 and 12.6-10.5 cal kyr BP intervals, may indicating the heat transport via AAIW. However, the tropical W-Atlantic Ocean ITW record has a much higher resolution by contrast to our Mg/Li results from core MD77-191, thus, it seems difficult to compare these two records during the last deglaciation.

The influence of [CO_3^{2-}] can be tested by using the other elemental proxies. The U/Ca of both calcite benthic calcite and planktonic foraminifera shows a negative correlation with [CO_3^{2-}] (Raitzsh et al., 2011; Russell et al., 2004; Keyl et al., 2013). Uranium speciation and solubility could be also additionally influenced by the redox state, as pore water has a much lower oxygen concentration, and leading to more depleted uranium concentration than bottom water (Barnes and Cochran, 1990). However, we performed the analyses on epi-benthic *H. elegans* in this study, therefore we do not expect a major effect of the redox state on U/Ca records. Even through there is no U/Ca studies performed on the *H. elegans*, it seems reliable that U/Ca ratio could represent a potential alternative to the B/Ca ratio to reconstruct bottom water [CO_3^{2-}]. Furthermore, Yu et al. (2014b) demonstrated that benthic species *Cibicidoides* genera, *Uvigerina* spp., *H. elegans* Sr/Ca could be used as a proxy to reconstruct deep water [CO_3^{2-}]. In addition, in cores MD77-191 and MD77-176, Mg/Ca and Sr/Ca records obtained on *H. elegans* strongly co-vary (Fig. 3). Records of Mg/Ca, Sr/Ca, Li/Ca and U/Ca from core MD77-191 show similar variations over the last 17 cal kyr BP (Fig.3). Thus, we suggest that the records of benthic elemental ratios (Mg/Ca, Sr/Ca, Li/Ca and U/Ca) seem to be mainly induced by the carbonate ion concentration changes.

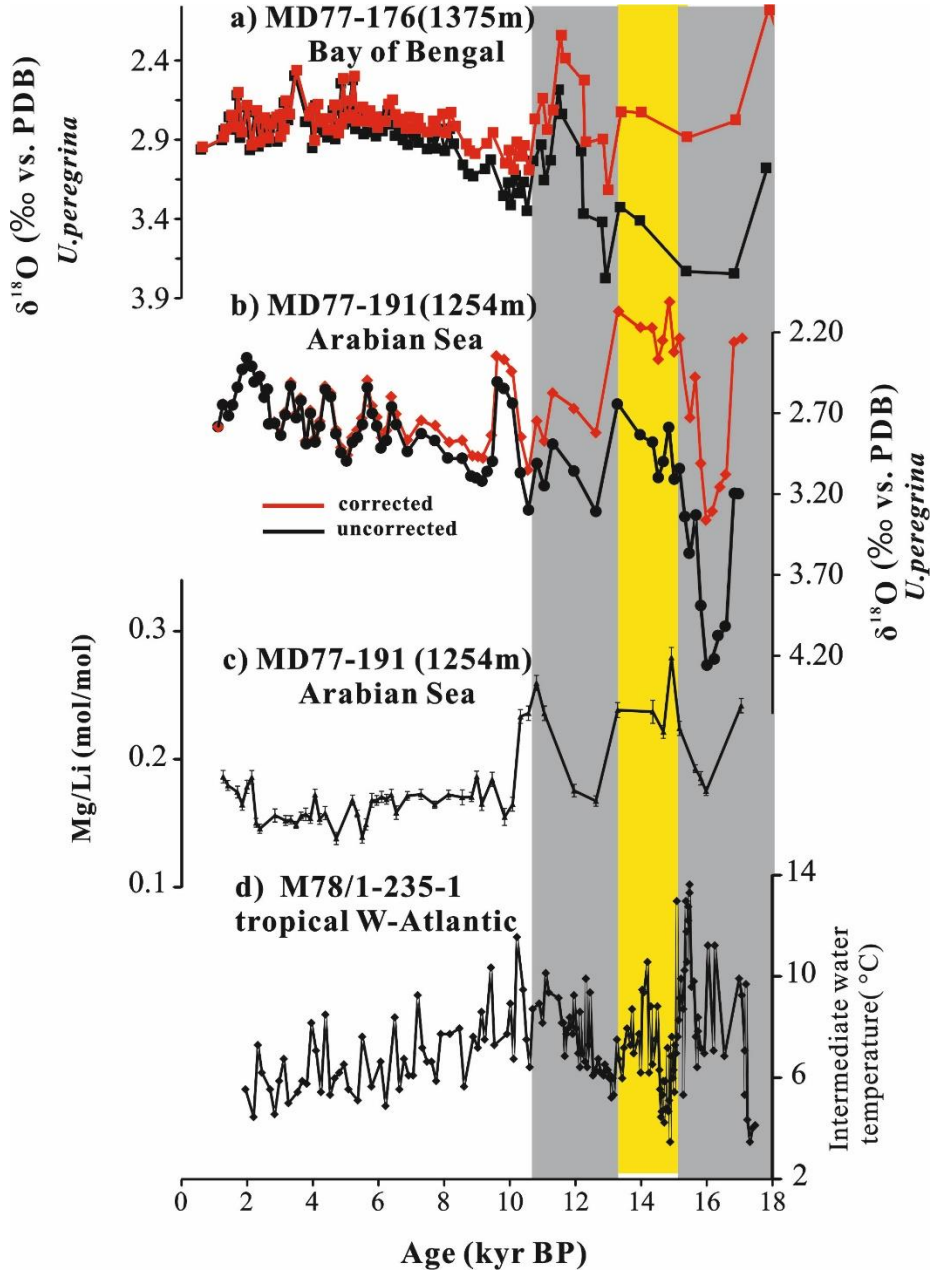

Fig. 4. *a) and b) benthic $\delta^{18}O$ obtained from MD77-176 (Bay of Bengal) and MD77-191 (Arabian Sea), respectively, The uncorrected benthic $\delta^{18}O$ is black line and correct benthic $\delta^{18}O$ by using the global ice volume $\delta^{18}O$ is red line; c) H. elegans Mg/Li ratios obtained from core MD77-191; d) IWT record based on the $Mg/Ca_{uvigerina}$ obtained from core M78/1-235-1 in the tropical W-Atlantic Ocean (Poggemann et al., 2018). The colour-shaded intervals are the same as in Figure 3.*

6.1.2. Calculation of past $[CO_3^{2-}]$

Records of Mg/Ca, Sr/Ca, Li/Ca and U/Ca from MD77-191 and of Mg/Ca and Sr/Ca from MD77-176 seem to be more sensitive to the variations of the $[CO_3^{2-}]$ concentrations. Studies of

benthic foraminifera U/Ca variations measured on calcite epifaunal species *C. wuellerstorfi*, *Cibicidoides mundulus* and *Ammonia* sp., showed a negative correlation with bottom water carbonate ion concentration (Raitzsch et al., 2011; Keul et al., 2013). However, to our knowledge, no such comparison work exists for aragonite benthic species *H. elegans*.

In addition, as mentioned before, *H. elegans* Sr/Ca could covary with $\Delta[CO_3^{2-}]$ bottom water when $\Delta[CO_3^{2-}]_{aragonite}$ is below 15 µmol/mol, and then being less sensitive with relatively constant values above 15 µmol/mol (Rosenthal et al., 2006). Yu et al. (2014b) summarized the literature calibration data of Sr/Ca for *C. wuellerstorfi*, *C. mundulus*, *Uvigerina* spp. and *H. elegans*. Although not yet tested thoroughly, they proposed that the benthic Sr/Ca may be used as an auxiliary proxy for sea water $\Delta[CO_3^{2-}]$. We collected the literature core-top data of paired $\Delta[CO_3^{2-}]_{aragonite}$ with *H. elegans* Sr/Ca at intermediate water depth (500-1500 m) (Rosenthal et al., 2006; Yu et al., 2014b) and plotted these Sr/Ca values together. Our database shows a positive relationship between Sr/Ca and bottom water $\Delta[CO_3^{2-}]_{aragonite}$ (Fig.5). When combined, the linear relationship between Sr/Ca and $\Delta[CO_3^{2-}]$ shows a sensitivity of 0.0167 mmol/mol of Sr/Ca per µmol/kg of $\Delta[CO_3^{2-}]$.

In order to compare our reconstructions with other records of $[CO_3^{2-}]$ obtained from B/Ca, we calculated the deep water $\Delta[CO_3^{2-}]$ from the *H. elegans* Sr/Ca by using the equation defined before: At $\Delta[CO_3^{2-}]_{aragonite}$ obtained from intermediate water depth (500-1500 m), Sr/Ca= -0.0002 $\Delta[CO_3^{2-}]^2_{aragonite}$ + 0.0292 $\Delta[CO_3^{2-}]_{aragonite}$ + 1.3189 (r^2=0.85). Seawater $[CO_3^{2-}]_{sat}$ is mainly affected by salinity, temperature and water depth (pressure). We calculated the $[CO_3^{2-}]_{sat}$ at the studied sites by using CO_2sys.xls (Ver. 12) (Pelletier et al., 2005).

The combined effects of salinity, temperature and pressure on the $[CO_3^{2-}]_{sat}$ are about ±0.5 µmol/kg on glacial-interglacial timescales, remaining roughly unchanged in the deep ocean at glacial-interglacial timescales (Yu et al., 2008; 2014a). Thus, we can make the calibration of the sea water $[CO_3^{2-}]$ concentration and reconstruct the paleo-$[CO_3^{2-}]$ of the intermediate water at our core sites based on the equation of $\Delta[CO_3^{2-}]=[CO_3^{2-}] - [CO_3^{2-}]_{sat}$.

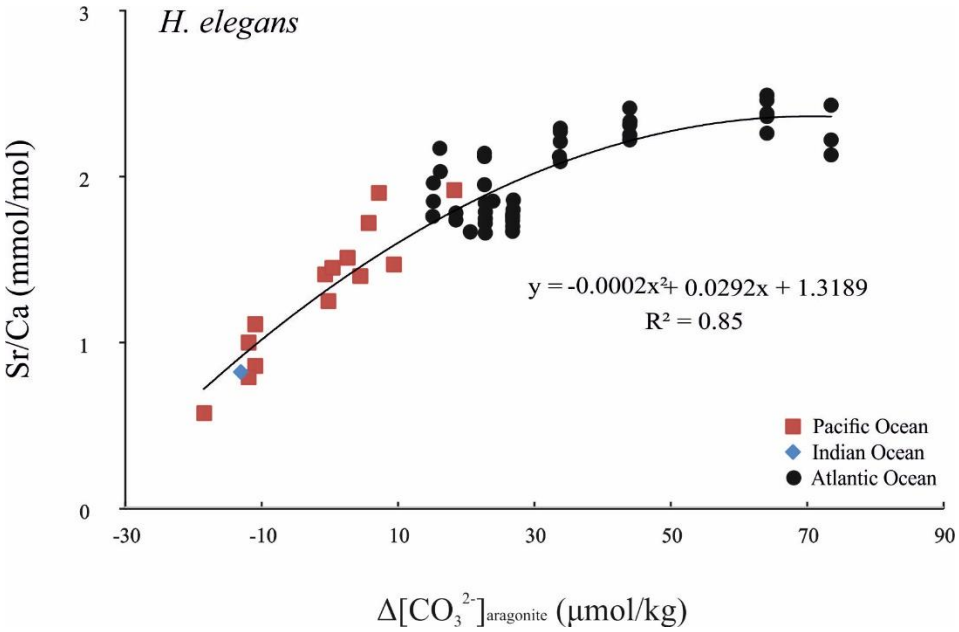

Fig. 5. *Core-top H. elegans Sr/Ca vs. deep water* $\Delta[CO_3^{2-}]_{aragonite}$.

Intermediate water [CO_3^{2-}] at core MD77-191 site calculated using changes in the Sr/Ca ratios display a decreasing trend during 17-15.2 kyr time interval and 12.6-10.5 cal kyr BP, which range between 97 and 77 µmol/kg, and between 95 and 84 µmol/kg, respectively. The [CO_3^{2-}] concentrations reach maximum values (~ 119 µmol/kg) in the 15-13.3 cal kyr BP time interval. Thereafter, the values of [CO_3^{2-}] keep decreasing and get a minimum value ~67 µmol/kg at the end of Holocene. In addition, compared with lower values (mean value of 73 µmol/kg) during the late Holocene (8.8-1.3 cal kyr BP), the record shows an increasing trend (mean value of 87 µmol/kg) during the early Holocene (10.3-9 cal ky BP).

We also calculated the [CO_3^{2-}] record of core MD77-176 from the northeastern BoB by using the *H. elegans* Sr/Ca ratios. The record of intermediate water [CO_3^{2-}] shows higher concentration of [CO_3^{2-}] during the LGM (~ 71 µmol/kg) than during the Holocene (~ 68 µmol/kg). During the last deglaciation, the intermediate water [CO_3^{2-}] record displays a decreasing trend to around ~67 µmol/kg at the 17-15.2 cal kyr BP interval, however, two extreme high values of the intermediate water [CO_3^{2-}] concentration (84–86 µmol/kg) occur at 11.7-11.5 cal kyr BP, it seems difficult to interpret this values and could not re-analysis these two samples limited by the *H. elegans* quantities. Furthermore, if we ignore these extremely high values, we also observed a decrease in the [CO_3^{2-}] (~ 70 µmol/kg) during the 12.6-10.5 cal kyr BP time intervals.

6.2. Possible controls on [CO_3^{2-}] records

To the first approximation, $[CO_3^{2-}] \approx ALK-DIC$ (Zeebe and Wolf-Gladrow, 2001). Thus, carbonate ion concentration in the seawater reflects the balance between mechanisms that affect changes in alkalinity (ALK) and total dissolved inorganic carbon (DIC). Those mechanisms are varied and most important ones deal with biological regeneration, changes of the water mass sources and/or mixing of different water masses and air-sea exchanges (Yu et al., 2008). Deep water $[CO_3^{2-}]$ affects the dissolution/ preservation of $CaCO_3$ on the sea floor by determining the seawater carbonate saturation, and provides therefore a control on global oceanic ALK inventory (Yu et al., 2014a).

Biological regeneration is linked to the sinking of organic matter and $CaCO_3$. The remineralization of sinking organic matter release CO_2 in the deep ocean (Holligan and Robertson, 1996; Yu et al., 2008). The released CO_2 will consume $[CO_3^{2-}]$ to produce bicarbonate ions (HCO_3^-), thus resulting in the decrease of carbonate ion (Holligan and Robertson, 1996). Thus, the ratio of organic to inorganic carbon (the so-called rain ratio) has an important effect on the $[CO_3^{2-}]$ concentration; an increasing rain ratio leading to the reduction of $[CO_3^{2-}]$ concentration of the deep ocean (Berger and Keir, 1984; Hollogan et al., 1996; Yu et al., 2008).

At core MD77-191 location, the paleo-productivity is controlled by the summer monsoon upwelling activity. High *G. bulloides* abundance results from cores MD77-191 and SK237-GC04 (10°58.65'N- 74°59.96'E, 1245 m water depth) indicate a progressive increase of surface productivity during the Holocene, and displays a significant increase since ~ 6 cal kyr BP (Bassinot et al., 2011; Naik et al., 2017; Fig.6). In addition, the total organic carbon (C_{org}) could be used as an indicator of paleo-productivity (e.g., Naidu et al., 1992; Calvert et al., 1995), the record of C_{org} obtained from core SK237-gc04 also shows an increase trend during the late Holocene and reaches the maximum value in the end of Holocene (Fig.6). An increasing rain ratio (more organic matter sinking) leads to decreased $[CO_3^{2-}]$ concentration of the deep ocean (Berger and Keir, 1984; Holligan and Robertson, 1996; Yu et al., 2008). In addition, we observed a decrease in the $[CO_3^{2-}]$ concentration, which is consistent with the high productivity during the Holocene (8.8-1.3 cal kyr BP; Fig.6). Thus, we suggest at site MD77-191 changes in paelo-productivity may be affected by the progressive increase of upwelling activity, resulting in more organic matter and a depletion of $[CO_3^{2-}]$.

However, for core MD77-176 obtained from northern BoB, the primary productivity is much lower than in the Arabian Sea in the modern time, and the distribution of chlorophyll in the surface water of the northeastern BoB indicates a slight increase of productivity in the winter monsoon (Thushara and Vinayachandran, 2016; O'malley, 2017). In addition, the deep water $[CO_3^{2-}]$ from the

Indian and Pacific Ocean are also lower during the Holocene compared with last deglaciation (Fig.7) (Yu et al., 2014a), which is in agreement with the decreasing trend of the intermediate [CO_3^{2-}] records obtained from cores MD77-191 and MD77-176 during the Holocene (8.8-1.3 cal kyr BP). This could likely result from a depletion in the oceanic ALK (Yu et al., 2014a), knowing that reducing the whole ocean ALK inventory may decrease the CO_2 solubility, thus driving up the atmospheric CO_2 over the last 8 cal kyr BP (Ridgwell et al., 2003; Menviel and Joos, 2012; Yu et al., 2014a). Thus, we suggest that paleo-productivity does not appear to a major control in affecting the variation of [CO_3^{2-}] concentrations from the northeastern BoB. Finally, the decrease in the intermediate-water [CO_3^{2-}] obtained from the north Indian Ocean (MD77-176 and MD77-191) during the Holocene may mainly indicate the contribution to atmospheric CO_2 rise since 8 cal kyr BP, due to the depleted global ocean alkalinity.

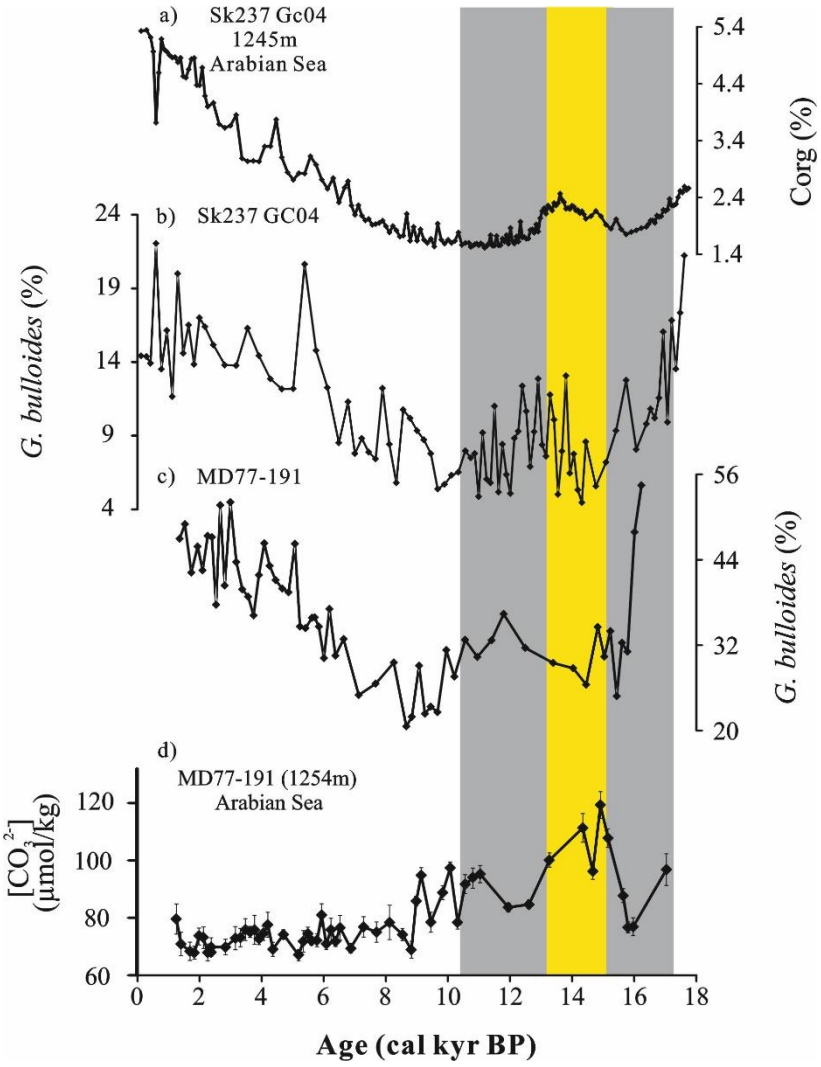

Fig. 6. *a) the total organic carbon percentage (%C_{org}) and b) G. bulloides percentage from core SK237-GC04 (1245m, Naik et al., 2017).c) relative abundance of G. bulloides and d) [CO_3^{2-}]*

record obtained from core MD77-191 (Arabian Sea). The colour-shaded intervals are the same as in Figure 3.

6.3. Significance to paleo-climate and atmospheric CO_2 changes

We compared the sea water [CO_3^{2-}] records of core MD77-191 (Arabian Sea) and core MD77-176 (northeastern BoB) with [CO_3^{2-}] records which were reconstructed by the benthic foraminiferal B/Ca at different water depths from the Atlantic Ocean (BOFS 17K, 58.0°N-16.5°E, 1150 m water depth), and the Indian Ocean (WIND 28K, 10.2°S-51.8°E, 4147 m water depth) (Yu et al., 2008, 2010) (Fig. 7). All of the [CO_3^{2-}] records at intermediate water depth display low values during the 17-15.2 and 12.6-10.5 kyr time intervals (last deglaciation). The record of intermediate [CO_3^{2-}] obtained from core MD77-176 shows maximum values (~84–86 μmol/kg) at 11.7-11.5 cal kyr BP, corresponding to a marked decrease (2.51‰) of benthic $\delta^{18}O$ at 11.5 cal kyr BP, by contrast, intermediate [CO_3^{2-}] from Arabian Sea and Atlantic Ocean all display a decreasing trend during 11.7-11.5 cal kyr BP (Figs. 7f and h), this seems to be associated to a local effect difficult to understand in this core. However, we could also observe a decrease in the [CO_3^{2-}] from core MD77-176 in the BoB during the 12.6-10.5 cal kyr BP time intervals except these two extreme high values (~84–86 μmol/kg) at 11.7-11.5 cal kyr BP. During the 17-15.2 and 12.6-10.5 cal kyr BP intervals, deep water [CO_3^{2-}] concentrations rose by about ～10 μmol/kg in the deep Atlantic, equatorial Pacific and Indian Oceans (Yu et al., 2008, 2010a, 2010b). The increased deep water [CO_3^{2-}] would promote deep-sea carbonate preservation and hence deplete the oceanic ALK inventory. Such an increase of deep-water [CO_3^{2-}] concentration is coeval with the two-step deglacial increase of atmospheric CO_2 (Fig. 7), likely suggesting that the deep-water carbonate ion increase results from a drop in DIC associated to the transfer of CO_2 from the deep ocean into the upper water depth and, ultimately, the atmosphere. The release of deep-sea CO_2 may induce a [CO_3^{2-}] decline at intermediate depths. Such a hypothesis is consistent with the variations of intermediate [CO_3^{2-}] concentration records from the Northern BoB, Arabian Sea and Northern Atlantic Ocean (Fig. 7).

Furthermore, we also observed that the decrease in [CO_3^{2-}] records correspond to an increase of benthic $\delta^{13}C$ during the last deglaciation. Such an increase in benthic $\delta^{13}C$ values has been observed in previous studies from the northern Indian Ocean (e.g., Duplessy et al., 1984; Curry et al., 1988; Naqvi et al., 1994; Jung et al., 2009; Ma et al., 2019). This increase of benthic $\delta^{13}C$ in the Holocene may reflect more invigorated circulation associated with better-ventilated waters at intermediate depth in the Northern Indian Ocean (Duplessy et al., 1984; Waelbroeck et al., 2006; Ma et al., 2019).

The similarity of the benthic $\delta^{13}C$-increases reflects the northward expansion of AAIW during time intervals 17-15.2 and 12.6-10.5 cal kyr BP in the western Arabian Sea, Pacific Ocean and BoB (Fig. S1) (Pahnke and Zahn, 2005; Jung et al., 2009; Ma et al., 2019). However, as AAIW is formed from the deep waters AABW, air-sea exchange could also affect the values of $\delta^{13}C$, as the intermediate benthic $\delta^{13}C$ in the Southern Ocean is dominated by the influence of air-sea exchange (Lynch-Stieglitz et al., 1994). Thus, values of intermediate benthic $\delta^{13}C$ could relatively increase via stronger upwelling during the formation of AAIW. In addition, the transition in the ε_{Nd} and $\Delta^{14}C$ records during the deglaciation also indicates a strong northward penetration of AAIW within the North Atlantic and Bay of Bengal (e.g., Cao et al., 2007; Pahnke et al., 2008; Pena et al., 2013; Yu et al., 2018; Ma et al., 2019). During the last deglaciation, core MD77-176 record of B-P age offsets display a decreasing trend in the 17-15.2 and 12.6-10.5 cal kyr intervals, corresponding to increases of benthic $\delta^{13}C$ values (Fig. 7). The variations in the B-P age offsets obtained from core MD77-176 (Northern Bay of Bengal), Arabian Sea and Pacific Ocean, all indicate a stronger upwelling and an enhanced northern flow of AAIW from the Southern Ocean during these two periods.

Therefore, during the 17-15.2 and 12.6-10.5 kyr time intervals, enhanced vertical ventilation in the Southern Ocean could have led to an increased production of intermediate water masses (AAIW) (Anderson et al., 2009). Values of intermediate benthic $\delta^{13}C$ and $[CO_3^{2-}]$ concentration could indicate stronger upwelling during the formation of AAIW (Yu et al., 2008, 2014a). Thus, decreased $[CO_3^{2-}]$ concentrations from cores MD77-191 and MD77-176 suggest the release of CO_2 from the deep ocean during the deglacial period.

7. Conclusions

Benthic foraminifera $\delta^{13}C$, $\delta^{18}O$ and elemental ratios of *H. elegans* have been analyzed on core MD77-191 (1254 m water depth) located in the south tip of India, as well as core MD77-176 (1375 m water depth) obtained from the northern BoB, in order to reconstruct the evolution of intermediate water masses in the northern Indian Ocean since last deglaciation. Benthic elemental ratios (Mg/Ca, Sr/Ca, Li/Ca and U/Ca) seem mainly influenced by the carbonate ion concentration changes.

We reconstructed seawater $[CO_3^{2-}]$ concentration by converting *H. elegans* Sr/Ca to $[CO_3^{2-}]$ using a modern, core-top based, empirical relationship. During the last deglaciation, increased benthic $\delta^{13}C$, depletion in $[CO_3^{2-}]$ and decreased B-P age offsets occurred in the 17-15.2 and 12.6-10.5 cal kyr BP intervals. All of these results suggest the strong linkage between Southern Ocean

enhanced ventilation via AAIW and release of CO_2 during the last deglaciation. The decreased [CO_3^{2-}] in intermediate water masses also provides evidence for the important influence of global ALK inventory variation during the late Holocene, corresponding to the atmospheric CO_2 rise since 8 kyr BP and/or increased productivity across the Holocene (at least for MD77-191).

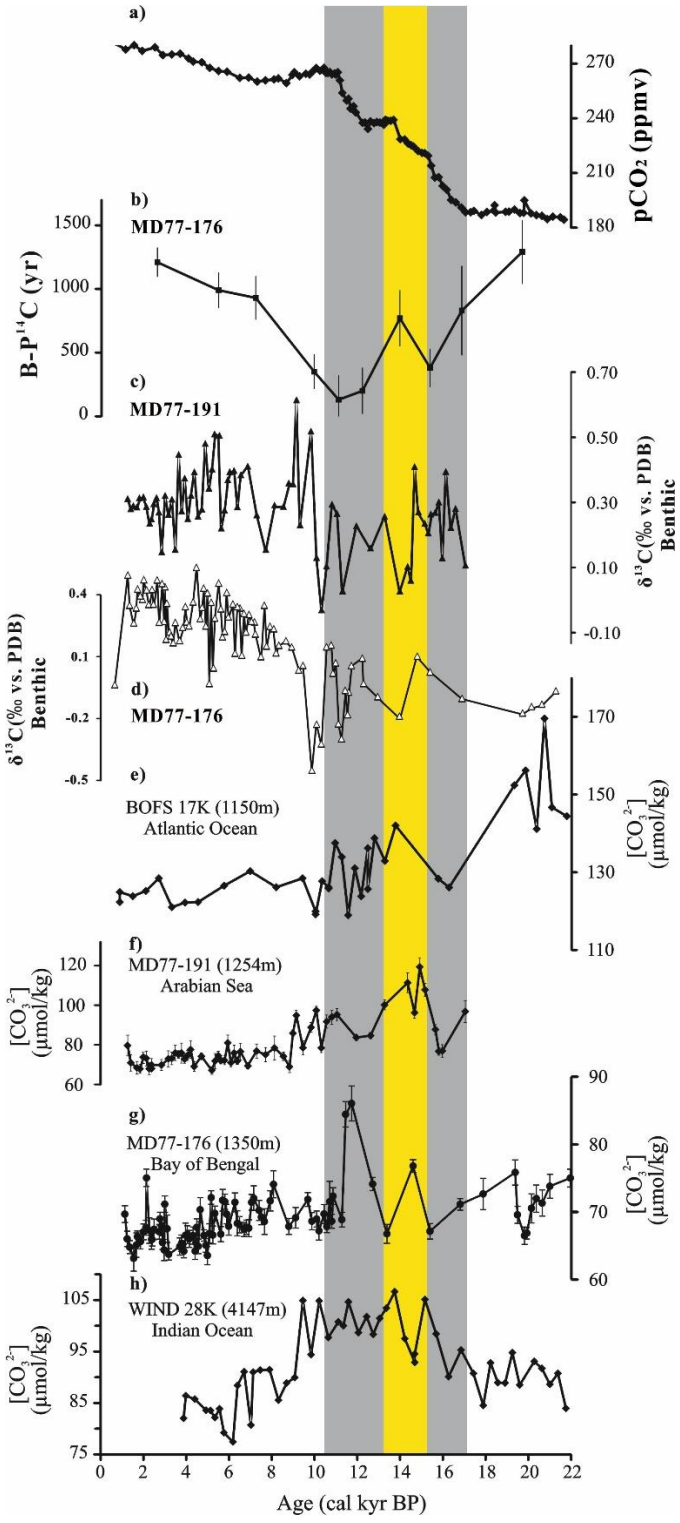

Fig. 7. *a) Ice core atmospheric CO_2 from Antarctic Dome C (Monnin et al., 2001), b) the*

intermediate water B-P ^{14}C age offset of MD77-176 in the BoB (Ma et al, 2019), c) and d) benthic $\delta^{13}C$ from MD77-176, MD77-191, respectively, e)- h) compilation of [CO_3^{2-}] records at different depths in the Indian Ocean and Atlantic Ocean (Yu et al., 2008). The colour-shaded intervals are the same as in Figure 3.

Acknowledgments

Authors acknowledge the China Scholarship Council for providing funding for the PhD study of R. Ma in France. The research leading to this paper was funded by the National Research Agency L-IPSL Project (Grant ANR-10-LABX-0018) and by the INSU-LEFE-IMAGO-CITRON GLACE project.

References

Ahmad, S. M., Babu, A. G., Padmakumari, V. M., Raza, W., 2008. Surface and deep water changes in the northeast Indian Ocean during the last 60 ka inferred from carbon and oxygen isotopes of planktonic and benthic foraminifera. Palaeogeogr. Palaeoclimatol. Palaeoecol. 262 (3), 182-188.

Ahmad, S. M., Zheng, H., Raza, W., Zhou, B., Lone, M. A., Raza, T., Suseela, G., 2012. Glacial to Holocene changes in the surface and deep waters of the northeast Indian Ocean. Marine Geology 329-331, 16-23.

Anderson, R. F., Ali, S., ., Bradtmiller, L. I., Nielsen, S. H. H., Fleisher, M. Q., Anderson, B. E., Burckle, L. H., 2009. Wind-driven upwelling in the Southern Ocean and the deglacial rise in atmospheric CO_2. Science 323 (5920), 1443-1448.

Barbero, L., González-Dávila, M., Santana-Casiano, J. M., Álvarez, M., 2010. Variability of the water mass transports and fluxes in the eastern north Atlantic during 2001. J. Geophys. Res. 115 (C3), 1-11.

Barker, S., Greaves, M., Elderfield, H., 2003. A study of cleaning procedures used for foraminiferal mg/ca paleothermometry. Geochem. Geophys. Geosyst. 4 (9), 1-20.

Barrientos, A., Lear, C. H., Jakobsson, M., Stranne, C., O'Regan, M., Cronin, T. M., Gukov, A. Y., Coxall, H. K., 2018. Arctic Ocean benthic foraminifera Mg/Ca ratios and global Mg/Ca-temperature calibrations: New constraints at low temperatures. Geochimica et Cosmochimica Acta 236, 240-259.

Bashmachnikov, I., Nascimento, Â., Neves, F., Menezes, T., Koldunov, N. V., 2015. Distribution of intermediate water masses in the subtropical northeast Atlantic. Ocean Sci. 11 (5), 803-827.

Bassinot, F. C., Marzin, C., Braconnot, P., Marti, O., Mathienblard, E., Lombard, F., Bopp, L., 2011. Holocene evolution of summer winds and marine productivity in the tropical Indian Ocean in response to insolation forcing: Data-model comparison. Clim. Past 7 (3), 815-829.

Barnes, C. E., and Cochran, J. K., 1990. Uranium removal in oceanic sediments and the oceanic U balance, Earth Planet. Sci. Lett., 97, 94–101.

Beal, L. M., Ffield, A., Gordon, A. L., 2000. Spreading of red sea overflow waters in the Indian Ocean. J. Geophys. Res. 105 (C4), 8549-8564.

Berger, W. H., Keir, R. S., 2013. Glacial-holocene changes in atmospheric CO_2 and the deep-sea record. In Climate Processes and Climate Sensitivity (eds J. E. Hansen and T. Takahashi). doi:10.1029/GM029p0337.

Bostock, H. C., Opdyke, B. N., Williams, M. J. M., 2010. Characterising the intermediate depth waters of the Pacific Ocean using $\delta^{13}C$ and other geochemical tracers. Deep-Sea Res. I 57 (7), 847-859.

Boyle, E. A., 1983. Manganese carbonate overgrowths on foraminifera tests. Geochim. Cosmochim. Acta 63 (18), 353-353.

Boyle, E. A., Keigwin, L. D., 1985. Comparison of Atlantic and Pacific paleochemical records for the last 215,000 years: Changes in deep ocean circulation and chemical inventories. Earth Planet. Sci. Lett. 76 (1), 135-150.

Boyle, E. A., Labeyrie, L., Duplessy, J. C., 1995. Calcitic foraminiferal data confirmed by cadmium in aragonite *Hoeglundina*: Application to the Last Glacial Maximum in the northern Indian Ocean. Paleoceanography 10 (5), 881-900.

Broecker, W. S., Peng, T.-H., 1982. Tracers in the sea. Published by Lamont-Doherty Geological Observatory, Eldigio Press, Columbia University, New York, 690pp.

Brovkin, V., Ganopolski, A., Archer, D., Rahmstorf, S., 2007. Lowering of glacial atmospheric CO_2 in response to changes in oceanic circulation and marine biogeochemistry. Paleoceanography 22 (4), 1-14.

Brown, R. E., Anderson, L. D., Thomas, E., Zachos, J. C., 2011. A core-top calibration of B/Ca in the benthic foraminifers nuttallides umbonifera and oridorsalis umbonatus: A proxy for cenozoic bottom water carbonate saturation. Earth Planet. Sci. Lett. 310 (3), 360-368.

Bryan, S. P., Marchitto, T. M., 2008. Mg/Ca–temperature proxy in benthic foraminifera: New calibrations from the florida straits and a hypothesis regarding Mg/Li. Paleoceanography 23 (PA2220), 1-17.

Bryan, S. P., Marchitto, T. M., Lehman, S. J., 2010. The release of ^{14}C-depleted carbon from the deep ocean during the last deglaciation: Evidence from the Arabian Sea. Earth Planet. Sci. Lett.

298 (1), 244-254.

Came, R. E., Oppo, D. W., Curry, W. B., Lynch-Stieglitz, J., 2008. Deglacial variability in the surface return flow of the Atlantic Meridional Overturning Circulation. Paleoceanography 23 (PA1217), 1-10.

Cao, L., Fairbanks, R. G., Mortlock, R. A., Risk, M. J., 2007. Radiocarbon reservoir age of high latitude North Atlantic surface water during the last deglacial. Quat. Sci. Rev. 26 (5), 732-742.

Curry, W. B., Duplessy, J. C., Labeyrie, L. D., Shackleton, N. J., 1988. Changes in the distribution of $\delta^{13}C$ of deep water σCO_2 between the last glaciation and the Holocene. Paleoceanography 3 (3), 317-341.

Doss, W., Marchitto, T. M., Eagle, R., Rashid, H., Tripati, A., 2018. Deconvolving the saturation state and temperature controls on benthic foraminiferal Li/Ca, based on downcore paired B/Ca measurements and coretop compilation. Geochim. Cosmochim. Acta 236, 297-314.

Duplessy, J.-C., Shackleton, N. J., Matthews, R. K., Prell, W., Ruddiman, W. F., Caralp, M., Hendy, C. H., 1984. ^{13}C record of benthic foraminifera in the last interglacial ocean: Implications for the carbon cycle and the global deep water circulation. Quat. Res. 21 (2), 225-243.

Hall, J.M., Chan, L.-H., 2004. Li/Ca in multiple species of benthic and plaktonic foraminifera: thermocline, latitudinal, and glacial-interglacial variation. Geochimica et Cosmochimica Acta, 68(3), 529-545.

Holligan, P. M., Robertson, J. E., 1996. Significance of ocean carbonate budgets for the global carbon cycle. Global Change Biology 2 (2), 85-95.

IPCC, 2013. Climate change 2013 : The physical science basis summary for policymakers. Intergovernmental Panel on Climate Change.

Jung, S. J. A., Kroon, D., Ganssen, G., Peeters, F., Ganeshram, R., 2009. Enhanced Arabian Sea intermediate water flow during glacial north Atlantic cold phases. Earth Planet. Sci. Lett. 280 (1), 220-228.

Keul, N., Langer, G., Nooijer, L. J. D., Nehrke, G., Reichart, G. J., Bijma, J., 2013. Incorporation of Uranium in benthic foraminiferal calcite reflects seawater carbonate ion concentration. Geochem. Geophys. Geosyst. 14 (1), 102-111.

Lüthi, D., Le Floch, M., Bereiter, B., Blunier, T., Barnola, J.-M., Siegenthaler, U., Raynaud, D., Jouzel, J., Fischer, H., Kawamura, K., Stocker, T. F., 2008. High-resolution carbon dioxide concentration record 650,000–800,000 years before present. Nature 453, 379.

Lear, C. H., Rosenthal, Y., Slowey, N., 2002. Benthic foraminiferal Mg/Ca-paleothermometry: A revised core-top calibration. Geochim. Cosmochim. Acta 66 (19), 3375-3387.

Lear, C. H., Rosenthal, Y., 2006. Benthic foraminiferal Li/Ca: insights into Cenozoic seawater

carbonate saturation state. Geology, 34, 985-988.

Lear, C. H., Mawbey, E. M., and Rosenthal, Y., 2010. Cenozoic benthic foraminiferal Mg/Ca and Li/Ca records: Toward unlocking temperatures and saturation states, Paleoceanography, 25, PA4215.

Lisiecki, L., Raymo, M., 2005. A Pliocene-Pleistocene stack of 57 globally distributed benthic ^{18}O records. Paleoceanography 20 (PA1003), 1-17.

Lutze, G. F., Thiel, H., 1989. Epibenthic foraminifera from elevated microhabitats; *Cibicidoides wuellerstorfi* and *Planulina ariminensis*. J. Foraminiferal Res. 19 (2), 153-158.

Lynch-Stieglitz, J., Adkins, J. F., Curry, W. B., Dokken, T., Hall, I. R., Herguera, J. C., Hirschi, J. J.-M., Ivanova, E. V., Kissel, C., Marchal, O., Marchitto, T. M., McCave, I. N., McManus, J. F., Mulitza, S., Ninnemann, U., Peeters, F., Yu, E.-F., Zahn, R., 2007. Atlantic Meridional Overturning Circulation during the Last Glacial Maximum. Science 316 (5821), 66-69.

Lynch-Stieglitz, J., Fairbanks, R. G., Charles, C. D., 1994. Glacial-interglacial history of Antarctic Intermediate Water: Relative strengths of Antarctic versus Indian Ocean sources. Paleoceanography 9 (1), 7-29.

Ma, R., Sépulcre, S., Licari, L., Bassinot, F., Liu, Z., Tisnérat-Laborde, N., Kallel, N., Yu, Z., Colin, C., 2019. Changes in intermediate circulation in the Bay of Bengal since the Last Glacial Maximum as inferred from benthic foraminifera assemblages and geochemical proxies. Geochem. Geophys. Geosyst. 20, 1-17.

Makou, M. C., Oppo, D. W., Curry, W. B., 2010. South atlantic intermediate water mass geometry for the Last Glacial Maximum from foraminiferal Cd/Ca. Paleoceanography 25 (PA4103), 1-7.

Mangini, A., Godoy, J. M., Godoy, M. L., Kowsmann, R., Santos, G. M., Ruckelshausen, M., Schroederritzrau, A., Wacker, L., 2010. Deep sea corals off Brazil verify a poorly ventilated southern Pacific Ocean during H2, H1 and the Younger Dryas. Earth Planet. Sci. Lett. 293 (3-4), 269-276.

Marchitto, T. M., Bryan, S. P., Doss, W., Mcculloch, M., Montagna, P., 2018. A simple biomineralization model to explain Li, Mg, and Sr incorporation into aragonitic foraminifera and corals. Earth Planet. Sci. Lett. 481, 20-29.

Marchitto, T. M., Bryan, S. P., Curry, W. B., McCorkle, D. C., 2007. Mg/Ca temperature calibration for the benthic foraminifera *Cibicidoides pachyderma*. Paleoceanography 22, 1-9.

Marchitto, C. S., Henderson, G. M., Crompoton, R., Staubwasser, M., Shaw, S., 2004. Effect of mineralogy, salinity and temperature on Li/Ca and Li isotope composition of calcium carbonate. Chemical Geology, 212, 5-15.

Marchitto, T. M., Lehman, S. J., Ortiz, J. D., Jacqueline, F., Alexander, V. G., 2007. Marine

radiocarbon evidence for the mechanism of deglacial atmospheric CO_2 rise. Science 316 (5830), 1456-1459.

Martin, P. A., Lea, D. W., Rosenthal, Y., Shackleton, N. J., Sarnthen, M., Papenfuss, T., (2002). Quaternary deep sea tempeature histories derived from benthic foraminiferal Mg/Ca. Earth Planet. Sci. Lett. 198, 193-209.

Marzin, C., Kallel, N., Kageyama, M., Duplessy, J. C., Braconnot, P., 2013. Glacial fluctuations of the Indian monsoon and their relationship with north Atlantic climate: New data and modelling experiments. Clim. Past 9 (5), 2135-2151.

Menviel, L., Joos, F., 2012. Toward explaining the Holocene carbon dioxide and carbon isotope records: Results from transient ocean carbon cycle-climate simulations. Palaeogeogr. Palaeoclimatol. Palaeoecol. 27 (PA1207), 1-17.

Mléneck, V. M., 1997. S´edimentation et dissolution des carbonates biog´eniques aux moyennes latitudes nord et sud, approche quantitative et relations avec les pal´eocirculations oc´eaniques des derniers 150 000 ans. PhD thesis, Universit´e Bordeaux I, pp. 277.

Monnin, E., Indermühle, A., Dällenbach, A., Flückiger, J., Stauffer, B., Stocker, T. F., Raynaud, D., Barnola, J. M., 2001. Atmospheric CO_2 concentrations over the last glacial termination. Science 291 (5501), 112-114.

Naik, D. K., Saraswat, R., Lea, D. W., Kurtarkar, S. R., Mackensen, A., 2017. Last glacial-interglacial productivity and associated changes in the eastern Arabian Sea. Palaeogeography, Palaeoclimatology, Palaeoecology 483, 147-156.

Naqvi, W. A., Charles, C. D., Fairbanks, R. G., 1994. Carbon and oxygen isotopic records of benthic foraminifera from the northeast Indian Ocean: Implications on glacial-interglacial atmospheric CO_2 changes. Earth Planet. Sci. Lett. 121 (1), 99-110.

O'Malley, R., 2017. Ocean productivity. http://www.science.oregonstate.edu/ocean. Productivity/index.php.

Pahnke, K., Goldstein, S. L., Hemming, S. R., 2008. Abrupt changes in Antarctic Intermediate Water circulation over the past 25,000 years. Nat. GeoSci. 1, 870.

Pahnke, K., Zahn, R., 2005. Southern Hemisphere water mass conversion linked with North Atlantic climate variability. Science 307 (5716), 1741-1746.

Pelletier, G., Lewis, E., Wallace, D., 2005. A calculator for the CO_2 system in seawater for microsoft excel/vba. Washington State Department of Ecology, Olympia, WA, Brookhaven National Laboratory Upton, NY.

Pena, L. D., Goldstein, S. L., Hemming, S. R., Jones, K. M., Calvo, E., Pelejero, C., Cacho, I., 2013. Rapid changes in meridional advection of Southern Ocean intermediate waters to the tropical

Pacific during the last 30kyr. Earth Planet. Sci. Lett. 368, 20-32.

Poggemann, D.-W., Nürnberg, D., Hathorne, E. C., Frank, M., Rath, W., Reißig, S., Bahr, A., 2018. Deglacial heat uptake by the Southern Ocean and rapid northward redistribution via Antarctic Intermediate Water. Palaeogeogr. Palaeoclimatol. Palaeoecol. 33 (11), 1292-1305.

Poggemann, D. W., Hathorne, E. C., Nürnberg, D., Frank, M., Bruhn, I., Reißig, S., Bahr, A., 2017. Rapid deglacial injection of nutrients into the tropical Atlantic via Antarctic Intermediate Water. Earth Planet. Sci. Lett. 463, 118-126.

Raitzsch, M., Kuhnert, H., Hathorne, E. C., Groeneveld, J., Bickert, T., 2011. U/Ca in benthic foraminifers: A proxy for the deep-sea carbonate saturation. Geochem. Geophys. Geosyst. 12 (6).

Ravichandran, M., Girishkumar, M. S., Riser, S., 2012. Observed variability of chlorophyll- a using argo profiling floats in the southeastern Arabian Sea. Deep-Sea Res. I 65 (65), 15-25.

Raza, T., Ahmad, S. M., Sahoo, M., Banerjee, B., Bal, I., Dash, S., Suseela, G., Mukherjee, I., 2014. Hydrographic changes in the southern Bay of Bengal during the last ~65,000 y inferred from carbon and oxygen isotopes of foraminiferal fossil shells. Quaternary International 333, 77-85.

Reichart, G. J., Jorissen, F., Mason, P. R. D., Anschutz, P., 2003. Single foraminiferal test chemistry records the marine environment. Geology 31 (2003), 355-358.

Reid, J. L., 2003. On the total geostrophic circulation of the South Pacific Ocean: Flow patterns, tracers and transports. Prog. Oceanogr. 16 (1), 1-61.

Reimer P. J., Bard E., Bayliss A., Beck J. W., Blackwell P. G., Bronk Ramsey C., Buck C. E., Cheng H., Edwards R. L., Friedrich M., Grootes P. M., Guilderson T. P., Haflidason H., Hajdas I., Hatté C., Heaton T. J., Hogg A. G., Hughen K. A., Kaiser K. F., Kromer B., Manning S. W., Niu M., Reimer R. W., Richards D. A., Scott E. M., Southon J. R., Turney C. S. M., van der Plicht J., 2013. IntCal13 and Marine13 radiocarbon age calibration curves 0-50000 years cal BP. Radiocarbon 55(4).

Ribbe, J., 2001. Intermediate water mass production controlled by Southern Hemisphere winds. Geophys. Res. Lett. 28 (3), 535-538.

Ridgwell, A., Zeebe, R. E., 2005. The role of the global carbonate cycle in the regulation and evolution of the earth system [rapid communication]. Earth Planet. Sci. Lett. 234 (3), 299-315.

Ridgwell, A. J., Watson, A. J., Maslin, M. A., Kaplan, J. O., 2003. Implications of coral reef buildup for the controls on atmospheric CO_2 since the Last Glacial Maximum. Paleoceanography 18 (4), 1-10.

Rosenthal, Y., Boyle, E. A., Slowey, N., 1997. Temperature control on the incorporation of magnesium, strontium, fluorine, and cadmium into benthic foraminiferal shells from little Bahama Bank: Prospects for thermocline paleoceanography. Geochim. Cosmochim. Acta 61

(17), 3633-3643.

Rosenthal, Y., Lear, C. H., Oppo, D. W., Linsley, B. K., 2006. Temperature and carbonate ion effects on Mg/Ca and Sr/Ca ratios in benthic foraminifera: Aragonitic species *Hoeglundina elegans*. Paleoceanography 21 (PA1007), 1-14.

Russell, A. D., Hönisch, B., Spero, H. J., Lea, D. W., 2004. Effects of seawater carbonate ion concentration and temperature on shell U, Mg, and Sr in cultured planktonic foraminifera. Geochim. Cosmochim. Acta 68 (21), 4347-4361.

Schlitzer, R., 2015. Ocean data view. http://odv.awi.de.

Shackleton, N. J., 1974. Attainment of isotopic equilibrium between ocean water and benthonic foraminifera genus uvigerina: Isotopic changes in the ocean during the last glacial. Les méthodes quantitatives d'étude des variations du climat au cours du pleistocène, gif-sur-yvette. Colloque international du CNRS 219, 203-210.

Sigman, D. M., Boyle, E. A., 2000. Glacial/interglacial variations in atmospheric carbon dioxide. Nature 407 (6806), 859-869.

Sijinkumar, A. V., Clemens, S., Nath, B. N., Prell, W., Benshila, R., Lengaigne, M., 2016. $\Delta^{18}O$ and salinity variability from the Last Glacial Maximum to recent in the Bay of Bengal and Andaman Sea. Quat. Sci. Rev. 135, 79-91.

Skinner, L. C., Claire, W., Scrivner, A. E., Fallon, S. J., 2014. Radiocarbon evidence for alternating northern and southern sources of ventilation of the deep Atlantic carbon pool during the last deglaciation. PNAS 111 (15), 5480-5484.

Stuiver, M., Braziunas, T. F., 1993. Modeling atmospheric ^{14}C influences and ^{14}C ages of marine samples to 10 000 BC. Radiocarbon 35 (1), 137-189.

Talley, L. D., Pickard, G. L., Emery, W. J., Swift, J. H., 2011; Preface. In Descriptive physical oceanography (sixth edition), Academic Press: Boston, pp. 1-383.

Thushara, V., Vinayachandran, P. N., 2016. Formation of summer phytoplankton bloom in the northwestern Bay of Bengal in a coupled physical-ecosystem model. J. Geophys. Res. 121 (12), 8535-8550.

Toggweiler, J.R., Russell, J.L., and Carson, S.R. (2006). Midlatitude westerlies, atmospheric CO_2, and climate change during the ice ages. Paleoceanography 21 (2).

Tomczak, M., Godfrey, J. S., 2003; Regional oceanography: An introduction. Daya Publishing House.

Waelbroeck, C., Levi, C., Duplessy, J. C., Labeyrie, L., Michel, E., Cortijo, E., Bassinot, F., Guichard, F., 2006. Distant origin of circulation changes in the Indian Ocean during the last deglaciation. Earth Planet. Sci. Lett. 243 (1), 244-251.

You, Y., 1998. Intermediate water circulation and ventilation of the Indian Ocean derived from water-mass contributions. J. Mar. Res. 56 (5), 1029-1067.

You, Y., Tomczak, M., 1993. Thermocline circulation and ventilation in the Indian Ocean derived from water mass analysis. Deep-Sea Res. I 40 (1), 13-56.

Yu, J., Anderson, R. F., Rohling, E. J., 2014a. Deep ocean carbonate chemistry and glacial-interglacial atmospheric CO_2 change. Oceanography 27 (1), 16-25.

Yu, J., Elderfield, H., 2007. Benthic foraminiferal B/Ca ratios reflect deep water carbonate saturation state. Earth Planet. Sci. Lett. 258 (1), 73-86.

Yu, J., Elderfield, H., 2008. Mg/Ca in the benthic foraminifera *Cibicidoides wuellerstorfi* and *Cibicidoides mundulus*: Temperature versus carbonate ion saturation. Earth Planet. Sci. Lett. 276 (1), 129-139.

Yu, J., Elderfield, H., Jin, Z., Tomascak, P., Rohling, E. J., 2014b. Controls on Sr/Ca in benthic foraminifera and implications for seawater Sr/Ca during the late pleistocene. Quat. Sci. Rev. 98 (15), 1-6.

Yu, J., Elderfield, H., Piotrowski, A. M., 2008. Seawater carbonate ion- $\delta^{13}C$ systematics and application to glacial-interglacial north atlantic ocean circulation. Earth Planet. Sci. Lett. 271 (1), 209-220.

Yu, J., Foster, G. L., Elderfield, H., Broecker, W. S., Clark, E., 2010a. An evaluation of benthic foraminiferal B/Ca and $\delta^{11}B$ for deep ocean carbonate ion and pH reconstructions. Earth Planet. Sci. Lett. 293 (1), 114-120.

Yu. J., Broecker, W., Elderfield, H., Jin, Z. D., McManus, J., Zhang, F., 2010b. Loss of carbon from the deep sea since the Last Glacial Macimum. Sicence 330, 1084-1087.

Yu, Z., Colin, C., Ma, R., Meynadier, L., Wan, S., Wu, Q., Kallel, N., Sepulcre, S., Dapoigny, A., Bassinot, F., 2018. Antarctic intermediate water penetration into the northern Indian Ocean during the last deglaciation. Earth Planet. Sci. Lett. 500, 67-75.

Zeebe, R. E., Wolf-Gladrow, D., 2001. CO_2 in seawater: Equilibrium, kinetics, isotopes. Amsterdam: Elsevier Science, B.V., pp. 346.

Supplementary figures

Fig. S1. Compilation of benthic $\delta^{13}C$ records obtained from core MD77-191 (water depth of 1254 m), MD77-176 (water depth of 1325 m) (Ma et al., 2019), core RC12-344 (2140 m water depth, Naqvi et al., 1994), MD97-2120 (1210 m water depth, Pahnke and Zahn, 2005), and Core 905 (1580 m water depth, Jung et al., 2009). The grey-shaded intervals mark the two-step increase in atmospheric CO_2, the yellow-shaded interval marks the 15-13.3 cal kyr BP interval. The colour-shaded intervals are the same as in Figure 3.

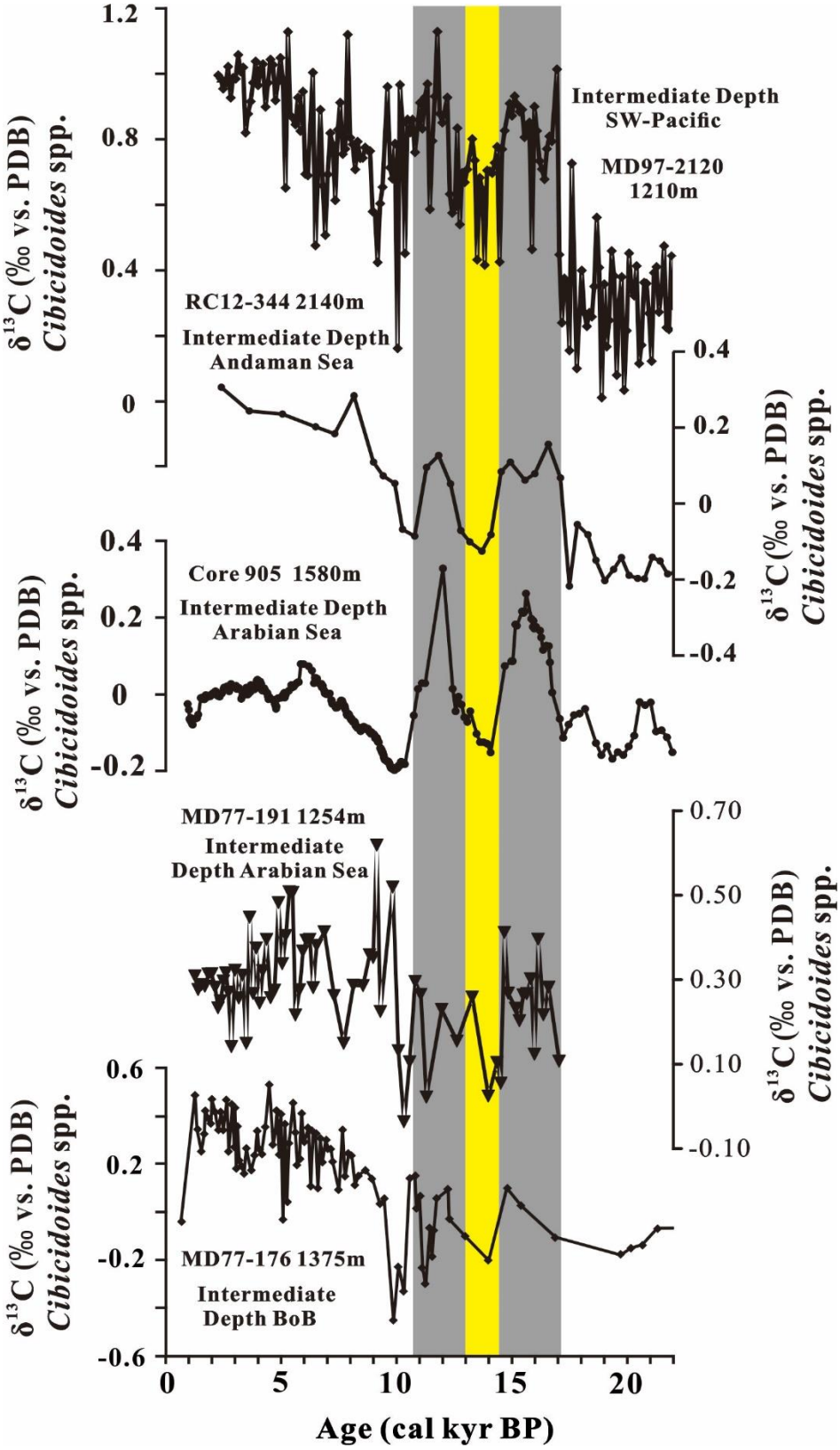
Intermediate Depth
SW-Pacific
MD97-2120
1210m
RC12-344 2140m
Intermediate Depth
Andaman Sea
Core 905 1580m
Intermediate Depth
Arabian Sea
MD77-191 1254m
Intermediate
Depth Arabian Sea
MD77-176 1375m
Intermediate
Depth BoB
δ13C (‰ vs. PDB)
Cibicidoides spp.
Age (cal kyr BP)

Fig. S1

Chapter 5: Changes in productivity and intermediate circulation in the northern Indian Ocean since the last deglaciation: new insights from benthic foraminiferal Cd/Ca and Ba/Ca records and benthic assemblages analysis

Past changes in the global Carbon cycle are involved in climate changes at different time-scales. As the productivity is a key process controlling the ocean Carbon pool, a better understanding of the processes controlling the productivity and their changes through time is a clue to better constrain past climate changes associated to variations in the Carbon Cycle. The nutrient content of water masses is a key factor influencing the productivity. In this context, the benthic foraminifera Cd/Ca is a robust proxy to reconstruct the paleo-nutrient, as the labile nutrient (phosphate and nitrate) shows a positive linear correlation with the seawater cadmium (Boyle et al., 1976; Boyle, 1988; Elderfield and Rickaby, 2000). In addition, benthic foraminifera Ba/Ca have also been explored to reconstruct paleo-nutrient, due to dissolved barium also exhibits a positive correlation with the ocean alkalinity and silica (refractory nutrients) (e.g., Lea and Boyle, 1989, 1990; Hall and Chan, 2004; Martin and Lea, 1998). However, the nutrient content associated to the AAIW has never been documented in the Indian Ocean, whereas it could also have an important role on the atmospheric CO_2 by controlling the primary productivity (e.g., Bauska et al., 2016; Kohfeld et al., 2005).

In this chapter, we present the first continuous and high resolution records of benthic foraminiferal Cd/Ca and Ba/Ca from two well time-scale constrained cores of the northern Indian Ocean (southeastern Arabian Sea and northern Bay of Bengal) in order to establish variations of intermediate circulation and paleo-nutrient content since the last deglaciation.

In addition, Arabian Sea is one of the most productivity regions in the modern time (Banse, 1987; Marra and Barber, 2005). Then, I also present the study of the benthic foraminiferal assemblages from the southeastern Arabian Sea, which permits to reconstruct the changes in the bottom water conditions (oxygen concentration and organic matter flow) and could be associated to the variations of the surface productivity since the last deglaciation in the Arabian Sea.

Changes in productivity and intermediate circulation in the northern Indian Ocean since the last deglaciation: new insights from benthic foraminiferal Cd/Ca and Ba/Ca records and benthic assemblages analysis

Ruifang MA[1], Sophie SEPULCRE[1], Franck BASSINOT[2], Frédéric HAURINE[1], Christophe COLIN[1]

[1]GEOPS, Université Paris-Sud, CNRS, Université Paris-Saclay, Rue du Belvédère, 91405, Orsay, France.

[2]LSCE/IPSL, CEA CNRS UVSQ, UMR 8212, F-91190 Gif Sur Yvette, France.

Abstract:

Cd/Ca and Ba/Ca ratios of several benthic foraminiferal species have been conducted on two well time-scale constrained cores of the northern Indian Ocean (Arabian Sea and northern Bay of Bengal), as well as benthic foraminiferal assemblages analyses obtained from core MD77-191 in the Arabian Sea, in order to establish variations of intermediate circulation and paleo-nutrient content since the last deglaciation. Intermediate water Cd_w estimated from the benthic Cd/Ca and Ba/Ca ratios were mainly affected by the surface productivity changes and/or variations of bottom water ventilation. The benthic foraminiferal analysis is consistent with the geochemical records. Results indicate that during the last deglaciation, millennial-scale events are marked by a decrease in the Cd_w and Ba/Ca values which indicate a decreasing surface productivity and high bottom water ventilation, coincident with increased benthic $\delta^{13}C$ values, low B-P ^{14}C age offsets and depleted [CO_3^{2-}]. All these records provide thus strong evidences for an increased northward penetration of Antarctic Intermediate Water (AAIW) in the northern Indian Ocean. This was associated with enhanced upwelling in the Southern Ocean, reflecting a strong sea-atmospheric CO_2 exchange through Southern Ocean ventilation during the last deglaciation. During the late Holocene (from 5.2 to 2.4 cal kyr BP), benthic foraminiferal assemblages indicate a meso- to eutrophic deep water conditions which correspond to high productivity, and consisent with a significant increase of intermediate water Cd_w obtained from southeastern Arabian Sea and northeastern BoB reflects an increase in the surface productivity. By contrast, the productivity during the early Holocene (from 10 to 6 cal kyr BP) seems to be weaker compared with 5.2-2.4 cal kyr BP time interval. The

comparison of intermediate water Cd_w with previous studies about Indian monsoon reconstruction suggests a seesaw relationship between intense monsoon rainfall and the surface productivity in the BoB and south tip of Arabian Sea during the Holocene.

Key words: paleo-nutrient, Cd/Ca, Ba/Ca, benthic assemblage, deglaciation, atmospheric CO_2, North Indian Ocean

1. Introduction

During the last deglaciation, a two-step rapid increase of atmospheric CO_2 occurred in the 18-14.7 and 12.8-11.7 cal kyr BP time intervals (e.g., Monnin et al., 2001). Several studies suggest that variations of the Southern Ocean circulation contribute to these increases of atmospheric CO_2 by transferring the deep ocean carbon to the upper ocean and atmosphere during the last deglaciation, by enhancing the upwelling and increasing the northward penetration of the Antarctic Intermediate Water (AAIW) in all ocean basins. (e.g., Anderson et al., 2009; Marchitto et al., 2007; Skinner et al., 2014). In the Pacific Ocean (e.g., Pahnke and Zahn, 2005; Bostock et al., 2010), and the northern Indian Ocean (Bryan et al., 2010; Raza et al., 2014; Yu et al., 2018; Ma et al., 2019), all studies indicate an increased northward propagation of AAIW during glacial periods, as well as at millennial time scale during the Heinrich events and stadials (e.g., Bryan et al., 2010; Pahnke et al., 2008). However, the role of AAIW is still controversial in the Atlantic Ocean, where several studies suggest a reduced northward flux of AAIW into the tropical Atlantic (e.g. Came et al., 2008; Xie et al., 2012; Howe et al., 2016; Gu et al., 2017) whereas others indicate an increased penetration (e,g., Pahnke et al., 2008; Dubois-Dauphin et al., 2016; Marchitto et al., 2007; Poggemann et al., 2017, 2018).

Thus, the northward extension of AAIW and the relationships with the atmospheric CO_2 variations still need to be constrained, as well as the relationships with enhanced upwelling in the Southern Ocean during the last deglaciation at millennial scales. Many proxies have been used to reconstruct past changes in intermediate circulation, such as $\Delta^{14}C$ (e.g., Bryan et al., 2010; Marchitto et al., 2007), benthic $\delta^{13}C$ (e.g., Jung et al., 2009; Pahnke and Zahn, 2005; Ma et al., 2019) and foraminifera ε_{Nd} (e.g., Xie et al., 2012; Pahnke et al., 2008; Yu et al., 2018). All these previous studies were focus on the close relationship between enhanced ventilation in the Southern Ocean and rising atmospheric CO_2 during the last deglaciation period. In addition, the intermediate-deep water circulation could affect the oceanic biological pump and nutrient upwelling, and thus could

also contribute to the observed CO_2 changes (e.g., Toggweiler, 1999; Marchitto and Broecker, 2005). Thus, recently reconstruction of the seawater nutrient to trace the variation of intermediate water masses have been received increasing attention, (e.g., Boyle and Keigwin, 1982; Oppo and Fairbanks, 1987; Came et al., 2008; Valley et al., 2017; Poggemann et al., 2017).

The benthic foraminifera Cd/Ca is a robust proxy to reconstruct the paleo-nutrient, as the labile nutrient (phosphate and nitrate) shows a positive linear correlation with the seawater cadmium (Boyle et al., 1976; Boyle, 1988; Elderfield and Rickaby, 2000). Dissolved barium also exhibits a positive correlation with the ocean alkalinity and silica (refractory nutrients), which both seems to mainly regenerate at deep depth (Chan et al., 1977; Lea and Boyle, 1989; Hall and Chan, 2004). Therefore, benthic foraminifera Ba/Ca have also been explored to reconstruct paleo-nutrient (e.g., Lea and Boyle, 1989, 1990; Hall and Chan, 2004; Martin and Lea, 1998). However, the nutrient content associated to the AAIW has never been documented in the Indian Ocean, whereas it could also have an important role on the atmospheric CO_2 by controlling the primary productivity (e.g., Bauska et al., 2016; Kohfeld et al., 2005).

In the modern time, Arabian Sea is one of the most productive regions (Banse, 1987; Marra and Barber, 2005), and surface productivity is dominated by the monsoon system due to the monsoon-driven vertical mixing and upwelling (Lévy et al., 2007). Different regions of Arabian Sea respond varyingly to the seasonal wind forcing, and thus could result in the variation of surface productivity at different seasons (Wiggert et al., 2005). In the western Arabian Sea, the southwestern wind associated to the summer monsoon, can lead to a high surface productivity via the enhanced coastal upwelling and Ekman pumping, inducing the lateral advection of nutrient-rich upwelling water (e.g., Wyrtki, 1973; Lévy et al., 2007) (Fig.1a). However, the upwelling is weaken and ceased during the winter season due to the changes in winds direction, leading a decrease of surface productivity (Fig.1b). Productivity in the eastern Arabian Sea off the India margin corresponds to the deepening of the mixed-layer and upwelling (e.g., Sharma, 1978; Shetye et al., 1990). Thus, the productivity of the southern tip of India is a key area to identify changes in the summer monsoon (Fig.1a).

Many previous studies have focused on the reconstruction of paleo-productivity of Arabian Sea during long time periods (e.g., Prell and Kutzbach, 1987; Naidu and Malmgren, 1996; Gupta et al., 2003; Bassinot et al., 2011; Singh et al., 2011). Monsoon-driven productivity of Arabian Sea could also be associated to global climate changes (Heinrich Stadials, glacial episodes) (e.g., Sigh et al., 2006; 2011; Saraswat et al., 2014). One of the most current proxies used to reconstruct the paleo-productivity is the relative abundance of the planktonic foraminifera *Globigerina bulloides* (Prell and Kutzbach, 1987; Naidu and Malmgren, 1996; Gupta et al., 2003; Bassinot et al., 2011). The

significant changes in the relative abundance of planktic foraminifera *G. bulloides* seem correspond to enhanced productivity (Curry et al., 1992; Naidu et al., 1992), and the immediate response of *G. bulloides* to the changes of the productivity makes it to be a useful proxy to reconstruct the paleo-productivity (e.g., Naidu and Malmgren, 1996; Zaric et al., 2005; Bassinot et al., 2011).

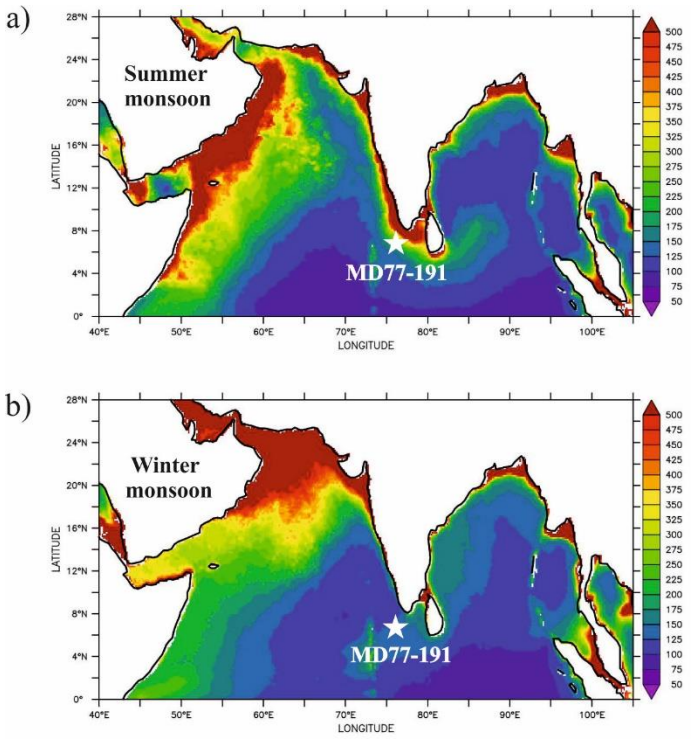

Fig. 1. *a) – b) Seasonal distribution of the Net primary productivity distribution (g C m^{-2} yr^{-1}) in Northern Indian Ocean during the summer and winter monsoon. Maps based on MODIS chlorophyll-a, SST, PAR satellite data, using the standard vertically Generalized Production Model (VGPM) (Behrenfeld and Falkowski, 1997) as the standard algorithm.*

At the deeper water depth, as the benthic foraminiferal microhabitat is related to organic flux and benthic ecosystem oxygenation, their distribution and abundance are powerful proxies to estimate the bottom water condition changes (e.g., Corliss et al., 1986; Schmiedl et al., 1998; Almogi-Labin et al., 2000), especially by indicating the organic matter flux to the seafloor (e.g., Altenbach et al., 1999; Caulle et al., 2015; Fontanier et al., 2002; Van der Zwaan et al., 1999). Thus, benthic foraminifera could be the indicator of the productivity especially in high carbon flux regions (Schnitker, 1994). By comparing past benthic foraminiferal assemblages to modern ones, changes of food supply and oxygen concentrations of the bottom water can be reconstructed (e.g., Peterson, 1984; Corliss, 1979; Murgese and De Deckker, 2005). Recently, the association between benthic foraminiferal assemblages and the geochemical proxies has received increasing attention, and their

comparison was used to reconstruct the evolution of surface productivity and upwelling intensity in the Indian Ocean (e.g., Den Dulk et al., 1998; Hermelin 1991, 1992; Hermelin and Shimmield, 1995; Murgese and De Deckker, 2005). Thus, by combining the benthic foraminiferal fauna analysis with the measurements of the geochemistry (benthic $\delta^{18}O$, $\delta^{13}C$, trace and minor elemental ratios) allows to constrain the paleoceanographic evolution (like oxygen, nutrient, …).

In this study, we have reconstructed benthic foraminifera Cd/Ca and Ba/Ca records at intermediate water depth in the northern Indian Ocean (Arabian Sea and northern Bay of Bengal) to estimate past changes in the paleo-nutrient content over the last 17 kyr and constrain relationships between AAIW circulation, Southern Ocean upwelling intensity and changes in the atmospheric CO_2. We provide in this work the first continuous and high-resolution benthic foraminifera Cd/Ca and Ba/Ca records in the northern Indian Ocean, whereas numerous records of benthic Cd/Ca have been published in the Atlantic Ocean (e.g., Came et al., 2008; Valley et al., 2017; Hall and Chan, 2004; Poggemann et al., 2017) and some in the Pacific Ocean (Boyle and Keigwin, 1982; Mccorkle et al., 1995; Umling et al., 2018). The intermediate and deep waters of the northern Indian Ocean are mainly from the south, due to the landlocked by Asia in the north (Talley et al., 2011). Thus, studying intermediate waters in the north Indian Ocean is important i) to understand the global intermediate circulation and its relationships with the Southern Ocean, and ii) to better constrain its potential role in global climate changes and the carbon cycle (Kallel et al., 1988; Jung et al., 2009; Yu et al., 2018; Ma et al., 2019).

We have also investigated benthic foraminiferal assemblages obtained from core MD77-191 (southeastern Arabian Sea) to help us to understand the changes in the bottom water conditions. Combined with benthic foraminiferal $\delta^{18}O$, $\delta^{13}C$, trace and minor elemental ratios obtained from the same core (chapter 4), our study allowed gathering information about past intermediate- and deep-water ventilation and changes in surface paleo-productivity.

2. Material and hydrological setting

We analyzed sediment core MD77-191 (07°30’N-76°43’E, 1254m) located in the Arabian Sea (southern tip of India), and core MD77-176 (14°30’5N-93°07’6E, 1375m), from the northeastern Bay of Bengal (BoB). These cores have been collected in 1977 during the OSIRIS III cruise of the N.0. Marion Dufresne (Fig. 2).

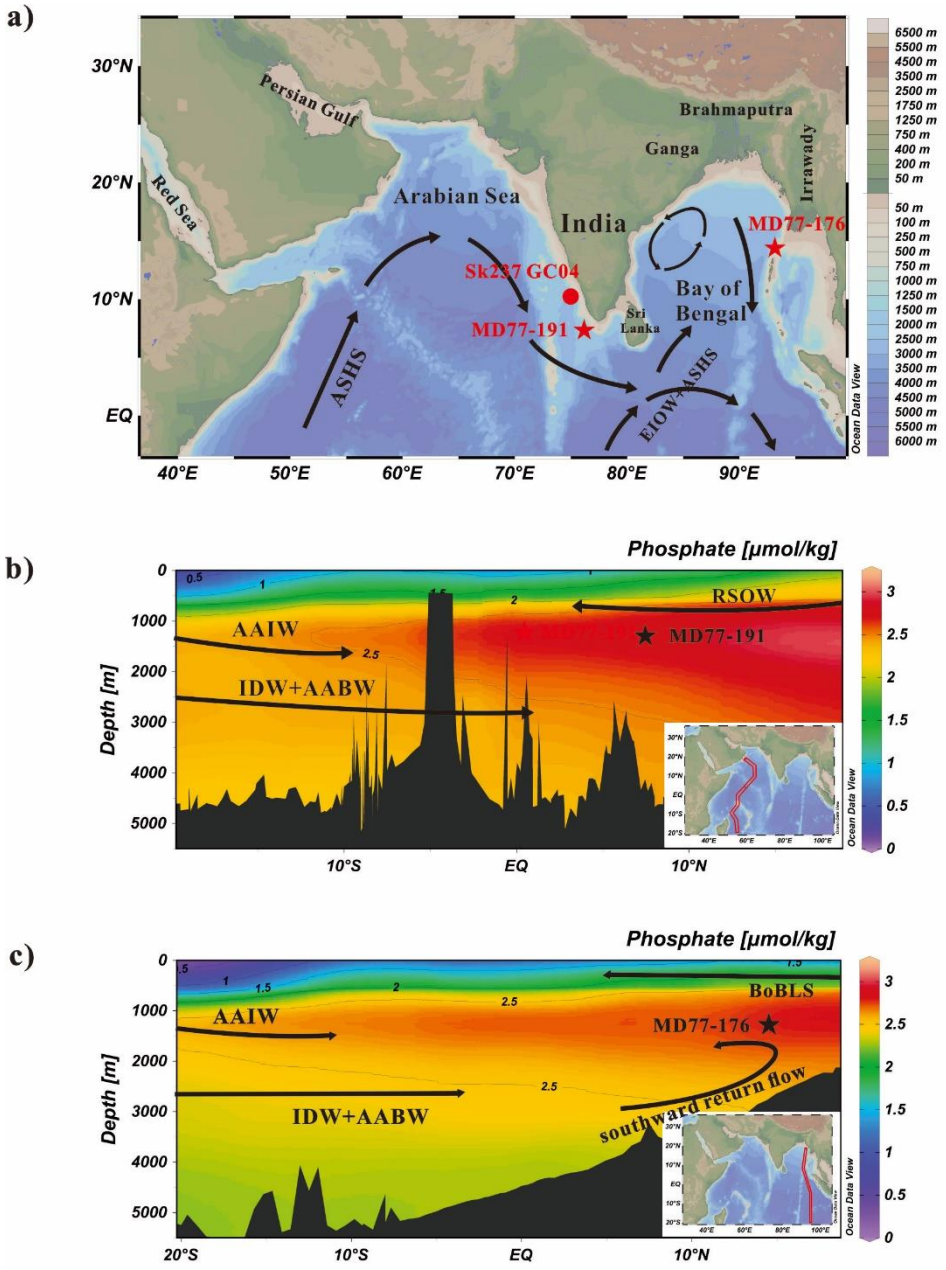

Fig. 2. *(a) Geographical setting and locations of MD77-191 in the Arabian Sea (red star), MD77-176 in the Bay of Bengal (red star) and reference site SK237 GC04 (red cirle, Naik et al., 2017). The black arrows are the general surface circulation direction in the Northern Indian Ocean drifted by Southwest Monsoon (Schott and Mccreary, 2001). (b) and (c) Phosphate (µmol/kg, coloured shading) depth-latitude section using the Ocean Data View (ODV) software (Schlitzer, 2015) and vertical distribution of water masses in the Arabian Sea and Bay of Bengal (N-S cross section). ASHS: Arabian Sea High Salinity Water. EIOW: Eastern Indian Ocean Water, BoBLS: Bay of Bengal low salinity Water, AAIW: Antarctic Intermediate Water, IIW: Indonesian Intermediate Water, RSW: Red Sea Intermediate Water, AABW: Antarctic Bottom Water, IDW: Indian Deep*

Water.

The age model of core MD77-191 was established by using 9 monospecific planktonic foraminifer *Globigerinoides bulloides* accelerator mass spectrometry (AMS) ^{14}C dating (Bassinot et al., 2011), one ^{14}C date made on pteropods (Mléneck, 1997), and three ^{14}C dates obtained on planktonic foraminifera *Globigerinoides ruber* measured at the LSCE, France (Ma et al., in prep.). The ^{14}C ages were converted to calendar ages by using the CALIB Rev. 7.1 software (Stuiver and Braziunas, 1993), the marine calibration data set (Reimer et al., 2013), and correcting for a surface marine reservoir of around 400 years. Core MD77-191 provides a continuous record since the last 17 cal kyr BP with an average sedimentation rate of about 53 cm/kyr and up to 90 cm/kyr for the Holocene. The age model of core MD77-176 was previously established by using 31 planktonic foraminifer (*G. ruber*) AMS ^{14}C dates combined with the core MD77-176 oxygen isotope record obtained on planktonic foraminifera *G. ruber*, which were correlated to the GISP2 Greenland ice core record (Marzin et al., 2013). Core MD77-176 displays high accumulation rates (average ~25 cm/kyr and up to 40 cm/kyr for the Holocene). Both cores have been characterized by high sedimentation rates (up to 90 cm/kyr) allowing to provide for the first time high-resolution benthic foraminifera Cd/Ca and Ba/Ca records in the northern Indian Ocean for the period since 40 cal kyr BP.

In the modern ocean, the surface waters of the Arabian Sea and BoB are characterized by seasonal reversal currents corresponding to the monsoon winds. The surface water masses shallower than 150m in the Arabian Sea are mainly Arabian Sea high Salinity Water (ASHS, 36.5 psu) (Talley et al., 2011). In the BoB, the surface waters above 100m are Bay of Bengal surface waters (BoBSW), with a low salinity (31 psu) due to large river inputs (Talley et al., 2011). The monsoon winds drive a strong vertical mixing in the Arabian Sea, which could cause a large variety of surface productivity during the summer monsoon season (Levy et al., 2007). In contrast, the productivity of the BoB is much lower than in the Arabian Sea due to strong salinity stratification of the upper water column caused by precipitation and Himalayan rivers freshwater discharge (Thushara and Vinayachandran, 2016). The distribution of chlorophyll in surface water of the northeastern BoB suggests a slight increase in productivity during the winter monsoon period (around January) (Thushara and Vinayachandran, 2016; O'malley, 2017).

Cores MD77-191 and MD77-176 are mainly bathed by North Indian Intermediate Water (NIIW) (Olson et al., 1993; Reid, 2003). However, core MD77-191 could also be influenced by the Red Sea Water (RSOW) (Beal et al., 2000; Talley et al., 2011). At core MD77-176 site in the northeastern BoB, there is no or very limited influence of RSOW, but this area could be affected by the southern return flow of deep water (North Indian Deep Water) (Talley et al., 2011). In addition, the

northward extension of AAIW today in the Indian Ocean rarely reaches beyond 10°S (Lynch-Stieglitz et al., 1994). The phosphate concentration of modern waters in the northern Indian Sea (BoB and Arabian Sea) at intermediate water depth is at around 2.5-3 µmol/kg (Figs. 2b and c). In addition, the modern data indicate that the southern sourced intermediate water (AAIW) in the south Indian Ocean shows a lower phosphate concentration at about 2-2.5 µmol/kg (Figs. 2b and c).

3. Methods

3.1. Cd/Ca and Ba/Ca analyses

We analyzed Cd/Ca and Ba/Ca in three calcite (*Cibicidoides pachyderma*, *Uvigerina peregrina*, and *Globobulimina* spp.) and one aragonite (*Hoeglundina elegans*) benthic foraminiferal species from core MD77-191. *C. pachyderma* is an epifaunal species, *U. peregrina* and *Globobulimina* spp. are endobenthic species with an intermediate and a deep microhabitats, respectively (Fontanier et al., 2002). In core MD77-176, we measured Cd/Ca and Ba/Ca ratios in *H. elegans* shells.

Each sample contained approximately 10-15 individuals from the 250-315µm fraction. Samples were gently crushed, cleaned to remove clays, organic matter and elemental oxides by using reductive and oxidative cleaned following previously published methods (Boyle and Keigwin, 1982; Barker et al., 2003). Each sample was dissolved in 0.075N HNO_3 and analyzed using a single collector sector field high resolution inductively coupled plasma mass spectrometer (HR-ICP-MS) Thermo Element XR hosted at the Laboratory GEOPS (University Paris-Sud, France).

The detailed instrumental settings and mother standard solution are described in Ma et al., (in preparation). A blank consisting of the same 0.1N HNO_3 used to dilute the standards and samples is also analyzed. On HR-ICP-MS, the elemental blanks are better than 6.5% for Cd and 1.8% for Ba/Ca. All raw intensities (including standards) are minus blank intensities, raw data are calculated by correcting the drift by using two-point linear standard curves interspersed between every four samples with a same standard. Standard curves are used to calculate elemental/Ca ratios, coefficients of determination (r^2) are always >0.9999 for all elemental ratios. The mean reproducibility and accuracy is Cd/Ca 7.5% and Ba/Ca 4.1%.

3.3. Faunal analysis

A total of 74 samples were collected for benthic foraminiferal assemblage determinations. In each sample, benthic foraminifera (>250 µm) were extracted, counted and identified to species level following the taxonomical descriptions of various authors (e.g., Jones, 1994; Holbourn et al., 2013; Loeblich and Tappan, 1988). Due to the lack of bulk samples' weight from core MD 77-191, we

could not perform the calculation of absolute abundance of foraminifera or accumulation rates, thus we coverted the individual counts as the percentage of total benthic foraminifera present in each sample. In order to describe major faunal variations, we performed principal component analysis (PCA) by using software PAST (Version 3.0, Hammer et al., 2001). Species present with a percentage >1% in at least 1 sample were used for statistical analysis and diversity calculation.

4. Results

4.1. Elemental ratios results

To check the validity of the elemental ratios results, Mn/Ca ratios from cores MD77-191 and MD77-176 were systematically measured. The Mn/Ca of *H. elegans* from cores MD77-191 and MD77-176 range between 6.5 and 10 µmol/mol and between 1 and 30 µmol/mol, respectively. Such ranges are much lower than the 100 µmol/mol limit proposed by Boyle (1983). The Mn/Ca obtained on three calcite benthic foraminifera species from core MD77-191, *C. pachyderma* (5-18 µmol/mol), *U. peregrina* (3-23 µmol/mol) and *Globobulimina* spp. (4-69 µmol/mol) are also all below 100 µmol/mol (Boyle, 1983). The Fe/Ca ratios are generally lower than 1 mmol/mol in all samples from cores MD77-191 and MD77-176. In addition, Barker et al. (2003) suggested a detection limit for uncleaned samples for Al/Ca at **>** 0.5 mmol/mol, and all Al/Ca results are below 0.5 mmol/mol, indicating that the sample cleaning procedure was efficient. This suggests that samples were not affected by clay contamination.

4.1.1 Cd/Ca

The Cd/Ca records of *C. pachyderma*, *U. peregrina* and *Globobulimina* spp. from core MD77-191 range between 0.07-0.2 µmol/mol, 0.07-0.14 µmol/mol and 0.03-0.09 µmol/mol, respectively (Figs. 3b-d). The calcite benthic species *C. pachyderma* and *U. peregrina* Cd/Ca values display a general increase trend during the time interval from the early to late Holocene (10-2.4 cal kyr BP). The Cd/Ca records of *C. pachyderma* and *U. peregrina* generally show a continuous increase during the Holocene with larger variations between 5.2 and 2.4 cal kyr BP. However, the Cd/Ca record of deep infanual *Globobulimina* spp., obtained at lower time resolution, shows different variations compared with the two calcite taxa without long term variations during the Holocene. During the last deglaciation, the Cd/Ca records of *C. pachyderma*, *U. peregrina* and *Globobulimina* spp. both have very low time resolutions. The Cd/Ca records of *C. pachyderma* and *U. peregrina* show low values during the 17-15.2 and 12-11 cal kyr BP time intervals, with average values of ~0.08

µmol/mol for *C. pachyderma* and ~0.09 µmol/mol for *U. peregrina*. By contrast, these two species (*C. pachyderma* and *U. peregrina*) Cd/Ca ratios display a higher value (~0.12 µmol/mol) at the 15-13.3 cal kyr BP time interval compared with 17-15.2 and 12-11 cal kyr BP time intervals.

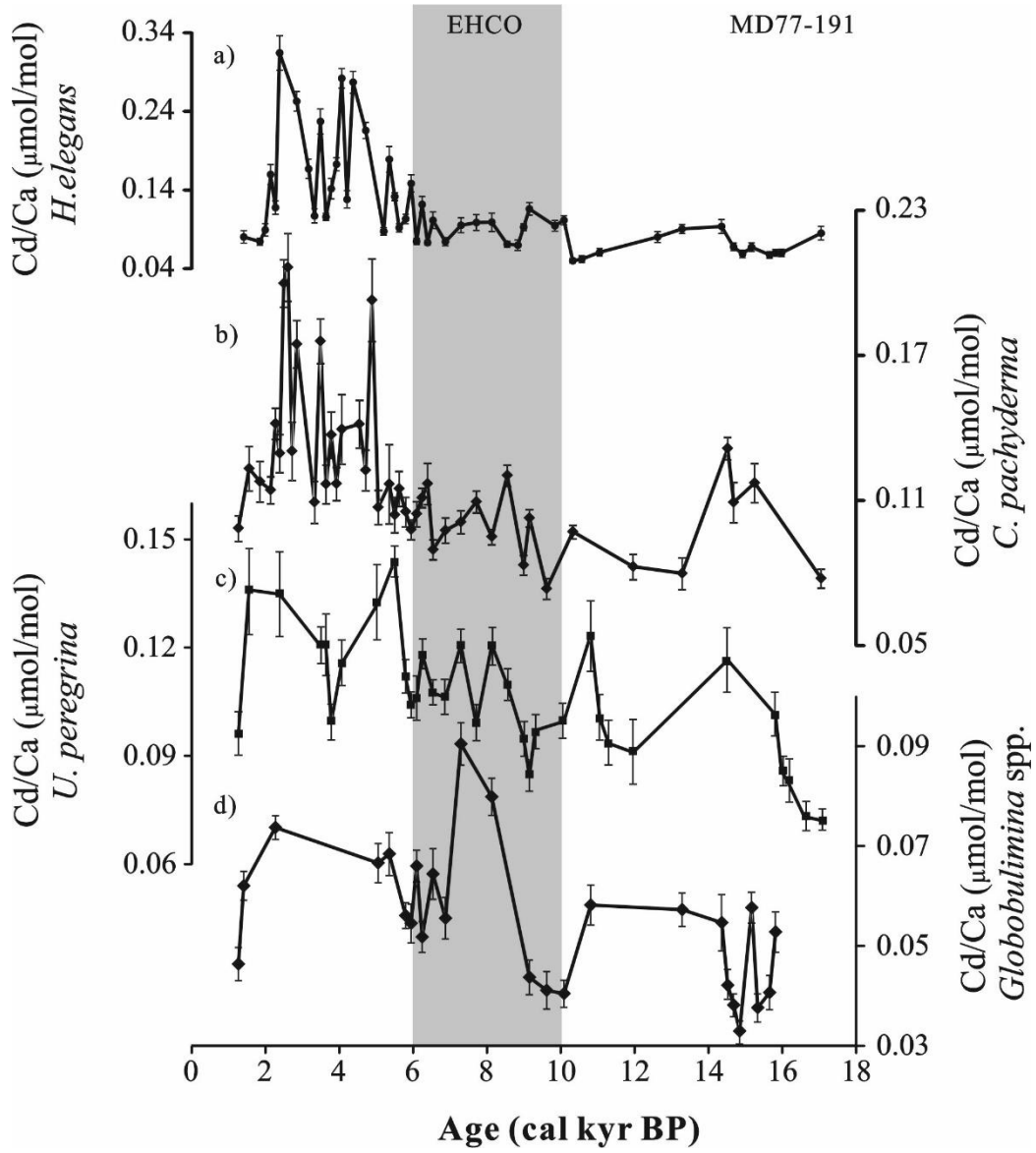

Fig. 3. *(a)-(d) Cd/Ca records of the benthic foraminifera Hoeglundina elegans, Cibicidoides pachyderma, Uvigerina peregrina, and Globobulimina* spp. *obtained from MD77-191. EHCO: Early Holocene Climate Optimum associated to intensified summer monsoon rainfall is also displayed.*

The *H. elegans* Cd/Ca values of core MD77-191 range from 0.05 to 0.31µmol/mol since 17 cal kyr BP (Fig. 3a). Compared with the lower values (0.07 µmol/mol) for the last deglaciation (17-11

cal kyr BP time interval), a continuous increase in the Cd/Ca begins at 10 cal kyr BP and reaches a maximum (0.31 μmol/mol) during the late Holocene (from 5.2 to 2.4 cal kyr BP). In addition, taking into consideration the analytical error bar (±0.02, 2σ) significant decreases of about ~0.05 μmol/mol occurred at 16-15.2 and 12.6-11 cal kyr BP time intervals during the last deglaciation, and a slightly increase (0.09 μmol/mol) between 15 and 13.3 cal kyr BP.

For core MD77-176, the *H. elegans* Cd/Ca records range between 0.06 and 0.17 μmol/mol over the past 18 cal kyr BP (Fig. 4a). The average benthic Cd/Ca values are similar at ~0.09 μmol/mol during the different time intervals (18-15.4 cal kyr BP, 12.7-10.5 cal kyr BP and Holocene). The analyses of MD77-176 are at low time resolution during the last deglaciation, moreover, compared with benthic Cd/Ca obtained from MD77-191, the Cd/Ca from MD77-176 record does not display a strong long-term trend since the last 18 cal kyr BP. However, the benthic Cd/Ca for the Holocene is associated to a slight increase both in value and range of variations after 6 cal kyr BP.

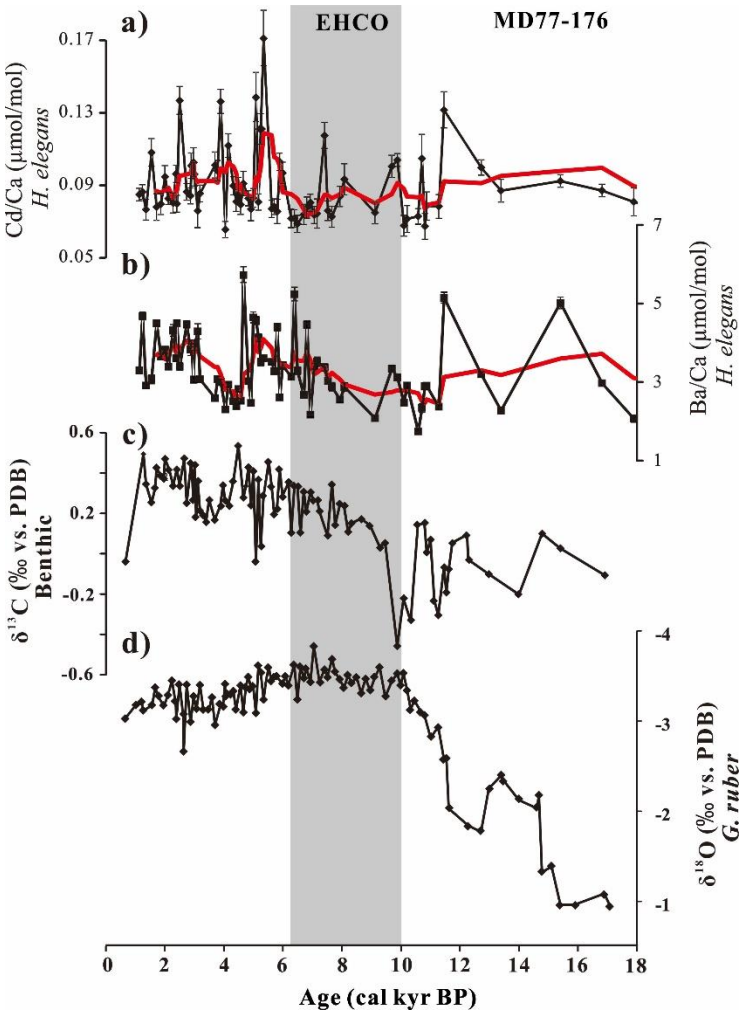

Fig. 4. *(a) Cd/Ca and (b) Ba/Ca records of the benthic foraminifera Hoeglundina elegans from*

MD77-176, the red lines are the smoothed curves using a five-point average. (c) benthic $\delta^{13}C$ (d) G. ruber $\delta^{18}O$ records for MD77-176. EHCO: Early Holocene Climate Optimum associated to intensified summer monsoon rainfall is also displayed.

4.1.2 Ba/Ca

The Ba/Ca records obtained on the four benthic foraminifera species from core MD77-191 range between 1.8-6.3 µmol/mol (*H. elegans*), 1.3-3.7 µmol/mol (*C. pachyderma*), 1.7-3.9 µmol/mol (*U. peregrina*) and 1.7-3.4 µmol/mol (*Globobulimina* spp.), respectively (Fig.5). For benthic calcite foraminifera *C. pachyderma*, *U. peregrina and Globobulimina* spp., the average Ba/Ca values during the last deglaciation (17-11 cal kyr BP) are 2.39, 2.21 and 1.96 µmol/mol, respectively. The mean Ba/Ca values during the Holocene are 3.03 µmol/mol (*C. pachyderma*), 2.62 µmol/mol (*U. peregrina*) and 2.69 µmol/mol (*Globobulimina* spp.), slightly higher than during the last deglaciation. The Ba/Ca record of *H. elegans* does not exhibit strong variations from the last deglaciation to the Holocene (mean values 3.51 and 3.17 µmol/mol, respectively) (Fig. 5a). In addition, the Ba/Ca record of the deep infauna species *Globobulimina* spp. is at a very low time resolution compared with other species, precluding observing the millennial scale variations since 16 cal kyr BP. However, the Ba/Ca values of *Globobulimina* spp. display a continuous increase trend from 16 cal kyr BP (～1.76 µmol/mol) to 6 cal kyr BP and reach maximum values (~ 3.4 µmol/mol) at the 6.8-6 cal kyr BP interval. Thereafter, the record shows a decrease trend until 1.3 cal kyr BP.

During the last deglaciation, short events have also been recorded at the core MD77-191 site during the 17-15.2, 15-14.3 and 13.3-11 cal kyr BP intervals. The Ba/Ca values all show a decreasing trend in the 16-15.2 cal kyr BP time interval (*C. pachyderma* ～2.35 µmol/mol, *U. peregrina* ～2.23 µmol/mol and *H. elegans* ～3.15 µmol/mol), followed by higher values during the 15-14.3 cal kyr BP time-period (*C. pachyderma* ～2.85 µmol/mol, *U. peregrina* ～2.7 µmol/mol and *H. elegans* ～4.15 µmol/mol). Then, a decrease occurs from 13.3 to 11 cal kyr BP.

In addition, Ba/Ca records obtained from *H. elegans*, *C. pachyderma* and *U. peregrina* all display a general increasing trend during the 8.8-3.5 cal kyr BP with a lager shift at around 6 cal kyr BP. However, the Ba/Ca records from these three benthic species seem to display different trend at some millennial scale events during the Holocene. For the Ba/Ca records of calcite species *C. pachyderma* and *U. peregrina*, significant decreases at 10-9 and 4.7-3.6 cal kyr BP intervals are observed, by contrast with the *H. elegans* Ba/Ca, showing an increasing trend during these two time intervals.

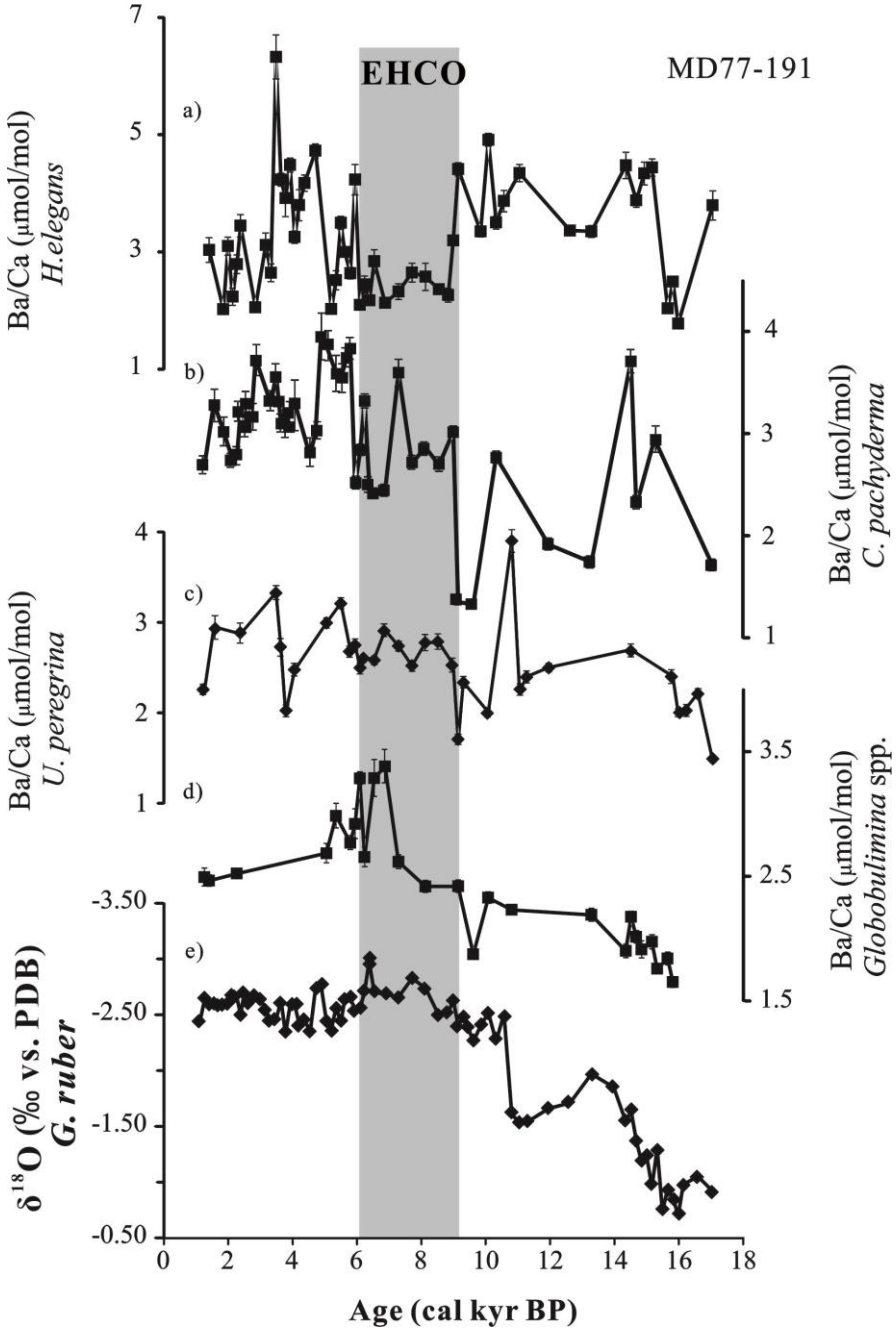

Fig. 5. *(a)-(d) Ba/Ca records of the benthic foraminifera Hoeglundina elegans, Cibicidoides pachyderma, Uvigerina peregrina, and Globobulimina* spp. *obtained from MD77-191; (e) G. ruber $\delta^{18}O$ records for MD77-191. EHCO: Early Holocene Climate Optimum associated to intensified summer monsoon rainfall is also displayed.*

The *H. elegans* Ba/Ca record from core MD77-176 ranges between 1.7 and 5.7 µmol/mol over the past 18 cal kyr BP (Fig.4b). The Ba/Ca record from core MD77-176 shows a similar value range (average ~3.4 µmol/mol) during the Holocene than the last deglaciation. The Ba/Ca record shows a much lower time resolution during the last deglaciation compared with Holocene, it seems less

reliable to describe the variations during the last deglaciation based on a low resolution record. Thus, we will only focus on changes in the Ba/Ca since 10 cal kyr BP. The values of Ba/Ca during the Holocene display a general increase since 10 cal kyr BP with significant shift (mean values of ~ 3.5 µmol/mol) at around 7-5 cal kyr BP.

4.2. Foraminifera assemblages

Benthic foraminiferal species richness ranges between 16 and 36, and total abundance fluctuates between 84 and 644 specimens. Hyaline species are the dominant constituents (＞80%), and consist mainly in *Bulimina aculeata*, *Hoeglundina elegans*, *Cibicidoides pachyderma*, *Uvigerina* spp., *Gyroidina broeckhiana*, *Globocassidulina subglobosa*, *Sphaeroidina bulloides*, *Gyroidinoides* spp., *Lenticulina* spp., *Melonis barleeanum*, and *Globobulimina* spp. (including *Praeglobobulimina* spp.) (in decreasing order of relative average abundance). Agglutinated taxon reach on average about 1.6%, and consist in *Textularia* sp., *Martinottiella communis*, and *Eggerella bradyi*. Average percentage of porcelaneous species is about 5.1%, characterized by *Pyrgo elongata*, *Pyrgo murrhina*, *Pyrgo depressa*, *Pyrgoella irregularis*, *Quinqueloculina* spp., *Sigmoilopsis schlumbergeri*, and *Spiroloculina* spp.

Furthermore, we merged species that have ecological similarity, such as *Globobulimina affinis*, *Globobulimina pacifica*, and *Praeglobobulimina* spp. into *Globobulimina* spp. The relative abundance of species >1% in at least 1 sample were used for statistical analyses. Around 74 samples and 55 groups/species were adopted to perform principal component analysis (PCA) in order to identify major faunal trends. The PCA analysis suggests that the benthic foraminifera could be grouped into two assemblages, and represents about 42% of the total variance (Table 1).

High positive loadings of PC1 are shown by *Bulimina aculeata* and *Cibicidoides pachyderma*, together with *Pullenia bulloides* and *Ehrenbergina trigona*. This assemblage, referred hereafter as assemblage 1, dominated the foraminiferal record during the late Holocene (between 6 and 1.4 cal kyr BP) (Fig. S1a). *Hoeglundina elegans* and *Bulimina manginata* exhibit high negative loadings on PC1 and dominate so-called assemblage 2, which dominate the record from the last deglaciation to early Holocene (Fig. S1b). Other quantitatively important contributors are *Cibicidoides wuellerstorfi*, *Globocassidulina subglobosa*, and *Gyroidinoides orbicularis.*

The total variance of PC2 is 21%, and the species composition consist of *Bulimina mexicana*, *Gyroidinoides orbicularis* and *Bolivina robusta* (Positive loadings); *Bulimina aculeata*, *Hoeglundina elegans* and *Uvigerina peregrina* (Negative loadings) (Table 1). It seems that the main composition of assemblage (PC2) is quite similar to PC1, and does not show more information

about the bottom conditions compared to PC1. Thus, we only use PC1 in the manuscript to recognize the two assemblages.

Table 1. *Species composition of benthic foraminiferal assemblages from core MD77-191.*

	Dominant species		**Important associated species**		**Variance (%)**
PC1					42
Positive loadings	*Bulimina aculeata*	0.82	*Pullenia bulloides*	0.15	
	Cibicidoides pachyderma	0.16	*Ehrenbergina trigona*	0.13	
Negative loadings	*Hoeglundina elegans*	-0.28	*Cibicidoides wuellerstorfi*	-0.03	
	Bulimina manginata	-0.07	*Globocassidulina subglobosa*	-0.03	
			Gyroidinoides orbicularis	-0.04	
PC2					21
Positive loadings	*Bulimina mexicana*	0.15	*Gyroidinoides orbicularis*	0.17	
	Bolivina robusta	0.14			
Negative loadings	*Bulimina aculeata*	-0.26	*Hoeglundina elegans*	-0.55	
	Uvigerina peregrina	-0.52			

5. Discussion

5.1. Intermediate Cd_w concentrations from Northern Indian Ocean

In the modern ocean, benthic foraminifera Cd/Ca have a positive correlation with Cd_w and labile nutrient (phosphate and nitrate) (Boyle et al., 1976; Hester and Boyle, 1982). As aragonite benthic foraminifera *H. elegans* faithfully records the bottom water Cd concentrations (Cd_w), Cd/Ca ratios could be converted to seawater Cd_w with the relationship (Eq.4.1), where the partition coefficient $D_p \approx 1$ for all water depth (Boyle et al., 1995; Bryan and Marchitto, 2010).

$$Dp = \frac{(Cd/Ca)_{foram}}{(Cd/Ca)_{water}} \quad \text{(Eq. 4.1)}$$

However, the partition coefficient in the calcite species changes with water depth. For water depths

below 3000m, $D_p \approx 2.9$ and for water depths between 1150-3000 m, was calculated based on the equation of Boyle, (1992; Eq. 4.2). The seawater Ca concentration is assumed to be a constant mean value of 0.01 mol/kg (Boyle, 1992).

$$D_p = 1.3 + (\text{depth} - 1150) \times (1.6/1850) \quad \text{(Eq. 4.2)}$$

The intermediate Cd_w based on the *H. elegans* Cd/Ca values of core MD77-191 range from 0.5 to 3.1µmol/kg since 17 cal kyr BP (Fig. 6a). Cd_w results from core MD77-191 indicate a shift from last deglaciation (~0.8 nmol/kg) to late Holocene (~1.31 nmol/kg). A continuous increase in the Cd_w begins at 10 cal kyr BP and is marked by a major shift at around 6.4 cal kyr BP with values up to 3.1 nmol/kg for 5.2-2.4 cal kyr BP time interval. In addition, variations of Cd_w obtained on *H. elegans* during the last deglaciation indicate a decrease of about ~0.5 nmol/kg at 16-15.2 and 12.6-11 cal kyr BP time intervals during the last deglaciation, with a slight increase (0.9 nmol/kg) between 15 and 13.3 cal kyr BP.

The intermediate Cd_w was also calculated for calcite benthic species *C. pachyderma*, *Globobulimina* spp. and *U. peregrina* obtained from core MD77-191. The Cd_w values of deep infanual *Globobulimina* spp. do not exhibit strong variations compared to the Cd_w records of *C. pachyderma* and *U. peregrina,* displaying a general increasing trend from the last deglaciation to the Holocene. In addition, the relatively lower change of *Globobulimina* spp. Cd/Ca compared to the other species investigated here may indicate a stable nutrient of the pore water, as *Globobulimina* spp. is a deep benthic infaunal species compared with other benthic taxa (Fig. 6d). During the last deglaciation, the Cd_w values show a decreasing trend during the 17-15.2 and 12-11 cal kyr BP intervals, with mean values of ~ 0.59 and 0.65 nmol/kg, respectively, for *C. pachyderma* and ~ 0.62 and 0.67 nmol/kg, respectively, for *U. peregrina*) (Fig. 6b and c). In addition, these two species (*C. pachyderma* and *U. peregrina*) Cd_w records all display a higher value (~0.94 and 0.84 nmol/kg) at the 15-14.3 cal kyr BP interval (Fig. 6b and c). Such variations of Cd_w obtained on *C. pachyderma* and *U. peregrina* are in good agreement with those obtained on *H. elegans*. Then, the Cd_w displays a general increase during the Holocene, with average values of ~0.87 nmol/mol for *C. pachyderma* and ~0.81 nmol/kg for *U. peregrina*.

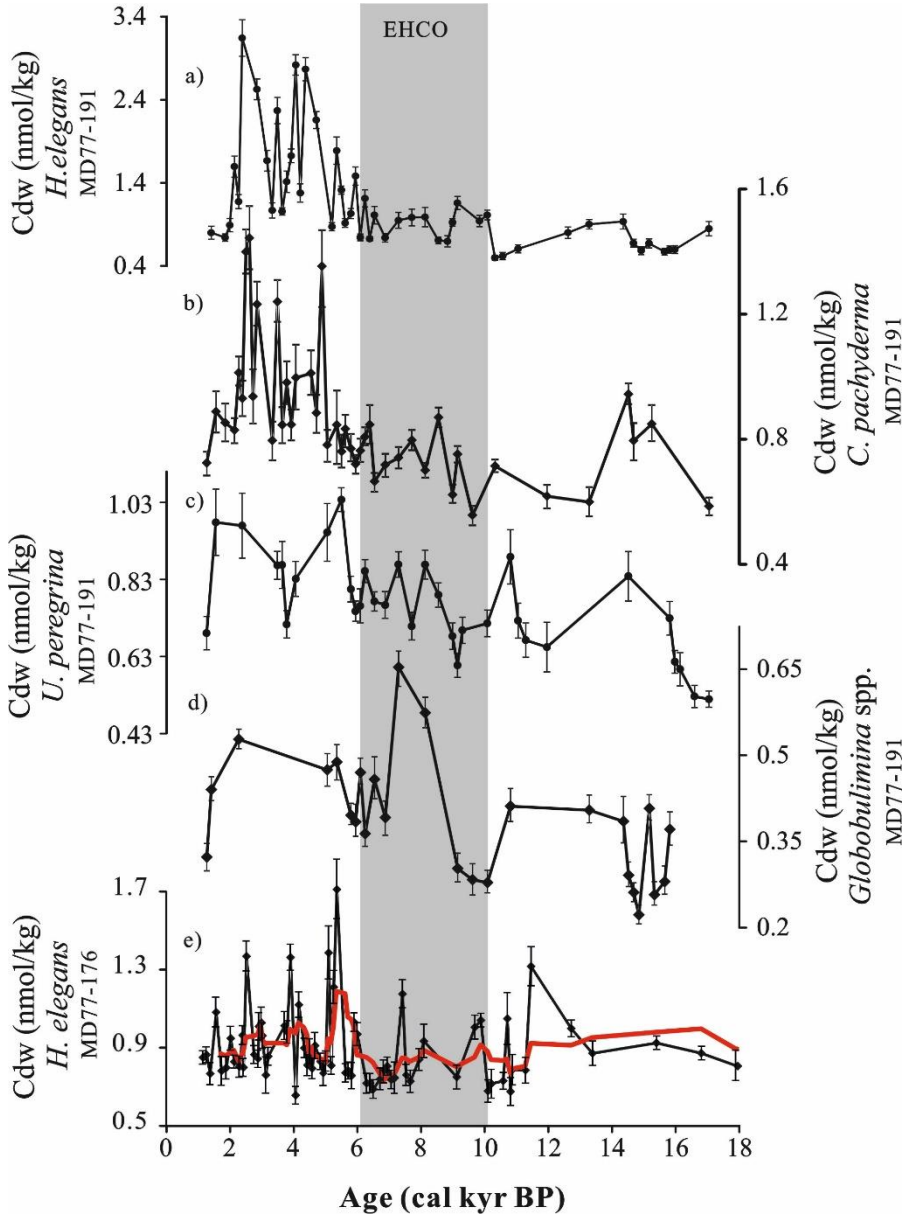

Fig. 6. *(a)-(d) Cd_w records calculated based on the Cd/Ca of benthic foraminifera Hoeglundina elegans, Cibicidoides pachyderma, Uvigerina peregrina, and Globobulimina* spp. *obtained from MD77-191, (e) Cd_w record from MD77-1761 reconstructed by H. elegans Cd/Ca, the red line is the smoothed curves using a five-point average. EHCO: Early Holocene Climate Optimum associated to intensified summer monsoon rainfall is also displayed.*

For core MD77-176, the intermediate Cd_w calculated from the *H. elegans* Cd/Ca records ranges between 0.6 and 1.7 nmol/kg over the past 18 cal kyr BP (Fig. 6e). Compared with intermediate Cd_w from MD77-191, the Cd_w record of core MD77-176 does not display a strong long-term trend from the last deglaciation to the Holocene. However, the trend of Cd_w during the Holocene also

displays a slight increase both in value and range of variations since 6 cal kyr BP, which is associated with the increased in MD77-191 intermediate Cd_w record at 6.4-2.2 cal kyr BP interval. In addition, the MD77-176 record was at a lower time resolution especially during the last deglaciation, and seems displaying a slight increase (1 nmol/kg) in the 18-15.4 cal kyr BP time interval, with a second shorter maximum (1.3 nmol/kg) at 13.4-11 cal kyr BP time interval.

As the labile nutrient regenerates by the decomposition of organic matter from the surface water, such variations of Cd_w could be due to a modification of the surface productivity. However, the Cd_w could also be modified by variations of the water masses sources and/or the renewal process of deep-water masses (Marchitto, 2004; Marchitto and Broecker, 2006).

5.2 Intermediate refractory nutrient variations since the last deglaciation

The distribution of barium has a positive relationship with the refractory nutrient (silica and alkalinity) (Chan et al., 1977; Lea and Boyle, 1989). Thus, the release of dissolved barium to the bottom water during organic matter remineralization can be recorded through the benthic Ba/Ca, a potential tracer proxy for the refractory nutrients.

The variations of the Ba/Ca records obtained on four benthic foraminiferal species (*H. elegans*, *C. pachyderma*, *U. peregrina* and *Globobulimina* spp.) are less clear compared with the Cd/Ca records from core MD77-191, especially at the millennial scales during the Holocene. However, the slight changes recorded at the millennial-scale in the Ba/Ca records are in agreement with the benthic Cd/Ca during the last deglaciation. Indeed, the records of Ba/Ca obtained from *C. pachyderma*, *U. peregrina* and *H. elegans* in MD77-191 all display decreasing trends during the 16-15.2 cal kyr BP and 13.3-11 cal kyr BP time intervals, consistent with the benthic Cd/Ca changes during the same time intervals (Fig. S2). In addition, although the records of Ba/Ca from *H. elegans*, *C. pachyderma* and *U. peregrina* show different trends at the 10-9, 4.7-3.6 cal kyr BP time intervals (during the Holocene) and seem difficult to interpret in the detail, the Ba/Ca records from these three species all display an increasing trend during the 8.8-3.5 cal kyr BP. A larger shift occurs at around 6 cal kyr BP, which is in agreement with the variations of Cd/Ca records from the same core (Fig. S2).

As both Ba/Ca and Cd/Ca records performed on *H. elegans* from core MD77-176 are at a much lower time resolution during the last deglaciation than the Holocene, it seems less reliable to describe the variations during the last deglaciation. Thus, we only focus on the variations since 10 cal kyr BP. In order to better observe the variations during the Holocene, we will use the Cd/Cd and Ba/Ca records on the smoothed curves using a five-point average for a comparison (Figs. 4a and b).

These smoothed curves show a covariation for the Holocene (Figs. 4a and b). The records display a general increase since 10 cal kyr BP with significant shift at around 7 cal kyr BP. Finally, we suggest that the Ba/Ca and Cd/Ca records seem in agreement in the long-term variations during the Holocene and at millennial scale changes during the last deglaciation for core MD77-191.

Changes in the Ba/Ca record indicates the influence of an additional source of Ba to the deep waters (surface productivity and river input), the source of water masses and/or the ventilation of deep-water masses (Martin and Lea, 1998; Ni Fhlaithearta et al., 2010). However, river inputs do not appear to play an important role in the variation of Ba/Ca. Although the River input is characterized by enriched Ba^{2+} relative to surface waters (Hall and Chan, 2004), but the transport of river barium is quite limited due the saturation of seawater related to $BaSO_4$ (Ni Fhlaithearta et al., 2010). In addition, we also compared the Ba/Ca record with the *G. ruber* $\delta^{18}O$ records of core MD77-176 (Marzin et al., 2013) and MD77-191 which indicates the surface salinity variations in the core site (Figs. 4b, d and 5). The lower salinities during the earliest Holocene (around 10-7 kyr) are associated with an intensified Indian monsoon, leading to more freshwater discharge from the Ganges-Brahmaputra river system and from the Irrawaddy River (e.g., Marzin et al., 2013; Contreras-Rosales et al., 2014). This should have led to more river barium, however, we do not observe a larger increase in the Ba/Ca values, the opposite of what would be expected from strong river barium input. Thus, the influence of the large river input on the benthic Ba/Ca values can be discounted. Moreover, the Ba^{2+} sourced from water masses also does not appear to be a major control at our core site. As in the modern Indian Ocean, the silica concentration of the core sites is similar with the southern sourced intermediate water (Fig.S3), and would reflect a stable refractory nutrient at the intermediate water depth.

In addition, previous works indicate that the enhanced benthic Ba/Ca ratios could be mainly related to increased surface productivity and/or lower ventilation (e.g., Hall and Chan, 2004; Martin and Lea, 1998; Ni Fhlaithearta et al., 2010). Moreover, the Cd_w could also reflect the surface productivity variations, source of water masses and/or the renewal process of deep water masses. Therefore, we will discuss these possible mechanisms below and will combine our data to enable us to decipher these different processes.

5.3. Intermediate water circulation versus productivity effects

In core MD77-191, we measured three calcite benthic taxa and one aragonite benthic species *H. elegans*, all of these records showing similar variations since 17 cal kyr BP. However, the Cd/Ca and Ba/Ca record of *H. elegans* has a higher resolution compared to other calcite benthic species,

especially during the last deglaciation. Moreover, we only produced a Cd/Ca record from *H. elegans* at core MD77-176 site. Thus, in the following discussion, we will only focus on the intermediate Cd_w which were calculated by the *H. elegans* Cd/Ca from cores MD77-191 and MD77-176. In addition, the time resolution of *H. elegans* Cd/Ca and Ba/Ca records from core MD77-176 during the last deglaciation is very low compared with the Holocene, then, we only focus on the high resolution period since 10 cal kyr BP (Holocene).

The significant changes in the relative abundance of planktonic foraminifera *Globigerina bulloides* seem correspond to enhanced productivity (Curry et al., 1992; Naidu et al., 1992), and the immediate response of *G. bulloides* to the changes of the productivity makes it to be a useful proxy to reconstruct the paleo-productivity (e.g., Naidu and Malmgren, 1996; Zaric et al., 2005; Bassinot et al., 2011). In addition, the total organic carbon (C_{org}) could be also used as an indicator of past productivity and/or bottom water ventilation changes (Naidu et al., 1992; Canfield, 1994; Calvert et al., 1995; Naik et al., 2017). In order to examine the relationships between intermediate Cd_w and surface productivity since the last deglaciation in the eastern Arabian Sea, we compared the MD77-191 Cd_w values with the relative abundance of *G. bulloides* from the same core MD77-191, the records of C_{org} and the *G. bulloides* percentage obtained from core SK237 GC04 (1245m, southeastern Arabian Sea, Naik et al., 2017) (Figs. 7a-d). These records display a strong co-variation since 17 cal kyr BP. Thus, we suggest the intermediate Cd_w could be mainly influenced by the surface productivity.

In addition, *B. aculeata* and *C. pachyderma* are major components to assemblage 1 (during the late Holocene), together with *Pullenia bulloides* and *Ehrenbergina trigona* (Figs. 8 and S1a). According to various authors, *B. aculeata* has a widespread distribution in the Southern Atlantic Ocean, the South China Sea and Arabian Sea, with preferred water depths from 1500 to 2500m (Miao and Thunell, 1993; Mackensen et al., 1995; Jian and Wang, 1997; Almogi-Labin et al., 2000). The distribution of *B. aculeata* is typically associated to high productivity and organic carbon flux (Mackensen et al., 1995; Altenbach et al., 1999). In the modern Arabian Sea, *B. aculeata* were observed in water with high phosphate and nitrate concentrations where surface productivity is high (De and Gupta, 2010). *Pullenia bulloides* is a shallow infaunal species, associated to mesotrophic environment in poorly ventilated deep waters in the northwestern Indian Ocean (Gupta and Thomas, 1999). *Ehrenbergina trigona* are recorded commonly in low oxygen habitats (Caulle et al., 2014). We thus interpret assemblage 1 as indicating relatively low-oxygen and meso- to eutrophic bottom water conditions during the late Holocene (6-1.4 cal kye BP). This environment could be associated to a higher surface productivity. In addition, strengthened increased of intermediate Cd_w records from MD77-191, all display larger increase during the 5.2-2.4 cal kyr BP associated to larger

variations in *G. bulloides* relative abundance from MD77-191 (Bassinot et al., 2011), which indicate an enhanced productivity during the late Holocene (Fig. 8). Benthic foraminifera assemblage 1 seem consistent with the geochemical proxies, reflecting a relatively low-oxygen level and meso- to eutrophic deep water conditions at the core site during the late Holocene that could correspond to high productivity.

By contrast, benthic foraminiferal assemblage 2 that dominate the last deglaciation to the early Holocene is characterized by *H. elegans* and *Bulimina manginata* as major contributors. The other quantitatively important contributors are *Cibicidoides wuellerstorfi, Globocassidulina subglobosa,* and *Gyroidinoides orbicularis* (Fig. S1b). In the northern Arabian Sea, Den Dulk et al. (1998) suggested that *H. elegans* preferred a high dissolved oxygen and low organic carbon level environment. Studies of living specimens from Bay of Biscay showed that the fauna dominated by *H. elegans* corresponds to rather oligotrophic settings (Fontanier et al., 2002). The live *C. wuellerstorfi* were found at low organic carbon flux rate (Mackensen et al., 1985; Burke et al., 1993; Altenbach et al., 1999). In addition, in the eastern Indian Ocean, it could indicate an environment characterized by a high oxygen concentration and a low carbon-flux rate (Murgese and De Deckker, 2005, 2007). *G. subglobsa* is an infaunal cosmopolitan species which is found throughout the Atlantic, Pacific and Southern Ocean. It reflects an oligotrophic environment, which is associated with a lower organic matter and higher dissolved-oxygen concentrations (Schönfeld, 2001; De and Gupta, 2010 and references therein).

Periods dominated by this taxon indicate then rather high oxygen levels and an oligotrophic environment. All evidences together suggest that intermediate water masses during the Holocene were characterized by high bottom water oxygen conditions and a low flux of organic matter. Thus, the assemblage 2 dominated during the (17-6 cal kyr BP interval) may be associated to the lower surface productivity compared with the late Holoecene (6-1.4 cal kyr BP). The benthic foraminiferal assemblages analysis seem difficult to be identified at millennial-scale variation during the last deglaciation (Fig. S1b). The records of *G. bulloides* percentage (Bassinot et al., 2011) and intermediate Cd_w during the 17-6 cal kyr BP all display a larger variation since 6 cal kyr BP and show a much lower values compared with the late Holocene, and the depleted values are in agreement with the assemblage 2 indicating a poor surface productivity from the last deglaciation to the early Holocene.

Thus, the benthic assemblages could indicate the organic matter flow, which may associated to the surface productivity especially in high carbon flux regions such as the Arabian Sea (Schnitker, 1994). In addition, the benthic foraminifera fauna are consist with the Cd_w record of core MD77-191

particularly during the late Holocene (6-1.4 cal kyr BP), and may indicate the record of Cd_w mainly link to changes of the surface productivity at the core site.

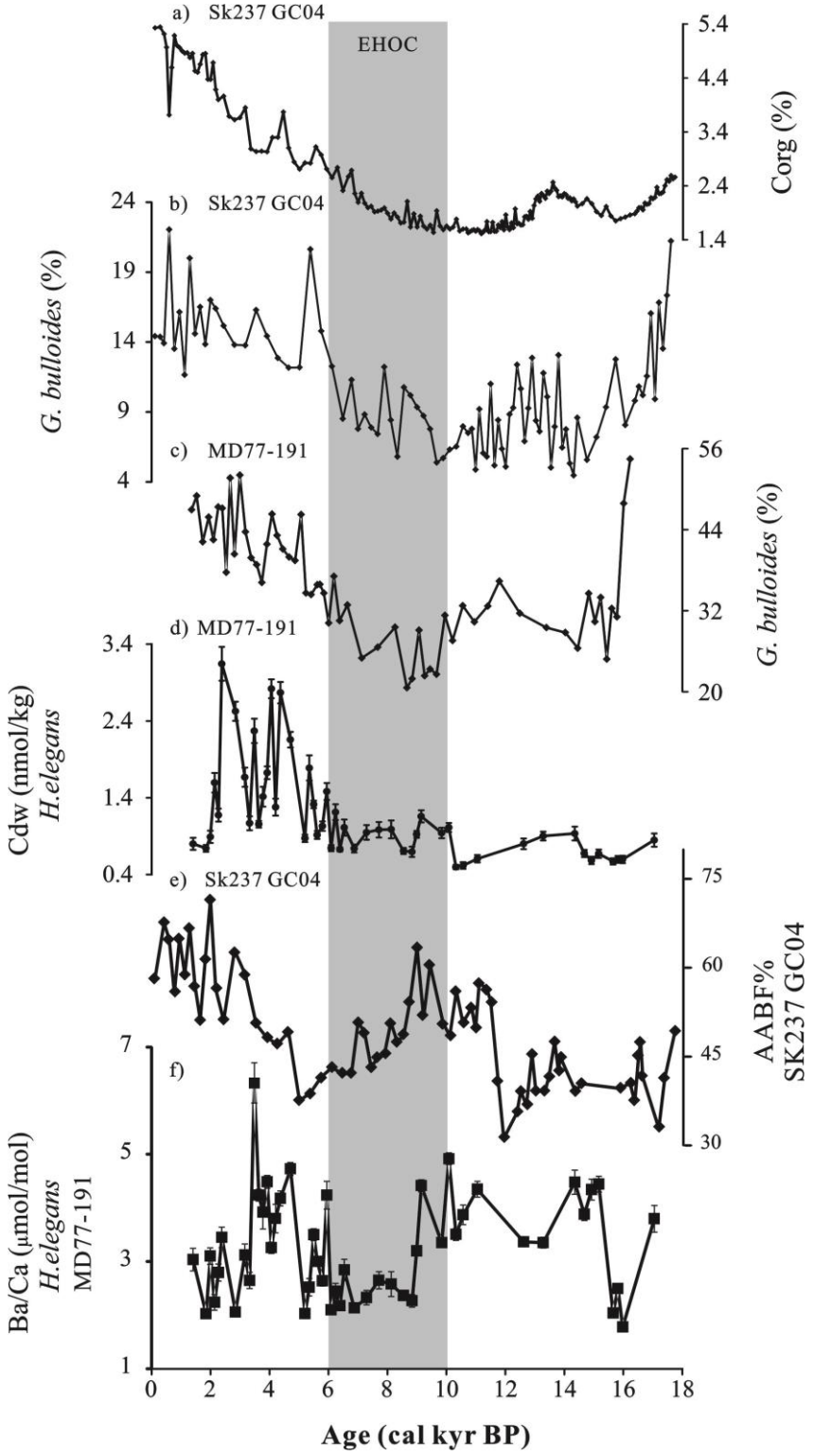

Fig. 7. *(a) Organic carbon weight percentage (%C_{org}) and (b) G. bulloides percentage from core SK237 GC04 (1245m, Arabian Sea, Naik et al., 2017). (c) relative abundance of G. bulloides and (d) Cd_w records from MD77-191 (Arabian Sea). (e) Relative abundance of angular asymmetrical benthic foraminifera (%AABF) from core SK237 GC04 (1245m, Arabian Sea, Naik et al., 2017). (f)*

H. elegans Ba/Ca records from MD77-191 (Arabian Sea). EHCO: Early Holocene Climate Optimum associated to intensified summer monsoon rainfall is also displayed.

The enhanced benthic Ba/Ca ratios could be mainly associated to the increased surface productivity and/or lower ventilation (e.g., Hall and Chan, 2004; Martin and Lea, 1998; Ni Fhlaithearta et al., 2010). We compared the *H. elegans* Ba/Ca record with the relative abundance of angular asymmetrical benthic foraminifera (%AABF) obtained from core SK237 GC04 (southeastern Arabian Sea, 10°58.65'N, 74°59.96'E, 1245m; Naik et al., 2017) to figure out the influence of the bottom water ventilation, as the dropped in %AABF suggest enhanced bottom water ventilation (Nigam et al., 2007; Mazumder and Nigman, 2014; Naik et al., 2017) (Figs.7e and f). All of these two records display decreasing trend during the 16-15.2 cal kyr BP and 13.3-11 cal kyr BP time intervals. In addition, during the early Holocene, these two records decrease from 9 to 6 cal kyr BP. However, the *H. elegans* Ba/Ca of MD77-191 and %AABF from SK237 GC04 display an opposite trend since 6 cal kyr BP. By contrast, the Ba/Ca record seems consistent with the increasing trend in Cd_w during the 6-3.5 cal kyr BP interval (Figs. 7 d and f). As we discussed before, the intermediate Cd_w from MD77-191 is mainly controlled by the surface productivity; thus, we suggest that the *H. elegans* Ba/Ca may also be affected by the productivity (during the late Holocene) and/or bottom water ventilation (from the late deglaciation to the early Holocene, the period with low productivity).

For core MD77-176 in the northern BoB, the smoothed curves of intermediate Cd_w and *H. elegans* Ba/Ca records show a covariation for the Holocene (Figs. 6e and 4b). These records display a general increase since 10 cal kyr BP with significant shift at around ~6 cal kyr BP, which is agreement with the larger variation of Cd_w obtained from MD77-191 during the Holocene, thus we suggest the *H. elegans* Ba/Ca and Cd_w may also reflect the surface productivity.

5.4. Changes in intermediate water circulation, paleo-productivity and global implications

During the Holocene, the intermediate Cd_w obtained from cores MD77-191 and MD77-176 display a continuous increasing trend since 10 cal kyr BP and with larger variations between 5.2 and 2.4 cal kyr BP. Compared with the late Holocene, the lower values of intermediate Cd_w between 10 and 6 cal kyr BP, corresponding to depleted values of *G. bulloides* relative abundance from cores SK237 GC04 and MD77-191 in the same time interval, and may indicate a poor surface productivity for the time interval from 10 to 6 cal kyr BP than during the late Holocene (Naik et al.,

2017) (Figs. 7b-c). The hypothesis to explain the lower surface productivity during the 10-6 cal kyr BP could be related by the intensified monsoon precipitation, and/or enhanced transport of low salinity water from the BoB (Sirocko et al., 2000; Naik et al., 2017). As the early Holocene Climate Optimum (10-6 cal kyr BP) is characterized by enhanced monsoon precipitation (Marzin et al., 2013; Contreras-Rosales et al., 2014) (Figs.9c-e), this should lead to more freshwater discharge from the Ganges-Brahmaputra river system and from the Irrawaddy River, then resulting in pronounced ocean stratification of the northern BoB and the south tip of India. Thus, this process may in turn decrease the surface productivity in the northern BoB and southeastern Arabian Sea.

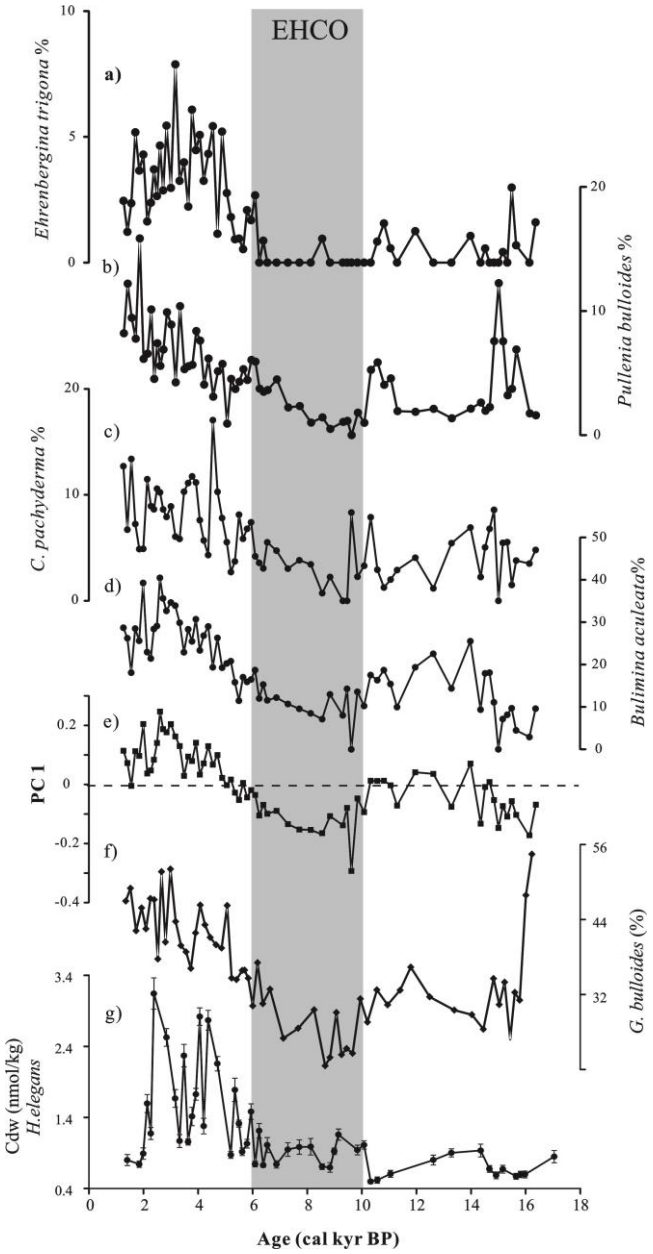

Fig. 8. *Comparison benthic assemblage 1 of MD77-191 with intermediate* Cd_w *and G. bulloides percentage from the same core. (a)-(d) relative abundance of dominated species from benthic*

assemblage 1, (e) PC 1 scores, (f) intermediate Cd_w and (g) G. bulloides percentage from core MD77-191. EHCO: Early Holocene Climate Optimum associated to intensified summer monsoon rainfall is also displayed.

In addition, strengthened increased of intermediate Cd_w records from cores MD77-191 and MD77-176 during the 5.2-2.4 cal kyr BP are associated to larger variations in *G. bulloides* relative abundance from cores SK237 GC04 and MD77-191, which indicate an enhanced productivity during the late Holocene (Naik et al., 2017) (Figs. 7b-c). Moreover, the changes in the Cd_w records are also consistent with the weakened summer monsoon intensity and rainfall during the late Holocene, which were observed in the BoB and Indian continent (Marzin et al., 2013; Contreras-Rosales et al., 2014; Sarkar et al., 2015) (Fig.9). This could also strongly support the hypothesis of the seesaw relationship between intense monsoon rainfall and the surface productivity in the BoB and south tip of Arabian Sea during the Holocene.

During the last deglaciation, short events have been recorded at the core MD77-191 site during the 16-15.2 and 12.6-11 cal kyr BP intervals. A significant decrease in *G. bulloides* relative abundance obtained from cores SK237 GC04 (Naik et al., 2017) and MD77-191, as well with depleted intermediate Cd_w from core MD77-191 during the time interval from 16 to 15.2 cal kyr BP, all suggest a decrease of surface productivity (Figs. 7b-d). A small decrease in the relative percentage *G. bulloides* of core SK237 GC04 and Cd_w occur in the 12.6-11 cal kyr BP may also indicate reduced productivity during this interval (Figs. 7b and d). In addition, the drop of %AABF from core SK237 GC04 and *H. elegans* Ba/Ca records indicate better ventilation bottom water, which result in a decreasing trend of $\%C_{org}$ due to a poor preservation (Figs. 7a, e and f).

The depleted Ba/Ca values in the 16-15.2 and 12.6-11 cal kyr BP intervals correspond to increase of benthic $\delta^{13}C$ and a decrease in $[CO_3^{2-}]$ records obtained from the same core (Fig. 10). In addition, the changes in the benthic $\delta^{13}C$ record, and B-P age offsets obtained on the sedimentary marine cores from Arabian Sea and Bay of Bengal at the 16-15.2 and 12.6-11 cal kyr BP intervals correspond to warming episodes in Antarctica and the Southern Hemisphere during the deglaciation (e.g., Epica, 2006; Cuffey et al., 2016). These time intervals also correspond to better ventilation in the South Ocean (e.g., Anderson et al., 2009; Skinner et al., 2010), which led to an enhanced vertical ventilation in the Southern Ocean resulting in an increased production of intermediate water masses (AAIW) (Anderson et al., 2009). Moreover, the decreased Ba/Ca obtained from MD77-191 may suggest better ventilated intermediate water during the 16-15.2 and 12.6-11 cal kyr BP intervals. These also provide the evidence for the enhanced northern flow of AAIW in the northern Indian Ocean.

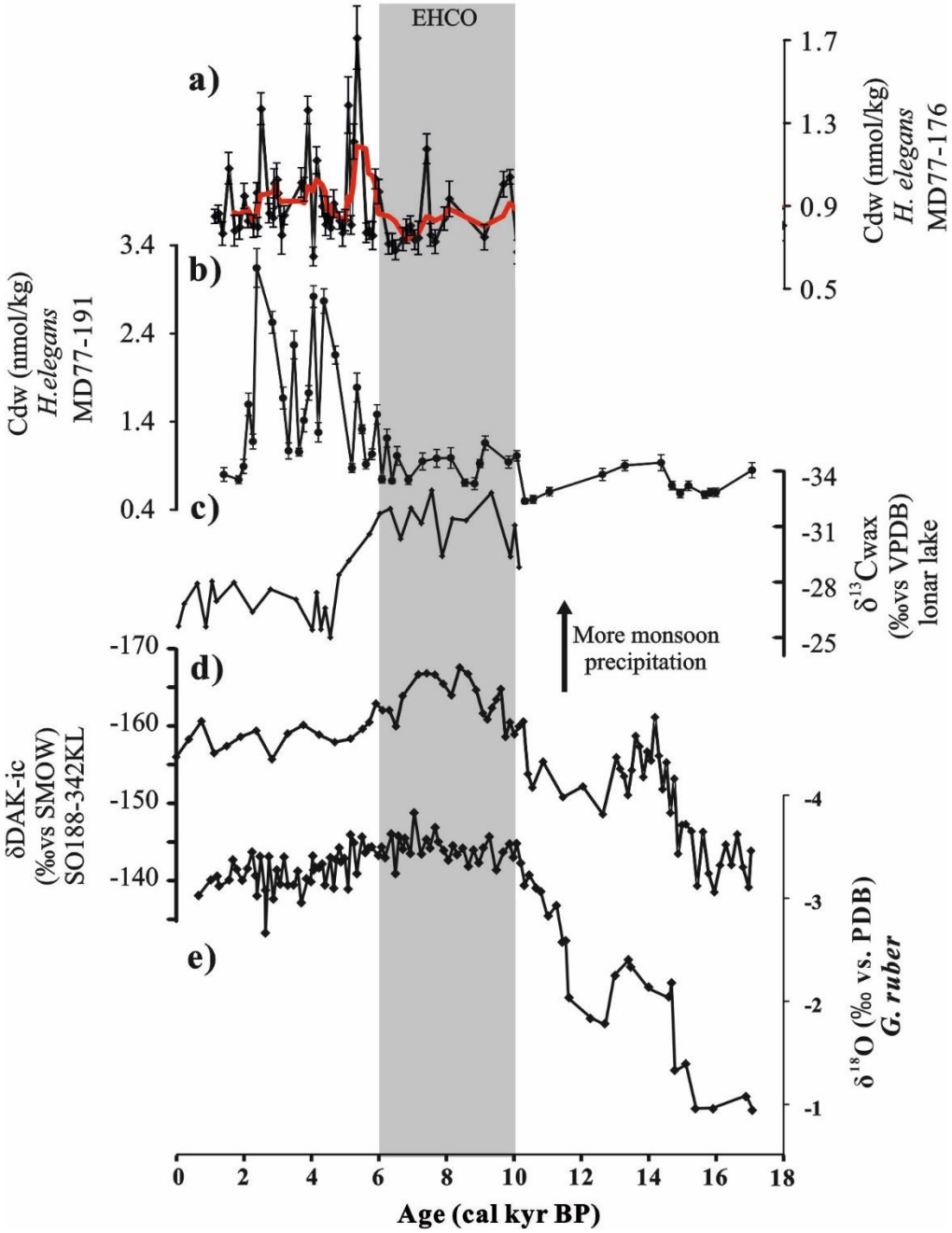

Fig. 9. *(a) and (b) intermediate Cd_w calculated by H. elegans obtained from MD77-176 and MD77-191, respectively. (c) Lonar Lake δ^{13}Cwax record (Sarkar et al., 2015). (d) δDAk-ic record from core SO188-342KL (Contreras-Rosales et al., 2014). (e) G. ruber δ^{18}O obtained from MD77-176 (Marzin et al., 2013). EHCO: Early Holocene Climate Optimum associated to intensified summer monsoon rainfall is also displayed.*

An increase in benthic δ^{13}C values is observed during the 17-15.2 and 12.6-11 cal kyr BP time intervals in the northern Indian Ocean (e.g., Duplessy et al., 1984; Curry et al., 1988; Naqvi et al.,

1994; Jung et al., 2009; Ma et al., 2019). The similarity between the benthic $\delta^{13}C$-increases reflects the northward expansion of AAIW during time intervals 17-15.2 and 12.6-11 cal kyr in the western Arabian Sea, Pacific Ocean and BoB (Jung et al., 2009; Pahnke and Zahn, 2005; Ma et al., 2019). However, as AAIW is formed from the deep waters AABW, air-sea exchange could also affect the values of $\delta^{13}C$, as the intermediate benthic $\delta^{13}C$ in the Southern Ocean is dominated by the influence of air-sea exchange (Lynch-Stieglitz et al., 1994). Thus, values of intermediate benthic $\delta^{13}C$ could increase relatively via stronger upwelling during the formation of AAIW.

Furthermore, the transition in the ε_{Nd} and $\Delta^{14}C$ records during the deglaciation also indicates a strong northward penetration of AAIW within the North Atlantic and Bay of Bengal (e.g., Cao et al., 2007; Pahnke et al., 2008; Pena et al., 2013; Yu et al., 2018). During the last deglaciation, core MD77-176 record of B-P age offsets displayed a decreasing trend in the 17-15.2 and 12.6-11 cal kyr intervals, and also indicated a stronger upwelling and an enhanced northern flow of AAIW from the Southern Ocean during these two periods (Ma et al., 2019). In addition, during the last deglaciation, a decrease in $[CO_3^{2-}]$ records of core MD77-191 also suggest the release CO_2 from the deep ocean in the deglacial period through the explanation of AAIW (Ma et al., in prep.).

In addition, the depleted Ba/Ca values obtained from the northern Indian Ocean at 16-15.2 and 12.6-11 cal kyr BP intervals are synchronous with a two-step increase of atmospheric CO_2 (Fig.10). Combined with variations in B-P age offset and benthic $\delta^{13}C$ records reported from the same region, all these signals could indicate strong upwelling and enhanced northern flow of AAIW from the Southern Ocean during these two periods. Thus, the variations of these records could provide strong evidence for the hypothesis that the Southern Ocean upwelling played a vital role for the CO_2 increase in the deglacial period (Anderson et al., 2009; Skinner et al., 2010, 2014). However, Kohfeld et al. (2005) suggested that although the physical processes (such as ventilation) could be involved for most of the glacial-interglacial CO_2 change, the biological pump may also contribute around less than half of the observed changes of CO_2 during the glacial-interglacial transitions. In addition, the depleted intermediate Cd_w and Ba/Ca records from the Arabian Sea indicate reduced surface productivity and/or enhanced ventilation, and thus a weaker biological production could also contribute to the two-step increase of atmospheric CO_2 during the 16-15.2 and 12.6-11 cal kyr BP intervals.

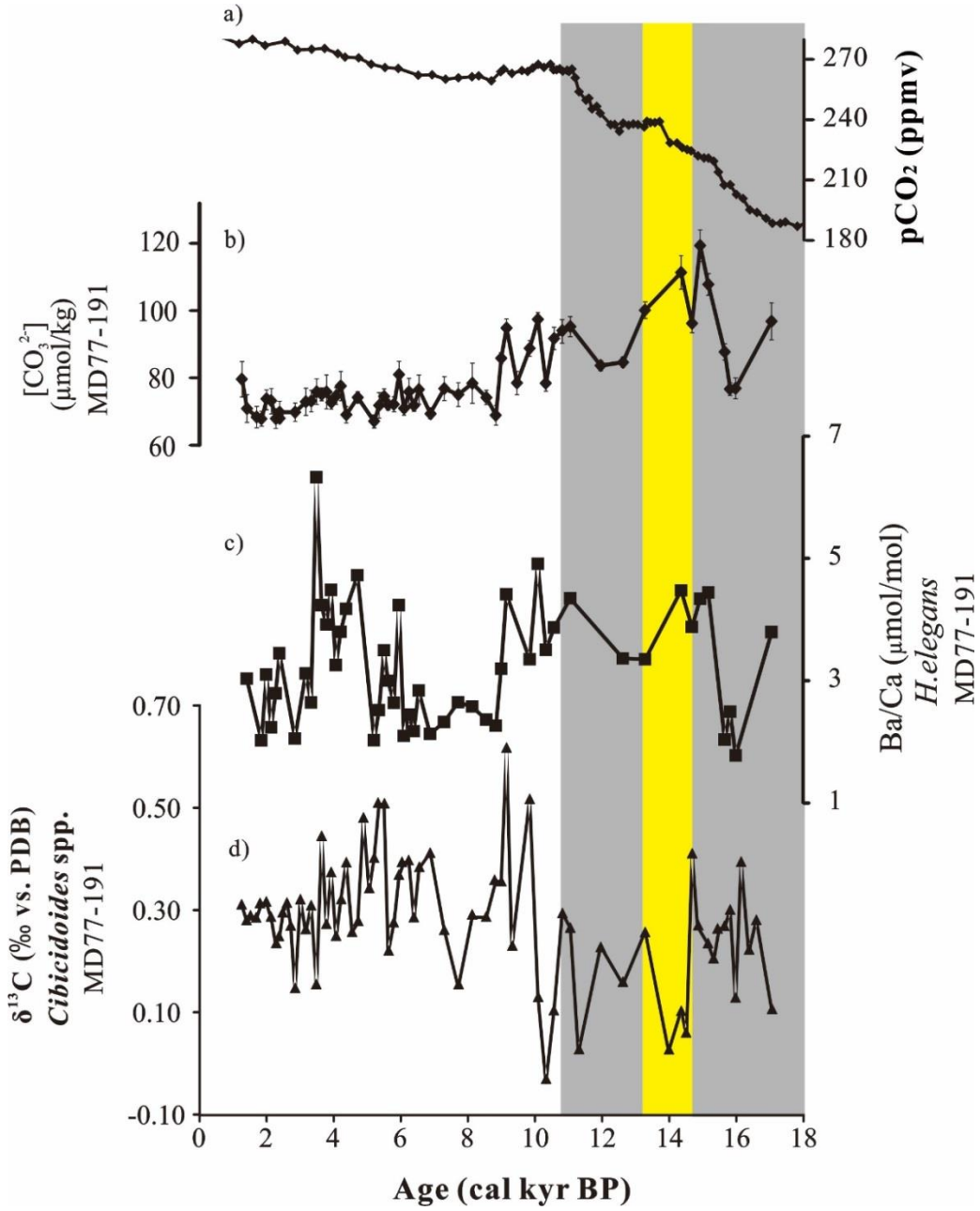

Fig. 10. *(a) Ice core atmospheric CO_2 from Antarctic Dome C (Monnin et al., 2001); (b) intermediate $[CO_3^{2-}]$ record, (c) H. elegans Ba/Ca ratios, and (d) benthic $\delta^{13}C$ records obtained from MD77-191. The grey-shaded intervals mark the two-step increase in atmospheric CO_2, the yellow-shaded interval marks the 15-13.3 cal kyr BP interval.*

6. Conclusion

Changes in benthic foraminiferal Cd/Ca and Ba/Ca were reconstructed on core MD77-191 (1254 m water depth) located in the south tip of India, as well as on core MD77-176 (1375 m water depth)

obtained from the northern BoB, in order to obtain the evolution of intermediate water circulation and paleo-nutrient changes in the northern Indian Ocean since the last deglaciation. Benthic elemental ratios Cd/Ca and Ba/Ca seem mainly influenced by the surface productivity changes and/or the intermediate-bottom water ventilation.

We reconstructed seawater Cd_w concentration by converting *H. elegans* Cd/Ca. During the late Holocene (5.2-2.4 cal kyr BP), the increased intermediate Cd_w concentrations of cores MD77-191 and MD77-176 indicate an enhanced surface productivity in the southeastern Arabian Sea and northeastern BoB, corresponding to weakened monsoon intensity and rainfall. By contrast, the lower values of intermediate Cd_w obtained from two cores indicate an enhanced monsoon precipitation and/or increased river input from the Himalayan rivers. In addition, benthic foraminiferal assemblages obtained from core MD77-191 were also investigated, and consistent with the records of *G. bulloides* relative abundance (Bassinot et al., 2011) and intermediate Cd_w obtained from the same core. Results indicate that assemblage 2 dominated the 17-6 cal kyr BP, reflecting a high bottom water oxygen conditions and a low flux of organic matter, corresponding to a poor productivity. The typically late Holocene assemblage indicates relatively low-oxygen level and meso- to eutrophic deep-water conditions, associated with high surface productivity during the late Holocene.

Moreover, during the last deglaciation, decreased intermediate Cd_w concentration and benthic Ba/Ca ratios are related to depleted surface productivity changes and/or the enhanced ventilation of intermediate-bottom water masses at the in the 16-15.2 and 12.6-11 cal kyr BP intervals. Combined with the increased benthic $\delta^{13}C$, depletion in $[CO_3^{2-}]$ and decreased B-P age offsets occurred during the same intervals, all of these changes indicate the increased northward flow of AAIW during 16-15.2 cal kyr BP and 12.6-11 cal kyr BP time intervals. These signals also provide strong evidence for the important role of enhanced Southern Ocean ventilation to the CO_2 increase during the last deglaciation.

Acknowledgements

R. Ma acknowledges the China Scholarship Council for providing funding for her study in France. This work has been supported by grants from the INSU-LEFE-IMAGO-CITRON GLACE program and the National Research Agency L-IPSL Project (Grant ANR-10-LABX-0018).

References

Anderson, R. F., Ali, S., Bradtmiller, L. I., Nielsen, S. H. H., Fleisher, M. Q., Anderson, B. E., Burckle, L. H., 2009. Wind-driven upwelling in the Southern Ocean and the deglacial rise in atmospheric CO_2. Science 323 (5920), 1443-1448.

Almogi-Labin, A., Schmiedl, G., Hemleben, C., Siman-Tov, R., Segl, M., Meischner, D., 2000. The influence of the NE winter monsoon on productivity changes in the Gulf of Aden, NW Arabian Sea, during the last 530ka as recorded by foraminifera. Marine Micropaleontology 40 (3), 295-319.

Altenbach, A. V., Pflaumann, U., Schiebel, R., Thies, A., Timm, S., Trauth, M., 1999. Scaling percentages and distributional patterns of benthic foraminifera with flux rates of organic carbon. Journal of Foraminiferal Research 29 (3), 173-185.

Banse, K., 1987. Seasonality of phytoplankton chlorophyll in the central and northern Arabian Sea. Deep Sea Research Part A Oceanographic Research Papers 34 (5), 713-723.

Barker, S., Greaves, M., Elderfield, H., 2003. A study of cleaning procedures used for foraminiferal Mg/Ca paleothermometry. Geochemistry Geophysics Geosystems 4 (9), 1-20.

Bassinot, F. C., Marzin, C., Braconnot, P., Marti, O., Mathienblard, E., Lombard, F., Bopp, L., 2011. Holocene evolution of summer winds and marine productivity in the tropical Indian Ocean in response to insolation forcing: Data-model comparison. Climate of the Past 7 (3), 815-829.

Bauska, T. K., Baggenstos, D., Brook, E. J., et al., 2016. Carbon isotopes characterize rapid changes in atmospheric carbon dioxide during the last deglaciation. Proceedings of the National Academy of Sciences, 113(13), 3465-3470.

Beal, L. M., Ffield, A., Gordon, A. L., 2000. Spreading of Red Sea overflow waters in the Indian Ocean. Journal of Geophysical Research: Oceans 105 (C4), 8549-8564.

Behrenfeld, M. J., Falkowski, P. G., 1997. Photosynthetic rates derived from satellite-based chlorophyll concentration. Limnology and Oceanography 42 (1), 1-20.

Bostock, H. C., Opdyke, B. N., Williams, M. J. M., 2010. Characterising the intermediate depth waters of the Pacific Ocean using $\delta^{13}C$ and other geochemical tracers. Deep-Sea Research I 57 (7), 847-859.

Boyle, E. A., 1992. Cadmium and $\delta^{13}C$ paleochemical ocean distributions during the stage 2 Glacial Maximum. Annual Review of Earth and Planetary Sciences 20 (1), 245-287.

Boyle, E. A., 1988. Cadmium: Chemical tracer of deepwater paleoceanography. Paleoceanography

3 (4), 471-489.

Boyle, E. A., 1983. Manganese carbonate overgrowths on foraminifera tests. Geochim. Cosmochim. Acta 63 (18), 353-353.

Boyle, E. A., Keigwin, L. D., 1982. Deep circulation of the north Atlantic over the last 200,000 years: Geochemical evidence. Science 218 (4574), 784-787.

Boyle, E. A., Labeyrie, L., Duplessly, J.-C., 1995. Calcitic foraminiferal data confirmed by cadmium in aragonitic Hoeglundina: Application to the Last Glacial Maximum in the northern Indian Ocean. Paleoceanography 10 (5), 881-900.

Boyle, E. A., Sclater, F., Edmond, J. M., 1976. On the marine geochemistry of Cadmium. Nature 263 (5572), 42-44.

Bryan, S. P., Marchitto, T. M., 2010. Testing the utility of paleonutrient proxies Cd/Ca and Zn/Ca in benthic foraminifera from thermocline waters. Geochemistry, Geophysics, Geosystems 11 (1).

Bryan, S. P., Marchitto, T. M., Lehman, S. J., 2010. The release of ^{14}C-depleted carbon from the deep ocean during the last deglaciation: Evidence from the Arabian Sea. Earth and Planetary Science Letters 298 (1), 244-254.

Burke, S. K., Berger, W. H., Coulbourn, W. T., Vincent, E., 1993. Benthic foraminifera in box core ERDC 112, Ontong Java Plateau. Journal of Foraminiferal Research 23 (1), 19-39.

Came, R. E., Oppo, D. W., Curry, W. B., Lynch-Stieglitz, J., 2008. Deglacial variability in the surface return flow of the Atlantic meridional overturning circulation. Paleoceanography 23 (PA1217), 1-10.

Canfield, D.E., 1994. Factors influencing organic carbon preservation inmarine sediments. Chem. Geol. 114, 315–329.

Cao, L., Fairbanks, R. G., Mortlock, R. A., Risk, M. J., 2007. Radiocarbon reservoir age of high latitude north Atlantic surface water during the last deglacial. Quaternary Science Reviews 26 (5), 732-742.

Calvert, S.E., Pedersen, T.F., Naidu, P.D., von Stackelberg, U., 1995. On the organic carbon maximum on the continental slope of the eastern Arabian Sea. J. Mar. Res. 53, 269-296.

Caulle, C., Mojtahid, M., Gooday, A. J., Jorissen, F. J., Kitazato, H., 2015. Living (rose-bengal-stained) benthic foraminiferal faunas along a strong bottom-water oxygen gradient on the Indian margin (Arabian Sea). Biogeosciences 12 (16), 5005-5019.

Chan, L. H., Drummond, D., Edmond, J. M., Grant, B., 1977. On the barium data from the Atlantic geosecs expedition. Deep Sea Research 24 (7), 613-649.

Cuffey, K. M., Clow, G. D., Steig, E. J., Buizert, C., Fudge, T. J., Koutnik, M., Waddington, E. D., Alley, R. B., Severinghaus, J. P., 2016. Deglacial temperature history of west Antarctica. Proceedings of the National Academy of Sciences 113 (50), 14249-14254.

Curry, W. B., Duplessy, J. C., Labeyrie, L. D., Shackleton, N. J., 1988. Changes in the distribution of $\delta^{13}C$ of deep water σCO_2 between the last glaciation and the Holocene. Paleoceanography 3 (3), 317-341.

Curry, W. B., Ostermann, D. R., Guptha, M. V. S., Ittekkot, V., 1992. Foraminiferal production and monsoonal upwelling in the Arabian Sea: evidence from sediment traps. Geological Society, London, Special Publications, 64, 93-106.

Contreras-Rosales, L.A., Jennerjahn, T., Tharammal, T., Meyer, V., Lückge, A., Paul, A., Schefuß, E., 2014. Evolution of the Indian Summer Monsoon and terrestrial vegetation in the Bengal region during the past 18 ka. Quaternary Science Reviews 102, 133-148.

Corliss, B. H., 1979. Recent deep-sea benthonic for aminiferal distributions in the southeast Indian Ocean: Inferred bottom-water routes and ecological implications. Marine Geology 31 (1-2), 115-138.

Corliss, B. H., Martinson, D. G., Keffer, T., 1986. Late Quaternary deep-ocean circulation. Geological Society of America Bulletin 97 (9), 1106.

Curry, W. B., Ostermann, D. R., Guptha, M. V. S., Ittekkot, V., 1992. Foraminiferal production and monsoonal upwelling in the Arabian Sea: Evidence from sediment traps. Upwelling System Evolution Since the Early Miocene Geological Society 64 (1), 93-106.

De, S., Gupta, A. K., 2010. Deep-sea faunal provinces and their inferred environments in the Indian Ocean based on distribution of recent benthic foraminifera. Palaeogeography, Palaeoclimatology, Palaeoecology 291 (3), 429-442.

Den Dulk, M., Reichart, G. J., Memon, G. M., Roelofs, E. M. P., Zachariasse, W. J., Zwaan, G. J. V. D., 1998. Benthic foraminiferal response to variations in surface water productivity and oxygenation in the northern Arabian Sea. Marine Micropaleontology 35 (1–2), 43-66.

Dubois-Dauphin, Q., Bonneau, L., Colin, C., Montero-Serrano, J.-C., Montagna, P., Blamart, D., Hebbeln, D., Van Rooij, D., Pons-Branchu, E., Hemsing, F., Wefing, A.-M., Frank, N., 2016.

South Atlantic intermediate water advances into the north-east Atlantic with reduced Atlantic Meridional Overturning Circulation during the last glacial period. Geochemistry, Geophysics, Geosystems 17 (6), 2336-2353.

Duplessy, J.-C., Shackleton, N. J., Matthews, R. K., Prell, W., Ruddiman, W. F., Caralp, M., Hendy, C. H., 1984. ^{13}C record of benthic foraminifera in the last interglacial ocean: Implications for the carbon cycle and the global deep water circulation. Quaternary Research 21 (2), 225-243.

Elderfield, H., Rickaby, R. E. M., 2000. Oceanic Cd/P ratio and nutrient utilization in the glacial Southern Ocean. Nature 405 (6784), 305-310.

EPICA, C. M., 2006. One-to-one coupling of glacial climate variability in Greenland and Antarctica. Nature 444, 195.

Fontanier, C., Jorissen, F. J., Licari, L., Alexandre, A., Anschutz, P., Carbonel, P., 2002. Live benthic foraminiferal faunas from the Bay of Biscay: Faunal density, composition, and microhabitats. Deep Sea Research Part I: Oceanographic Research Papers 49 (4), 751-785.

Gu, S., Liu, Z., Zhang, J., Rempfer, J., Joos, F., Oppo, D. W., . 2017. Coherent response of Antarctic Intermediate Water and Atlantic Meridional Overturning Circulation during the last deglaciation: Reconciling contrasting Neodymium isotope reconstructions from the tropical Atlantic. Paleoceanography and Paleoclimatology, 32.

Gupta, A. K., Anderson, D. M., Overpeck, J. T., 2003. Abrupt changes in the Asian Southwest Monsoon during the Holocene and their links to the North Atlantic Ocean. Nature 421 (6921), 354-357.

Gupta, S. B. K., 1999. Introduction to modern foraminifera. in Sen Gupta B.K., Ed., Modern Foraminifera, Kluwer, Dordrecht, , pp. 3-6.

Hammer, Ø., Harper, D. A. T., Ryan, P. D., 2001. Past: Paleontological statistics software package for education and data analysis.

Hall, J., Chan, L. H., 2004. Ba/Ca in benthic foraminifera: Thermocline and middepth circulation in the north Atlantic during the last glaciation. Paleoceanography 19 (PA4018), 1-13.

Hermelin, J. O. R., 1991. Relative abundances of benthic foraminifera in ODP hole 117-728A, PANGAEA.

Hermelin, J. O. R., 1992. Variations in the benthic foraminiferal fauna of the Arabian Sea: A response to changes in upwelling intensity? Geological Society, London, Special Publications 64, 151-166.

Hermelin, J. O. R., Shimmield, G. B., 1995. Impact of productivity events on the benthic foraminiferal fauna in the Arabian Sea over the last 150,000 years. Paleoceanography 10 (1), 85-116.

Hester, K., Boyle, E., 1982. Water chemistry control of Cadmium content in recent benthic foraminifera. Nature 298, 260-262.

Howe, J., Piotrowski, A. M., Oppo, D. W., Huang, K.-F., Mulitza, S., Chiessi, C. M., Blusztajn, J., Antarctic intermediate water circulation in the south Atlantic over the past 25,000years. 2016.

Holbourn, A., Henderson, A. S., Macleod, N., 2013; Front matter. In Atlas of benthic foraminifera, pp. 1-641.

Jian, Z., Wang, L., 1997. Late quaternary benthic foraminifera and deep-water paleoceanography in the South China Sea. Marine Micropaleontology 32 (1), 127-154.

Jones, R. W., The challenger foraminifera. Oxford University Press: 1994; p. 149. 37.

Jung, S. J. A., Kroon, D., Ganssen, G., Peeters, F., Ganeshram, R., 2009. Enhanced Arabian Sea intermediate water flow during glacial North Atlantic cold phases. Earth and Planetary Science Letters 280 (1), 220-228.

Kallel, N., Labeyrie, L. D., Juillet-Leclerc, A., Duplessy, J.-C., 1988. A deep hydrological front between intermediate and deep-water masses in the glacial Indian Ocean. Nature 333, 651.

Kohfeld, K.E., Quéré, C.L., Harrison, S.P., Anderson, R.F., 2005. Role of marine biology in Glacial-interglacial CO2 cycles. Science 308, 74.

Lea, D. W., Boyle, E., 1989. Barium content of benthic foraminifera controlled by bottom-water composition. Nature 338 (338), 751-753.

Lea, D. W., Boyle, E., 1990. Foraminiferal reconstitution of barium distribution in water masses of the glacial oceans. Paleoceanography 5 (5), 719-742.

Levy, M., Shankar, D., André, J.-M., Shenoi, S., Durand, F., De Boyer Montegut, C., 2007. Basin-wide seasonal evolution of the Indian Ocean's phytoplankton blooms. Journal of Geophysical Research 112 (C12014), 1-14.

Loeblich, A. R., Tappan, H., 1988; Generic taxa erroneously regarded as foraminifers. In

Foraminiferal genera and their classification, Loeblich, A. R.; Tappan, H., Eds. Springer US: Boston, MA, pp. 726-730.

Lynch-Stieglitz, J., Fairbanks, R. G., Charles, C. D., 1994. Glacial-interglacial history of Antarctic Intermediate Water: Relative strengths of Antarctic versus Indian Ocean sources. Paleoceanography 9 (1), 7-29.

Ma, R., Sépulcre, S., Licari, L., Bassinot, F., Liu, Z., Tisnérat-Laborde, N., Kallel, N., Yu, Z., Colin, C., 2019. Changes in intermediate circulation in the Bay of Bengal since the Last Glacial Maximum as inferred from benthic foraminifera assemblages and geochemical proxies. Geochemistry, Geophysics, Geosystems 20, 1-17.

Mackensen, A., Schmiedl, G., Harloff, J., Giese, M., 1995. Deep-sea foraminifera in the South Atlantic Ocean; ecology and assemblage generation. Micropaleontology 41 (4), 342-358.

Mackensen, A., Sejrup, H. P., Jansen, E., 1985. The distribution of living benthic foraminifera on the continental slope and rise off southwest Norway. Marine Micropaleontology 9 (4), 275-306.

Marchitto, T. M., 2004. Lack of a significant temperature influence on the incorporation of Cd into benthic foraminiferal tests. Geochemistry, Geophysics, Geosystems 5.

Marchitto, T. M., Broecker, W. S., 2006. Deep water mass geometry in the glacial atlantic ocean: A review of constraints from the paleonutrient proxy Cd/Ca. Geochemistry, Geophysics, Geosystems 7.

Marchitto, T. M., Lehman, S. J., Ortiz, J. D., Flückiger, J., Geen, A. v., 2007. Marine radiocarbon evidence for the mechanism of deglacial atmospheric CO_2 rise. Science 316, 1456-1459.

Marra, J., Barber, R. T., 2005. Primary productivity in the Arabian Sea: A synthesis of JGOFS data. Progress in Oceanography 65 (2), 159-175.

Martin, P., Lea, D. W., 1998. Comparison of water mass changes in the deep tropical Atlantic derived from Cd/Ca and carbon isotope records: Implications for changing Ba composition of deep Atlantic water masses. Paleoceanography 13 (6), 572-585.

Marzin, C., Kallel, N., Kageyama, M., Duplessy, J. C., Braconnot, P., 2013. Glacial fluctuations of the Indian monsoon and their relationship with north Atlantic climate: New data and modelling experiments. Clim. Past 9 (5), 2135-2151.

Mazumder, A., Nigam, R., 2014. Bathymetric preference of fourmajor genera of rectilinear benthic foraminifera within oxygen minimum zone in Arabian Sea off central west coast of India. J.

Earth Syst. Sci. 123, 633–639.

McCorkle, D., Martin, P., W. Lea, D., P. Klinkhammer, G., 1995. Evidence of a dissolution effect on benthic foraminiferal shell chemistry: $\delta^{13}C$, Cd/Ca, Ba/Ca, and Sr/Ca results from the ontong Java Plateau. Paleoceanography 10 (4), 699-714.

Miao, Q., Thunell, R. C., 1993. Recent deep-sea benthic foraminiferal distributions in the South China and Sulu Seas. Marine Micropaleontology 22 (1), 1-32.

Mléneck, V. M., 1997. S´edimentation et dissolution des carbonates biog´eniques aux moyennes latitudes nord et sud, approche quantitative et relations avec les pal´eocirculations oc´eaniques des derniers 150 000 ans. PhD thesis, Universit´e Bordeaux I, pp. 277

Monnin, E., Indermühle, A., Dällenbach, A., Flückiger, J., Stauffer, B., Stocker, T. F., Raynaud, D., Barnola, J.-M., 2001. Atmospheric CO_2 concentrations over the last glacial termination. Science 291 (5501), 112-114.

Murgese, D. S., De Deckker, P., 2005. The distribution of deep-sea benthic foraminifera in core tops from the eastern Indian Ocean. Marine Micropaleontology 56 (1), 25-49.

Murgese, D. S., De Deckker, P., 2007. The late quaternary evolution of water masses in the eastern Indian Ocean between Australia and Indonesia, based on benthic foraminifera faunal and carbon isotopes analyses. Palaeogeography, Palaeoclimatology, Palaeoecology 247 (3), 382-401.

Naqvi, W. A., Charles, C. D., Fairbanks, R. G., 1994. Carbon and oxygen isotopic records of benthic foraminifera from the northeast indian ocean: Implications on glacial-interglacial atmospheric CO_2 changes. Earth and Planetary Science Letters 121 (1), 99-110.

Naidu, P.D., Prakash Babu, C., Rao, C.M., 1992. The upwelling record in the sediments of the western continental margin of India. Deep-Sea Res. 39, 715–723.

Naidu, P.D., Malmgren, B.A., 1996. A high-resolution record of late Quaternary upwelling along the Oman margin, Arabian Sea based on planktonic foraminifera. Paleoceanography 11, 129–140.

Naik, D. K., Saraswat, R., Lea, D. W., Kurtarkar, S. R., Mackensen, A., 2017. Last glacial-interglacial productivity and associated changes in the eastern Arabian Sea. Palaeogeography, Palaeoclimatology, Palaeoecology 483, 147-156.

Nigam, R.,Mazumder, A., Henriques, P.J., Saraswat, R., 2007. Benthic foraminifera as proxy for oxygen-depleted conditions off the central west coast of India. J. Geol. Soc. India 70, 1047–1054.

Ni Fhlaithearta, S., Reichart, G. J., Jorissen, F., Fontanier, C., Rohling, E. J., Thomson, J., de Lange,

G., Reconstructing the seafloor environment during sapropel formation using benthic foraminiferal trace metals, stable isotopes, and sediment composition. 2010; Vol. 25.

Olson, D., L. Hitchcock, G., Fine, R., A. Warren, B., Maintenance of the low-oxygen layer in the central Arabian Sea. 1993; Vol. 40, p 673-685.

Oppo, D. W., Fairbanks, R. G., 1987. Variability in the deep and intermediate water circulation of the Atlantic Ocean during the past 25,000 years: Northern Hemisphere modulation of the Southern Ocean. Earth and Planetary Science Letters 86, 1-15.

Pahnke, K., Goldstein, S. L., Hemming, S. R., 2008. Abrupt changes in Antarctic Intermediate Water circulation over the past 25,000 years. Nature Geoscience 1, 870.

Pahnke, K., Zahn, R., 2005. Southern Hemisphere water mass conversion linked with north Atlantic climate variability. Science 307 (5716), 1741-1746.

Pena, L. D., Goldstein, S. L., Hemming, S. R., Jones, K. M., Calvo, E., Pelejero, C., Cacho, I., 2013. Rapid changes in meridional advection of Southern Ocean intermediate waters to the tropical Pacific during the last 30kyr. Earth and Planetary Science Letters 368, 20-32.

Peterson, L. C., 1984. Recent abyssal benthic foraminiferal biofacies of the eastern Equatorial Indian Ocean. Marine Micropaleontology 8 (6), 479-519.

Prell, W. L., Kutzbach, J. L., 1987. Monsoon variability over the past 150,000 years. Journal of Geophysical Research Atmospheres 92 (D7), 8411-8425.

Poggemann, D.-W., Hathorne, E., Nuernberg, D., Frank, M., Bruhn, I., Reißig, S., Bahr, A., 2017. Rapid deglacial injection of nutrients into the tropical Atlantic via Antarctic Intermediate Water. Earth and Planetary Science Letters 463, 118-126.

Poggemann, D.-W., Nürnberg, D., Hathorne, E. C., Frank, M., Rath, W., Reißig, S., Bahr, A., 2018. Deglacial heat uptake by the Southern Ocean and rapid northward redistribution via Antarctic Intermediate Water. Paleoceanography and Paleoclimatology 33 (11), 1292-1305.

Raza, T., Ahmad, S. M., Sahoo, M., Banerjee, B., Bal, I., Dash, S., Suseela, G., Mukherjee, I., 2014. Hydrographic changes in the southern Bay of Bengal during the last ~65,000 y inferred from carbon and oxygen isotopes of foraminiferal fossil shells. Quaternary International 333, 77-85.

Reid, J. L., 2003. On the total geostrophic circulation of the south Pacific Ocean: Flow patterns, tracers and transports. Progress in Oceanography 16 (1), 1-61.

Reimer P. J., Bard E., Bayliss A., Beck J. W., Blackwell P. G., Bronk Ramsey C., Buck C. E.,

Cheng H., Edwards R. L., Friedrich M., Grootes P. M., Guilderson T. P., Haflidason H., Hajdas I., Hatté C., Heaton T. J., Hogg A. G., Hughen K. A., Kaiser KF., Kromer B., Manning S. W., Niu M., Reimer R. W., Richards D. A., Scott E. M., Southon J. R., Turney C. S. M., van der Plicht J., 2013. IntCal13 and Marine13 radiocarbon age calibration curves 0-50000 years cal BP. Radiocarbon 55(4).

Sarkar, S., Prasad, S., Wilkes, H., Riedel, N., Stebich, M., Basavaiah, N., Sachse, D., 2015. Monsoon source shifts during the drying mid-Holocene: Biomarker isotope based evidence from the core 'monsoon zone'(CMZ) of India. Quaternary Science Reviews 123, 144-157.

Saraswat, R., Nigam, R., Correge, T., 2014. A glimpse of the Quaternary monsoon history from India and adjoining seas. Palaeogeography, Palaeoclimatology, Palaeoecology 397, 1-6.

Schilman, B., Almogi-Labin, A., Bar-Matthews, M., Labeyrie, L., Paterne, M., Luz, B., Long and short-term carbon fluctuations in the eastern Mediterranean during the late Holocene. 2001; Vol. 29.

Schlitzer, R., 2015. Ocean data view. http://odv.awi.de.

Schmiedl, G., Hemleben, C., Keller, J., Segl, M., 1998. Impact of climatic changes on the benthic foraminiferal fauna in the Ionian Sea during the last 330,000 years. Paleoceanography 13 (5), 447-458.

Schmiedl, G., Mackensen, A., Multispecies stable isotopes of benthic foraminifers reveal past changes of organic matter decomposition and deepwater oxygenation in the Arabian Sea. 2006; Vol. 21.

Schnitker, D., 1994. Deep-sea benthic foraminifers: Food and bottom water masses. In: Zahn r., pedersent. F., kaminski m.A., labeyrie l. (eds). Carbon cycling in the glacial ocean: Constraints on the ocean's role in global change. . NATO ASI Series (Series I: Global Environmental Change), vol 17. Springer, Berlin, Heidelberg.

Schonfeld, J., 2001. Benthic foraminifera and pore-water oxygen profiles: A re-assessment of species boundary conditions at the western Iberian margin. Vol. 31, p 86-107.

Schott, F. A., McCreary, J. P., The monsoon circulation of the Indian Ocean. 2001; Vol. 51, p 1-123.

Sharma, G. S., 1978. Upwelling off the southwest coast of India. Indian Journal of Marine Sciences.

Shetye, S. R., Gouveia, A. D., Shenoi, S. S. C., Sundar, D., Michael, G. S., Almeida, A. M., Santanam, K., 1990. Hydrography and circulation off the west coast of India during the southwest monsoon 1987.

Sirocko, F., Schonberg, D.G., Devey, C., 2000. Processes controlling trace element geochemistry of Arabian Sea sediments during the last 25,000 years. Glob. Planet. Chang. 26, 217–303.

Singh, A. D., Jung, S. J. A., Darling, K., Ganeshram, R., Ivanochko, T., Kroon, D., 2011. Productivity collapses in the Arabian Sea during glacial cold phases. Paleoceanography 26 (3).

Singh, A. D., Kroon, D., Ganeshram, R., 2006. Millennial scale variations in productivity and OMZ intensity in the eastern Arabian Sea. Journal of the Geological Society of India 68 (3), 369-377.

Skinner, L. C., Claire, W., Scrivner, A. E., Fallon, S. J., 2014. Radiocarbon evidence for alternating northern and southern sources of ventilation of the deep Atlantic carbon pool during the last deglaciation. PNAS 111 (15), 5480-5484.

Skinner, L. C., Fallon, S., Waelbroeck, C., Michel, E., Barker, S., 2010. Ventilation of the deep Southern Ocean and deglacial CO_2 rise. Science 328 (5982), 1147-1151.

Stuiver, M., Braziunas, T. F., 1993. Modeling atmospheric ^{14}C influences and ^{14}C ages of marine samples to 10 000 BC. Radiocarbon 35 (1), 137-189.

Talley, L. D., Pickard, G. L., Emery, W. J., Swift, J. H., 2011; Preface. In Descriptive physical oceanography (sixth edition), Academic Press: Boston, pp. 1-383.

Thushara, V., Vinayachandran, P. N., 2016. Formation of summer phytoplankton bloom in the northwestern Bay of Bengal in a coupled physical-ecosystem model. Journal of Geophysical Research: Oceans 121 (12), 8535-8550.

Toggweiler, J. R., 1999. Variation of atmospheric CO_2 by ventilation of the ocean's deepest water, Paleoceanography 14, 571-588.

Umling, N. E., Thunell, R. C., Bizimis, M., 2018. Deepwater expansion and enhanced remineralization in the eastern equatorial Pacific during the Last Glacial Maximum. Paleoceanography and Paleoclimatology 33 (6), 563-578.

Valley, S., Lynch-Stieglitz, J., M. Marchitto, T., 2017. Timing of deglacial amoc variability from a high-resolution seawater Cadmium reconstruction: Timing deglacial upper amoc variability. Paleoceanography 32, 1195-1203.

Van der Zwaan, G. J., Duijnstee, I. A. P., Den Dulk, M., Ernst, S. R., Jannink, N. T., Kouwenhoven, T. J., 1999. Benthic foraminifers: Proxies or problems? A review of paleocological concepts. Earth-Science Reviews 46 (1), 213-236.

Wiggert, J. D., Hood, R. R., Banse, K., Kindle, J. C., 2005. Monsoon-driven biogeochemical processes in the Arabian Sea. Progress in Oceanography 65 (2), 176-213.

Wyrtki, K., 1973; Physical oceanography of the Indian Ocean. In The biology of the Indian Ocean, Zeitzschel, B.; Gerlach, S. A., Eds. Springer Berlin Heidelberg: Berlin, Heidelberg, pp. 18-36.

Xie, R. C., Marcantonio, F., Schmidt, M. W., 2012. Deglacial variability of Antarctic Intermediate Water penetration into the north Atlantic from authigenic Neodymium isotope ratios. Paleoceanography 27 (3).

Yu, Z., Colin, C., Ma, R., Meynadier, L., Wan, S., Wu, Q., Kallel, N., Sepulcre, S., Dapoigny, A., Bassinot, F., 2018. Antarctic Intermediate Water penetration into the northern Indian Ocean during the last deglaciation. Earth and Planetary Science Letters 500, 67-75.

Zahn, R., Winn, K., Sarnthein, M., 1986. Benthic foraminiferal $\delta^{13}C$ and accumulation rates of organic carbon: *Uvigerina peregrina* group and *Cibicidoides wuellerstorfi*. Paleoceanography 1 (1), 27-42.

Zaric, S., Donner, B., Fischer, G., Mulitza, S.,Wefer, G., 2005. Sensitivity of planktic foraminifera to sea surface temperature and export production as derived from sediment trap data. Mar. Micropaleontol. 55, 75–105.

Supplementary figures

Fig. S1. Down core variations of PC 1 scores and the percentages of major species in: (a) benthic assemblage 1 and (b) benthic assemblage 2.

Fig. S2: comparison of Cd/Ca and Ba/Ca obtained from MD77-191. (a) Cd/Ca and (b) Ba/Ca records from *Hoeglundina elegans*; (c) Cd/Ca and (d) Ba/Ca records from *Cibicidoides pachyderma*; (e) Cd/Ca and (f) Ba/Ca records from *Uvigerina peregrina*; (g) Cd/Ca and (h) Ba/Ca records from *Globobulimina* spp. EHCO: Early Holocene Climate Optimum associated to intensified summer monsoon rainfall is also displayed.

Fig. S3: Silica (µmol/kg, coloured shading) depth-latitude section using the Ocean Data View (ODV) software (Schlitzer, 2015) and vertical distribution of water masses in the Arabian Sea and Bay of Bengal (N-S cross section).

a)

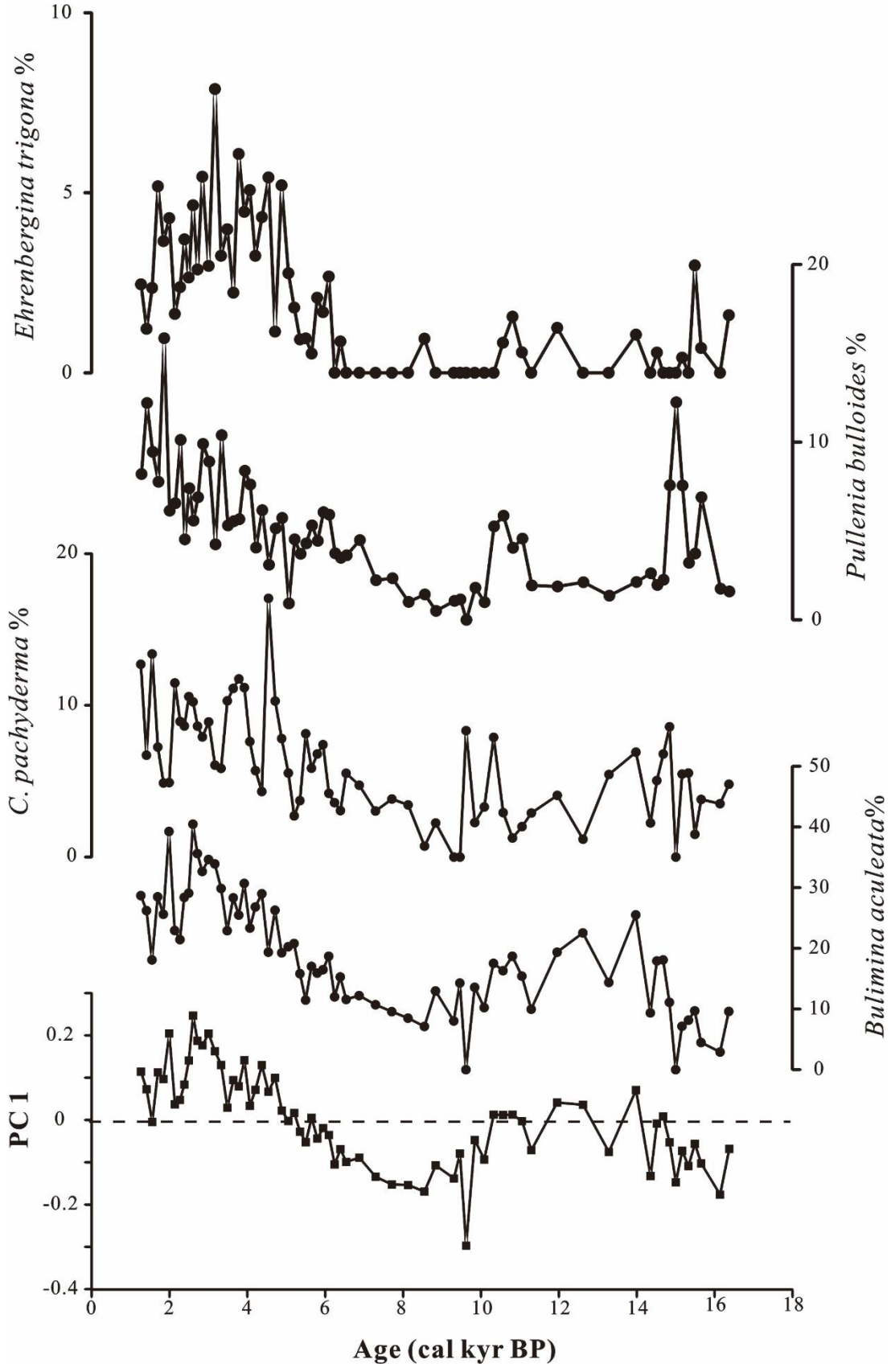
Ehrenbergina trigona %
Pullenia bulloides %
C. pachyderma %
Bulimina aculeata%
PC 1
Age (cal kyr BP)

Fig. S1

b)

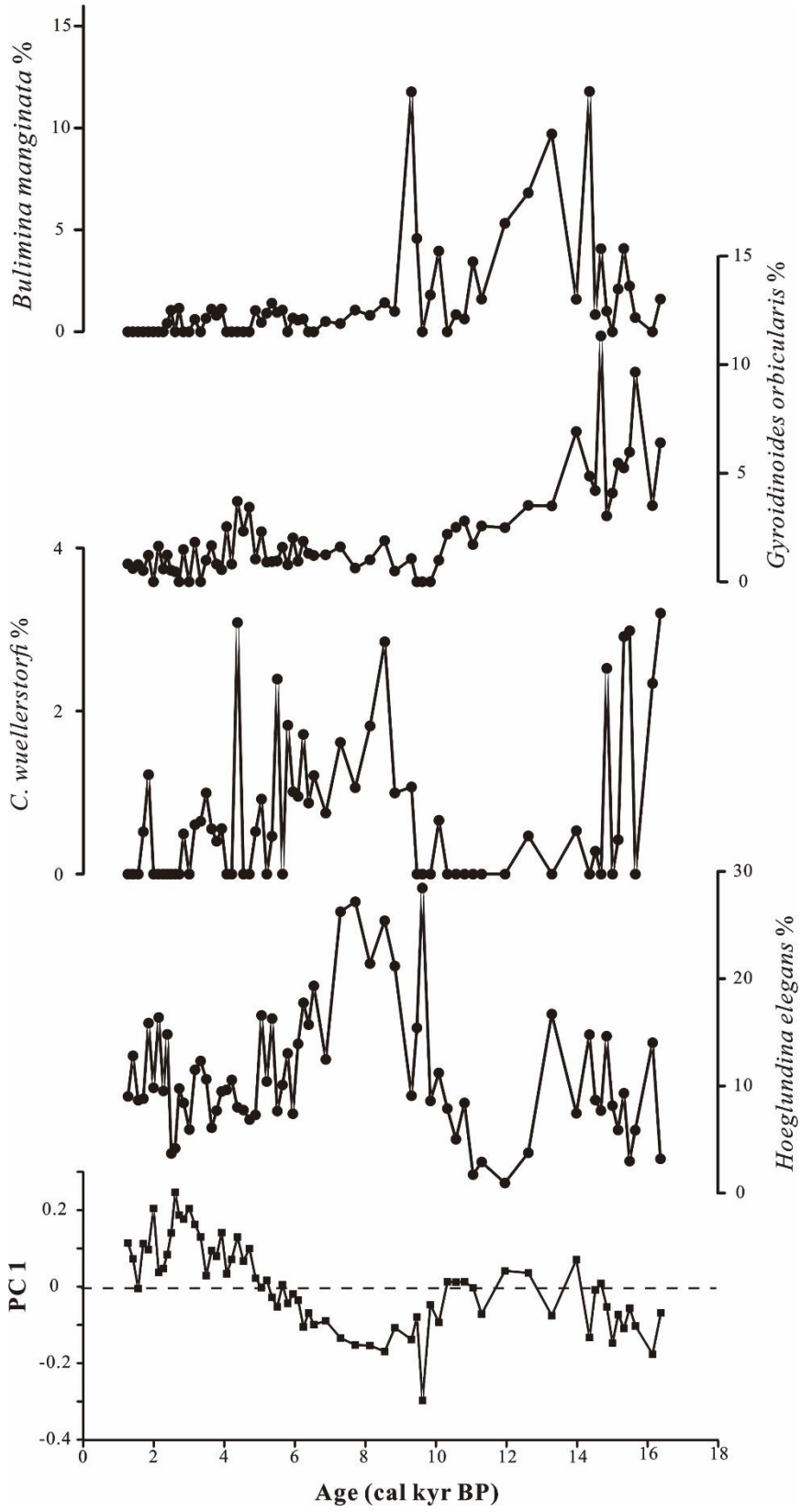
Bulimina manginata %
15
10
5
0
Gyroidinoides orbicularis %
15
10
5
0
C. wuellerstorfi %
4
2
0
Hoeglundina elegans %
30
20
10
0
PC 1
0.2
0
-0.2
-0.4
0
2
4
6
8
10
12
14
16
18
Age (cal kyr BP)

Fig. S1

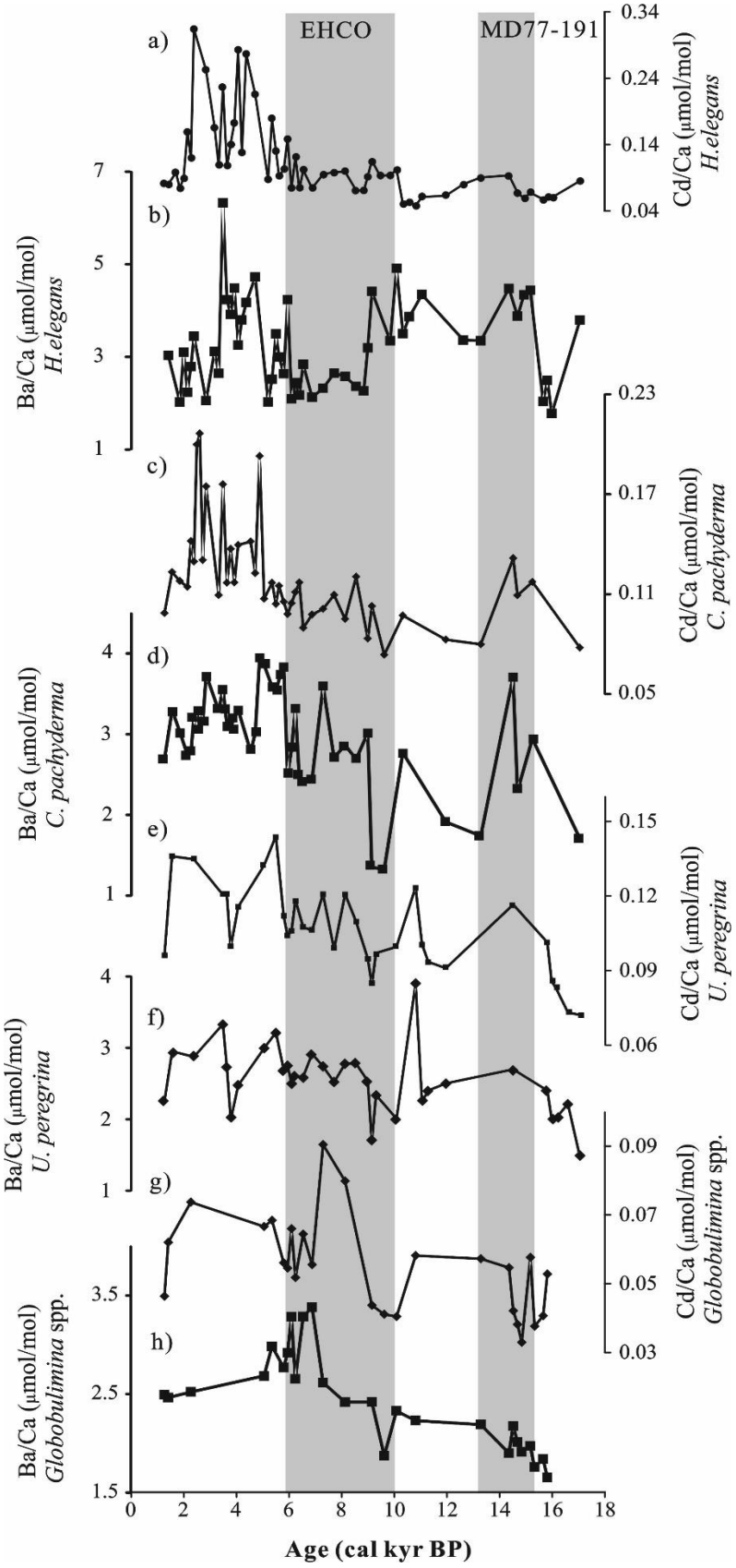
EHCO
MD77-191
a)
b)
c)
d)
e)
f)
g)
h)
Cd/Ca (µmol/mol) H.elegans
Ba/Ca (µmol/mol) H.elegans
Cd/Ca (µmol/mol) C. pachyderma
Ba/Ca (µmol/mol) C. pachyderma
Cd/Ca (µmol/mol) U. peregrina
Ba/Ca (µmol/mol) U. peregrina
Cd/Ca (µmol/mol) Globobulimina spp.
Ba/Ca (µmol/mol) Globobulimina spp.
Age (cal kyr BP)

Fig. S2

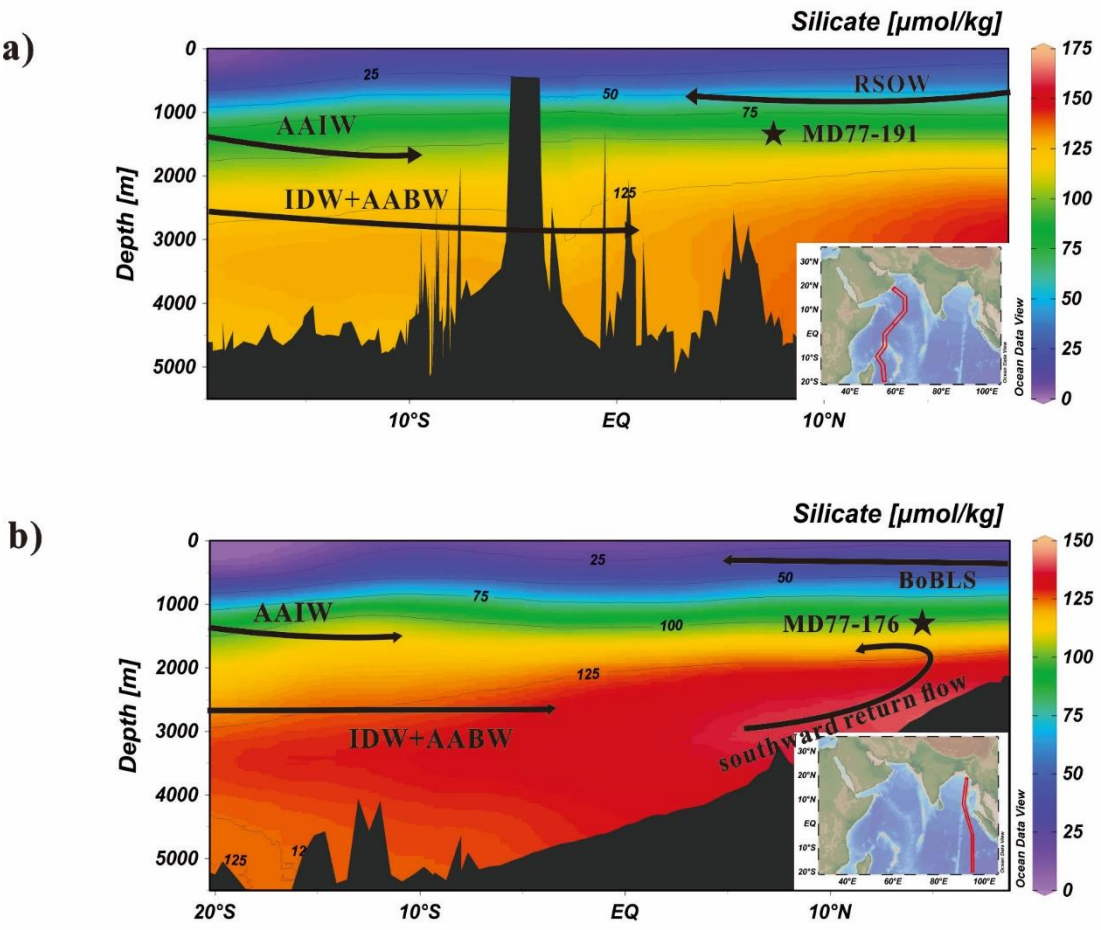
a)
Silicate [µmol/kg]
AAIW
IDW+AABW
RSOW
MD77-191
Depth [m]
10°S
EQ
10°N
b)
Silicate [µmol/kg]
AAIW
IDW+AABW
BoBLS
MD77-176
southward return flow
Depth [m]
20°S
10°S
EQ
10°N
Ocean Data View

Fig. S3

Chapter 6: Changes in the intermediate circulation from Eastern Equatorial Indian Ocean since MIS 17 based on the benthic elemental ratios

In this chapter, I present the preliminary interpretation of geochemical records of benthic elemental ratios from SHI9001. The stable isotope analysis used to build the age model have been performed very lately during the PhD work, preventing thus a complete interpretation of the results that will be further developed in the future. Hereafter, I present the preliminary age model, as well as some interpretation tracks to be followed to understand the elemental ratio and stable isotopes results.

6.1. Introduction

The Eastern Equatorial Indian Ocean is a key area to study the connections between the Pacific Ocean and the Indian Ocean through the Indonesian Throughflow (ITF). Indeed, the ITF transports about 10 Sv of warm, low salinity water from the Pacific Ocean through the passageways of the Indonesian archipelago into the eastern Indian Ocean (e.g., You and Tomczak, 1993; You, 1998; Tomczak and Godfrey, 2003). North Pacific thermocline and intermediate water masses are leaving the oceanic gateway via the Makassar Strait, Lombok Channel (1.2 Sv), Ombai Strait (4.5 Sv) and Timor Sea (4.3 Sv), to form a major heat source for the Indian Ocean and contribute about one third to the upper water mass transport in the North Atlantic at 20°N (Schiller et al., 1998; Speich et al., 2001). The ITF contributes to the intermediate water circulation in the Northern Indian Ocean through the Indonesian Intermediate Water, flowing through the Bay of Bengal off Sumatra, the Southern Ocean along the Australian coast and the Arabian Sea via the Equatorial Indian Ocean (You, 1998). The IIW enter into the Indian Ocean just south of the Java Island, making this area a key point to study past exchanges between the Pacific and the Indian Ocean, and to decipher how changes in Pacific Ocean circulation can affect the IIW.

Past studies of the ITF have mainly focused on surface and thermocline depths, and give different results:

i) at the surface, changes in the sea-surface temperatures SST and marine paleoproductivity seem to be related to variations in the upwelling intensity, associated to the monsoon strength, with a processional cyclicity and at a longer timescale, due to low-latitude climate phenomena such as El Niño–Southern Oscillation or the Indian Ocean Dipole or Zonal Mode (Lückge et al., 2009). However, a recent work (Wang et al., 2018) has pointed out changes in the SST related to glacial-interglacial changes. Another study has exhibited the role of the southern high-latitude climate on SST at glacial-interglacial timescale (Mohtadi et al., 2010). In addition, studies on marine records from the Sumatran continental margin (De Deckker and Gingele, 2002; Gingele et al., 2002), or the oceanic realm off south Java (Martinez et al., 1999; Takahashi and Okada, 2000), suggest that changes in the East Asian Monsoon (EAM) intensity have been driving the surface oceanic mixing and paleo-productivity in the eastern Indian Ocean, without assigning any significant role to the Pacific Ocean or the ITF. To finish, the connection with the Northern Indian Ocean remains unclear since a SST reconstruction from the Andaman Sea exhibiting a 3° cooler SSTs during the last glacial compared to today has established a direct link between local hydrography and changes in the intensity of the Asian monsoon system, rather than a global climatic mechanism connecting

both areas (Rashid et al., 2007);

ii) at the thermocline depth, variations in the thermocline water temperature TWT mainly exhibit a precession cyclicity associated to the austral winter monsoon and independent from the glacial-interglacial conditions (Wang et al., 2018). These variations have also been related to changes in the TWT changes in the North Indian Ocean, with a warmer TWT during glacial stages (Mohtadi et al., 2010);

iii) finally, none of these previous works has extended back in time older than 300 kyr, and most of them have focused on surface and thermocline depths, without any record for intermediate water.

The aim of this work is to better understand past changes in the intermediate water circulation, by using geochemical proxies measured on benthic foraminifera from a marine sediment core retrieved off Java (core SHI9001 6°11.57' S 103°11.80' E) at 1348m water depth. This study will help to better understand the connections between the Pacific Ocean and the Indian Ocean through the ITF and the IIW at glacial-interglacial as well as at longer timescale.

6.2. Studied area

Surface circulation in the study area is dominated by the monsoon wind regime. During the NW monsoon season (December–March), the South Java Current (SJC) (coming from the Equatorial Counter Current ECC), is flowing to the southeast to mix with the Leeuwin Current (LC), forming from warm and saline water coming from the eastern part of the Indonesian Archipelago (Tomczak and Godfrey, 1994). The mixing of the SJC and the LC feeds the South Equatorial Current (SEC) flowing westward. Lower salinities are observed in the SJC because of fresher water coming from the Java Sea and runoff from Sumatra and Java. During the SE monsoon (July–October), the SJC is moving northwestward to give origin to the SEC without any significant contribution of the LC (Quadfasel and Cresswell, 1992). This is also the season during which an active upwelling system off S Java and SW Sumatra is established (Tomczak and Godfrey, 1994). At the thermocline depth, the dominant water masses are the North Indian Water (NIW) and the ITF (Gordon et al., 1997; Wijffels et al., 2002). The NIW is forming from the Indian Central Water (ICW), and mixes with the outflow of salty marginal seas (Red Sea and Persian Gulf) when crossing the equator. The NIW are flowing northward following the SJC. The ITF is made of intermediate waters from the North and South Pacific. The ITF strength increases during the boreal summer, transferring cooler and fresher thermocline waters, and warmer and fresher surface waters to the Indian Ocean (Gordon et al., 1997).

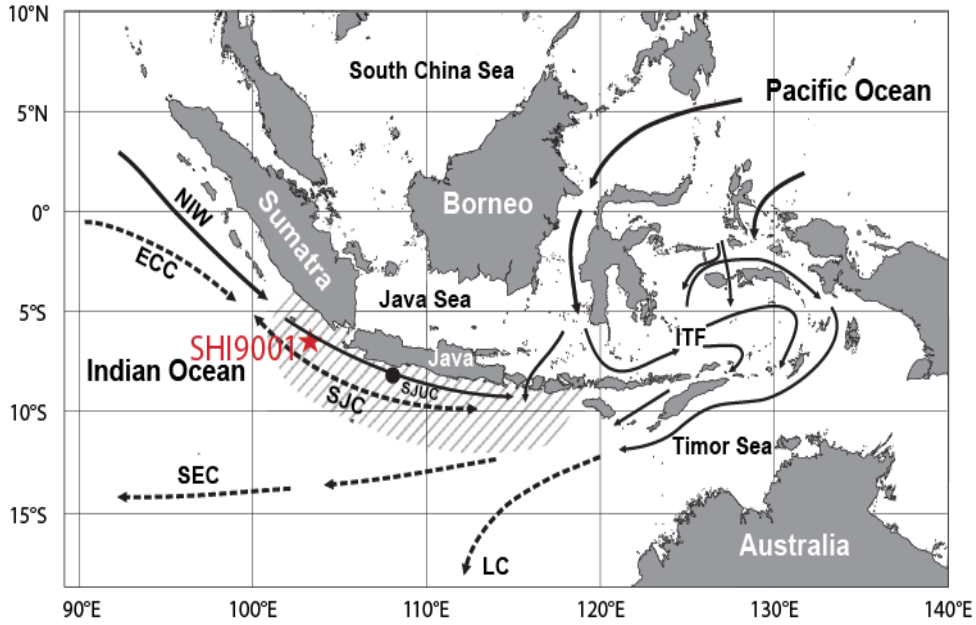

Fig. 6.1. *Mean surface (dashed arrows) and subsurface (solid arrows) currents in the studied area with core SHI9001 location. Gray dashed area roughly indicates the spatial extension of the Java upwelling. ECC, Equatorial Counter Current; ITF, Indonesian Throughflow; LC, Leeuwin Current; NIW, North Indian Water; SEC, South Equatorial Current; SJC, South Java Current; SJUC, South Java Undercurrent. Note the seasonal reversal in the flow direction of the SJC. Adapted from Mohtadi et al. (2010).*

6.3. Material and Methods

Core SHI9001 (6°11.57' S 103°11.80' E, 1348m) is located in the Eastern Equatorial Indian Ocean EEIO and was collected during the SHIVA cruise. A total of 88 samples were sieved for benthic foraminiferal analysis.

Oxygen and Carbon stable isotope have been performed on 70 samples of *C. wuellerstorfi* at the State Key Laboratory of Marine Geology of Tongji University (Shanghai, People's Republic of China). Approximately 4-8 clean and well-preserved specimens (>250 µm) were selected per sample. Stable isotope analyses were performed using a Finnigan MAT 253 mass spectrometer, with a mean external reproducibility better than ±0.07‰ for $\delta^{18}O$ and ±0.04‰ for $\delta^{13}C$. $\delta^{18}O$ and $\delta^{13}C$ values were calibrated versus PDB by using National Bureau of Standards (NBS) standards. Further analysis of planktonic foraminifera *Globigerinoides ruber* are going to be performed during summer 2019 in order to complete the benthic record.

Mg/Ca, Sr/Ca, U/Ca, Li/Ca, Cd/Ca and Ba/Ca ratios were measured in shells of the epi-faunal benthic foraminifera *H. elegans* (aragonite) and shallow endo-benthic *Uvigerina peregrina* (calcite)

from cores SHI9001. An epi-faunal species that growths on the sediment-seawater interface minimizes the influence of pore water composition in the elemental ratios (Lutze and Thiel, 1989) whereas *U. peregrina* is an endo-benthic species with an intermediate microhabitat (Fontanier et al., 2002).

Each sample contained approximately 8-15 individual foraminifers larger than 250μm. The foraminiferal tests were crushed open between two glass plates. The resulting fragments were ultrasonically cleaned to remove clays, and then submitted to oxidative and reductive protocols to remove organic matter and oxides following methods described by Boyle and Keigwin (1985) and Barker et al. (2003). Samples were dissolved in 0.075N HNO_3 and analyzed using a single collector sector field high resolution inductively coupled plasma mass spectrometer (HR-ICP-MS) Thermo Element XR hosted at the Laboratory GEOPS (University Paris-Sud, France).

The detailed instrumental settings and mother standard solution have been described in previous Chapters. A blank consisting of the same 0.1N HNO_3 used to dilute the standards and samples is also analyzed. On HR-ICP-MS, the elemental blanks are better than ±0.12% for Mg, ±0.02% for Sr, ±5.5% for Li, ±0.05% for U, ±6% for Cd and ±1.6% for Ba/Ca. All raw intensities (including standards) are corrected by removing the specific blank intensity values. Drift corrections during the course of daily analyses were performed through bracketing and linear regression estimated using standards interspersed every four samples. Standard curves are used to calculate elemental/Ca ratios, coefficients of determination (r^2) are always >0.9999 for all elemental ratios. The mean reproducibility and accuracy is Mg/Ca 2.1%, Sr/Ca 0.8%, Li/Ca 0.1%, U/Ca 3%, Cd/Ca 7.5% and Ba/Ca 4.5%.

6.4. Benthic foraminiferal records

6.4.1. Stable isotope records

The *C. wuellerstorfi* $\delta^{18}O$ record ranges from 2.40‰ to 3.89‰ at 240 and 510 cm, respectively. Cyclic variations are observed, and seem to correlate with glacial-interglacial changes.

$\delta^{13}C$ results range from -1.17‰ at 740 cm to 0.47‰ at 90 cm. Variations in the $\delta^{13}C$ seem to be anti-correlated to the $\delta^{18}O$ record. Moreover, a long-term trend is observed, with an average increase from ≈-0.5 to ≈0.3 ‰ from the bottom to the core-top.

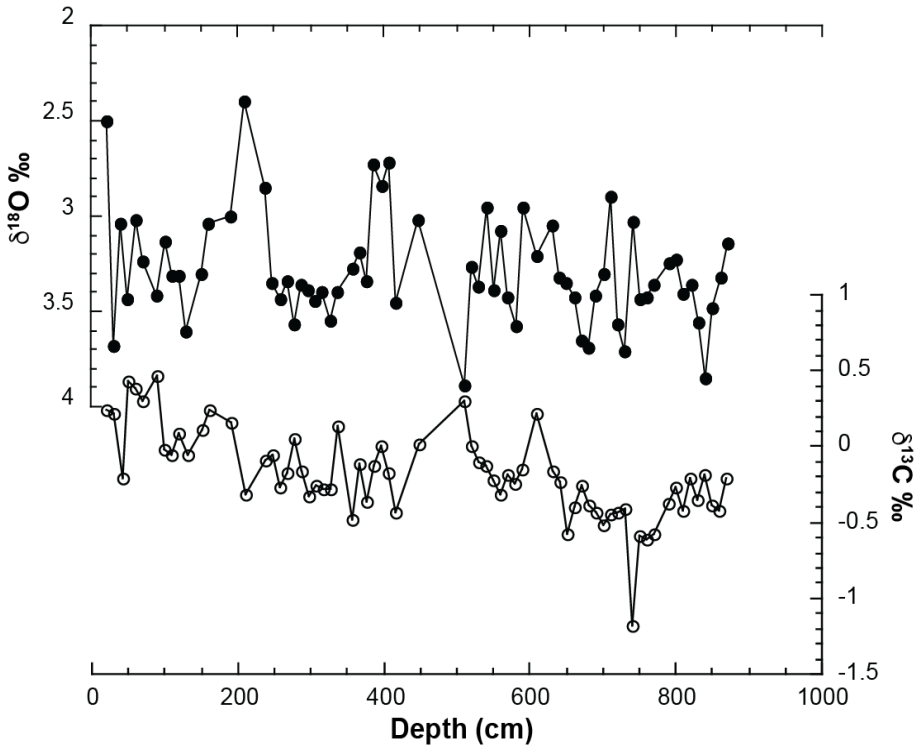

Fig. 6.2. *C. wuellerstorfi stable isotopes records from core SHI9001.*

6.4.2. Elemental ratios results

To check the validity of the elemental ratios results, the Mn/Ca from SHI9001 was systematically measured. The Mn/Ca of *H. elegans* and *U. peregrina* range between 0.5-5 µmol/mol and 1-25 µmol/mol, respectively, which is much lower than the 100 µmol/mol limit proposed by Boyle, (1983). The Fe/Ca values of *H. elegans* and *U. peregrina* are generally lower than 0.5 mmol/mol in all samples from core SHI9001. In addition, Barker et al., (2003) suggested a detection limit for uncleaned samples for Al/Ca at > 0.5 mmol/mol, and all Al/Ca results are below 0.5 mmol/mol, indicating the efficiency of the sample cleaning, suggesting the lack of sedimentary clay contamination.

6.4.2.1. Elemental ratios results of H. elegans

Mg/Ca and Sr/Ca ratios of core SHI9001 range from 0.3-0.6 mmol/mol and 0.4-1.3 mmol/mol, respectively (Fig. 6.3). The *H. elegans* Mg/Ca and Sr/Ca records show a strong covariation. These

elemental ratios records display a decrease from 870 cm to 407 cm, reaching minimum values of Mg/Ca (0.3 mmol/mol) and Sr/Ca (0.4 mmol/mol). Then, records show a continuous decrease from 400 to the core top (10 cm).

Cd/Ca and Ba/Ca records range from 0.07-0.15 µmol/mol and 1.2-7 µmol/mol (Fig. 6.3). The Cd/Ca and Ba/Ca values show an increasing trend during the 870-630 cm and 590-520 cm intervals, with average values of ~0.13 µmol/mol for Cd/Ca and ~5.4 µmol/mol for Ba/Ca. Then, the elemental ratios display a decrease since 510 cm. Compared with benthic Ba/Ca variations, the Cd/Ca variations are less clear from 510 to the core-top. By comparison, the Ba/Ca record reaches an increase in the 407-248 cm depth interval, with a maximum (7 µmol/mol) at 248 cm depth.

Li/Ca and U/Ca records range between 0.6-4 µmol/mol and 17-64 nmol/mol (Fig. 6.3). Li/Ca and U/Ca records keep a stable value (~2.5 µmol/mol and ~20 nmol/mol) between 870-550cm. Thereafter, Li/Ca values display a significant decrease in the 520-480 cm interval reaching a minimum value (0.6 µmol/mol), and then show a continuous increase from 470 to the core-top. By contrast, U/Ca records display a significant increase from 510 cm to the core top and reach a maximum value (64 nmol/mol) in 210 cm depth.

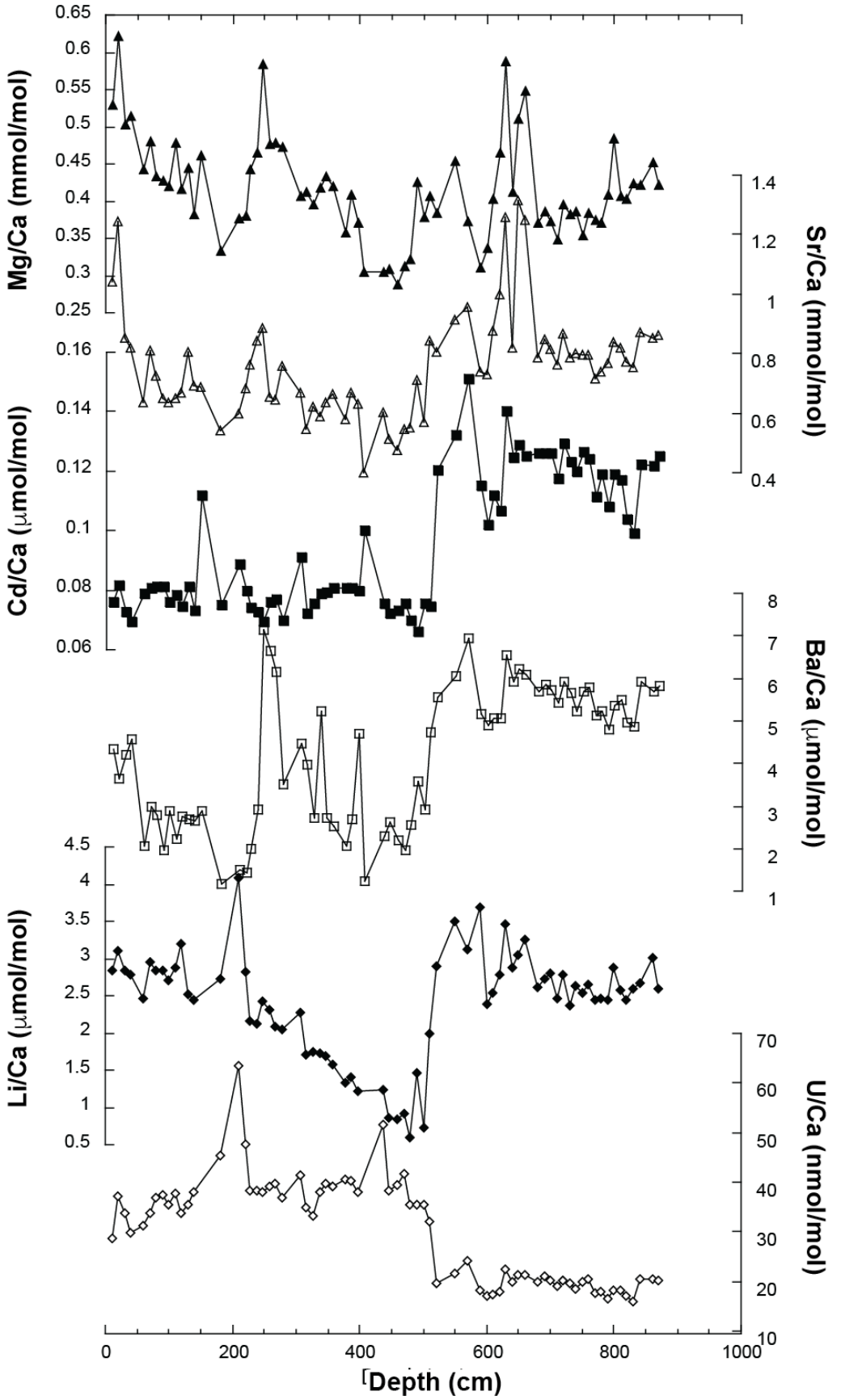

Fig. 6.3. *Core SHI9001 H. elegans Mg/Ca, Sr/Ca, Cd/Ca, Ba/Ca Li/Ca and U/Ca records.*

6.4.2.2. Elemental ratios results of U. peregrina

Mg/Ca, Sr/Ca, Cd/Ca, Ba/Ca, Li/Ca and U/Ca *U. peregrina* ratios from core SHI9001 range from 0.9-2 mmol/mol, 1.1-1.7 mmol/mol, 0.12-0.2 µmol/mol, 4.5-9.4 µmol/mol, 14-21 µmol/mol and 8.7-35 nmol/mol, respectively (Fig. 6.4). Mg/Ca, Sr/Ca and U/Ca show an increasing trend between 800 and 447 cm depth interval, and reach a maximum value (2 mmol/mol, 1.7 mmol/mol and 35 nmol/mol, respectively). Thereafter, the records of Mg/Ca, Sr/Ca and U/Ca generally decrease until the core-top. In addition, an increasing trend is observed in the Li/Ca record from 800 cm to 307 cm, and the maximum value (21 µmol/mol) is reached at 307 cm depth. Then, the record of Li/Ca shows a decreasing trend in the core-top (278-80 cm depth interval). The Cd/Ca and Ba/Ca elemental ratios display a slight increase in the 800-307 cm depth interval. The Cd/Ca and Ba/Ca records generally show a continuous decrease from 278 cm to 20 cm. The lowest values are found in this depth interval reaching 0.12 µmol/mol and 4.5 µmol/mol, respectively. However, the continuous decrease is interrupted by an increase during the 259 -190 cm depth interval.

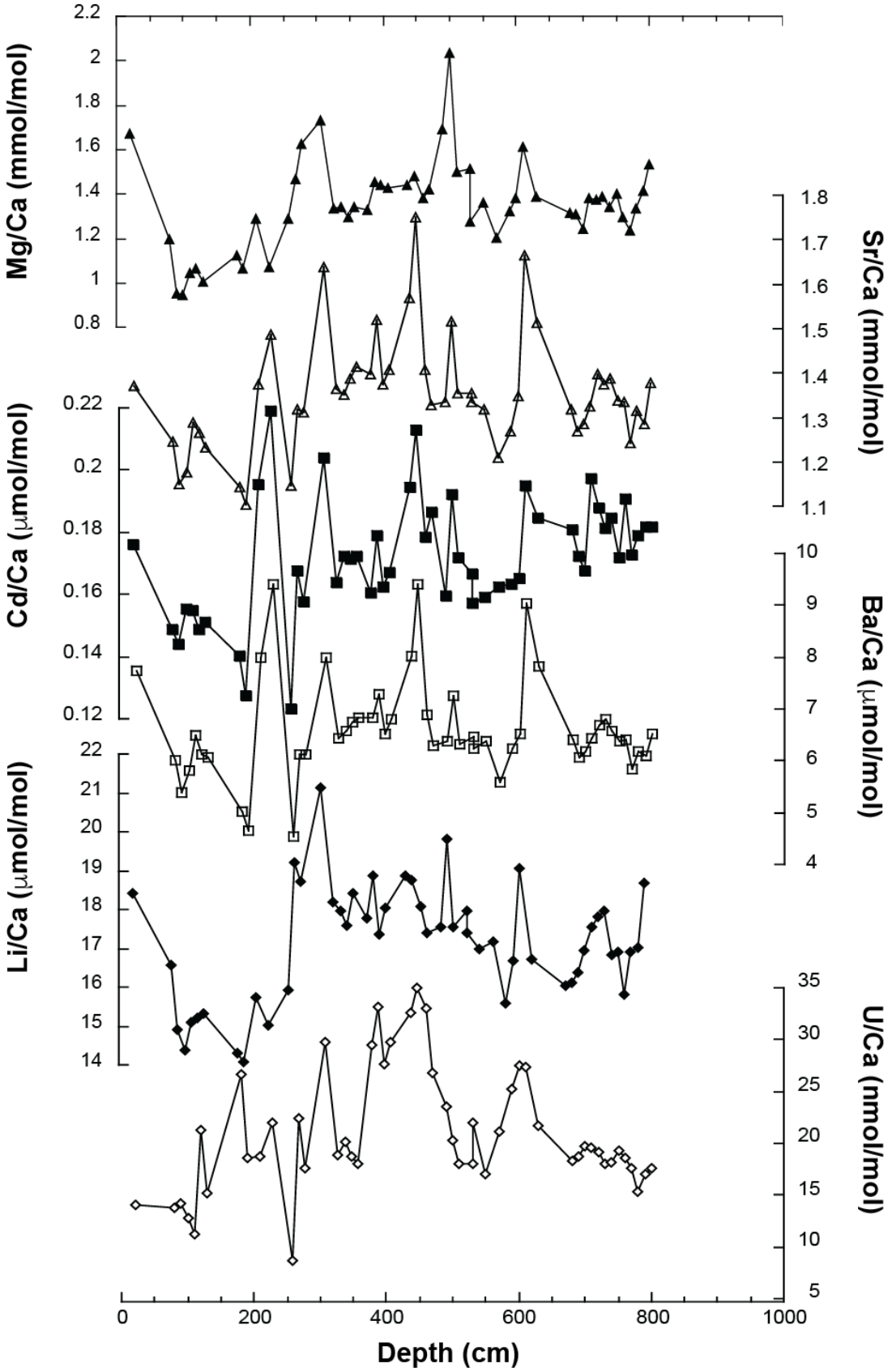

Fig. 6.4. *Core SHI9001 U. peregrina Mg/Ca, Sr/Ca, Cd/Ca, Ba/Ca Li/Ca and U/Ca records.*

6.5. Discussion

6.5.1. Age model

The age model for core SHI9001 was obtained by correlating the benthic $\delta^{18}O$ record (Figure 6.5) with the reference record LR04 (Lisiecki and Raymo, 2005) using the Analyseries software (Paillard et al., 1996). We also tested the comparison with the planktonic $\delta^{18}O$ record of core SO139-74KL off Sumatra (6°543'S, 103°833'E, 1690m) spanning the last 290 kyr (Wang et al., 2018). Both age models are in agreement for the last 290kyr, and for the older time-period, we only used the LR04 reference record. However, because of the low resolution of the record, the oldest Marine Isotope Stages MIS were more difficult to be compared to the LR04 benthic stack. We chose the two maximum values of the $\delta^{18}O$ at 3.89‰ and 3.85‰ at 510 and 840 cm depths, respectively, as indicating MIS 10 and 16, respectively. Following this method, the record in core SHI9001 extended down to MIS 17 that spans the last ≈685 ka. Sedimentation rates are variable from glacial to interglacial stages, with a constant trend of low to high values, respectively. On average, sedimentation rates for interglacial and glacial periods were determined as 2.5 and 1 cm/ka, respectively.

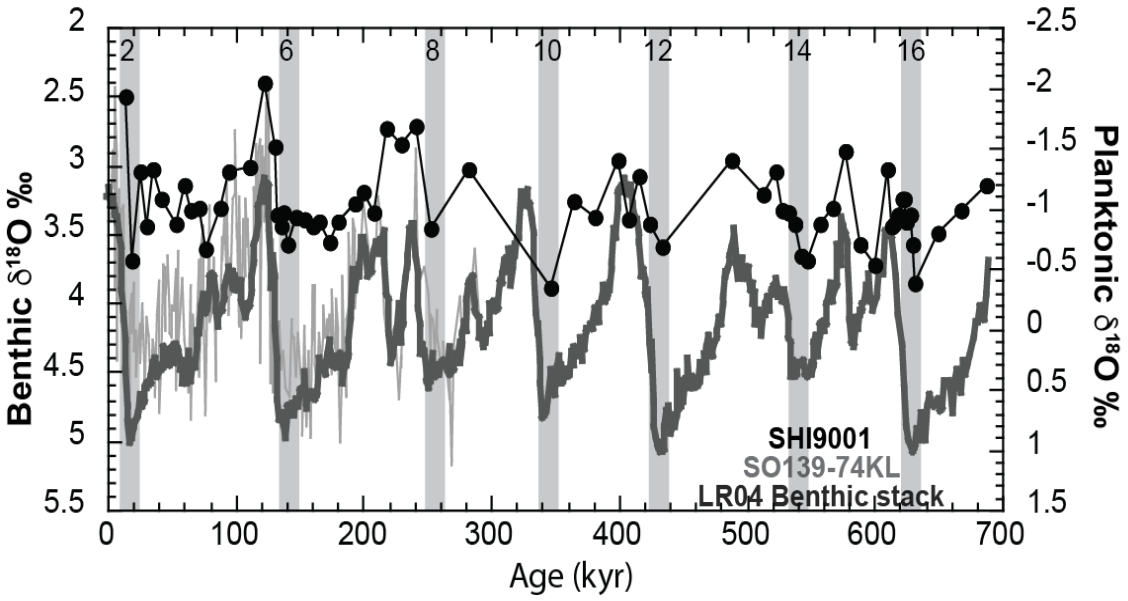

Fig. 6.5. *Core SHI9001 $\delta^{18}O$ versus age (black dots and curve). Age model based on LR04 benthic stack (dark grey, Lisiecki and Raymo, 2005) and core SO139-74KL $\delta^{18}O$ planktonic record (light*

grey, Wang et al., 2018). Gray band and peer numbers indicate glacial stages.

The SHI9001 benthic $\delta^{13}C$ record exhibits less clear variations related to glacial-interglacial cycles, but seems to show a longer trend. In order to better understand core SHI9001 $\delta^{13}C$ record, we compare it to the benthic $\delta^{13}C$ stack from Hoogakker et al., (2006) and to records from the South China Sea (ODP1143, 9°36198'N, 113°28503'E, 2771m, Wang et al., 2004) and the Timor Sea (core MD01-2378, 13°0825'S, 121°788'E, 1783m, Holbourn et al., 2005) (Fig. 6.6).

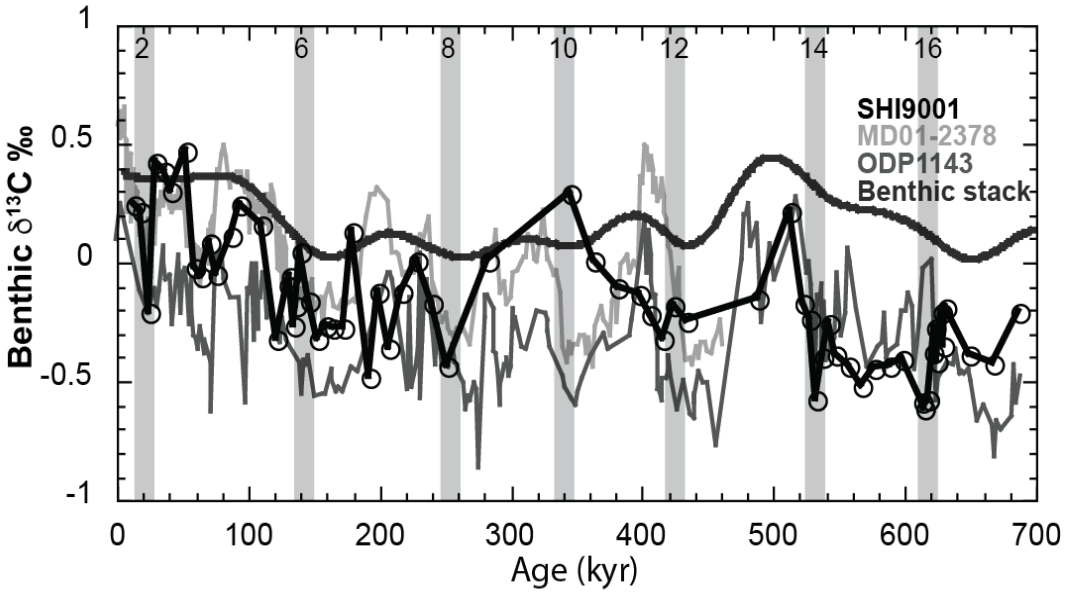

Fig. 6.6. *Core SHI9001 $\delta^{13}C$ record (black curve and dots) compared to a $\delta^{13}C$ benthic stack (dark grey, Hoogakker et al., 2006), and $\delta^{13}C$ records from the South China Sea (medium grey, ODP1143, Wang et al., 2004) and the Timor Sea (light grey, core MD01-2378, Holbourn et al., 2005). Gray band and peer numbers indicate glacial stages.*

Global trends for the different records are quite similar, even if because of the low-resolution of core SHI9001, the variations are sometimes less clear. These variations of about 400 kyr duration have been associated in the literature to concomitant changes in the burial fluxes of organic and inorganic carbon due to ventilation changes and/or changes in the production and export ratio (Hoogakker et al., 2006). In particular, 2 major events punctuated the last million-year period, the mid-Pleistocene transition (MPT) centered at 0.9 Ma and the mid-Brunhes event (MBE) around 0.4 Ma, both of them marked by a $\delta^{13}C$ maximum values (Wang et al., 2004). Although now well documented, the underlying causes for these large-scale variations in the $\delta^{13}C$ are still under debate, implying changes in the changes in ratio between particulate and dissolved organic carbon

(POC/DOC) in the ocean, as well as changes in the ocean circulation and in the global Carbon pool, also implying exchanges with the atmosphere. The role of the Southern Ocean is in particular invoked, because of its central role in the connection between all ocean basins, as well as in the biogeochemical processes (Wang et al., 2004).

6.5.2. Comparison between stable isotope records and elemental ratio results

In order to better decipher the variations observed in the elemental ratio records, we processed cross-comparison between the results for each species (Tables 6.1. and 6.2.).

Table 6.1. *Correlation coefficient (R^2) calculated between the different element/Ca ratios for H. elegans. The observed negative correlations are indicated in red and the highest R^2 are highlighted in yellow.*

	Mg/Ca	Sr/Ca	Li/Ca	Cd/Ca	Ba/Ca	U/Ca
Mg/Ca		0,46950	0,17925	0,00118	0,08497	0,00155
Sr/Ca	0,46950		0,34731	0,2695	0,35924	0,24727
Li/Ca	0,17925	0,34731		0,27044	0,13506	0,11875
Cd/Ca	0,00118	0,26950	0,27044		0,47221	0,60486
Ba/Ca	0,08497	0,35924	0,13506	0,47221		0,5255
U/Ca	0,00155	0,24727	0,11875	0,60486	0,5255	

Table 6.2. *Correlation coefficient (R^2) calculated between the different element/Ca ratios for U. peregrina. The highest R^2 are highlighted in yellow.*

	Mg/Ca	Sr/Ca	Li/Ca	Cd/Ca	Ba/Ca	U/Ca
Mg/Ca		0,36061	0,69647	0,19595	0,15739	0,10489
Sr/Ca	0,36061		0,51947	0,61521	0,82266	0,37823
Li/Ca	0,69647	0,51947		0,24461	0,22436	0,18209
Cd/Ca	0,19595	0,61521	0,24461		0,67818	0,15476
Ba/Ca	0,15739	0,82266	0,22436	0,67818		0,23558
U/Ca	0,10489	0,37823	0,18209	0,15476	0,23558	

Different groups emerge from these results:

1) *H. elegans* Mg/Ca, Sr/Ca and, with a lowest R^2, the Li/Ca, seem to be in agreement. The highest R^2 are observed between the Cd/Ca, Ba/Ca and U/Ca, with negative trends between the U/Ca and the two other ratios. However, we can notice that the Cd/Ca, Ba/Ca and Li/Ca records exhibit a longer trend with an abrupt decrease of the values at about 400 kyr, whereas the U/Ca ratio increases at the same time.

2) Strong correlations between the Mg/Ca and the Li/Ca in the one hand, and between the Sr/Ca, Cd/Ca and Ba/Ca and to a lesser extent, with the U/Ca, are observed for *U. peregrina* (Table 6.2.).

When comparing the elemental ratio records from both species to the stable isotope records, some trends emerge:

i) As already described, the $\delta^{18}O$ of *C. wuellerstorfi* clearly exhibit the "classical" glacial-interglacial changes, whereas the $\delta^{13}C$ record shows a longer trend;

ii) *U. peregrina* Mg/Ca and Li/Ca seem to be in agreement with the *C. wuellerstorfi* $\delta^{18}O$, exhibiting the glacial-interglacial cyclicity, as well as the Mg/Ca and the Sr/Ca of *H. elegans* (Fig.6.7);

iii) Sr/Ca, Cd/Ca and Ba/Ca records (and U/Ca, to a lesser extent) from *U. peregrina* are similar, and part of the variations is in agreement with the long-term trends of the $\delta^{13}C$ record. Moreover, the Cd/Ca and the Ba/Ca ratios from *H. elegans* display an opposite variations compared to the $\delta^{13}C$ (Fig. 6.8);

v) A more complex pattern is observed in the Li/Ca and U/Ca records from *H. elegans*, also partly exhibited by the Ba/Ca and Cd/Ca ratios, as well as in the Mg/Ca and Sr/Ca (Fig. 6.3).

The difference between both species can be explained by their different microhabitats: indeed, *H. elegans* is an epifaunal species that is supposed to record the deep-water geochemical properties whereas *U. peregrina* has a deeper microhabitat inside the sediment, and thus may reflect the pore-water signature. However, as common features have also emerged from the different records from both species at glacial-interglacial as well as at longer timescales, the same processes as described in the following could drive their variations.

6.5.2.1. Glacial-interglacial variability

As already observed in previous records (e.g., Bryan and Marchitto, 2008), the covariation of the Mg/Ca and Li/Ca ratios of *U. peregrina* can be used to propose a new proxy for bottom-temperature, the Mg/Li ratio. We calculated this ratio, and we used the equation from Bryan and Marchitto, (2008) to reconstruct past bottom water temperature (BWT): Mg/Li = 0.0061*T+0.033 (Fig. 6.8). In order to compare the results with another calibration method, we also calculated the BWT from the Mg/Ca ration with the 2 equations given by Bryan and Marchitto: Mg/Ca = 0.079T+0.77 and Mg/Ca = $0.98e^{(0.045*T)}$ and another one from of Elderfield et al., (2010) Mg/Ca = 0.07T+0.9 (Fig. 6.8.). We also used the Mg/Ca from *H. elegans* and the following equation from Bryan and Marchitto, (2008) to check the validity of our reconstructions: Mg/Ca = 0.006*T+0.03.

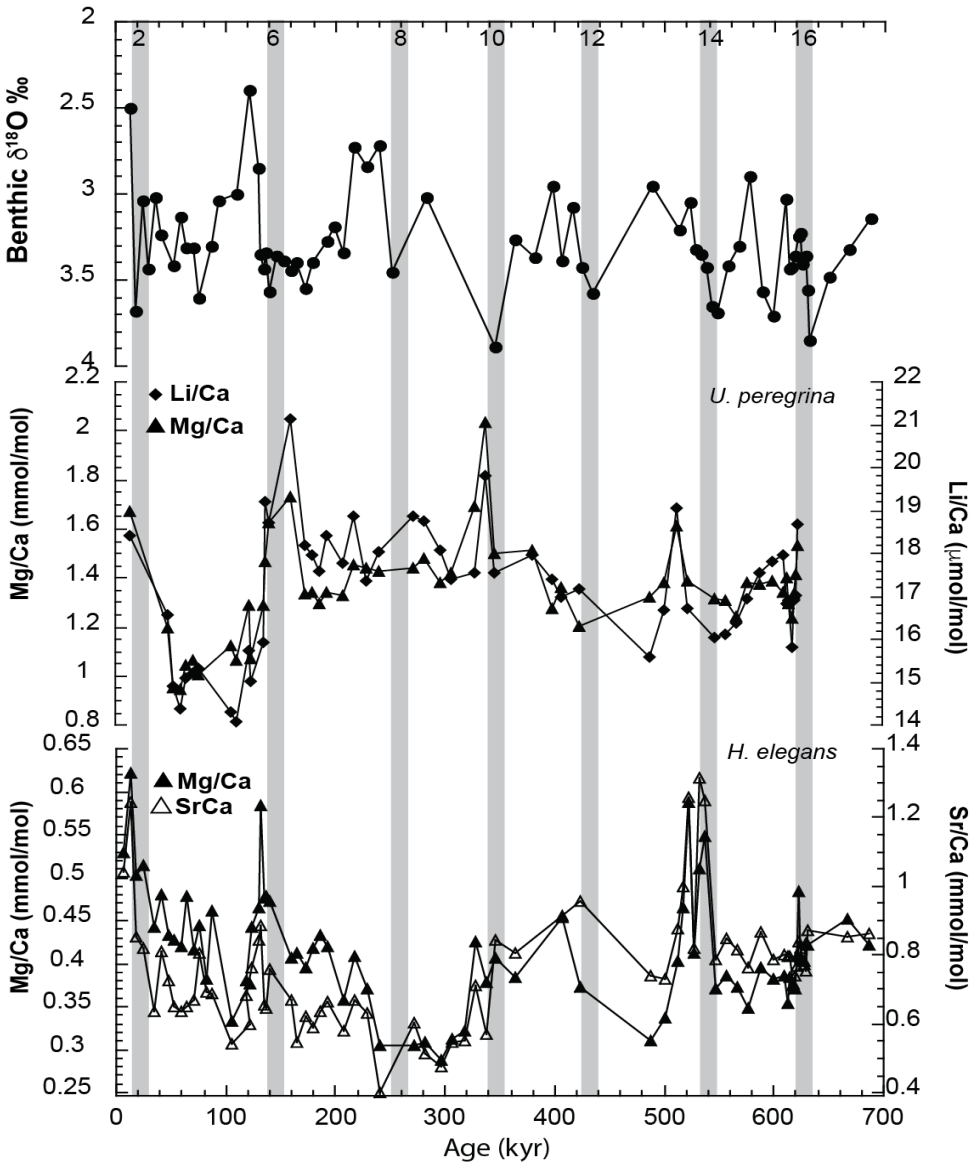

Fig. 6.7. *Comparison between the $\delta^{18}O$ and the H. elegans Mg/Ca and Li/Ca form U. peregrina and Mg/Ca and the Sr/Ca from H. elegans. Gray band and peer numbers indicate glacial stages.*

On *U. peregrina* species, the BWT calculated from the Mg/Li ratio vary between 5.03°C at 53 kyr and 11.45°C at 338kyr. The different reconstructions from the Mg/Ca ratio are in agreement BWT range between -0.66 and 16.25°C at 56 and 338 kyr, respectively, but the amplitudes of the BWT, as well as the maximum values calculated with this latter method seems slightly unrealistic. Moreover, the BWT from the Mg/Li calculation are in good agreement with the calculations from the Mg/Ca ratio of *H. elegans*, ranging from 4.29°C to 9.9°C at 296 and 12 kyr, respectively. These values are slightly higher than the modern BWT of about 5°C at the studied site, but the trends are in agreement with the glacial-interglacial variability, suggesting colder water masses during glacial

periods compared to interglacial intervals. These changes in the BWT could reflect a change in the water source, as well as a difference in the contribution from the ITF, affected by the sea level variations during glacial times. Moreover, this BWT change could also reflect a more local effect associated to the strength of the upwelling, as already observed for subsurface water (Lückge et al., 2009). Further work will help to decipher between these different mechanisms.

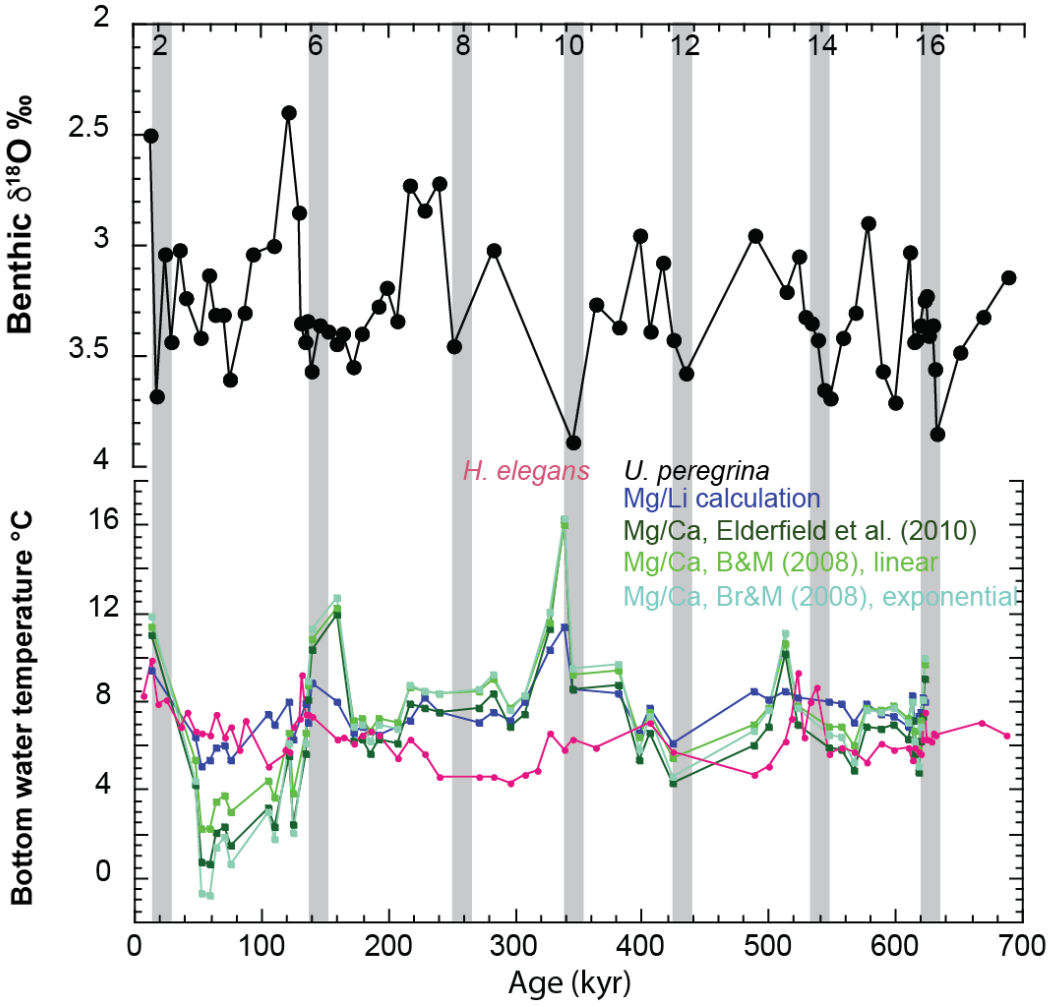

Fig. 6.8. *Comparison between the $\delta^{18}O$ and the bottom water temperatures reconstructed from the Mg/Ca of H. elegans (calibration from Bryan and Marchitto, 2008, pink curve) and the Mg/Li (calibration from Bryan and Marchitto, 2008, blue curve) and the Mg/Ca (calibration from Elderfield et al., 2010, dark green curve, from Bryan and Marchitto, 2008, linear calculation, light green curve, exponential calculation, light blue curve) from U. peregrina. Gray band and peer numbers indicate glacial stages.*

6.5.3. Long-term changes

The Sr/Ca, Cd/Ca and Ba/Ca ratios from *U. peregrina*, as well as the Cd/Ba and the Ba/Ca from *H. elegans* tend to exhibit opposite variations to the $\delta^{13}C$ record from *C. wuellerstorfi* (Fig. 6.9). According to the literature, the Cd/Ca and the Ba/Ca ratios are related to the nutrient content of the water masses (e.g., Boyle and Keigwin, 1982; Came et al., 2008; Elderfield and Rickaby, 2000; Hall and Chan, 2004; Oppo and Fairbanks, 1987; Valley et al., 2017; Poggemann et al., 2017).

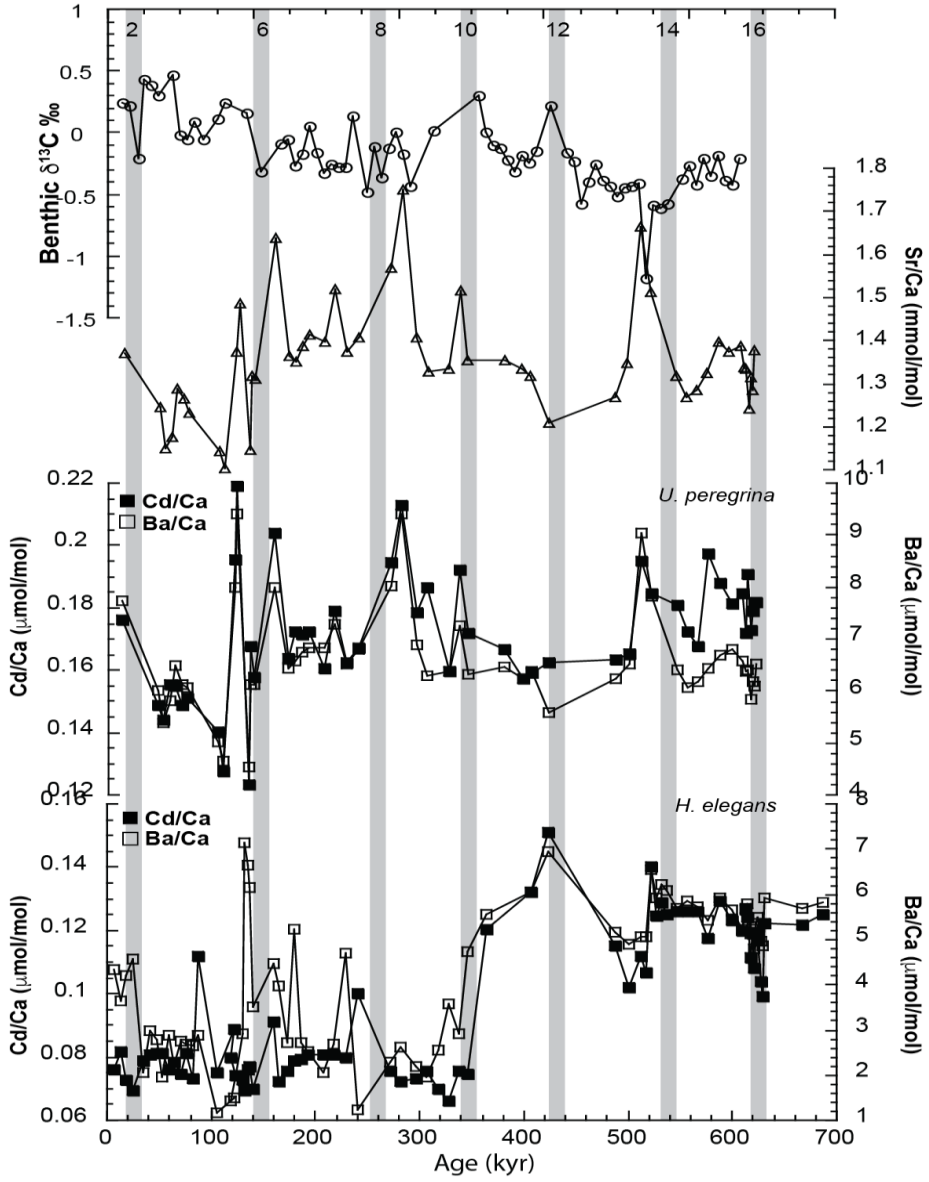

Fig. 6.9. *Comparison between the $\delta^{13}C$ and Sr/Ca, Cd/Ca and Ba/Ca records from U. peregrina and the Cd/Ca and Ba/Ca records from H. elegans. Gray band and peer numbers indicate glacial stages.*

Thus, an increase in these ratios associated to a decrease in the $\delta^{13}C$ tend to prove that the nutrient content of the water masses at the core site have varied through time. This is in agreement with the global variations in the ocean $\delta^{13}C$, related to changes in the Organic versus Inorganic carbon ratios and associated to global biogeochemical cycle changes. However, part of these variations could also reflect changes in the water source, with a varying contribution from water masses from the Southern Ocean. Moreover, as already noticed for the glacial-interglacial variability, local changes related to the relationships between the monsoon and the upwelling, could also have influenced the paleo-nutrient concentrations.

6.5.4. Abrupt variations during the 400 kyr event

Finally, the Li/Ca and the U/Ca records of *H. elegans* display an abrupt opposite variation at around 400 kyr, that does not seem to mirror the glacial-intergalcial variability nor the long-term trends described in the $\delta^{13}C$ record (Fig. 6.10). However, this abrupt change occurs during a $\delta^{13}C$ maximum observed in various $\delta^{13}C$ records (Fig. 6.6 and 6.10). As the Li/Ca and the U/Ca proxies can reflect the carbonate ion concentration (e.g., Doss et al., 2018; Marchitto et al., 2018; Keul et al., 2013), these records could indicate a strong change in the ocean Carbon cycle at intermediate water depths, that could be in relation with the global C change recorded in the $\delta^{13}C$.

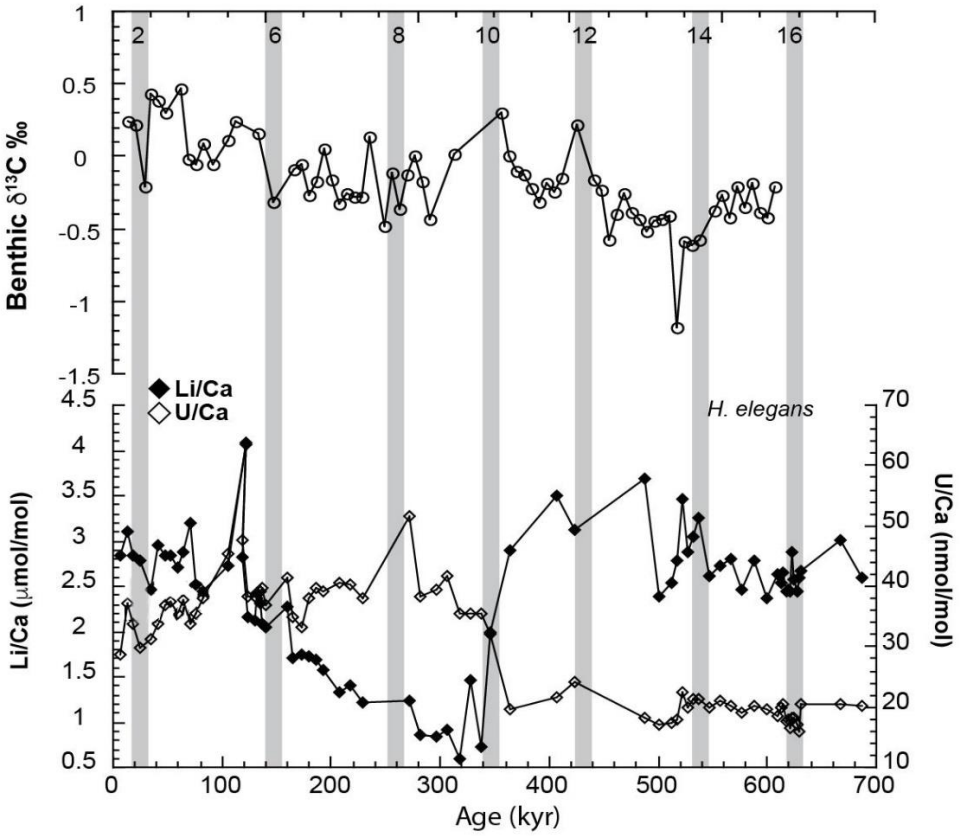

Fig. 6.10. *Comparison between the $\delta^{13}C$ and Li/Ca and U/Ca records from H. elegans. Gray band and peer numbers indicate glacial stages.*

References

Barker, S., Greaves, M., Elderfield, H., 2003. A study of cleaning procedures used for foraminiferal Mg/Ca paleothermometry. Geochemistry Geophysics Geosystems 4 (9), 1-20.

Boyle, E. A., 1983. Manganese carbonate overgrowths on foraminifera tests. Geochim. Cosmochim. Acta 63 (18), 353-353.

Boyle, E. A., Keigwin, L. D., 1985. Comparison of Atlantic and Pacific paleochemical records for the last 215,000 years: Changes in deep ocean circulation and chemical inventories. Earth and Planetary Science Letters 76 (1), 135-150.

Boyle, E. A., Keigwin, L. D., 1982. Deep circulation of the North Atlantic over the last 200,000 years: Geochemical evidence. Science 218 (4574), 784-787.

Bryan, S. P., Marchitto, T. M., 2008. Mg/Ca–temperature proxy in benthic foraminifera: New calibrations from the florida straits and a hypothesis regarding Mg/Li. Paleoceanography 23 (PA2220), 1-17.

Came, R. E., Oppo, D. W., Curry, W. B., Lynch-Stieglitz, J., 2008. Deglacial variability in the surface return flow of the Atlantic Meridional Overturning Circulation. Paleoceanography 23 (1).

De Deckker, P., Gingele, F. X., 2002. On the occurrence of the giant diatom ethmodiscus rex in an 80-ka record from a deep-sea core, southeast of Sumatra, Indonesia: Implications for tropical palaeoceanography. Marine Geology 183 (1), 31-43.

Doss, W., Marchitto, T. M., Eagle, R., Rashid, H., Tripati, A., 2018. Deconvolving the saturation state and temperature controls on benthic foraminiferal Li/Ca, based on downcore paired B/Ca measurements and core-top compilation. Geochimica Et Cosmochimica Acta 236, 297-314.

Elderfield, H., Greaves, M., Barker, S., Hall, I. R., Tripati, A., Ferretti, P., Crowhurst, S., Booth, L., Daunt, C., 2010. A record of bottom water temperature and seawater $\delta^{18}O$ for the Southern Ocean over the past 440 kyr based on Mg/Ca of benthic foraminiferal *Uvigerina* spp. Quaternary Science Reviews 29 (1), 160-169.

Elderfield, H., Rickaby, R. E. M., 2000. Oceanic Cd/P ratio and nutrient utilization in the glacial Southern Ocean. Nature 405 (6784), 305-310.

Fontanier, C., Jorissen, F. J., Licari, L., Alexandre, A., Anschutz, P., Carbonel, P., 2002. Live benthic foraminiferal faunas from the Bay of Biscay: Faunal density, composition, and microhabitats. Deep Sea Research Part I: Oceanographic Research Papers 49 (4), 751-785.

Gingele, F. X., Deckker, P. D., Girault, A., Guichard, F., 2002. History of the south Java current over the past 80 ka. Palaeogeography Palaeoclimatology Palaeoecology 183 (3), 247-260.

Gordon, A. L., Ma, S., Olson, D. B., Hacker, P., Ffield, A., Talley, L. D., Wilson, D., Baringer, M.,

1997. Advection and diffusion of Indonesian Throughflow Water within the Indian Ocean South Equatorial Current. Geophysical Research Letters 24 (21), 2573-2576.

Hall, J., Chan, L. H., 2004. Ba/Ca in benthic foraminifera: Thermocline and middepth circulation in the North Atlantic during the last glaciation. Paleoceanography 19 (PA4018), 1-13.

Holbourn, A., Kuhnt, W., Kawamura, H., Jian, Z., Grootes, P., Erlenkeuser, H., Jian, X., 2005. Orbitally paced paleoproductivity variations in the timor sea and Indonesian Throughflow variability during the last 460 kyr. Paleoceanography 20 (3).

Hoogakker, B. A. A., Rohling, E. J., Palmer, M. R., Tyrrell, T., Rothwell, R. G., 2006. Underlying causes for long-term global ocean $\delta^{13}C$ fluctuations over the last 1.20 myr. Earth and Planetary Science Letters 248 (1), 15-29.

Keul, N., Langer, G., Nooijer, L. J. D., Nehrke, G., Reichart, G. J., Bijma, J., 2013. Incorporation of uranium in benthic foraminiferal calcite reflects seawater carbonate ion concentration. Geochemistry Geophysics Geosystems 14 (1), 102-111.

Lückge, A., Mohtadi, M., Rühlemann, C., Scheeder, G., Vink, A., Reinhardt, L., Wiedicke, M., 2009. Monsoon versus ocean circulation controls on paleoenvironmental conditions off southern Sumatra during the past 300,000 years. Paleoceanography 24 (1).

Lisiecki, L., Raymo, M., 2005. A Pliocene-Pleistocene stack of 57 globally distributed benthic ^{18}O records. Paleoceanography 20 (PA1003), 1-17.

Lutze, G. F., Thiel, H., 1989. Epibenthic foraminifera from elevated microhabitats; *Cibicidoides wuellerstorfi* and *Planulina ariminensis*. Journal of Foraminiferal Research 19 (2), 153-158.

Marchitto, T. M., Bryan, S. P., Doss, W., Mcculloch, M., Montagna, P., 2018. A simple biomineralization model to explain Li, Mg, and Sr incorporation into aragonitic foraminifera and corals. Earth and Planetary Science Letters 481, 20-29.

Martinez, J. I., De Deckker, P., Barrows, T. T., 1999. Palaeoceanography of the Last Glacial Maximum in the eastern Indian Ocean: Planktonic foraminiferal evidence. Palaeogeography Palaeoclimatology Palaeoecology 147 (1), 73-99.

Mohtadi, M., Lückge, A., Steinke, S., 2010. Late Pleistocene surface and thermocline conditions of the eastern tropical Indian Ocean. Quaternary Science Reviews 29 (7), 887-896.

Oppo, D. W., Fairbanks, R. G., 1987. Variability in the deep and intermediate water circulation of the Atlantic Ocean during the past 25,000 years: Northern Hemisphere modulation of the Southern Ocean. Earth and Planetary Science Letters 86 (1), 1-15.

Paillard, D., Labeyrie, L., Yiou, P., 1996. Macintosh program performs time-series analysis. Eos Transactions American Geophysical Union 77 (39), 379-379.

Poggemann, D. W., Hathorne, E. C., Nürnberg, D., Frank, M., Bruhn, I., Reißig, S., Bahr, A., 2017.

Rapid deglacial injection of nutrients into the tropical Atlantic via Antarctic Intermediate Water. Earth and Planetary Science Letters 463, 118-126.

Quadfasel, D., Cresswell, G. R., 1992. A note on the seasonal variability of the south Java current. Journal of Geophysical Research Oceans 97 (C3), 3685-3688.

Rashid, H., Flower, B. P., Poore, R. Z., Quinn, T. M., 2007. A ~25 ka Indian Ocean Monsoon variability record from the Andaman Sea. Quaternary Science Reviews 26 (19), 2586-2597.

Schiller, A., Godfrey, J. S., McIntosh, P. C., Meyers, G., Wijffels, S. E., 1998. Seasonal near-surface dynamics and thermodynamics of the Indian Ocean and Indonesian Throughflow in a global ocean general circulation model. Journal of Physical Oceanography 28 (11), 2288-2312.

Speich, S., Blanke, B., Madec, G., 2001. Warm cold water routes of an OGCM Thermohaline conveyor belt. Geophysical Research Letters 28 (2), 311–314.

Takahashi, K., Okada, H., 2000. The paleoceanography for the last 30,000 years in the southeastern Indian Ocean by means of calcareous nannofossils. Marine Micropaleontology 40 (1), 83-103.

Tomczak, M., Godfrey, J. S., 2003; Regional oceanography: An introduction. Daya Publishing House.

Tomczak, M., Godfrey, S., *Regional oceanography*. 1994.

Valley, S., Lynch-Stieglitz, J., M. Marchitto, T., 2017. Timing of deglacial AMOC variability from a high-resolution seawater Cadmium reconstruction: Timing deglacial upper amoc variability. Paleoceanography 32, 1195-1203.

Wang, P., Tian, J., Cheng, X., Liu, C., Jian, X., 2004. Major Pleistocene stages in a carbon perspective: The South China Sea record and its global comparison. Paleoceanography 19:Pa4005. Paleoceanography 19 (4).

Wang, X., Jian, Z., Lückge, A., Wang, Y., Dang, H., Mohtadi, M., 2018. Precession-paced thermocline water temperature changes in response to upwelling conditions off southern Sumatra over the past 300,000 years. Quaternary Science Reviews.

Wijffels, S., Sprintal, J., Fieux, M., Bray, N., 2002. The jade and WOCE I10/IR6 throughflow sections in the southeast Indian Ocean. Part 1: Water mass distribution and variability. Deep-Sea Research Part II 49 (7), 1341-1362.

You, Y., 1998. Intermediate water circulation and ventilation of the Indian Ocean derived from water-mass contributions. Journal of Marine Research 56 (5), 1029-1067.

You, Y., Tomczak, M., 1993. Thermocline circulation and ventilation in the Indian Ocean derived from water mass analysis. Deep Sea Research Part I: Oceanographic Research Papers 40 (1), 13-56.

General conclusions and perspectives

The main objectives of this study were to reconstruct the evolution of intermediate water circulation in the Indian Ocean at glacial-interglacial as well as at millennial timescales, and to better understand the relationships between ocean circulation (especially the role of Antarctic Intermediate Water AAIW), Southern Ocean upwelling intensity and changes in the atmospheric CO_2 by the investigation of marine cores at intermediate water depth collected from the northern Indian Ocean (Bay of Bengal and Arabian Sea) and in the Eastern Equatorial Indian Ocean. In this study, we have investigated benthic foraminiferal assemblages together with stable isotopes ($\delta^{13}C$, $\delta^{18}O$), and ^{14}C of benthic foraminiferal in order to reconstruct hydrological changes of intermediate water masses at high temporal resolution since the Last Glacial Maximum (LGM). The analyses of benthic foraminiferal elemental ratios were made to reconstruct the chemical properties of intermediate water masses such as paleo-carbonate ion concentration (Mg/Ca, Sr/Ca, Li/Ca, and U/Ca), bottom-water temperature (Mg/Li) or the paleo-nutrient changes (Cd/Ca and Ba/Ca). This strategy allowed us to better understand the temporal evolution of the source and ventilation of intermediate water masses in the northern Indian Ocean and, in particular, the millennial-scale variations during the last deglaciation in the Northern Indian Ocean, or longer-trend changes in the Equatorial Indian Ocean.

In the northeastern Bay of Bengal, benthic foraminiferal assemblages, $\delta^{13}C$, $\delta^{18}O$, and ^{14}C have been conducted from core MD77-176 at intermediate water depths to reconstruct the evolution of intermediate water masses of the Northeast Indian Ocean since the Last Glacial Maximum (LGM). Our results seem to indicate that the LGM was mainly influenced by the southern sourced waters at the core site. A high relative abundance of intermediate and deep infaunal species during the LGM reflects low oxygen concentration and/or meso- to eutrophic deep-water conditions, associated with depleted benthic $\delta^{13}C$ values. During the Holocene, benthic foraminiferal assemblages indicate an oligo– to mesotrophic environment with well-ventilated bottom water conditions compared with LGM. Millennial-scale events (17-14 and 13-10.6 cal kyr BP intervals) punctuated the last deglaciation, displaying an increase in the benthic $\delta^{13}C$ and in the ε_{Nd} values coincident with depleted B-P ^{14}C age offsets. Strengthened upward mixing could move much younger ^{14}C age surface water to deep water masses, leading to a decreasing in B-P age offsets. In addition, benthic $\delta^{13}C$ could also increase via strong upwelling during the formation of AAIW/SAMW due to the influence of air-sea exchange (Lynch-Stieglitz et al., 1994). Thus, these records indicate an increased contribution of AAIW at the studied site accompanied by enhanced upwelling in the

Southern Ocean. This could be associated to a strong sea-atmospheric CO_2 exchange through the Southern Ocean ventilation during the last deglaciation.

In the northern Indian Ocean, benthic foraminiferal $\delta^{13}C$ and $\delta^{18}O$ combined with *H. elegans* elemental ratios (Mg/Ca, Sr/Ca, Li/Ca and U/Ca) were analyzed on core MD77-191 located at 1254 m water depth from the south tip of India, and core MD77-176 (1375 m water depth) collected from the northern BoB. We highlighted that benthic elemental ratios (Mg/Ca, Sr/Ca, Li/Ca and U/Ca) seem to be mainly influenced by the carbonate ion concentration changes, and that bottom water temperature does not seem to strongly influence these ratios. We reconstructed seawater $[CO_3^{2-}]$ concentration by converting *H. elegans* Sr/Ca to $[CO_3^{2-}]$, by collecting the literature core-top data of paired $\Delta[CO_3^{2-}]_{aragonite}$ with *H. elegans* Sr/Ca at intermediate water depth (500-1500 m) (Rosenthal et al., 2006; Yu et al., 2014) and plotted these Sr/Ca values together to build an empirical relationship. Then, we compared the seawater $[CO_3^{2-}]$ records of core MD77-191 (Arabian Sea) and core MD77-176 (northeastern BoB) with $[CO_3^{2-}]$ records at different water depths from the Atlantic Ocean (BOFS 17K, at 1150 m water depth), and the Indian Ocean (WIND 28K, at 4147 m water depth) (Yu et al., 2008, 2010). All of the $[CO_3^{2-}]$ records at intermediate water depths display low values during the 17-15.2 and 12.6-10.5 kyr time intervals (last deglaciation), indicating the transfer of CO_2 from the deep ocean into the upper water depth. In addition, the decrease in $[CO_3^{2-}]$ records also correspond to an increase of benthic $\delta^{13}C$ during the last deglaciation, which could be also observed in previous benthic $\delta^{13}C$ studies from the northeastern Bay of Bengal, Arabian Sea and Pacific Ocean (e.g., Duplessy et al., 1984; Curry et al., 1988; Naqvi et al., 1994; Jung et al., 2009; Ma et al., 2019). Furthermore, increased benthic $\delta^{13}C$, depletion in $[CO_3^{2-}]$ were also associated with decreased B-P age offsets from the Bay of Bengal occurred in the 17-15.2 and 12.6-10.5 cal kyr BP time intervals. All of these results suggest the strong linkage between Southern Ocean enhanced ventilation via AAIW and release of CO_2 during the last deglaciation. During the Holocene, the decreased $[CO_3^{2-}]$ in intermediate water masses also provides evidence for the important influence of global alkalinity inventory variation, corresponding to the atmospheric CO_2 rise since 8 cal kyr BP and/or increased productivity through the Holocene (at least for MD77-191), as the biological regeneration may also lead to the decrease of carbonate ion (Holligan and Robertson, 1996).

We also performed analyses of benthic foraminiferal Cd/Ca and Ba/Ca on cores MD77-176 and MD77-191, to obtain the evolution of intermediate water circulation and paleo-nutrient changes in the northern Indian Ocean since the last deglaciation. Indeed, benthic Cd/Ca and Ba/Ca ratios seem mainly influenced by the surface productivity changes and/or the intermediate-bottom water

ventilation. The intermediate seawater Cd_w concentration was calculated from the *H. elegans* Cd/Ca based on the equation of Boyle (1992). During the late Holocene (from 5.2 to 2.4 cal kyr BP), the increased intermediate Cd_w concentrations of two marine cores MD77-191 and MD77-176 indicate an enhanced surface productivity in the south tip of India. For the northeastern Bay of Bengal, by contrast, the lower values of intermediate Cd_w during the early Holocene (from 10 to 6 cal kyr BP) indicate a poor surface productivity. This large variation of the intermediate Cd_w during the Holocene is in agreement with the changes in the monsoon precipitation observed in the BoB and Indian continent (Marzin et al., 2013; Contreras-Rosales et al., 2014; Sarkar et al., 2015), and could provide strong evidence for the hypothesis of the seesaw relationship between intense monsoon rainfall and the surface productivity in the BoB and south tip of Arabian Sea during the Holocene. Moreover, during the last deglaciation, decreased intermediate Cd_w concentration and benthic Ba/Ca ratios are related to depleted surface productivity changes and/or the enhanced ventilation of intermediate-bottom water masses at the in the 16-15.2 and 12.6-11 cal kyr BP intervals. The enhanced intermediate water masses ventilation are associated with the increased benthic $\delta^{13}C$, depletion in $[CO_3^{2-}]$ and decreased B-P age offsets obtained from the same cores and occur during the same intervals. All of these changes could also provide strong evidence for the increased northward flow of AAIW during 16-15.2 cal kyr BP and 12.6-11 cal kyr BP intervals. In addition, the study of benthic foraminifera assemblages from core MD77-191 collected from the south tip of India have permitted to establish two main assemblage characterized mainly by *B. aculeata, C. pachyderma, Pullenia bulloides* and *Ehrenbergina trigona* for assemblage 1 and *H. elegans, Bulimina manginata C. wuellerstorfi* and *Globocassidulina subglobosa* for assemblage 2. Benthic foramnifera assemblages are broadly in agreement with the records of *G. bulloides* relative abundance (Bassinot et al., 2011) and intermediate Cd_w obtained from the same core, which could reflect the changes in the surface productivity since the 17 cal kyr BP. The benthic foraminiferal assemblage analysis indicates that assemblage 2 (during 17-6 cal kyr BP interval) reflects a high bottom water oxygen conditions and a low flux of organic matter, corresponding to a poor productivity. The late Holocene assemblage indicates relatively low-oxygen level and meso- to eutrophic deep water conditions compared with assemblage 2 during 17-6 cal kyr BP interval, and associated with high surface productivity during the late Holocene.

In the eastern Equatorial Indian Ocean, the age model of core SHI9001 was based on the correlation between the $\delta^{18}O$ record obtained on benthic foraminifera (*C. wuellerstorfi*) with a reference record (LR04 benthic stack, Lisieki and Raymo, 2005). Core SHI9001 spans the last 685 kyr, reaching Marine Isotope Stage (MIS) 17. The bottom water temperature calculated from the *U. peregrina* Mg/Li calculation is in good agreement with the calculations from the Mg/Ca ratio of *H.*

elegans, ranging from 4.29 to 9.9°C. The trends of bottom water temperature are in agreement with the glacial-interglacial variability, suggesting colder water masses during glacial periods compared to interglacial ones. The Sr/Ca, Cd/Ca and Ba/Ca ratios from *U. peregrina*, as well as the Cd/Ba and the Ba/Ca from *H. elegans* tend to exhibit opposite variations to the $\delta^{13}C$ record obtained on *C. wuellerstorfi*, which may indicate changes in the water source, with a varying contribution from water masses from the Southern Ocean. In addition, the Li/Ca and the U/Ca records of *H. elegans* display an abrupt opposite variation at around 400 kyr, that does not seem to mirror the glacial-interglacial variability nor the long-term trends described in the $\delta^{13}C$ record. All these records could indicate a strong change in the ocean Carbon cycle at intermediate water depths, which could be in relation with the global C change recorded in the $\delta^{13}C$. Further work will help to decipher between these different mechanisms.

All the records obtained during this study provide a better understanding of the temporal evolution of the source and ventilation of intermediate water masses in the northern Indian Ocean and their relationships with the other ocean basins and the global C cycle. The main results are:

(1). During the LGM, Southern Sourced Water (SSW) masses were dominant in the north Indian Ocean, and characterized by low oxygen concentration and/or meso- to eutrophic deep water conditions.

(2). During the last deglaciation, increased northward flow of AAIW in the north Indian Ocean were highlighted, associated to the enhanced upwelling in the Southern Ocean. In addition, the geochemical records also provide strong evidence that enhanced Southern Ocean ventilation could play an important role in a two-step rapid increase of atmospheric CO_2 during the 18-14.7 and 12.8-11.7 cal kyr BP time intervals.

(3). During the Holocene, the hydrology of the northern Indian Ocean is characterized by a progressive increase influence of NADW. In addition, the enhanced surface productivity occurs during the late Holocene (5.2-2.4 cal kyr BP), by contrast, the early-mid Holocene (10-6 cal kyr BP) display a poor surface productivity induced by a greater stratification of the upper water column link to intensified Indian summer monsoon condition (and associated increase of Asian rivers freshwater discharge).

(4). At a longer timescale, the connection between the Indian Ocean and the Southern Ocean, with the related consequences on the global Carbon cycle, have also been pointed out although further investigations have to be performed to better understand these processes.

To go further in the reconstruction of past changes in the intermediate water circulation and the understanding of the relationships between the Indian Ocean, the Southern Ocean and the C exchanges, the following points could be developed:

(1). For core SHI9001 collected from the eastern equatorial Indian Ocean, the age spans the last

685 kyr, and could reach Marine Isotope Stage MIS 17. Thus, the geochemical records show glacial-interglacial variability and/or the long-term trends, and which are quite different from the climate changes from two cores in the north Indian Ocean (MD77-191 and MD77-176, since the LGM). Thus, further study to develop the interpretation of the results of trace elemental ratios that will be help us understand the evolution of the source and ventilation of intermediate water masses in the eastern equatorial Indian Ocean, as well as global Carbon cycle during the glacial-interglacial periods. In addition, a more detailed stratigraphic structure of core SHI9001 will be necessary improved by higher resolution in sampling, and could also performed the planktonic foraminiferal oxygen isotope analysis as glacial-interglacial variability range should be easily recognized compared with benthic foraminifera.

(2). As the weights of the bulk samples of cores MD77-176 (northeastern Bay of Bengal) and MD77-191 (southeastern Arabian Sea) were missing, these methods were not fully interpreted. For example, the abundance of foraminifera could not be calculated, thus the accumulation rate for the benthic foraminifera (BFAR) and the species (AR) also could not be used for these two cores. However, BFAR and AR seem to directly reflect the organic matter flux rates (e.g., Schmiedl and Mackensen, 1997; Murgese and De Deckker, 2007). For core SHI9001, the primary data about sampling and sieving of foraminiferal samples (weight of the bulk and dry foraminiferal samples) are available. Thus, in the future, we could be able to perform more calculations for the benthic foraminifera. In addition, performing on core SHI9001 the benthic assemblage analysis, and combined with the benthic geochemical proxies records (oxygen and carbon isotopes, trace elemental ratios), could help us get more information about the bottom water condition variations and better constrain the paleoceanographic evolution (like oxygen, nutrient, …) at a longer timescale.

(3). Records of multiply geochemical proxies in the northern Indian Ocean all indicate that enhanced upwelling in the Southern Ocean leads to strong northward flow of AAIW, and could also associated to the two-step rapid increase of CO_2 during the last deglaciation. It will be quite interesting to modeling changes in the strength of the AAIW and the impact on the Carbon ocean pool and the air-sea Carbon exchanges in the future.

References

Ahmad, S. M., Babu, A. G., Padmakumari, V. M., Raza, W., 2008. Surface and deep water changes in the northeast Indian Ocean during the last 60 ka inferred from carbon and oxygen isotopes of planktonic and benthic foraminifera. Palaeogeography, Palaeoclimatology, Palaeoecology 262 (3), 182-188.

Ahmad, S. M., Zheng, H., Raza, W., Zhou, B., Lone, M. A., Raza, T., Suseela, G., 2012. Glacial to holocene changes in the surface and deep waters of the northeast Indian Ocean. Marine Geology 329-331, 16-23.

Alagarsamy, R., Zhang, J., Comparative studies on trace metal geochemistry in Indian and Chinese rivers. 2005; Vol. 89.

Almogi-Labin, A., Schmiedl, G., Hemleben, C., Siman-Tov, R., Segl, M., Meischner, D., 2000. The influence of the NE winter monsoon on productivity changes in the Gulf of Aden, NW Arabian Sea, during the last 530 ka as recorded by foraminifera. Marine Micropaleontology 40 (3), 295-319.

Altenbach, A. V., Pflaumann, U., Schiebel, R., Thies, A., Timm, S., Trauth, M., 1999. Scaling percentages and distributional patterns of benthic foraminifera with flux rates of organic carbon. Journal of Foraminiferal Research 29 (3), 173-185.

Anderson, R. F., Ali, S., ., Bradtmiller, L. I., Nielsen, S. H. H., Fleisher, M. Q., Anderson, B. E., Burckle, L. H., 2009. Wind-driven upwelling in the Southern Ocean and the deglacial rise in atmospheric CO_2. Science 323 (5920), 1443-1448.

Andrews, J. T. S., Abrupt changes (Heinrich Events) in late Quaternary north Atlantic marine environments. 1998; Vol. 13.

Barbero, L., González-Dávila, M., Santana-Casiano, J. M., Álvarez, M., 2010. Variability of the water mass transports and fluxes in the eastern north Atlantic during 2001. Journal of Geophysical Research: Oceans 115 (C3), 1-11.

Barker, S., Greaves, M., Elderfield, H., 2003. A study of cleaning procedures used for foraminiferal Mg/Ca paleothermometry. Geochemistry Geophysics Geosystems 4 (9), 1-20.

Barker, S., Knorr, G., Edwards, R. L., Parrenin, F., Putnam, A. E., Skinner, L. C., Eric, W., Martin, Z., 2011. 800,000 years of abrupt climate variability. Science 334 (6054), 347-51.

Bashmachnikov, I., Nascimento, Â., Neves, F., Menezes, T., Koldunov, N. V., 2015. Distribution of

intermediate water masses in the subtropical northeast Atlantic. Ocean Sci. 11 (5), 803-827.

Barnes, C. E., and Cochran, J. K., 1990. Uranium removal in oceanic sediments and the oceanic U balance, Earth Planet. Sci. Lett., 97, 94–101.

Banse, K., 1987. Seasonality of phytoplankton chlorophyll in the central and northern Arabian Sea. Deep Sea Research Part A Oceanographic Research Papers 34 (5), 713-723.

Barrientos, A., Lear, C. H., Jakobsson, M., Stranne, C., O'Regan, M., Cronin, T. M., Gukov, A. Y., Coxall, H. K., 2018. Arctic Ocean benthic foraminifera Mg/Ca ratios and global Mg/Ca-temperature calibrations: New constraints at low temperatures. Geochimica et Cosmochimica Acta 236, 240-259.

Bassinot, F. C., Marzin, C., Braconnot, P., Marti, O., Mathienblard, E., Lombard, F., Bopp, L., 2011. Holocene evolution of summer winds and marine productivity in the tropical Indian Ocean in response to insolation forcing: Data-model comparison. Climate of the Past 7 (3), 815-829.

Bauska, T. K., Baggenstos, D., Brook, E. J., et al., 2016. Carbon isotopes characterize rapid changes in atmospheric carbon dioxide during the last Deglaciation. Proceedings of the National Academy of Sciences, 113(13), 3465-3470.

Beal, L. M., Ffield, A., Gordon, A. L., 2000. Spreading of Red Sea overflow waters in the Indian Ocean. Journal of Geophysical Research: Oceans 105 (C4), 8549-8564.

Behrenfeld, M. J., Falkowski, P. G., 1997. Photosynthetic rates derived from satellite-based chlorophyll concentration. Limnology and Oceanography 42 (1), 1-20.

Berger, W. H., Keir, R. S., 2013. Glacial-holocene changes in atmospheric CO_2 and the deep-sea record. In Climate Processes and Climate Sensitivity (eds J. E. Hansen and T. Takahashi). doi:10.1029/GM029p0337.

Böhm, E., Lippold, J., Gutjahr, M., Frank, M., Blaser, P., Antz, B., Fohlmeister, J., Frank, N., Andersen, M. B., Deininger, M., 2015. Strong and Deep Atlantic Meridional Overturning circulation during the last glacial cycle. Nature 517, 73.

Bond, G., Broecker, W., Johnsen, S., McManus, J., Labeyrie, L., Jouzel, J., Bonani, G., Correlations between climate records from north Atlantic sediments and Greenland ice. 1993; Vol. 365, p 143-147.

Bond, G., Showers, W., Cheseby, M., Lotti, R., Almasi, P., deMenocal, P., Priore, P., Cullen, H., Hajdas, I., Bonani, G., 1997. A pervasive millennial-scale cycle in orth Atlantic Holocene and glacial climates. Science 278 (5341), 1257-1266.

Bostock, H. C., Opdyke, B. N., Williams, M. J. M., 2010. Characterising the intermediate depth waters of the Pacific Ocean using $\delta^{13}C$ and other geochemical tracers. Deep Sea Research Part I: Oceanographic Research Papers 57 (7), 847-859.

Boyle, E. A., 1983. Manganese carbonate overgrowths on foraminifera tests. Geochim. Cosmochim. Acta 63 (18), 353-353.

Boyle, E. A., 1992. Cadmium and $\delta^{13}C$ paleochemical ocean distributions during the stage 2 Glacial Maximum. Annual Review of Earth and Planetary Sciences 20 (1), 245-287.

Boyle, E. A., 1988. Cadmium: Chemical tracer of deepwater paleoceanography. Paleoceanography 3 (4), 471-489.

Boyle, E. A., Keigwin, L. D., 1982. Deep circulation of the North Atlantic over the last 200,000 years: Geochemical evidence. Science 218 (4574), 784-787.

Boyle, E. A., Keigwin, L. D., 1985. Comparison of Atlantic and Pacific paleochemical records for the last 215,000 years: Changes in deep ocean circulation and chemical inventories. Earth and Planetary Science Letters 76 (1), 135-150.

Boyle, E. A., Labeyrie, L., Duplessly, J.-C., 1995. Calcitic foraminiferal data confirmed by Cadmium in aragonitic *Hoeglundina*: Application to the Last Glacial Maximum in the northern Indian Ocean. Paleoceanography 10 (5), 881-900.

Boyle, E. A., Sclater, F., Edmond, J. M., 1976. On the marine geochemistry of Cadmium. Nature 263 (5572), 42-44.

Broecker, W. S., Peng, T.-H., 1984. Tracers in the sea. Published by Lamont-Doherty Geological Observatory, Eldigio Press, Columbia University, New York, 10964.

Brovkin, V., Ganopolski, A., Archer, D., Rahmstorf, S., 2007. Lowering of glacial atmospheric CO_2 in response to changes in oceanic circulation and marine biogeochemistry. Paleoceanography 22 (4), 1-14.

Brown, R. E., Anderson, L. D., Thomas, E., Zachos, J. C., 2011. A core-top calibration of B/Ca in the benthic foraminifers *Nuttallides umbonifera* and *Oridorsalis umbonatus*: A proxy for Cenozoic bottom water carbonate saturation. Earth and Planetary Science Letters 310 (3), 360-368

Bryan, S. P., Marchitto, T. M., 2008. Mg/Ca–temperature proxy in benthic foraminifera: New calibrations from the Florida Straits and a hypothesis regarding Mg/Li. Paleoceanography 23 (PA2220), 1-17.

Bryan, S. P., Marchitto, T. M., 2010. Testing the utility of paleonutrient proxies Cd/Ca and Zn/Ca in benthic foraminifera from thermocline waters. Geochemistry, Geophysics, Geosystems 11 (1).

Bryan, S. P., Marchitto, T. M., Lehman, S. J., 2010. The release of ^{14}C-depleted carbon from the deep ocean during the last Deglaciation: Evidence from the Arabian Sea. Earth and Planetary Science Letters 298 (1), 244-254.

Burton, K.W., and Vance, D. (2000). Glacial–interglacial variations in the neodymium isotope composition of seawater in the Bay of Bengal recorded by planktonic foraminifera. Earth and Planetary Science Letters 176 (3), 425-441.

Burke, S. K., Berger, W. H., Coulbourn, W. T., Vincent, E., 1993. Benthic foraminifera in box core ERDC 112, Ontong Java Plateau. Journal of Foraminiferal Research 23 (1), 19-39.

Calvert, S.E., Pedersen, T.F., Naidu, P.D., von Stackelberg, U., 1995. On the organic carbon maximum on the continental slope of the eastern Arabian Sea. J. Mar. Res. 53, 269-296.

Came, R. E., Oppo, D. W., Curry, W. B., Lynch-Stieglitz, J., 2008. Deglacial variability in the surface return flow of the Atlantic Meridional Overturning Circulation. Paleoceanography 23 (1).

Canfield, D.E., 1994. Factors influencing organic carbon preservation inmarine sediments. Chem. Geol. 114, 315–329.

Cao, L., Fairbanks, R. G., Mortlock, R. A., Risk, M. J., 2007. Radiocarbon reservoir age of high latitude north Atlantic surface water during the last deglacial. Quaternary Science Reviews 26 (5), 732-742.

Caulle, C., Mojtahid, M., Gooday, A. J., Jorissen, F. J., Kitazato, H., 2015. Living (rose-bengal-stained) benthic foraminiferal faunas along a strong bottom-water oxygen gradient on the Indian margin (Arabian Sea). Biogeosciences 12 (16), 5005-5019.

Chan, L. H., Drummond, D., Edmond, J. M., Grant, B., 1977. On the Barium data from the Atlantic geosecs expedition. Deep Sea Research 24 (7), 613-649.

Chandramohan, T., Balchand, A., Regional sediment yield pattern for the west flowing rivers of kerala state India. 2007; Vol. 54, p 501-511.

Collison, P. M., Vertical distribution of foraminifera off the coast of northumberland, england. 1980; Vol. 10, p 75-78.

Contreras-Rosales, L.A., Jennerjahn, T., Tharammal, T., Meyer, V., Lückge, A., Paul, A., Schefuß, E., 2014. Evolution of the Indian Summer Monsoon and terrestrial vegetation in the Bengal region during the past 18 ka. Quaternary Science Reviews 102, 133-148.

Corliss, B. H., 1979. Recent deep-sea benthonic for aminiferal distributions in the southeast Indian

Ocean: Inferred bottom-water routes and ecological implications. Marine Geology 31 (1-2), 115-138.

Corliss, B. H., 1985. Microhabitats of benthic foraminifera within deep-sea sediments. Nature 314, 435.

Corliss, B. H., Martinson, D. G., Keffer, T., 1986. Late Quaternary deep-ocean circulation. GSA Bulletin 97 (9), 1106-1121.

Cuffey, K.M., Clow, G.D., Steig, E.J., Buizert, C., Fudge, T.J., Koutnik, M., Waddington, E.D., Alley, R.B., and Severinghaus, J.P. (2016). Deglacial temperature history of west Antarctica. Proceedings of the National Academy of Sciences 113 (50), 14249-14254.

Curray, J. R., Moore, D. G., Growth of the Bengal deep-sea Fan and denudation in the Himalayas. 1971; Vol. 82.

Curry, W. B., Duplessy, J. C., Labeyrie, L. D., Shackleton, N. J., 1988. Changes in the distribution of $\delta^{13}C$ of deep water σCO_2 between the last glaciation and the Holocene. Paleoceanography 3 (3), 317-341.

Curry, W. B., Ostermann, D. R., Guptha, M. V. S., Ittekkot, V., 1992. Foraminiferal production and monsoonal upwelling in the Arabian Sea: evidence from sediment traps. Geological Society, London, Special Publications, 64, 93-106.

Dansgaard, W., Johnsen, S. J., Clausen, H. B., Dahl-Jensen, D., Gundestrup, N. S., Hammer, C. U., Hvidberg, C. S., Steffensen, J. P., Sveinbjörnsdottir, A. E., Jouzel, J., Bond, G., 1993. Evidence for general instability of past climate from a 250-kyr ice-core record. Nature 364, 218.

De Deckker, P., Gingele, F. X., 2002. On the occurrence of the giant diatom ethmodiscus rex in an 80-ka record from a deep-sea core, southeast of Sumatra, Indonesia: Implications for tropical palaeoceanography. Marine Geology 183 (1), 31-43.

De Pol-Holz, R., Keigwin, L., Southon, J., Hebbeln, D., Mohtadi, M., 2010. No signature of abyssal carbon in intermediate waters off Chile during Deglaciation. Nature Geoscience 3, 192.

De, S., and Gupta, A.K. (2010). Deep-sea faunal provinces and their inferred environments in the Indian Ocean based on distribution of recent benthic foraminifera. Palaeogeography, Palaeoclimatology, Palaeoecology 291 (3), 429-442.

Deschamps, P., Durand, N., Bard, E., Hamelin, B., Camoin, G., Thomas, A.L., Henderson, G.M., Okuno, J. and Yokoyama Y., 2012. Ice-sheet collapse and sea-level rise at the Bolling Warming 14600 years ago. Nature, 483, 559-564.

De Villiers, S., Greaves, M., Elderfield, H., 2002. An intensity ratio calibration method for the

accurate determination of Mg/Ca and Sr/Ca of marine carbonates by ICP-AES. Geochemistry Geophysics Geosystems 3,

Den Dulk, M., Reichart, G. J., Memon, G. M., Roelofs, E. M. P., Zachariasse, W. J., Zwaan, G. J. V. D., 1998. Benthic foraminiferal response to variations in surface water productivity and oxygenation in the northern Arabian Sea. Marine Micropaleontology 35 (1–2), 43-66.

Doss, W., Marchitto, T. M., Eagle, R., Rashid, H., Tripati, A., 2018. Deconvolving the saturation state and temperature controls on benthic foraminiferal Li/Ca, based on downcore paired B/Ca measurements and coretop compilation. Geochimica Et Cosmochimica Acta 236, 297-314.

Dubois-Dauphin, Q., Bonneau, L., Colin, C., Montero-Serrano, J.-C., Montagna, P., Blamart, D., Hebbeln, D., Van Rooij, D., Pons-Branchu, E., Hemsing, F., Wefing, A.-M., Frank, N., 2016. South atlantic intermediate water advances into the north-east Atlantic with reduced Atlantic Meridional Overturning circulation during the last glacial period. Geochemistry, Geophysics, Geosystems 17 (6), 2336-2353.

Duplessy, J. C., Shackleton, N. J., Fairbanks, R. G., Labeyrie, L., Oppo, D., Kallel, N., Deepwater source variations during the last climatic cycle and their impact on the global deepwater circulation. 1988; Vol. 3, p 343-360.

Duplessy, J.-C., Shackleton, N. J., Matthews, R. K., Prell, W., Ruddiman, W. F., Caralp, M., Hendy, C. H., 1984. ^{13}C record of benthic foraminifera in the last interglacial ocean: Implications for the carbon cycle and the global deep water circulation. Quaternary Research 21 (2), 225-243.

Elderfield, H., Greaves, M., Barker, S., Hall, I. R., Tripati, A., Ferretti, P., Crowhurst, S., Booth, L., Daunt, C., 2010. A record of bottom water temperature and seawater $\delta^{18}O$ for the Southern Ocean over the past 440 kyr based on Mg/Ca of benthic foraminiferal *Uvigerina* spp. Quaternary Science Reviews 29 (1), 160-169.

Elderfield, H., Rickaby, R. E. M., 2000. Oceanic Cd/P ratio and nutrient utilization in the glacial Southern Ocean. Nature 405 (6784), 305-310.

Elderfield, H., Yu, J., Anand, P., Kiefer, T., Nyland, B., 2006. Calibrations for benthic foraminiferal Mg/Ca paleothermometry and the carbonate ion hypothesis. Earth and Planetary Science Letters 250 (3), 633-649.

EPICA, C.M. (2006). One-to-one coupling of glacial climate variability in Greenland and Antarctica. Nature 444, 195.

Escalante, A. A., Ayala, F. J., 1996. Molecular paleogenetics: The evolutionary history of plasmodium and related protists. In: Jablonski, D., Erwin, D. H., Lipps, J. H. Eds., Evolutionary

Paleobiology. The University of Chigago Press, Chicago, pp. 21–41.

Fairbanks, R.G., Mortlock, R.A., Chiu, T., Cao, L., Kaplan, A., Guilderson, T.P., Fairbanks, T.W., Bloom, A.L., Grootes, P.M., Nadeau, M., (2005). Radiocarbon calibrationcurve spanning 0 to 50000 years BP based on paired $^{230}Th/^{234}U/^{238}U$ and ^{14}C dates on pristine corals. Quat. Sci. Rev. 24, 1781–1796.

Fontanier, C., Jorissen, F. J., Licari, L., Alexandre, A., Anschutz, P., Carbonel, P., 2002. Live benthic foraminiferal faunas from the Bay of Biscay: Faunal density, composition, and microhabitats. Deep Sea Research Part I: Oceanographic Research Papers 49 (4), 751-785.

Gingele, F. X., Deckker, P. D., Girault, A., Guichard, F., 2002. History of the south Java current over the past 80 ka. Palaeogeography Palaeoclimatology Palaeoecology 183 (3), 247-260.

Gordon, A. L., Ma, S., Olson, D. B., Hacker, P., Ffield, A., Talley, L. D., Wilson, D., Baringer, M., 1997. Advection and diffusion of Indonesian Throughflow Water within the Indian Ocean South Equatorial Current. Geophysical Research Letters 24 (21), 2573-2576.

Gomes, H., Goes, J., Saino, T., 2000. Influence of physical processes and freshwater discharge on the seasonality of phytoplankton regime in the Bay of Bengal. Continental Shelf Research 20, 313-330.

Gooday, A. J., 2003. Benthic foraminifera (protista) as tools in deep-water palaeoceanography: Environmental influences on faunal characteristics. Advances in Marine Biology 46, 1-90.

Green, D. R. H., Cooper, M. J., German, C. R., Wilson, P. A., 2013. Optimization of an inductively coupled plasma-optical emission spectrometry method for the rapid determination of high-precision Mg/Ca and Sr/Ca in foraminiferal calcite. Geochemistry Geophysics Geosystems 4 (6), 1-11.

Grootes, P. M., Stuiver, M., 1997. Oxygen 18/16 variability in greenland snow and ice with 10^{-3}- to 10^{5}-year time resolution. Journal of Geophysical Research Oceans 102 (C12), 26455-26470.

Gu, S., Liu, Z., Zhang, J., Rempfer, J., Joos, F., Oppo, D.W., 2017. Coherent response of Antarctic Intermediate Water and Atlantic Meridional Overturning during the last deglaciation: Reconciling contrasting Neodymium isotope reconstructions from the tropical Atlantic. Paleoceanography, 32, 1036-1053.

Gupta, S. B. K., 1999. Introduction to modern foraminifera. in Sen Gupta B. K., Ed., Modern Foraminifera, Kluwer, Dordrecht, pp. 3-6.

Gupta, A. K., Anderson, D. M., Overpeck, J. T., 2003. Abrupt changes in the Asian Southwest Monsoon during the Holocene and their links to the North Atlantic Ocean. Nature 421 (6921),

354-357.

Hall, J., Chan, L. H., 2004. Ba/Ca in benthic foraminifera: Thermocline and middepth circulation in the north Atlantic during the last glaciation. Paleoceanography 19 (PA4018), 1-13.

Hall, J.M., Chan, L.-H., 2004. Li/Ca in multiple species of benthic and plaktonic foraminifera: thermocline, latitudinal, and glacial-interglacial variation. Geochimica et Cosmochimica Acta, 68(3), 529-545.

Hammer, Ø., Harper, D. A. T., Ryan, P. D., 2001. Past: Paleontological statistics software package for education and data analysis.

Hendry, K.R., Robinson, L.F., Meredith, M.P., Mulitza, S., Chiessi, C.M., Arz, H., 2012. Abrupt changes in high-latitude nutrient supply to the Atlantic during the last glacial cycle. Geology 40, 123–126.

Hermelin, J. O. R., 1991. Relative abundances of benthic foraminifera in ODP hole 117-728A, PANGAEA.

Hermelin, J. O. R., 1992. Variations in the benthic foraminiferal fauna of the Arabian Sea: A response to changes in upwelling intensity? Geological Society, London, Special Publications 64, 151-166.

Hermelin, J. O. R., Shimmield, G. B., 1995. Impact of productivity events on the benthic foraminiferal fauna in the Arabian Sea over the last 150,000 years. Paleoceanography 10 (1), 85-116.

Hester, K., Boyle, E., 1982. Water chemistry control of Cadmium content in recent benthic foraminifera. Nature 298, 260-262.

Holbourn, A., Kuhnt, W., Kawamura, H., Jian, Z., Grootes, P., Erlenkeuser, H., Jian, X., 2005. Orbitally paced paleoproductivity variations in the Timor Sea and Indonesian Throughflow variability during the last 460 kyr. Paleoceanography 20 (3).

Holbourn, A., Henderson, A. S., Macleod, N., 2013; Front matter. In Atlas of benthic foraminifera, pp. 1-641.

Holligan, P. M., Robertson, J. E., 1996. Significance of ocean carbonate budgets for the global carbon cycle. Global Change Biology 2 (2), 85-95.

Hoogakker, B. A. A., Rohling, E. J., Palmer, M. R., Tyrrell, T., Rothwell, R. G., 2006. Underlying causes for long-term global ocean $\delta^{13}C$ fluctuations over the last 1.20 myr. Earth and Planetary Science Letters 248 (1), 15-29.

Howe, J. N. W., Piotrowski, A. M., Oppo, D. W., Huang, K. F., Mulitza, S., Chiessi, C. M., and Blusztajn, J., 2016. Antarctic intermediate water circulation in the South Atlantic over the past 25,000 years. Paleoceanography, 31(10), 1302-1314.

IPCC, 2013. Climate change 2013 : The physical science basis summary for policymakers. Intergovernmental Panel on Climate Change.

Jian, Z., Wang, L., 1997. Late quaternary benthic foraminifera and deep-water paleoceanography in the South China Sea. Marine Micropaleontology 32 (1), 127-154.

Johnsen, S. J., Dansgaard, W., Clausen, H. B., Langway, C. C., 1972. Oxygen isotope profiles through the Antarctic and Greenland ice sheets. Nature 235 (5339), 429-434.

Jones, R. W., The challenger foraminifera. Oxford University Press: 1994; p. 149. 37.

Jorissen, F. J., 1999; Benthic foraminiferal microhabitats below the sediment-water interface. In: Sen gupta, b.K. , ed., modern foraminifera. Dordrecht: Kluwer, pp. 161-179.

Jorissen, F. J., Fontanier, C., Thomas, E., Chapter seven paleoceanographical proxies based on deep-sea benthic foraminiferal assemblage characteristics. Elsevier Science and Technology: 2007.

Jorissen, F. J., Wittling, I., Peypouquet, J. P., Rabouille, C., Relexans, J. C., 1998. Live benthic foraminiferal faunas off cape blanc, NW-africa: Community structure and microhabitats. Deep Sea Research Part I Oceanographic Research Papers 45 (12), 0-2188.

Jung, S. J. A., Kroon, D., Ganssen, G., Peeters, F., Ganeshram, R., 2009. Enhanced Arabian Sea intermediate water flow during glacial north Atlantic cold phases. Earth and Planetary Science Letters 280 (1), 220-228.

Kallel, N., Labeyrie, L. D., Juillet-Leclerc, A., Duplessy, J.-C., 1988. A deep hydrological front between intermediate and deep-wafpr , masses in the glacial indian ocean. Nature 333, 651.

Katz, M., Cramer, B., Franzese, A., Honisch, B., Miller, K., Rosenthal, Y., Wright, J., 2010. Traditional and emerging geochemical proxies in foraminifera. Journal of Foraminiferal Research 40 (2), 165-192.

Keul, N., Langer, G., Nooijer, L. J. D., Nehrke, G., Reichart, G. J., Bijma, J., 2013. Incorporation of uranium in benthic foraminiferal calcite reflects seawater carbonate ion concentration. Geochemistry Geophysics Geosystems 14 (1), 102-111.

Key, R. M., Kozyr, A., Sabine, C. L., Lee, V., Wanninkhof, R., Bullister, J. L., Feely, R. A., Millero, F. J., Mordy, C., Peng, T.-H., 2004. A global ocean carbon climatology: Results from global data

analysis project (glodap). Glob Biogeochem. Cy 18 (GB4031), 1-23.

Khatiwala, S., Primeau, F., Holzer, M., 2012. Ventilation of the deep ocean constrained with tracer observations and implications for radiocarbon estimates of ideal mean age. Earth and Planetary Science Letters 325-326 (4), 116-125.

Kohfeld, K.E., Quéré, C.L., Harrison, S.P., Anderson, R.F., 2005. Role of marine biology in Glacial-interglacial CO2 cycles. Science 308, 74.

Kolla, V., Moore, D. G., Curray, J. R., 1976. Recent bottom-current activity in the deep western Bay of Bengal. Marine Geology 21, 255-270.

Lea, D. W., Boyle, E., 1989. Barium content of benthic foraminifera controlled by bottom-water composition. Nature 338 (338), 751-753.

Lea, D. W., Boyle, E., 1990. Foraminiferal reconstitution of Barium distribution in water masses of the glacial oceans. Paleoceanography 5 (5), 719-742.

Lear, C. H., Mawbey, E. M., Rosenthal, Y., 2010. Cenozoic benthic foraminiferal Mg/Ca and Li/Ca records: Toward unlocking temperatures and saturation states. Paleoceanography 25 (4), 1-11.

Lear, C. H., Rosenthal, Y., Slowey, N., 2002. Benthic foraminiferal Mg/Ca-paleothermometry: A revised core-top calibration. Geochimica Et Cosmochimica Acta 66 (19), 3375-3387.

Lear, C. H., Rosenthal, Y., 2006. Benthic foraminiferal Li/Ca: insights into Cenozoic seawater carbonate saturation state. Geology, 34, 985-988.

Lévy, M., Shankar, D., André, J.-M., Shenoi, S., Durand, F., De Boyer Montegut, C., 2007. Basin-wide seasonal evolution of the Indian Ocean's phytoplankton blooms. Journal of Geophysical Research 112 (C12014), 1-14.

Lisiecki, L., Raymo, M., 2005. A pliocene-pleistocene stack of 57 globally distributed benthic 18o records. Paleoceanography 20 (PA1003,), 1-17.

Locke, S., and Thunell, R.C. (1988). Paleoceanographic record of the last glacial/interglacial cycle in the Red Sea and Gulf of Aden. Palaeogeography, Palaeoclimatology, Palaeoecology 64 (3), 163-187.

Loeblich, A. R., Tappan, H., 1988; Generic taxa erroneously regarded as foraminifers. In Foraminiferal genera and their classification, Loeblich, A. R.; Tappan, H., Eds. Springer US: Boston, MA, pp. 726-730.

Lutze, G. F., Thiel, H., 1989. Epibenthic foraminifera from elevated microhabitats; *Cibicidoides wuellerstorfi* and *Planulina ariminensis*. J. Foraminiferal Res. 19 (2), 153-158.

Lüthi, D., Le Floch, M., Bereiter, B., Blunier, T., Barnola, J.-M., Siegenthaler, U., Raynaud, D., Jouzel, J., Fischer, H., Kawamura, K., 2008. High-resolution carbon dioxide concentration record 650,000-800,000 years before present. Nature 453 (7193), 379-82.

Lückge, A., Mohtadi, M., Rühlemann, C., Scheeder, G., Vink, A., Reinhardt, L., Wiedicke, M., 2009. Monsoon versus ocean circulation controls on paleoenvironmental conditions off southern Sumatra during the past 300,000 years. Paleoceanography 24 (1).

Lynch-Stieglitz, J., Adkins, J. F., Curry, W. B., Dokken, T., Hall, I. R., Herguera, J. C., Hirschi, J. J.-M., Ivanova, E. V., Kissel, C., Marchal, O., Marchitto, T. M., McCave, I. N., McManus, J. F., Mulitza, S., Ninnemann, U., Peeters, F., Yu, E.-F., Zahn, R., 2007. Atlantic Meridional Overturning Circulation during the Last Glacial Maximum. Science 316 (5821), 66-69.

Lynch-Stieglitz, J., Fairbanks, R. G., Charles, C. D., 1994. Glacial-interglacial history of Antarctic Intermediate Water: Relative strengths of Antarctic versus Indian Ocean sources. Paleoceanography 9 (1), 7-29.

Lynch-Stieglitz, J., S. Broecker, W., G. Fairbanks, R., The influence of air-sea exchange on the isotopic composition of oceanic carbon: Observations and modeling. 1995; Vol. 9, p 653-665.

Ma, R., Sépulcre, S., Licari, L., Bassinot, F., Liu, Z., Tisnérat-Laborde, N., Kallel, N., Yu, Z., Colin, C., 2019. Changes in intermediate circulation in the bay of bengal since the Last Glacial Maximum as inferred from benthic foraminifera assemblages and geochemical proxies. Geochemistry, Geophysics, Geosystems 20, 1-17.

Mackensen, A., Sejrup, H. P., Jansen, E., 1985. The distribution of living benthic foraminifera on the continental slope and rise off southwest Norway. Marine Micropaleontology 9 (4), 275-306.

Mackensen, A., Hubberten, H.W., Bickert, T., Fischer, G., and Fütterer, D.K., 1993. The $\delta^{13}C$ in benthic foraminiferal tests of *Fontbotia wuellerstorfi* (*schwager*) relative to the $\delta^{13}C$ of dissolved inorganic carbon in Southern Ocean Deep Water: Implications for glacial ocean circulation models. Paleoceanography 8 (5), 587-610.

Mackensen, A., Schmiedl, G., Harloff, J., Giese, M., 1995. Deep-sea foraminifera in the South Atlantic Ocean; ecology and assemblage generation. Micropaleontology 41 (4), 342-358.

Mackensen, A., Licari, L., 2004. Carbon isotopes of live benthic foraminifera from the south atlantic ocean: Sensitivity to bottom water carbonate saturation state and organic matter rain rates. In: Wefer, G., Mulitza, S., Rathmeyer, V. (Eds.), The South Atlantic in the Late Quaternary - Reconstruction of Material Budget and Current Systems, SpringerVerlag, Berlin, pp. 623-644.

Mackensen, A., Schumacher, S., Radke, J., Schmidt, D. N., 2000. Microhabitat preferences and stable carbon isotopes of endobenthic foraminifera: Clue to quantitative reconstruction of oceanic new production? Marine Micropaleontology 40 (3), 233-258.

Makou, M. C., Oppo, D. W., Curry, W. B., 2010. South atlantic intermediate water mass geometry for the Last Glacial Maximum from foraminiferal Cd/Ca. Paleoceanography 25 (PA4103), 1-7.

Mangini, A., Godoy, J. M., Godoy, M. L., Kowsmann, R., Santos, G. M., Ruckelshausen, M., Schroederritzrau, A., Wacker, L., 2010. Deep sea corals off brazil verify a poorly ventilated southern Pacific Ocean during H2, H1 and the Younger Dryas. Earth Planet. Sci. Lett. 293 (3-4), 269-276.

Makou, M. C., Oppo, D. W., Curry, W. B., 2010. South atlantic intermediate water mass geometry for the Last Glacial Maximum from foraminiferal Cd/Ca. Paleoceanography 25 (PA4103).

Marchitto, T. M., 2004. Lack of a significant temperature influence on the incorporation of Cd into benthic foraminiferal tests. Geochemistry, Geophysics, Geosystems 5.

Marchitto, T. M., Broecker, W. S., 2006. Deep water mass geometry in the glacial atlantic ocean: A review of constraints from the paleonutrient proxy Cd/Ca. Geochemistry, Geophysics, Geosystems 7.

Marchitto, C. S., Henderson, G. M., Crompoton, R., Staubwasser, M., Shaw, S., 2004. Effect of mineralogy, salinity and temperature on Li/Ca and Li isotope composition of Calcium carbonate. Chemical Geology, 212, 5-15.

Marchitto, T. M., Bryan, S. P., Curry, W. B., McCorkle, D. C., 2007. Mg/Ca temperature calibration for the benthic foraminifera *Cibicidoides pachyderma*. Paleoceanography 22, 1-9.

Marchitto, T. M., Bryan, S. P., Doss, W., Mcculloch, M., Montagna, P., 2018. A simple biomineralization model to explain Li, Mg, and Sr incorporation into aragonitic foraminifera and corals. Earth and Planetary Science Letters 481, 20-29.

Marchitto, T. M., Lehman, S. J., Ortiz, J. D., Jacqueline, F., Alexander, V. G., 2007. Marine radiocarbon evidence for the mechanism of deglacial atmospheric CO_2 rise. Science 316 (5830), 1456-1459.

Marra, J., Barber, R. T., 2005. Primary productivity in the Arabian Sea: A synthesis of JGOFS data. Progress in Oceanography 65 (2), 159-175.

Martin, P., Lea, D. W., 1998. Comparison of water mass changes in the deep tropical Atlantic derived from Cd/Ca and carbon isotope records: Implications for changing ba composition of deep Atlantic water masses. Paleoceanography 13 (6), 572-585.

Martin, P. A., Lea, D. W., Rosenthal, Y., Shackleton, N. J., Sarnthen, M., Papenfuss, T., (2002). Quaternary deep sea tempeature histories derived from benthic foraminiferal Mg/Ca. Earth Planet. Sci. Lett. 198, 193-209.

Martinez, J. I., De Deckker, P., Barrows, T. T., 1999. Palaeoceanography of the Last Glacial Maximum in the eastern Indian Ocean: Planktonic foraminiferal evidence. Palaeogeography Palaeoclimatology Palaeoecology 147 (1), 73-99.

Marzin, C., Kallel, N., Kageyama, M., Duplessy, J. C., Braconnot, P., 2013. Glacial fluctuations of the Indian Monsoon and their relationship with north Atlantic climate: New data and modelling experiments. Clim. Past 9 (5), 2135-2151.

Matsumoto, K., 2007. Radiocarbon-based circulation age of the world oceans. Journal of Geophysical Research 112 (C09004), 1-7.

Mazumder, A., Nigam, R., 2014. Bathymetric preference of fourmajor genera of rectilinear benthic foraminifera within oxygen minimum zone in Arabian Sea off central west coast of India. J. Earth Syst. Sci. 123, 633–639.

McCorkle, D. C., Corliss, B. H., Farnham, C. A., 1997. Vertical distributions and stable isotopic compositions of live (stained) benthic foraminifera from the north Carolina and California continental margins. Deep Sea Research Part I Oceanographic Research 44 (6), 983-1024.

McCorkle, D., Keigwin, L. D., 1990. The influence of microhabitats on the carbon isotopic composition of deep-sea benthic foraminifera. Paleoceanography 5 (2), 161-185.

McCorkle, D., Martin, P., W. Lea, D., P. Klinkhammer, G., 1995. Evidence of a dissolution effect on benthic foraminiferal shell chemistry: $\delta^{13}C$, Cd/Ca, Ba/Ca, and Sr/Ca results from the ontong Java Plateau. Paleoceanography 10 (4), 699-714.

McManus, J. F., Bond, G. C., Broecker, W. S., Johnsen, S., Labeyrie, L., Higgins, S., High-resolution climate records from the north Atlantic during the last interglacial. 1994; Vol. 371.

McManus, J. F., Francois, R., Gherardi, J. M., Keigwin, L. D., Brown-Leger, S., 2004. Collapse and rapid resumption of Atlantic Meridional circulation linked to deglacial climate changes. Nature 428, 834.

Menviel, L., Joos, F., 2012. Toward explaining the Holocene carbon dioxide and carbon isotope records: Results from transient ocean carbon cycle-climate simulations. Palaeogeogr. Palaeoclimatol. Palaeoecol. 27 (PA1207), 1-17.

Miao, Q., Thunell, R. C., 1993. Recent deep-sea benthic foraminiferal distributions in the South China and Sulu Seas. Marine Micropaleontology 22 (1), 1-32.

Milliman, J. D., Meade, R. H., World-wide delivery of river sediment to the oceans. 1983; Vol. 91, p 1-21.

Mix, A. C., Fairbanks, R. G., 1985. North Atlantic surface-ocean control of Pleistocene deep-ocean circulation. Earth and Planetary Science Letters 73 (2), 231-243.

Mix, A. C., Pisias, N. G., Zahn, R., Rugh, W., Lopez, C., Nelson, K., 1991. Carbon 13 in Pacific Deep and Intermediate waters, 0-370 ka: Implications for ocean circulation and Pleistocene CO_2. Paleoceanography 6 (2), 205-226.

Mléneck, V. M., 1997. S´edimentation et dissolution des carbonates biog´eniques aux moyennes latitudes nord et sud, approche quantitative et relations avec les pal´eocirculations oc´eaniques des derniers 150 000 ans. PhD thesis, Universit´e Bordeaux I, pp. 277.

Mohtadi, M., Lückge, A., Steinke, S., 2010. Late Pleistocene surface and thermocline conditions of the eastern tropical Indian Ocean. Quaternary Science Reviews 29 (7), 887-896.

Monnin, E., Indermühle, A., Dällenbach, A., Flückiger, J., Stauffer, B., Stocker, T. F., Raynaud, D., Barnola, J. M., 2001. Atmospheric CO_2 concentrations over the last glacial termination. Science 291 (5501), 112-114.

Mortyn, P., Martinez-Boti, M., Planktonic foraminifera and their proxies for the reconstruction of surface-ocean climate parameters. 2007.

Murgese, D. S., De Deckker, P., 2005. The distribution of deep-sea benthic foraminifera in core tops from the eastern Indian Ocean. Marine Micropaleontology 56 (1), 25-49.

Murgese, D.S., De Deckker, P., 2007. The late Quaternary evolution of water masses in the eastern Indian Ocean between Australia and Indonesia, based on benthic foraminifera faunal and carbon isotopes analyses. Palaeogeography, Palaeoclimatology, Palaeoecology 247 (3), 382-401.

Naqvi, W. A., Charles, C. D., Fairbanks, R. G., 1994. Carbon and oxygen isotopic records of benthic foraminifera from the northeast Indian Ocean: Implications on glacial-interglacial atmospheric CO_2 changes. Earth and Planetary Science Letters 121 (1), 99-110.

Naidu, P.D., Prakash Babu, C., Rao, C.M., 1992. The upwelling record in the sediments of the western continental margin of India. Deep-Sea Res. 39, 715–723.

Naidu, P.D., Malmgren, B.A., 1996. A high-resolution record of late Quaternary upwelling along the Oman margin, Arabian Sea based on planktonic foraminifera. Paleoceanography 11, 129–140.

Naik, D. K., Saraswat, R., Lea, D. W., Kurtarkar, S. R., Mackensen, A., 2017. Last glacial-interglacial productivity and associated changes in the eastern Arabian Sea. Palaeogeography, Palaeoclimatology, Palaeoecology 483, 147-156.

Naik, S.S., Basak, C., Goldstein, S.L., Naidu, P.D., and Naik, S.M. (2019). A 16 kyr record of ocean circulation and monsoon intensification from the central Bay of Bengal. Geochemistry, Geophysics, Geosystems, accepted.

Nigam, R.,Mazumder, A., Henriques, P.J., Saraswat, R., 2007. Benthic foraminifera as proxy for oxygen-depleted conditions off the central west coast of India. J. Geol. Soc. India 70, 1047–1054.

Ni Fhlaithearta, S., Reichart, G. J., Jorissen, F., Fontanier, C., Rohling, E. J., Thomson, J., de Lange, G., Reconstructing the seafloor environment during sapropel formation using benthic foraminiferal trace metals, stable isotopes, and sediment composition. 2010; Vol. 25.

Olson, D., L. Hitchcock, G., Fine, R., A. Warren, B., Maintenance of the low-oxygen layer in the central Arabian Sea. 1993; Vol. 40, p 673-685.

O'Malley, R., 2017. Ocean productivity. http://www.science.oregonstate.edu/ocean.Productivity/index.php.

Oppo, D. W., Fairbanks, R. G., 1987. Variability in the deep and intermediate water circulation of the Atlantic Ocean during the past 25,000 years: Northern hemisphere modulation of the Southern Ocean. Earth and Planetary Science Letters 86 (1), 1-15.

Pahnke, K., Goldstein, S. L., Hemming, S. R., 2008. Abrupt changes in Antarctic Intermediate Water circulation over the past 25,000 years. Nature Geoscience 1, 870.

Pahnke, K., Zahn, R., 2005. Southern hemisphere water mass conversion linked with North Atlantic climate variability. Science 307 (5716), 1741-1746.

Paillard, D., Labeyrie, L., Yiou, P., 1996. Macintosh program performs time-series analysis. Eos Transactions American Geophysical Union 77 (39), 379-379.

Pena, L. D., Goldstein, S. L., Hemming, S. R., Jones, K. M., Calvo, E., Pelejero, C., Cacho, I., 2013. Rapid changes in meridional advection of Southern Ocean intermediate waters to the tropical Pacific during the last 30kyr. Earth Planet. Sci. Lett. 368, 20-32.

Pérez, F. F., Mintrop, L., Llinás, O., Glez-Dávila, M., Castro, C. G., Alvarez, M., Körtzinger, A., Santana-Casiano, M., Rueda, M. J., Ríos, A. F., 2001. Mixing analysis of nutrients, oxygen and inorganic carbon in the canary islands region. Journal of Marine Systems 28 (3), 183-201.

Peterson, L. C., 1984. Recent abyssal benthic foraminiferal biofacies of the eastern equatorial Indian Ocean. Marine Micropaleontology 8 (6), 479-519.

Peterson, C.D., Lisiecki, L.E., and Stern, J.V. (2014), Deglacial whole-ocean $\delta^{13}C$ change estimated from 480 benthic foraminiferal records, Paleoceanography 29, 549-563.

Pelletier, G., Lewis, E., Wallace, D., 2005. A calculator for the CO_2 system in seawater for

microsoft excel/vba. Washington State Department of Ecology, Olympia, WA, Brookhaven National Laboratory Upton, NY.

Peltier, W.R., and Fairbanks, R.G. (2006). Global glacial ice volume and Last Glacial Maximum duration from an extended Barbados sea level record. Quat. Sci. Rev. 25, 3322–3337.

Poggemann, D. W., Hathorne, E. C., Nürnberg, D., Frank, M., Bruhn, I., Reißig, S., Bahr, A., 2017. Rapid deglacial injection of nutrients into the tropical Atlantic via Antarctic Intermediate Water. Earth and Planetary Science Letters 463, 118-126.

Poggemann, D.-W., Nürnberg, D., Hathorne, E. C., Frank, M., Rath, W., Reißig, S., Bahr, A., 2018. Deglacial heat uptake by the Southern Ocean and rapid northward redistribution via Antarctic Intermediate Water. Paleoceanography and Paleoclimatology 33 (11), 1292-1305.

Prasanna Kumar, S., Muraleedharan, P. M., Prasad, T. G., Gauns, M., Ramaiah, N., de Souza, S. N., Sardesai, S., Madhupratap, M., 2002. Why is the Bay of Bengal less productive during summer monsoon compared to the Arabian Sea? Geophysical Research Letters 29 (24), 88-1-88-4.

Prell, W. L., Kutzbach, J. L., 1987. Monsoon variability over the past 150,000 years. Journal of Geophysical Research Atmospheres 92 (D7), 8411-8425.

Quadfasel, D., Cresswell, G. R., 1992. A note on the seasonal variability of the south Java current. Journal of Geophysical Research Oceans 97 (C3), 3685-3688.

Rahmstorf, S., 1995. Bifurcations of the atlantic thermohaline circulation in response to changes in the hydrological cycle. Nature 378, 145.

Rahmstorf, S.: Thermohaline Ocean Circulation. In: Encyclopedia of Quaternary Sciences , Edited by S. A. Elias. Elsevier, Amsterdam, 2006.

Raitzsch, M., Kuhnert, H., Hathorne, E. C., Groeneveld, J., Bickert, T., 2011. U/Ca in benthic foraminifers: A proxy for the deep-sea carbonate saturation. Geochemistry, Geophysics, Geosystems 12 (6).

Ravichandran, M., Girishkumar, M. S., Riser, S., 2012. Observed variability of chlorophyll- a using argo profiling floats in the southeastern Arabian Sea. Deep-Sea Res. I 65 (65), 15-25.

Ramaswamy, V., Nair, R. R., Fluxes of material in the Arabian Sea and Bay of Bengal- sediment trap studies. 1994; Vol. 103, p 189-210.

Ramaswamy, V., Gaye, B., Shirodkar, P.V., Rao, P.S., Chivas, A.R., Wheeler, D., and Thwin, S. (2008). Distribution and sources of organic carbon, nitrogen and their isotopic signatures in sediments from the Ayeyarwady (Irrawaddy) continental shelf, northern Andaman Sea. Marine Chemistry 111, 137-150.

Rashid, H., Flower, B. P., Poore, R. Z., Quinn, T. M., 2007. A ~25 ka Indian Ocean Monsoon variability record from the Andaman Sea. Quaternary Science Reviews 26 (19), 2586-2597.

Raza, T., Ahmad, S. M., Sahoo, M., Banerjee, B., Bal, I., Dash, S., Suseela, G., Mukherjee, I., 2014. Hydrographic changes in the southern Bay of Bengal during the last ~65,000 y inferred from carbon and oxygen isotopes of foraminiferal fossil shells. Quaternary International 333, 77-85.

Reichart, G. J., Jorissen, F., Mason, P. R. D., Anschutz, P., 2003. Single foraminiferal test chemistry records the marine environment. Geology 31 (2003), 355-358.

Reid, J. L., 2003. On the total geostrophic circulation of the south Pacific Ocean: Flow patterns, tracers and transports. Progress in Oceanography 16 (1), 1-61.

Reimer P. J., Bard E., Bayliss A., Beck J. W., Blackwell P. G., Bronk Ramsey C., Buck C. E., Cheng H., Edwards R. L., Friedrich M., Grootes P. M., Guilderson T. P., Haflidason H., Hajdas I., Hatté C., Heaton T. J., Hogg A. G., Hughen K. A., Kaiser K. F., Kromer B., Manning S. W., Niu M., Reimer R. W., Richards D. A., Scott E. M., Southon J. R., Turney C. S. M., van der Plicht J., 2013. IntCal13 and Marine13 radiocarbon age calibration curves 0-50000 years cal BP. Radiocarbon 55(4).

Ribbe, J., 2001. Intermediate water mass production controlled by Southern Hemisphere winds. Geophys. Res. Lett. 28 (3), 535-538.

Ridgwell, A. J., Watson, A. J., Maslin, M. A., Kaplan, J. O., 2003. Implications of coral reef buildup for the controls on atmospheric CO_2 since the Last Glacial Maximum. Paleoceanography 18 (4), 1-10.

Ridgwell, A., Zeebe, R. E., 2005. The role of the global carbonate cycle in the regulation and evolution of the earth system [rapid communication]. Earth and Planetary Science Letters 234 (3), 299-315.

Roberts, N. L., Piotrowski, A. M., McManus, J. F., Keigwin, L. D., 2010. Synchronous deglacial overturning and water mass source changes. Science 327 (5961), 75-78.

Robinson, R. A. J., Bird, M., Oo, N. W., Hoey, T., Aye, M. M., Higgitt, D., Lu, X., Swe, A., Tun, T., Win, S. L., 2007. The Irrawaddy River sediment flux to the Indian Ocean: the original nineteenth- century data revisited. The Journal of Geology 115, 629-640.

Rosenthal, Y., Boyle, E. A., Slowey, N., 1997. Temperature control on the incorporation of Magnesium, Strontium, Fuorine, and Cadmium into benthic foraminiferal shells from little Bahama Bank: Prospects for thermocline paleoceanography. Geochim. Cosmochim. Acta 61 (17), 3633-3643.

Rosenthal, Y., Lear, C. H., Oppo, D. W., Linsley, B. K., 2006. Temperature and carbonate ion effects on Mg/Ca and sr/ca ratios in benthic foraminifera: Aragonitic species *Hoeglundina elegans*. Paleoceanography 21 (PA1007), 1-14.

Ruddiman, W. F., 2014. Earth's climate past present and future.

Russell, A. D., Hönisch, B., Spero, H. J., Lea, D. W., 2004. Effects of seawater carbonate ion concentration and temperature on shell U, Mg, and Sr in cultured planktonic foraminifera. Geochim. Cosmochim. Acta 68 (21), 4347-4361.

Sarin, M. M., Krishnaswami, S., Major ion chemistry of the Ganga–Brahmaputra river systems, india. 1984; Vol. 312, p 538-541.

Saraswat, R., Nigam, R., Correge, T., 2014. A glimpse of the Quaternary Monsoon history from India and Adjoining Seas. Palaeogeography, Palaeoclimatology, Palaeoecology 397, 1-6.

Sarkar, S., Prasad, S., Wilkes, H., Riedel, N., Stebich, M., Basavaiah, N., Sachse, D., 2015. Monsoon source shifts during the drying mid-Holocene: Biomarker isotope based evidence from the core 'monsoon zone'(CMZ) of India. Quaternary Science Reviews 123, 144-157.

Sarmiento, J. L., Gruber, N., Brzezinski, M. A., Dunne, J. P., 2004. High-latitude controls of thermocline nutrients and low latitude biological productivity. Nature 427, 56–60.

Schiller, A., Godfrey, J. S., McIntosh, P. C., Meyers, G., Wijffels, S. E., 1998. Seasonal near-surface dynamics and thermodynamics of the Indian Ocean and Indonesian Throughflow in a global ocean general circulation model. Journal of Physical Oceanography 28 (11), 2288-2312.

Schilman, B., Almogi-Labin, A., Bar-Matthews, M., Labeyrie, L., Paterne, M., Luz, B., Long and short-term carbon fluctuations in the eastern Mediterranean during the late Holocene. 2001; Vol. 29.

Schlitzer, R., 2015. Ocean data view. http://odv.awi.de.

Schmiedl, G., Hemleben, C., Keller, J., Segl, M., 1998. Impact of climatic changes on the benthic foraminiferal fauna in the Ionian Sea during the last 330,000 years. Paleoceanography 13 (5), 447-458.

Schmiedl, G., Mackensen, A., Multispecies stable isotopes of benthic foraminifers reveal past changes of organic matter decomposition and deepwater oxygenation in the Arabian Sea. 2006; Vol. 21.

Schmiedl, G., Mackensen, A., 1997. Late Quaternary paleoproductivity and deep water circulation in the eatern South Atlantic Ocean: evidence from benthic foramiknifera. Palaeogeogr.,

Palaeoclimatol., Palaeoecol. 130, 43-80.

Schnitker, D., 1994. Deep-sea benthic foraminifers: Food and bottom water masses. In: Zahn r., pedersen t.F., kaminski m.A., labeyrie l. (eds). Carbon cycling in the glacial ocean: Constraints on the ocean's role in global change. . NATO ASI Series (Series I: Global Environmental Change), vol 17. Springer, Berlin, Heidelberg.

Schott, F. A., McCreary, J. P., The monsoon circulation of the Indian Ocean. 2001; Vol. 51, p 1-123.

Schonfeld, J., 2001. Benthic foraminifera and pore-water oxygen profiles: A re-assessment of species boundary conditions at the western Iberian margin. Vol. 31, p 86-107.

Schrag, D. P., 1999. Rapid analysis of high-precision Sr/Ca ratios in corals and other marine carbonates. Paleoceanography 14 (2), 97-102.

Sengupta, D., Bharath Raj, G. N., Shenoi, S. S. C., Surface freshwater from Bay of Bengal runoff and Indonesian throughflow in the tropical Indian Ocean. 2006; Vol. 33.

Shackleton, N. J., Opdyke, N. D., 1973. Oxygen isotope and paleomangetic stratigraphy of equatorial pacific core v28-238:Oxygen isotope temperatures and ice volume on a 105 and 106 year scale. Quaternary Research 3 (1), 39-55.

Shackleton, N.J. (1974). Attainment of isotopic equilibrium between ocean water and benthonic foraminifera genus uvigerina: Isotopic changes in the ocean during the last glacial. Les méthodes quantitatives d'étude des variations du climat au cours du pleistocène, gif-sur-yvette. . Colloque international du CNRS 219, 203-210.

Shankar, D., Vinayachandran, P. N., Unnikrishnan, A. S., 2002. The monsoon currents in the north Indian Ocean. Progress in Oceanography 52 (1), 63-120.

Sharma, G. S., 1978. Upwelling off the southwest coast of India. Indian Journal of Marine Sciences.

Shetye, S. R., Gouveia, A. D., Shenoi, S. S. C., Sundar, D., Michael, G. S., Almeida, A. M., Santanam, K., 1990. Hydrography and circulation off the west coast of India during the southwest monsoon 1987.

Shemesh, A., Hodell, D., Crosta, X., Kanfoush, S., Charles, C., and Guilderson, T., 2002. Sequence of events during the last deglaciation in Southern Ocean sediments and Antarctic ice cores. Paleoceanography 17.

Siani, G., Michel, E., De Pol-Holz, R., DeVries, T., Lamy, F., Carel, M., Isguder, G., Dewilde, F., Lourantou, A., 2013. Carbon isotope records reveal precise timing of enhanced Southern Ocean upwelling during the last Deglaciation. Nature Communications 4, 2758.

Sigman, D. M., Boyle, E. A., 2000. Glacial/interglacial variations in atmospheric carbon dioxide.

Nature 407 (6806), 859-869.

Sijinkumar, A. V., Clemens, S., Nath, B. N., Prell, W., Benshila, R., Lengaigne, M., 2016. $\Delta^{18}O$ and salinity variability from the Last Glacial Maximum to recent in the Bay of Bengal and Andaman Sea. Quat. Sci. Rev. 135, 79-91.

Siddall, M., Rohling, E.J., Almogi-Labin, A., Hemleben, C., Meischner, D., Schmelzer, I., and Smeed, D. A. (2003). Sea-level fluctuations during the last glacial cycle. Nature 423, 853.

Singh, A. D., Jung, S. J. A., Darling, K., Ganeshram, R., Ivanochko, T., Kroon, D., 2011. Productivity collapses in the Arabian Sea during glacial cold phases. Paleoceanography 26 (3).

Singh, A. D., Kroon, D., Ganeshram, R., 2006. Millennial scale variations in productivity and OMZ intensity in the eastern Arabian Sea. Journal of the Geological Society of India 68 (3), 369-377.

Sikes, E. L., Allen, K. A., Lund, D. C., 2017. Enhanced $\delta^{13}C$ and $\delta^{18}O$ differences between the south Atlantic and south Pacific during the last glaciation: The deep gateway hypothesis. Paleoceanography 32 (10).

Sirocko, F., Sarnthein, M., 1989; Wind-borne deposits in the northwestern Indian Ocean: Record of holocene sediments versus modern satellite data. pp. 401-433.

Sirocko, F., Schonberg, D.G., Devey, C., 2000. Processes controlling trace element geochemistry of Arabian Sea sediments during the last 25,000 years. Glob. Planet. Chang. 26, 217–303.

Skinner, L. C., Claire, W., Scrivner, A. E., Fallon, S. J., 2014. Radiocarbon evidence for alternating northern and southern sources of ventilation of the deep Atlantic carbon pool during the last deglaciation. PNAS 111 (15), 5480-5484.

Skinner, L. C., Fallon, S., Waelbroeck, C., Michel, E., Barker, S., 2010. Ventilation of the deep Southern Ocean and deglacial CO_2 rise. Science 328 (5982), 1147-1151.

Smith, R. L., Huyer, A., Godfrey, J. S., Church, J. A., 1991. The Leeuwin current off western Australia, 1986–1987. Journal of Physical Oceanography 21, 323-345.

Speich, S., Blanke, B., Madec, G., 2001. Warm cold water routes of an OGCM Thermohaline conveyor belt. Geophysical Research Letters 28 (2), 311–314.

Stocker, T. F., Wright, D. G., 1996. Rapid changes in ocean circulation and atmospheric radiocarbon. Paleoceanography 11 (6), 773-795.

Stoll, H.M., Vance, D., and Arevalos, A. (2007). Records of the Nd isotope composition of seawater from the Bay of Bengal: Implications for the impact of northern hemisphere cooling on itcz movement. Earth and Planetary Science Letters 255 (1), 213-228.

Stuiver, M., Braziunas, T. F., 1993. Modeling atmospheric ^{14}C influences and ^{14}C ages of marine

samples to 10 000 bc. Radiocarbon 35 (1), 137-189.

Szarek, R., Kuhnt, W., Kawamura, H., and Nishi, H. (2009). Distribution of recent benthic foraminifera along continental slope of the Sunda Shelf (South China Sea). Marine Micropaleontology 71 (1), 41-59.

Takahashi, K., Okada, H., 2000. The paleoceanography for the last 30,000 years in the southeastern Indian Ocean by means of calcareous nannofossils. Marine Micropaleontology 40 (1), 83-103.

Talley, L. D., Pickard, G. L., Emery, W. J., Swift, J. H., 2011; Preface. In Descriptive physical oceanography (sixth edition), Academic Press: Boston, pp. 1-383.

Taylor, K. C., Lamorey, G. W., Doyle, G. A., Alley, R. B., Grootes, P. M., Mayewski, P. A., White, J. W. C., Barlow, L. K., 1993. The 'flickering switch' of late Pleistocene climate change. Nature 361 (6411), 432-436.

Thushara, V., Vinayachandran, P. N., 2016. Formation of summer phytoplankton bloom in the northwestern Bay of Bengal in a coupled physical-ecosystem model. Journal of Geophysical Research: Oceans 121 (12), 8535-8550.

Tisnérat-Laborde, N., Poupeau, J. J., Tannau, J. F., Paterne, M., 2001. Development of a semi-automated system for routine preparation of carbonate samples. Radiocarbon 43 (2A), 299-304.

Toggweiler, J. R., 1999. Variation of atmospheric CO_2 by ventilation of the ocean's deepest water, Paleoceanography 14, 571-588.

Toggweiler, J.R., Russell, J.L., and Carson, S.R. (2006). Midlatitude westerlies, atmospheric CO_2, and climate change during the ice ages. Paleoceanography 21 (2).

Tomczak, M., Godfrey, J. S., 2003; Regional oceanography: An introduction. Daya Publishing House.

Tripathy, G., Sunil, Singh, S., Bhushan, R., Ramaswamy, V., Sr–Nd isotope composition of the Bay of Bengal sediments: Impact of climate on erosion in the himalaya. 2011; Vol. 45, p 175-186.

Tsuchiya, M., Talley, L. D., McCartney, M. S., 1992. An eastern atlantic section from Iceland southward across the equator. Deep Sea Research Part A. Oceanographic Research Papers 39 (11), 1885-1917.

Umling, N. E., Thunell, R. C., Bizimis, M., 2018. Deepwater expansion and enhanced remineralization in the eastern equatorial Pacific during the Last Glacial Maximum. Paleoceanography and Paleoclimatology 33 (6), 563-578.

Van der Zwaan, G. J., Duijnstee, I. A. P., Den Dulk, M., Ernst, S. R., Jannink, N. T., Kouwenhoven,

T. J., 1999. Benthic foraminifers: Proxies or problems? A review of paleocological concepts. Earth-Science Reviews 46 (1), 213-236.

Valley, S., Lynch-Stieglitz, J., M. Marchitto, T., 2017. Timing of deglacial AMOC variability from a high-resolution seawater Cadmium reconstruction: Timing deglacial upper amoc variability. Paleoceanography 32, 1195-1203.

Venkatarathnam, K., Biscaye, P. E., 1973. Clay mineralogy and sedimentation in the western Indian Ocean. Deep Sea Research and Oceanographic Abstracts 23 (10), 949-961.

Vinayachandran, P. N., Murty, V. S. N., Ramesh Babu, V., 2002. Observations of barrier layer formation in the Bay of Bengal during summer monsoon. Journal of Geophysical Research: Oceans 107 (C12), SRF 19-1-SRF 19-9.

Wacker, L., Fahrni, S. M., Hajdas, I., Molnar, M., Synal, H. A., Szidat, S., Zhang, Y. L., 2013. A versatile gas interface for routine radiocarbon analysis with a gas ion source. Nuclear Instruments and Methods in Physics Research Section B: Beam Interactions with Materials and Atoms 294, 315-319.

Waelbroeck, C., Levi, C., Duplessy, J. C., Labeyrie, L., Michel, E., Cortijo, E., Bassinot, F., Guichard, F., 2006. Distant origin of circulation changes in the Indian Ocean during the last Deglaciation. Earth and Planetary Science Letters 243 (1), 244-251.

Wais, D.P.M. (2013). Onset of deglacial warming in west Antarctica driven by local orbital forcing. Nature 500, 440.

Wan, S., Jian, Z., 2014. Deep water exchanges between the South China Sea and the Pacific since the last glacial period, Paleoceanography, 29, 1162–1178.

Wang, P., Tian, J., Cheng, X., Liu, C., Jian, X., 2004. Major Pleistocene stages in a carbon perspective: The South China Sea record and its global comparison. Paleoceanography 19:Pa4005. Paleoceanography 19 (4).

Wang, X., Jian, Z., Lückge, A., Wang, Y., Dang, H., Mohtadi, M., 2018. Precession-paced thermocline water temperature changes in response to upwelling conditions off southern Sumatra over the past 300,000 years. Quaternary Science Reviews.

Warren, B. A., 1981. Deep circulation of the world ocean. Evolution of physical oceanography 641.

Wen, X., Liu, Z., Wang, S., Cheng, J., and Zhu, J. (2016). Correlation and anti-correlation of the East Asian summer and winter monsoons during the last 21,000 years. Nature Communications 7, 11999.

Wiggert, J. D., Hood, R. R., Banse, K., Kindle, J. C., 2005. Monsoon-driven biogeochemical

processes in the Arabian Sea. Progress in Oceanography 65 (2), 176-213.

Wijffels, S., Sprintal, J., Fieux, M., Bray, N., 2002. The Jade and WOCE I10/IR6 throughflow sections in the southeast Indian Ocean. Part 1: Water mass distribution and variability. Deep-Sea Research Part II 49 (7), 1341-1362.

Wunsch, C., 2002. What is thermohaline circulation? Science 298 (5596), 1179-1181.

Wyrtki, K., 1973. Physical oceanography of the Indian Ocean, The biology of the Indian Ocean. Springer, pp. 18-36.

Xie, R.C., Marcantonio, F., and Schmidt, M.W., 2012. Deglacial variability of Antarctic Intermediate Water penetration into the north Atlantic from authigenic Neodymium isotope ratios. Paleoceanography 27 (3).

Yasuda, I., 2004. North pacific intermediate water: Progress in sage (subarctic gyre experiment) and related projects. Journal of Oceanography 60 (2), 385-395.

You, Y., 1998. Intermediate water circulation and ventilation of the Indian Ocean derived from water-mass contributions. Journal of Marine Research 56 (5), 1029-1067.

You, Y., Tomczak, M., 1993. Thermocline circulation and ventilation in the Indian Ocean derived from water mass analysis. Deep Sea Research Part I: Oceanographic Research Papers 40 (1), 13-56.

Yu, J., Anderson, R. F., Rohling, E. J., 2014a. Deep ocean carbonate chemistry and glacial-interglacial atmospheric CO_2 change. Oceanography 27 (1), 16-25.

Yu, J., Elderfield, H., Jin, Z., Tomascak, P., Rohling, E. J., 2014b. Controls on Sr/Ca in benthic foraminifera and implications for seawater Sr/Ca during the late Pleistocene. Quaternary Science Reviews 98 (15), 1-6.

Yu, J., Day, J., Greaves, M., Elderfield, H., 2005. Determination of multiple element/Calcium ratios in foraminiferal calcite by quadrupole ICP-MS. Geochemistry, Geophysics, Geosystems 6 (8), 1-9.

Yu, J., Elderfield, H., 2007. Benthic foraminiferal B/Ca ratios reflect deep water carbonate saturation state. Earth and Planetary Science Letters 258 (1), 73-86.

Yu, J., Elderfield, H., 2008. Mg/Ca in the benthic foraminifera *Cibicidoides wuellerstorfi* and *Cibicidoides mundulus*: Temperature versus carbonate ion saturation. Earth and Planetary Science Letters 276 (1), 129-139.

Yu, J., Elderfield, H., Piotrowski, A. M., 2008. Seawater carbonate ion- $\delta^{13}C$ systematics and

application to glacial-interglacial north Atlantic Ocean circulation. Earth and Planetary Science Letters 271 (1), 209-220.

Yu, J., Foster, G. L., Elderfield, H., Broecker, W. S., Clark, E., 2010a. An evaluation of benthic foraminiferal B/Ca and $\delta^{11}B$ for deep ocean carbonate ion and pH reconstructions. Earth and Planetary Science Letters 293 (1), 114-120.

Yu. J., Broecker, W., Elderfield, H., Jin, Z. D., McManus, J., Zhang, F., 2010b. Loss of carbon from the deep sea since the Last Glacial Macimum. Sicence 330, 1084-1087.

Yu, Z., Colin, C., Ma, R., Meynadier, L., Wan, S., Wu, Q., Kallel, N., Sepulcre, S., Dapoigny, A., Bassinot, F., 2018. Antarctic Intermediate Water penetration into the northern Indian Ocean during the last Deglaciation. Earth and Planetary Science Letters 500, 67-75.

Zahn, R., Winn, K., and Sarnthein, M. (1986). Benthic foraminiferal $\delta^{13}C$ and accumulation rates of organic carbon: *Uvigerina peregrina* group and *Cibicidoides wuellerstorfi*. Paleoceanography 1 (1), 27-42.

Zaric, S., Donner, B., Fischer, G., Mulitza, S.,Wefer, G., 2005. Sensitivity of planktic foraminifera to sea surface temperature and export production as derived from sediment trap data. Mar. Micropaleontol. 55, 75–105.

Zarriess, M., Mackensen, A., 2011. Testing the impact of seasonal phytodetritus deposition on d13C of epibenthic foraminifer *Cibicidoides wuellerstorfi*: a 31,000 year highresolution record from the northwest African continental slope. Paleoceanography 26 (2), PA2202.

Zeebe, R. E., Wolf-Gladrow, D., 2001. CO_2 in seawater: Equilibrium, kinetics, isotopes. Amsterdam: Elsevier Science, B.V., pp. 346.

Appendix 1

Earth and Planetary Science Letters 500 (2018) 67–75

Contents lists available at ScienceDirect

Earth and Planetary Science Letters

www.elsevier.com/locate/epsl

Antarctic Intermediate Water penetration into the Northern Indian Ocean during the last deglaciation

Zhaojie Yu [a,b,d,*], Christophe Colin [b], Ruifang Ma [b], Laure Meynadier [e], Shiming Wan [a,c], Qiong Wu [f], Nejib Kallel [g], Sophie Sepulcre [b], Arnaud Dapoigny [h], Frank Bassinot [h]

[a] Key Laboratory of Marine Geology and Environment, Institute of Oceanology, Chinese Academy of Sciences, Qingdao 266071, PR China
[b] Laboratoire GEOsciences Paris-Sud (GEOPS), UMR 8148, CNRS-Université de Paris-Sud, Université Paris-Saclay, Bâtiment 504, 91405 Orsay Cedex, France
[c] Laboratory for Marine Geology, Qingdao National Laboratory for Marine Science and Technology, Qingdao 266061, PR China
[d] Center for Ocean Mega-Science, Chinese Academy of Sciences, 7 Nanhai Road, Qingdao, 266071, PR China
[e] Equipe de Géochimie et Cosmochimie, Institut de Physique du Globe de Paris-Sorbonne Paris Cité, UMR 7154, Université Paris Diderot, France
[f] College of Oceanography, Hohai University, Nanjing, China
[g] Université de Sfax, Faculté des Sciences, Laboratoire GEOGLOB, BP 802, 3038 Sfax, Tunisia
[h] Laboratoire des Sciences du Climat et de l'Environnement, Domaine du CNRS, Gif-sur-Yvette, 91198, France

ARTICLE INFO

Article history:
Received 11 May 2018
Received in revised form 1 August 2018
Accepted 2 August 2018
Available online xxxx
Editor: D. Vance

Keywords:
Nd isotopic composition
AAIW
deglaciation
atmospheric CO_2
Northern Indian Ocean

ABSTRACT

The two-stage increase in atmospheric carbon dioxide (CO_2), and the associated decrease in radiocarbon (^{14}C) during the last deglaciation, are thought to have been linked to enhanced Southern Ocean upwelling and the rapid release of sequestered ^{14}C-depleted CO_2. Antarctic Intermediate Water (AAIW), originating from the Southern Ocean, reflects variations in the Southern Ocean and, crucially, mirrors the chemical signature of upwelling deep water. However, the penetration of AAIW into the Northern Indian Ocean and its relationship with deglacial climate changes have not been thoroughly elucidated to date. Here, we present the neodymium isotopic composition (ε_{Nd}) of mixed planktonic foraminifera from core MD77-176 from an intermediate depth in the Northern Indian Ocean to reconstruct the past evolution of intermediate water during deglaciation. The ε_{Nd} record in the Northern Indian Ocean displays two pulse-like shifts towards more radiogenic Southern Ocean values during the deglaciation, and these shifts coincide with excursions in $\Delta^{14}C$ and ε_{Nd} records in the Pacific and Atlantic Oceans. These results suggest invasion of AAIW into the Northern Hemisphere oceans associated with enhanced Southern Ocean ventilation during deglaciation. Our new ε_{Nd} record strongly supports the close linkage of AAIW propagation and atmospheric CO_2 rise through Southern Ocean ventilation during deglaciation.

1. Introduction

During deglaciation (~18–10 kyr BP), atmospheric carbon dioxide (CO_2) increased from 180 to 265 parts per million (ppm); meanwhile, its radiocarbon content (^{14}C) decreased by ~35%. These changes occurred in two steps during the periods ~18 to 14.7 kyr BP and ~12.8 to 11.7 kyr BP (Monnin and Barnola, 2001). A mechanism of enhanced Southern Ocean ventilation and release of excess ^{14}C-depleted CO_2 by upwelled deep water has been invoked to explain this extraordinary phenomenon (Anderson et al., 2009; Bryan et al., 2010; Marchitto et al., 2007; Skinner et al., 2014). This explanation is based on the fact that the deep ocean is the largest and relatively most ^{14}C-depleted carbon reservoir that can interact with the atmosphere on a millennial timescale (Sigman and Boyle, 2000). However, the specific processes involved in Southern Ocean ventilation and/or atmospheric CO_2 leakage during the deglaciation remain unclear (Anderson et al., 2009; Burke and Robinson, 2012; Jaccard et al., 2016; Skinner et al., 2014). More evidence is needed to clarify the role of Southern Ocean variations and their influence on global thermohaline circulation. The formation and advection of AAIW, which is highly sensitive to the perturbation of the Southern Ocean and westerly wind stress (Ribbe, 2001), is therefore key for understanding the deglacial variations in the Southern Ocean. The propagation of Antarctic Intermediate Water (AAIW) is also important for regulating heat and freshwater distribution, and for ventilation associated with intermediate thermohaline circulation of the ocean (Lynch-Stieglitz et al., 1994; Ribbe, 2001).

* Corresponding author at: Institute of Oceanology, Chinese Academy of Sciences, Qingdao 266071, China.
E-mail address: yuzhaojie@qdio.ac.cn (Z. Yu).

https://doi.org/10.1016/j.epsl.2018.08.006
0012-821X/

A reconstruction of intermediate water $\Delta^{14}C$ values near Baja California in the Pacific Ocean shows two oscillations associated with old ^{14}C-depleted waters during Heinrich Stadial 1 (HS1) and the Younger Dryas (YD), consistent with the timing of atmospheric CO_2 rise during the deglaciation (Marchitto et al., 2007). These observations have also been confirmed by the Nd isotopic compositions (reported as ε_{Nd}) of fish teeth/debris from the same core, which indicated a shift in the ε_{Nd} values towards Southern Ocean values at the beginning of the deglaciation (Basak et al., 2010). Both studies suggest that this intermediate water observed near Baja California was sourced from the Southern Ocean, and was advected to the Northern Pacific Ocean via AAIW (Basak et al., 2010; Marchitto et al., 2007). Direct evidence of strong Southern Ocean upwelling has been reported based on ^{14}C (Skinner et al., 2010) and opal flux records (Anderson et al., 2009) in the Southern Ocean during the deglaciation, and the existence of strong upwelling also suggests strong production and advection of the AAIW at this time. In contrast, a $\Delta^{14}C$ reconstruction of the AAIW signature off the coast of Chile showed no impact of old abyssal carbon during deglaciation (De Pol-Holz et al., 2010). Furthermore, a modelling study was also not able to achieve the observed mid-depth ^{14}C anomalies, even with a totally ^{14}C-free deep reservoir (Hain et al., 2011), suggesting that the linkage between Southern Ocean overturning and ^{14}C-depleted AAIW penetration is complicated.

If Southern Ocean ventilation was accompanied by strong northward invasion of the AAIW during the deglaciation, the specific $\Delta^{14}C$ and ε_{Nd} signal should also be observed in intermediate-depth cores from other oceans. However, while such a possible invasion of AAIW during the deglaciation has been fully discussed in the Atlantic (Cao et al., 2005; Mangini et al., 2010; Pahnke et al., 2008), it is poorly established in the Indian Ocean. The only $\Delta^{14}C$ study from the northern Arabian Sea suggested that ^{14}C-depleted carbon from the deep Southern Ocean could have greatly influenced the intermediate water in the Arabian Sea during deglaciation (Bryan et al., 2010). However, there is a possibility that the $\Delta^{14}C$ record is contaminated with other upwelling ^{14}C-depleted water, such as local deep water and/or North Indian Intermediate Water (Basak et al., 2010; Bryan et al., 2010). In contrast, foraminiferal ε_{Nd} values have been widely used as a quasi-conservative tracer for past deep oceanic circulation (Frank, 2002; Piotrowski et al., 2012). Dissolved Nd in the ocean is characterized by a short residence time (from 360 to 700 yr) (Frank, 2002; Tachikawa et al., 2003), meaning different water masses carry distinct ε_{Nd} signatures that are generally altered only by mixing and/or local lithogenic Nd inputs from continents and marginal oceans.

In this study, we present the ε_{Nd} values of mixed planktonic foraminifera from core MD77-176 (Fig. 1), collected at an intermediate water depth in the Northern Indian Ocean to establish its intermediate water evolutionary history. Modern seawater ε_{Nd} in the Northern Indian Ocean can be used to discriminate between the relative contributions of Nd from the input of Himalayan rivers (mainly the Ganges–Brahmaputra river system) and water masses originating from the Southern Ocean (Yu et al., 2017a). Here, we constrain the relative contributions of lithogenic Nd inputs since the last glacial period and track deep- and intermediate-water masses originating from the Southern Ocean. In a broader context, the ε_{Nd} record reported in this study is compared with previous ^{14}C and ε_{Nd} records from Northern Hemisphere oceans in order to better understand the potential northward penetration of AAIW during deglaciation.

2. Materials and methods

2.1. Sediment core and age models

Cores MD77-176 (14°30′5″N–93°07′6″E, 1375 m water depth, Fig. 1) was collected in the northeastern Bay of Bengal (BoB) during cruise OSIRIS III of the R.V. Marion Dufresne in 1977. Core MD77-176 was extracted from a site located near the continental slope, 200 km away from the modern Irrawaddy River mouth. This core's lithology consists of intercalated olive grey terrigenous clay and silty clay layers with foraminifera- or nannofossil-bearing ooze. The age model was established using accelerator mass spectrometry (AMS) ^{14}C dates (31 monospecific planktonic foraminifera dates) and oxygen isotope measurements (correlating the $\delta^{18}O$ values of the MD77-176 core and the GISP2-Greenland ice core record) performed on planktonic foraminifera *Globigerinoides ruber* (Fig. 2) (Marzin et al., 2013). The Calib 4.1 program has been used to convert the ^{14}C ages into calendar ages over the last 20 kyr (Stuiver and Reimer, 1993; Stuiver et al., 1998) and includes a correction for the ocean surface reservoir age of 400 yr (Broecker and Peng, 1982). Ages older than 20 kyr ^{14}C BP were established using the Fairbanks et al. (2005) calibration model. The local $\delta^{18}O_{sw}$ values of MD77-176 display large millennial-scale oscillations, suggesting a correlation with the GISP2 record (Marzin et al., 2013). Using the Heinrich events as tie points, Marzin et al. (2013) developed a second age model for core MD77-176 by tuning the $\delta^{18}O_{sw}$ values of MD77-176 with respect to the GISP2 record. As evidenced by a comparison, these two age models are consistent (Marzin et al., 2013). The core MD77-176 thus provides a continuous record over the last 40 kyr BP, with an average sedimentation rate of approximately 25 cm/kyr and a sedimentation rate of up to 40 cm/kyr during the Holocene.

2.2. Analytical methods

Approximately 30 mg of mixed planktonic foraminifera species were picked from the size fraction ranging between 150 and 300 μm. The samples were gently crushed between glass slides under the microscope to ensure that all chambers were open, and ultrasonicated with MilliQ water. Samples were allowed to settle between ultrasonication steps before removing the supernatant. Each sample was rinsed thoroughly with MilliQ water until the solution was clear and free of clay. After the cleaning step, the foraminifera were dissolved using stepwise 100 μl nitric acid (0.5 M HNO_3) until the dissolution reaction was complete. The dissolved samples were centrifuged, and the supernatant was immediately transferred to Teflon beakers to prevent the leaching of any possible remaining phases.

Nd was separated from the carbonate matrix using Eichrom TRU and LN resins, following the analytical procedure described in detail by Copard et al. (2010). In brief, samples were loaded using 2 ml of 1 M HNO_3 on preconditioned TRU Spec columns (83 mg portion of TRU Spec). The unwanted cations were eluted using five aliquots of 0.5 ml of 1 M HNO_3. The TRU Spec columns were then placed over Ln Spec columns. The light REEs were then eluted from the upper (TRU Spec) column using seven aliquots of 0.1 ml of 0.05 M HNO_3. After decoupling from the TRU Spec columns, La, Ce, and most of the Pr were removed from the Ln Spec columns using 2.5 ml of 0.25 M HCl. Nd was then eluted with an additional 3.25 ml of 0.25 M HCl.

The $^{143}Nd/^{144}Nd$ ratios of all purified Nd fractions were analysed using a Thermo Fisher multi-collector inductively coupled plasma mass spectrometer (MC-ICPMS Neptune ^{Plus}) at the Laboratoire des Sciences du Climat et de l'Environnement (LSCE) in Gif-sur-Yvette, France (Table 1). The mass-fractionation correction was

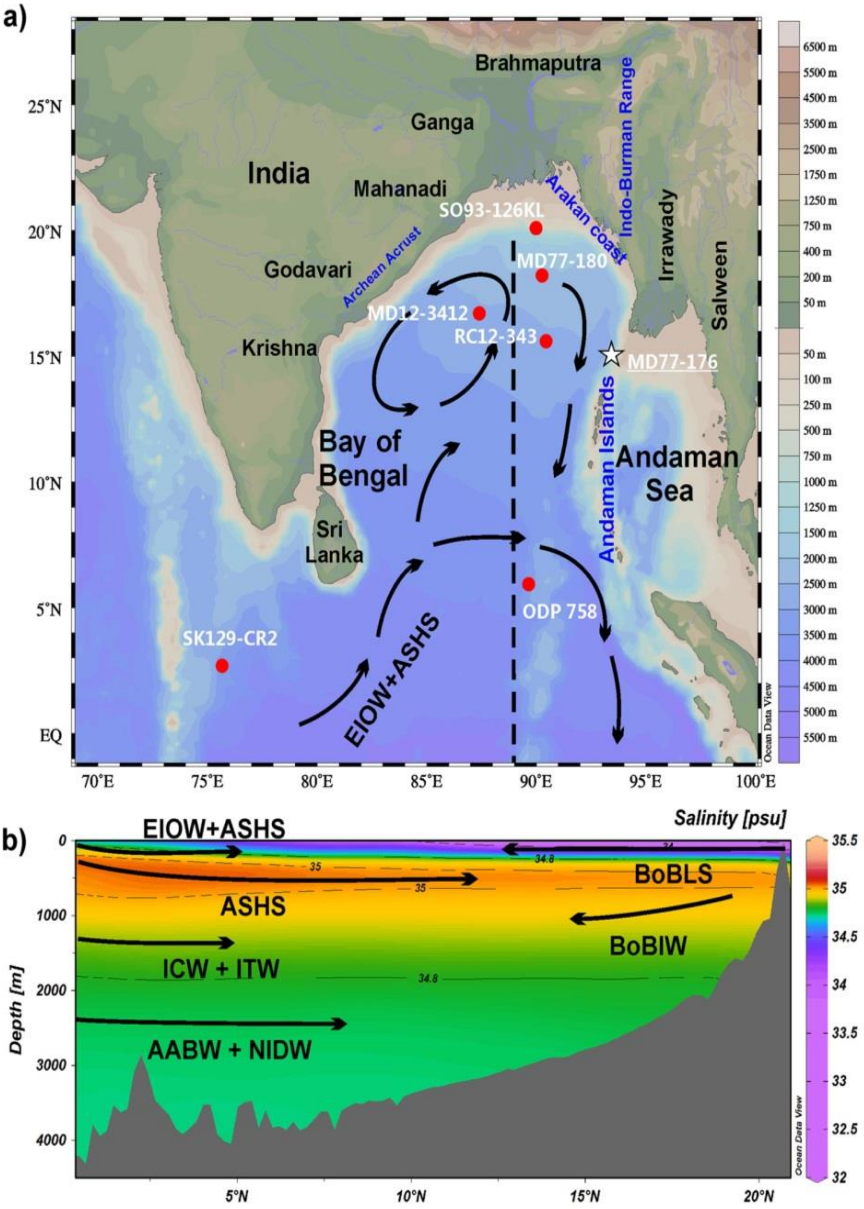

Fig. 1. a) Geographical setting and locations of reference sites (red circles) in the Bay of Bengal (BoB). The black arrows illustrate the general surface circulation pattern in the BoB during boreal summer (June–September) (Shankar et al., 2002). All the colour contours (bathymetry) in this and subsequent figures are plotted with the help of ODV4 software (Schlitzer, 2015). b) Salinity distribution along a N–S cross-section in the BoB. EIOW: Eastern Indian Ocean Surface Water; ASHS: Arabian Sea High Salinity Water; BoBLS: BoB Lower Salinity Water; BoBIW: BoB Intermediate Water; ICW: Indian Central Water; ITW: Indonesian Throughflow Water; AABW: Antarctic Bottom Water; NIDW: North Indian Deep Water. (For interpretation of the colours in the figure(s), the reader is referred to the web version of this article.)

made by normalizing $^{146}Nd/^{144}Nd$ to 0.7219 and applying an exponential law. During each analytical session, samples were systematically bracketed with analyses of JNdi-1 and La Jolla standard solutions, which are characterized by accepted values of 0.512115 ± 0.000006 (Tanaka et al., 2000) and 0.511855 ± 0.000007 (Lugmair et al., 1983), respectively. Standard JNdi-1 and La Jolla solutions were analysed at concentrations similar to those of the samples (from 10 to 15 ppb). Repeated ($n = 15$–20) measurements of standard JNdi-1 and La Jolla solutions within one session gave values from 0.512110 ± 0.000005 to 0. 0.512119 ± 0.000005 (2σ), and from 0.511848 ± 0.000008 to 0.511858 ± 0.000005 (2σ), respectively. The external reproducibility (2σ) for time resolved measurements, deduced from repeated analyses of JNdi-1 and La Jolla standards, is approximately 0.3 ε_{Nd} units (Table 1). The analytical error for each sample analysis was taken as the external reproducibility of the La Jolla standard. Nd isotopic composition is expressed as $\varepsilon_{Nd} = [(^{143}Nd/^{144}Nd)_{Sample}/(^{143}Nd/^{144}Nd)_{CHUR} - 1] \times 10{,}000$, where $(^{143}Nd/^{144}Nd)_{CHUR}$ represents the chondritic uniform reservoir and corresponds to the modern average earth value $(^{143}Nd/^{144}Nd)_{CHUR} = 0.512638$ (Jacobsen and Wasserburg, 1980).

3. Results and discussion

3.1. Revisiting the significance of foraminiferal ε_{Nd} in the BoB

It has been demonstrated that the ε_{Nd} values of fossil planktonic foraminifera are not related to the ambient seawater at calcification depths, but instead reflect the bottom and/or porewater ε_{Nd} values due to the presence of authigenic Fe–Mn coating precipitated onto the carbonate shells (Piotrowski et al., 2012; Roberts et al., 2010). Therefore, the ε_{Nd} values of planktonic foraminifera can be used as a useful tracer of deep-water circulation changes in the past (Tachikawa et al., 2014).

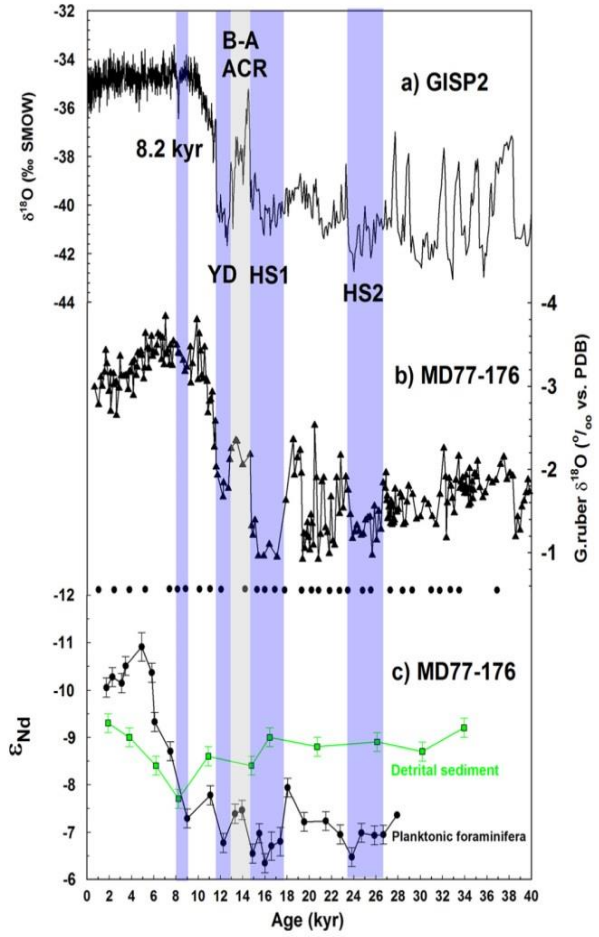

Fig. 2. Information on core MD77-176 from the Northern Indian Ocean. a) Greenland ice core $\delta^{18}O$ record GISP2 (Grootes and Stuiver, 1997); b) Age-*G. ruber* $\delta^{18}O$ plot for core MD77-176 (Marzin et al., 2013). The black circles represent the ^{14}C age points (^{14}C ages were converted into calendar ages using the Calib 4.1 program for ages younger than 20 kyr ^{14}C BP and the Fairbanks et al. (2005) calibration for ages older than 20 kyr ^{14}C BP; c) ε_{Nd} of detrital sediment (Colin et al., 2006) and mixed planktonic foraminifera (this study) from core MD77-176. $\varepsilon_{Nd} = [(^{143}Nd/^{144}Nd)_{Sample}/(^{143}Nd/^{144}Nd)_{CHUR} - 1] \times 10{,}000$. Note that the detrital and foraminifera ε_{Nd} variabilities are quite different, indicating that they may be controlled by distinct processes. The terms 8.2 kyr, YD, B-A ACR (grey bar), HS1 and HS2 stand for the 8.2 kyr cooling event, Younger Dryas, Bølling-Allerød, Antarctic Cold Reversal and Heinrich Stadial 1 intervals, respectively. The foraminifera ε_{Nd} values are more radiogenic during the Northern Hemisphere cold intervals (blue bars).

Table 1
ε_{Nd} of mixed planktonic foraminifera from core MD77-176.

Sample depth (cm)	Calendar age (kyr BP)	ε_{Nd}	$\pm 2\sigma$
30–32	1.7	−10.0	0.2
55–57	2.3	−10.3	0.2
85–87	3.1	−10.1	0.2
105–107	3.5	−10.5	0.2
185–187	4.9	−10.9	0.2
235–237	5.8	−10.4	0.3
250–252	6.1	−9.3	0.2
315–317	7.5	−8.7	0.2
365–367	9.0	−7.3	0.2
450–452	11.1	−7.8	0.2
495–497	12.3	−6.8	0.2
525–527	13.3	−7.4	0.2
535–537	13.9	−7.5	0.2
555–557	14.9	−6.5	0.2
560–562	15.5	−7.0	0.2
570–572	16.0	−6.3	0.2
580–582	16.6	−6.7	0.2
590–592	17.4	−6.8	0.3
600–602	18.1	−7.9	0.3
615–617	19.5	−7.2	0.2
650–652	21.5	−7.2	0.2
670–672	22.8	−6.9	0.2
685–687	23.8	−6.5	0.2
695–697	24.7	−7.0	0.2
715–717	25.9	−6.9	0.2
720–722	26.7	−6.9	0.2
770–772	27.9	−7.4	0.2

All measured $^{143}Nd/^{144}Nd$ ratios are reported relative to ε_{Nd} values of La Jolla of 0.511858 ± 0.000020 (Lugmair et al., 1983) and Jndi-1 of 0.512115 ± 0.000007 (Tanaka et al., 2000), and ε_{Nd} values were calculated using a CHUR of 0.512638 (Jacobsen and Wasserburg, 1980). Error bars represent external reproducibility unless the internal error is larger.

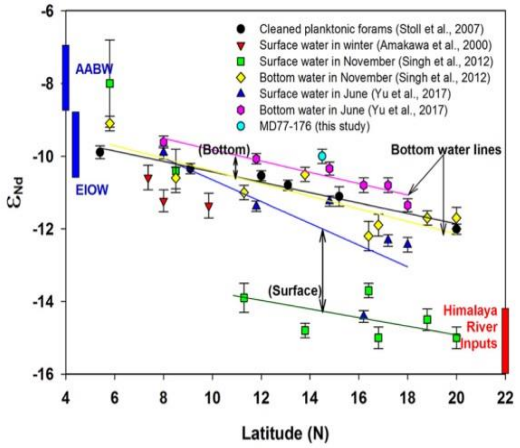

Fig. 3. Comparison of planktonic foraminiferal ε_{Nd} with bottom and surface water ε_{Nd} values in the Bay of Bengal. The ε_{Nd} values of reductive-oxidative cleaned planktonic foraminifera from the late Holocene intervals are from Stoll et al. (2007). The surface and bottom water ε_{Nd} values in November and June are from Singh et al. (2012) and Yu et al. (2017a). The surface water ε_{Nd} values in winter are from Amakawa et al. (2000). The core top ε_{Nd} value of MD77-176 is also plotted for comparison. The blue and red rectangles mark the modern seawater ε_{Nd} ranges of AABW, EIOW and Himalayan river inputs, respectively. The straight lines are trend lines of ε_{Nd} records using the same colour as their original data sets. These straight lines generally indicate mixing between unradiogenic Himalaya River inputs (ε_{Nd} from −16 to −14) with the radiogenic Eastern Indian Ocean water (EIOW: ε_{Nd} from −10 to −9) and Antarctic bottom water (AABW: ε_{Nd} from −9 to −7) (Goswami et al., 2012; Piepgras and Wasserburg, 1982; Yu et al., 2017a). Two double-sided black arrows highlight the offset in the surface water ε_{Nd} trend lines in the months of November and June, as well as the offset in the bottom ε_{Nd} trend lines in these two months. Note that the difference in the surface water ε_{Nd} values (approximately 2 ε_{Nd}) is generally four-fold greater than the difference in the bottom ε_{Nd} values (approximately 0.5 ε_{Nd}) in the months of November and June.

Prior to these recent studies, foraminifera ε_{Nd} records obtained from several cores located between 1253 m and 3173 m water depth in the BoB have been interpreted as surface seawater signals (Burton and Vance, 2000; Stoll et al., 2007). Therefore, the significance of these ε_{Nd} records in the BoB should be re-evaluated (Fig. 3). Based on modern seawater studies, seawater ε_{Nd} values in the BoB display strong latitudinal and vertical gradients, resulting from the mixture of nonradiogenic Nd inputs from Himalayan rivers and more radiogenic deep water originating from the Southern Ocean (Singh et al., 2012; Yu et al., 2017a). Therefore, the BoB constitutes an ideal region to better constrain the significance of the ε_{Nd} data obtained from planktonic foraminifera.

A strong seasonal variation in ε_{Nd} values has been reported in the BoB (Yu et al., 2017a). Seawater samples collected in June 2012 were more radiogenic (~2 ε_{Nd} for the upper 2000 m and ~0.5 ε_{Nd} below 2000 m) than seawater samples collected nearby in November 2008 (Singh et al., 2012; Yu et al., 2017a). The difference in surface water ε_{Nd} values between June and November is attributed to the summer monsoon-induced lithogenic inputs from Himalayan rivers (Yu et al., 2017a). The ε_{Nd} values

of surface and deep waters in the BoB display strong latitudinal changes (Fig. 3). This pattern is mainly due to the mixing of non-radiogenic Himalayan river inputs (ε_{Nd} values from −16 to −14) with the radiogenic Eastern Indian Ocean Water (EIOW: ε_{Nd} values from −10 to −9), Arabian Sea High Salinity Water (ASHS: $\varepsilon_{Nd} = \sim -8$) and Antarctic Bottom Water (AABW: ε_{Nd} from −9 to −7) (Goswami et al., 2012; Piepgras and Wasserburg, 1982; Yu et al., 2017a).

However, the ε_{Nd} values of cleaned planktonic foraminifera along a latitudinal transect are consistent with spatial variation in the bottom water ε_{Nd} values rather than the surface water ε_{Nd} values (Fig. 3). North of 11°N, the ε_{Nd} values of cleaned planktonic foraminifera are in the range of the deep-water masses but are not far from the ε_{Nd} values of surface water in winter (Fig. 3). However, although some winter species are present (Anand et al., 2003), the planktonic foraminifera in this area grow mainly in the summer, and the ε_{Nd} values of surface water in winter are unlikely to be recorded. South of 11°N, the ε_{Nd} values of surface and deep water are more homogeneous, and both are similar to those of the cleaned planktonic foraminifera. One exception is at 6°N, where the ε_{Nd} values of cleaned planktonic foraminifera are similar to the deep water values but differ from the surface water values (Fig. 3). Therefore, we confirm that planktonic foraminifera record the ε_{Nd} values of deep-water masses. North of 11°N, the ε_{Nd} values of cleaned planktonic foraminifera record the signatures of deep-water masses that are not strongly modified by the lithogenic input from Himalayan rivers.

3.2. Intermediate water ε_{Nd} values in the Northern Indian Ocean over the last 28 kyr

The foraminiferal ε_{Nd} values obtained from core RC12-343 (water depth of 2666 m) (Stoll et al., 2007) and ODP Site 758 (water depth of 2925 m) (Burton and Vance, 2000; Gourlan et al., 2010), therefore, represent past variations in the deep-water compositions in the northern and southern BoB, respectively. Meanwhile, the seawater ε_{Nd} record obtained from core MD77-176 (water depth of 1325 m) reflects the intermediate-water signal in the northern BoB (Figs. 2 and 3). Interestingly, ε_{Nd} variations in the deep water of northern BoB (RC12-343), southern BoB (ODP Site 758) and equatorial Indian Ocean (SK129-CR2) (Wilson et al., 2015) reveal a comparable, but not always consistent, pattern of variation to intermediate water as indicated by core MD77-176 (Fig. 4a).

Similar radiogenic ε_{Nd} values, ranging between −8 and −7, were observed in all of the seawater ε_{Nd} records obtained in the BoB during the late last glaciation from 28 to 18 kyr BP (Fig. 4a). However, during the deglaciation, from 18 to 10 kyr BP, the ε_{Nd} values of deep water display a decreasing trend down to ∼−9, while intermediate water (MD77-176) maintains a relatively radiogenic ε_{Nd} range between −8 and −6 until the early Holocene. The intermediate- and deep water ε_{Nd} values converge and decrease to approximately −10.5 during the time interval from 10 to 5 kyr BP. Similarly, the deep and intermediate water ε_{Nd} values in the late Holocene (after 5 kyr) display an increasing trend (Fig. 4a).

The radiogenic ε_{Nd} results during the last glacial suggest that both the northern and southern BoB seawater ε_{Nd} values were considerably more radiogenic than modern values (Yu et al., 2017a) and without any north-south gradient. This observation contrasts strongly with the modern seawater ε_{Nd} values of deep- and intermediate-water masses that show a north-south ε_{Nd} gradient (from −12 to −10 for water masses below 2000 m and from −13 to −10 for water masses between 2000 and 1000 m) (Yu et al., 2017a). This discrepancy implies a considerable change in the lithogenic Nd input and/or a modification in the deep-circulation during the last glacial period (Burton and Vance, 2000).

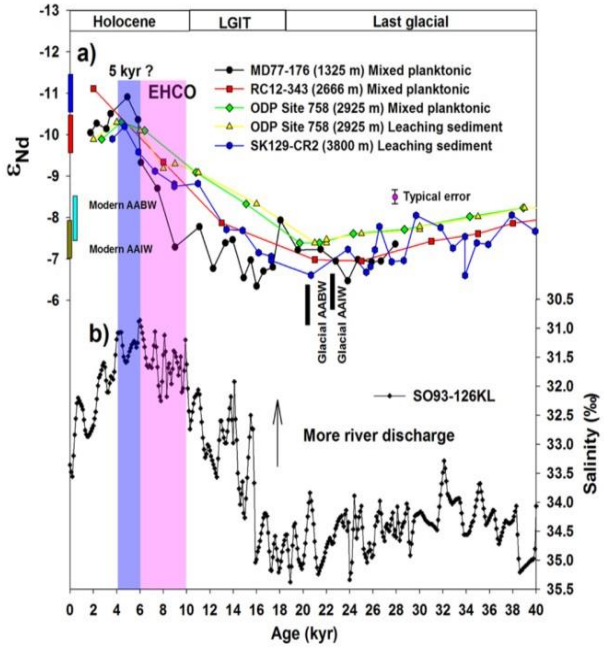

Fig. 4. Intermediate and deep water ε_{Nd} values in the Northern Indian Ocean over the last 28 kyr. a) Compilation of seawater ε_{Nd} records obtained from planktonic foraminifera in core MD77-176 (water depth of 1325 m) (this study), core RC12-343 (water depth of 2666 m) (Stoll et al., 2007), ODP site 758 (water depth of 2925 m) (Burton and Vance, 2000), and leached sediments from ODP site 758 (Gourlan et al., 2010) and from SK129-CR2 (Wilson et al., 2015). The variability in the deep water ε_{Nd} records (water depths greater than 1500 m) is similar to that in the intermediate water ε_{Nd} records (water depths shallower than 1500 m, core MD77-176) over the last 28 kyr BP, except for a period during the deglaciation (black line, intermediate water is approximately 0.5–2 ε_{Nd} more radiogenic than those of the deep water); b) Sea surface salinity calculated from marine $\delta^{18}O$ record and $U^{K'}_{37}$ temperature in core SO93-126KL located in the northern Bay of Bengal (Kudrass et al., 2001). Greater river discharge would lead to a lower sea surface salinity. LGIT: Last glacial–interglacial transition. EHCO: The Early Holocene Climatic Optimum. The blue and red rectangles in panel (a) mark the modern seawater ε_{Nd} ranges in intermediate and deep water, respectively. The ε_{Nd} ranges of glacial and modern AABW and AAIW are also indicated by black, brown and blue rectangles.

Numerous studies have concluded that the intensity of Indian monsoon precipitation was weaker during the late stage of the last glaciation than it is today (Kudrass et al., 2001; Marzin et al., 2013), and that the lithogenic input from Himalayan rivers (ε_{Nd} values of ∼−16) to the Bengal Fan was consequently lower (Burton and Vance, 2000; Colin et al., 1999; Joussain et al., 2016). Modelling studies have indicated that radiogenic dust (with ε_{Nd} values of −11 to −4) (Scheuvens et al., 2013) from the Arabian peninsula or Persian Gulf regions could have been transported to the BoB, thereby elevating the mean ε_{Nd} value of the BoB, during the last glaciation (Mahowald et al., 2006). However, increased dust delivery during the last glaciation could have modified surface water ε_{Nd} values (Tachikawa et al., 1999), but would have only slightly influenced the deep water ε_{Nd} values. Therefore, the observed variations in glacial seawater ε_{Nd} values mainly reflect a decrease in the amount of unradiogenic lithogenic Nd inputs from Himalayan rivers during weak monsoon intervals and/or the consequent increase in the proportion of radiogenic Nd derived from the southern deep-water mass.

The ε_{Nd} values of the present AABW range between −9 and −7 (Piepgras and Wasserburg, 1982). Seawater ε_{Nd} reconstructions of the AABW in the South Atlantic during the last glaciation based on planktonic foraminifera revealed values of -6 ± 0.4 ($n = 8$; 2σ) (Howe et al., 2016). Similarly, the ε_{Nd} values of the modern AAIW vary from −8.4 to −7.9, as has been observed in the Atlantic sector of the Southern Ocean (Stichel et al., 2012). More radiogenic AAIW values of −6.8 to −6.0 during the last glacia-

tion were also reported from the South Atlantic Ocean (Howe et al., 2016) and Southwest Pacific Ocean (Hu et al., 2016), which may indicate a higher Pacific contribution to the AAIW supplied through the Drake Passage. Indeed, a shift towards more radiogenic values was identified during HS1 for the AAIW in cold-water corals (ε_{Nd} value of −6.5) from the Drake Passage (Hu et al., 2016; Robinson and van de Flierdt, 2009). Radiogenic ε_{Nd} values for water from southern sources during the last glacial (AABW and AAIW) are a consequence of reduced export of North Atlantic Deep Water (NADW) due to re-organization of the Atlantic Meridional Overturning Circulation (AMOC) (Piotrowski et al., 2012; Robinson and van de Flierdt, 2009). Therefore, glacial ε_{Nd} values of deep water in the BoB (before 18 kyr BP) may indicate a reduction in the contribution of the NADW and a higher proportion of radiogenic water from southern sources.

The deglacial decoupling of ε_{Nd} values between various water depths may reflect stratification between deep and intermediate water during the deglacial period. The decrease in ε_{Nd} in deep water of the Northern Indian Ocean could be due to enhanced nonradiogenic Nd inputs from Himalayan rivers, associated with an intensified summer monsoon (Fig. 4b) (Burton and Vance, 2000; Stoll et al., 2007), and/or an increased NADW (−13) contribution to the deep water of the BoB. These results suggest that the influence of the AABW in the deep water of the BoB weakened during deglaciation.

Furthermore, the sediments in core MD77-176 are the result of mixing between unradiogenic Ganges–Brahmaputra river sediments ($\varepsilon_{Nd} = \sim -16$) and more radiogenic materials from the Indo–Burman Ranges (ε_{Nd} range from −7.4 to −4.0) drained by rivers along the Arakan coast, with an additional contribution of sediments from the Irrawaddy River ($\varepsilon_{Nd} = \sim -10$) (Colin et al., 1999; Joussain et al., 2016). The sediment ε_{Nd} values of these rivers have generally been stable since the last glaciation (Joussain et al., 2016). Variable contributions of these sediments to the deep water ε_{Nd} values during the deglaciation cannot be entirely excluded. However, despite proximity to the Himalayan rivers, the intermediate water ε_{Nd} values in the northern BoB during the deglaciation are more radiogenic (between -7.9 ± 0.3 and -6.3 ± 0.2) than the detrital ε_{Nd} values collected from the same core (Fig. 1) and the ε_{Nd} values of foraminifera from deep-water masses at this time (Fig. 4a). These results are best explained by a higher contribution of southern-sourced water (mainly AAIW) in the northern BoB. The AAIW ε_{Nd} values during the last glaciation (from −6.8 to −6.0) (Hu et al., 2016) are comparable to the radiogenic intermediate water values in the northern BoB at this time.

The convergence of ε_{Nd} values in the early Holocene could be due to enhanced unradiogenic Nd input from Himalayan rivers, especially the Ganges–Brahmaputra river system (Fig. 4b). The Early Holocene Climatic Optimum (from 10 to 6 kyr BP) was characterized by intensified Indian monsoon precipitation (Contreras-Rosales et al., 2014; Marzin et al., 2013) and increased sediment transfer from the Ganges–Brahmaputra river system to the Bengal Fan (Joussain et al., 2017). However, the peak in intermediate and deep water ε_{Nd} appears at ∼5 kyr BP, which is not associated with the Early Holocene Climatic Optimum but is concurrent with a peak in Himalayan river discharge, as indicated by a sea surface salinity (SSS) reconstruction from core SO93-126KL from the northern BoB (Fig. 4b) (Kudrass et al., 2001). The wet climate at this time (Kudrass et al., 2001) might have been a result of the interaction between the summer monsoon and the migration of the Intertropical Convergence Zone.

Nevertheless, the increasing input of unradiogenic Nd from the Himalayas since the early Holocene could have modified the ε_{Nd} values of seawater in the BoB and dominated the sharply decreasing trend in the BoB. Similarly, the increasing ε_{Nd} trend in the late Holocene is probably associated with the decrease in monsoon rainfall and river input since 5 kyr BP (Fig. 4). Weakened monsoon rainfall in the late Holocene has been observed in the BoB and Indian continent (Contreras-Rosales et al., 2014; Marzin et al., 2013), suggesting a decrease in the volume of sediment transferred to the BoB during this period (Joussain et al., 2017). The influence of sea-level variation can be ignored, as it generally remains at a highstand during the Holocene and is not correlated with the seawater ε_{Nd} record of the BoB (Fig. 4). Recent sedimentology studies also suggest that the lithogenic input to the BoB is more sensitive to precipitation intensity rather than to sea-level variations (Joussain et al., 2017). The ASHS (including Red Sea/Persian Gulf outflows) mainly impacts the surface and subsurface water of the northern BoB (upper 500 m) (Yu et al., 2017b) and therefore seems insignificant in determining the ε_{Nd} record of MD77-176. The possibly delayed influence of terrigenous inputs on the ε_{Nd} record can also be excluded, as a previous study indicated that the ε_{Nd} record of BoB seawater could vary seasonally (Yu et al., 2017a).

3.3. Deglacial invasion of AAIW in the Northern Hemisphere oceans and its linkage to atmospheric CO_2

It is suggested that the formation and convection of the AAIW are linked to many factors, such as westerly wind stress-influenced mixing, Ekman transport and upwelling Circumpolar Deep Water (CDW), associated with Southern Ocean overturning (Ribbe, 2001). At present, the northward flow of the AAIW is found as far as 20°N in the Atlantic and Pacific Oceans but only as far as 10°S in the Indian Ocean (Lynch-Stieglitz et al., 1994). However, compared to the interglacial period, the global intermediate water circulation during the deglaciation was very different. Strong northward invasion of the AAIW during the deglaciation has been reported in the Atlantic (Cao et al., 2005; Mangini et al., 2010; Pahnke et al., 2008) and Pacific Oceans (Basak et al., 2010; Marchitto et al., 2007; Stott et al., 2009) on the basis of ε_{Nd} and/or $\Delta^{14}C$ data, suggesting enhanced production and propagation of AAIW from the Southern Ocean. The ε_{Nd} data from core MD77-176 reported in this study indicate the presence of the AAIW in the Northern Indian Ocean, at least at 14.5°N. Our ε_{Nd} data, combined with a ^{14}C record (Bryan et al., 2010) from the Northern Indian Ocean (Figs. 5 and 6), imply that intermediate water with a radiogenic ε_{Nd} and ^{14}C-depleted composition was sourced from the Southern Ocean through northern penetration of AAIW.

The timing of AAIW fluctuations during the deglaciation (mainly the cold intervals, i.e., HS1: ∼18 to 14.7 kyr BP and YD: ∼12.8 to 11.7 kyr BP) is broadly consistent among ε_{Nd} records in the three oceans (Fig. 5). The agreement between the ε_{Nd} and $\Delta^{14}C$ records is also striking during these intervals, with similar patterns of variability being observed in all three oceans, indicating that the feature illustrated in this study is widespread (Figs. 4 and 5). The deglacial transition in the ε_{Nd} and $\Delta^{14}C$ records started at ∼18 kyr BP, which probably indicates that the first enhanced invasion of AAIW into the Northern Hemisphere originated from the initiation of Southern Ocean ventilation following the breakup of extensive sea-ice during the Last Glacial Maximum (Basak et al., 2010). This observation is also supported by a clear covariation between the deglacial shift in $\delta^{13}C$ values of *Neogloboquadrina dutertrei* and a corresponding increase in the opal flux observed in the Eastern Equatorial Pacific, suggesting that the enhanced upwelling in the Southern Ocean during deglaciation introduced more nutrient-rich and $\delta^{13}C$-depleted water to the Eastern Equatorial Pacific surface via upward mixing (Anderson et al., 2009; Basak et al., 2010; Spero and Lea, 2002). Moreover, a multiproxy study of surface ocean productivity, dust inputs, and thermocline conditions at ODP Site 1240 from the Eastern Equatorial Pacific shows that diatoms

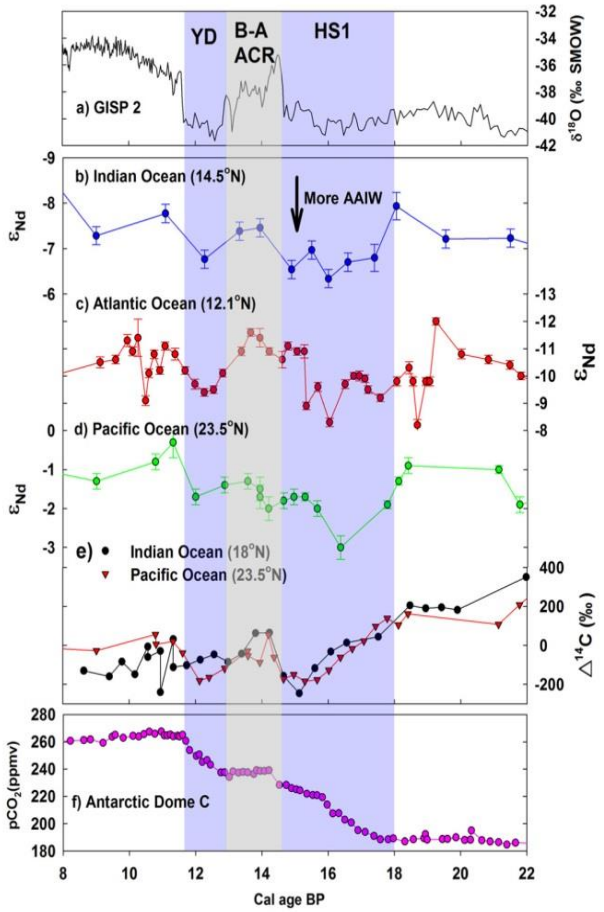

Fig. 5. Intermediate water circulation reorganization during the deglaciation (8–22 kyr BP). a) Greenland ice core $\delta^{18}O$ record GISP2 (Grootes and Stuiver, 1997); b) ε_{Nd} from core MD77-176 in the Indian Ocean (this study); c) εNd from core MD99-2198 in the Atlantic Ocean (Pahnke et al., 2008); d) ε_{Nd} from core MV99-GC31/PC08 in the Pacific Ocean (Basak et al., 2010); e) $\Delta^{14}C$ records from core RC27-23 in the Indian Ocean (Bryan et al., 2010) and core MV99-GC31/PC08 in the Pacific Ocean (Marchitto et al., 2007); f) Atmospheric CO_2 from Antarctic Dome C placed on the GISP2 timescale (Monnin and Barnola, 2001). The terms YD, B-A, ACR (grey bar) and HS1 indicate the Younger Dryas, Bølling-Allerød, Antarctic Cold Reversal and Heinrich Stadial 1 intervals, respectively. Note that the ε_{Nd} records show a clear shift during the Northern Hemisphere cold intervals (YD and HS1, blue bars), which correspond to the sharp rise of atmospheric CO_2.

outcompeted coccolithophores during deglaciation, which also indicates that the influence of Si-rich Southern Ocean intermediate waters was greater at this time (Calvo et al., 2011).

The variations in ε_{Nd} and $\Delta^{14}C$ records in the northern oceans during the cold intervals (HS1 and YD) are generally synchronous with the two-step increase in atmospheric CO_2 concentration, implying that the strong production and greater activity of AAIW from the Southern Ocean were linked to the release of CO_2 from the deep sea to the atmosphere (Fig. 5). Skinner et al. (2010) has used the ^{14}C content of planktonic and benthic foraminifera recovered from the Southern Ocean to verify the existence of an exceptionally old abyssal carbon reservoir before HS1, and to further reveal that the CO_2 was transferred from this reservoir to the atmosphere via intensified Southern Ocean upwelling during the deglaciation. Other evidence that favours strong Southern Ocean ventilation and associated atmospheric CO_2 leakage during the cold HS1 and YD includes ^{14}C reconstructions from core MD99-2334K (Skinner et al., 2014), and opal flux reconstructions, and $^{231}Pa/^{230}Th$ ratios from a variety of Southern Ocean cores (Anderson et al., 2009). In contrast, the changes in the ε_{Nd} and $\Delta^{14}C$ records are more subtle during the warming Bølling-Allerød (B-A) period, associated with stable atmospheric CO_2, suggesting that weakened AAIW production and propagation were correlated with subdued upwelling of the Southern Ocean and limited leakage of CO_2 to the atmosphere (Fig. 5). This evidence implies that the northward invasion of AAIW was coupled to enhanced Southern Ocean ventilation during the deglaciation, and was associated with atmospheric CO_2 leakage (see also Fig. 6).

The intermediate ε_{Nd} and $\Delta^{14}C$ patterns support the concept of a bipolar seesaw. Periods of sudden shifts in intermediate ε_{Nd} and $\Delta^{14}C$ patterns during the Northern Hemisphere cold intervals (HS1 and YD) are concurrent with Southern Hemisphere warm episodes and atmospheric CO_2 increases. This relationship supports the idea that fresh water inputs to the North Atlantic Ocean weakened northward heat transport and that the Southern Hemisphere retained more heat, allowing the sea ice cover to melt and permitting the winds to drive more effective Southern Ocean upwelling and strong AAIW advection (Broecker, 1998; Skinner et al., 2014). In contrast, the generally stable ε_{Nd} and $\Delta^{14}C$ patterns during the warming B-A period suggest the reverse, implying a direct control of the cooling Southern Ocean on the weakened AAIW formation and advection. This interpretation also rationalizes the synchronous changes in Southern Hemisphere temperature and atmospheric CO_2 (Monnin and Barnola, 2001).

4. Conclusions

In this study, we use the ε_{Nd} values of mixed planktonic foraminifera from core MD77-176 collected in the Northern Indian Ocean to establish the evolutionary history of intermediate water, and the potential influence of radiogenic Southern Ocean-sourced AAIW and unradiogenic Himalayan river inputs. A re-evaluation of the ε_{Nd} records in the BoB indicates that the ε_{Nd} values of fossil planktonic foraminifera are consistent with bottom water ε_{Nd} values. Our results reveal that the last glacial period and the last deglaciation, until approximately 10.5 kyr were characterized by ε_{Nd} values between -7.9 ± 0.3 and -6.3 ± 0.2. In contrast, lower ε_{Nd} values (from -7.3 ± 0.2 to -10.9 ± 0.2) were observed between 10 and 5 cal kyr BP in the Holocene, later increasing to -10 during the very late Holocene. The radiogenic ε_{Nd} values during the last deglaciation are best explained by strong propagation of AAIW into the Northern Indian Ocean (during HS1 and YD). Compared with existing data from other seas, we suggest that the global northward propagating intermediate water was sourced from the Southern Ocean and was associated with atmospheric CO_2 leakage during deglaciation. Our new intermediate water ε_{Nd} record from the Northern Indian Ocean sheds light on the history of Southern Ocean ventilation during the deglaciation and, more specifically, on the linkage between AAIW propagation and atmospheric CO_2 rise.

Acknowledgements

This work was supported by the National Natural Science Foundation of China (41622603 and 41576034), National Programme on Global Change and Air–Sea Interaction (GASI-GEOGE-03), Innovation Project (2016ASKJ13) and Aoshan Talents programme (2017ASTCP-ES01) of Qingdao National Laboratory for Marine Science and Technology and CAS Interdisciplinary Innovation Team, Open Fund of the Key Laboratory of Marine Geology and Environment, Chinese Academy of Sciences (No. MGE2018KG01). Z. Yu acknowledges the China Scholarship Council for providing funding for his study in France. This study was supported by the Labex L-IPSL and the MONOPOL projects, which are funded by the ANR (grant nos. ANR-10-LABX-0018 and ANR 2011 Blanc SIMI 5-6 024 04).

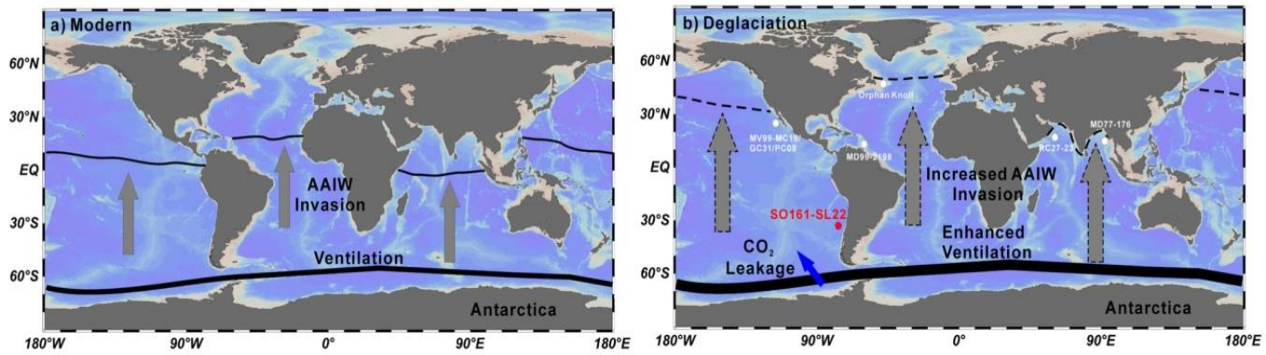

Fig. 6. Schematic illustration of the northward invasion of Antarctic Intermediate Water (AAIW) at present and during the last deglaciation at a depth range from 500 to 1500 m. a) Present: the northward flow of AAIW is found as far as 20°N in the Atlantic and Pacific Oceans but extends only as far as 10°S in the Indian Ocean (Lynch-Stieglitz et al., 1994); b) Last deglaciation: the northward flow of AAIW was associated with enhanced Southern Ocean ventilation and atmospheric CO_2 leakage, and might have reached ~50°N in the Atlantic based on orphan knoll corals (Cao et al., 2005) and MD99-2198 (Pahnke et al., 2008), at least 23.5°N in the Pacific Ocean based on MV99-MC19/GC31/PC08 (Basak et al., 2010; Marchitto et al., 2007) and almost the entire Indian Ocean based on RC27-23 (Bryan et al., 2010) and MD77-176 (this study). The white dots indicate the cores that show strong penetration of AAIW during the deglaciation. The red dot indicates the core SO161-SL22, that does not show strong penetration of AAIW during the deglaciation.

References

Amakawa, H., Alibo, D.S., Nozaki, Y., 2000. Nd isotopic composition and REE pattern in the surface waters of the eastern Indian Ocean and its adjacent seas. Geochim. Cosmochim. Acta 64, 1715–1727.

Anand, P., Elderfield, H., Conte, M.H., 2003. Calibration of Mg/Ca thermometry in planktonic foraminifera from a sediment trap time series. Paleoceanography 18.

Anderson, R.F., Ali, S., Bradtmiller, L.I., Nielsen, S.H.H., Fleisher, M.Q., Anderson, B.E., Burckle, L.H., 2009. Wind-driven upwelling in the Southern Ocean and the deglacial rise in atmospheric CO_2. Science 323, 1443–1448.

Basak, C., Martin, E.E., Horikawa, K., Marchitto, T.M., 2010. Southern Ocean source of ^{14}C-depleted carbon in the North Pacific Ocean during the last deglaciation. Nat. Geosci. 3, 770–773.

Broecker, W.S., 1998. Paleocean circulation during the last deglaciation: a bipolar seesaw? Paleoceanography 13, 119–121.

Broecker, W.S., Peng, T.H., 1982. The Tracers in the Sea. LamontDoherty Geological Observatory, Palisades, NY.

Bryan, S.P., Marchitto, T.M., Lehman, S.J., 2010. The release of ^{14}C-depleted carbon from the deep ocean during the last deglaciation: evidence from the Arabian Sea. Earth Planet. Sci. Lett. 298, 244–254.

Burke, A., Robinson, L.F., 2012. The Southern Ocean's role in carbon exchange during the last deglaciation. Science 335, 557–561.

Burton, K.W., Vance, D., 2000. Glacial–interglacial variations in the neodymium isotope composition of seawater in the Bay of Bengal recorded by planktonic foraminifera. Earth Planet. Sci. Lett. 176, 425–441.

Calvo, E., Pelejero, C., Pena, L.D., Cacho, I., Logan, G.A., 2011. Eastern equatorial pacific productivity and related-CO_2 changes since the last glacial period. Proc. Natl. Acad. Sci. USA 108, 5537–5541.

Cao, L., Fairbanks, R.G., Mortlock, R.A., Kaplan, A., Risk, M.J., 2005. Radiocarbon Reservoir Age of High Latitude North Atlantic Surface Water During the Past 20,000 Years Inferred From Deep-Sea Corals and Foraminifera. AGU Fall Meeting.

Colin, C., Turpin, L., Bertaux, J., Desprairies, A., Kissel, C., 1999. Erosional history of the Himalayan and Burman ranges during the last two glacial–interglacial cycles. Earth Planet. Sci. Lett. 171, 647–660.

Colin, C., Turpin, L., Blamart, D., Frank, N., Kissel, C., Duchamp, S., 2006. Evolution of weathering patterns in the Indo-Burman Ranges over the last 280 kyr: effects of sediment provenance on $^{87}Sr/^{86}Sr$ ratios tracer. Geochem. Geophys. Geosyst. 7.

Contreras-Rosales, L.A., Jennerjahn, T., Tharammal, T., Meyer, V., Lückge, A., Paul, A., Schefuß, E., 2014. Evolution of the Indian Summer Monsoon and terrestrial vegetation in the Bengal region during the past 18 ka. Quat. Sci. Rev. 102, 133–148.

Copard, K., Colin, C., Douville, E., Freiwald, A., Gudmundsson, G., De Mol, B., Frank, N., 2010. Nd isotopes in deep-sea corals in the North-eastern Atlantic. Quat. Sci. Rev. 29, 2499–2508.

De Pol-Holz, R., Keigwin, L., Southon, J., Hebbeln, D., Mohtadi, M., 2010. No signature of abyssal carbon in intermediate waters off Chile during deglaciation. Nat. Geosci. 3, 192–195.

Fairbanks, R.G., Mortlock, R.A., Chiu, T.C., Cao, L., Kaplan, A., Guilderson, T.P., Fairbanks, T.W., Bloom, A.L., Grootes, P.M., Nadeau, M.J., 2005. Radiocarbon calibration curve spanning 0 to 50,000 years BP based on paired 230 Th/234 U/238 U and 14 C dates on pristine corals. Quat. Sci. Rev. 24, 1781–1796.

Frank, M., 2002. Radiogenic isotopes: tracers of past ocean circulation and erosional input. Rev. Geophys. 40.

Goswami, V., Singh, S.K., Bhushan, R., Rai, V.K., 2012. Temporal variations in $^{87}Sr/^{86}Sr$ and εNd in sediments of the southeastern Arabian Sea: impact of monsoon and surface water circulation. Geochem. Geophys. Geosyst. 13.

Gourlan, A.T., Meynadier, L., Allègre, C.J., Tapponnier, P., Birck, J.-L., Joron, J.-L., 2010. Northern Hemisphere climate control of the Bengali rivers discharge during the past 4 Ma. Quat. Sci. Rev. 29, 2484–2498.

Grootes, P.M., Stuiver, M., 1997. Oxygen 18/16 variability in Greenland snow and ice with 10^3- to 10^5-year time resolution. J. Geophys. Res., Oceans 102, 26455–26470.

Hain, M.P., Sigman, D.M., Haug, G.H., 2011. Shortcomings of the isolated abyssal reservoir model for deglacial radiocarbon changes in the mid-depth Indo-Pacific Ocean. Geophys. Res. Lett. 38, 155–170.

Howe, J.N., Piotrowski, A.M., Noble, T.L., Mulitza, S., Chiessi, C.M., Bayon, G., 2016. North Atlantic deep water production during the last glacial maximum. Nat. Commun. 7.

Hu, R., Noble, T.L., Piotrowski, A.M., Mccave, I.N., Bostock, H.C., Neil, H.L., 2016. Neodymium isotopic evidence for linked changes in Southeast Atlantic and Southwest Pacific circulation over the last 200 kyr. Earth Planet. Sci. Lett. 455, 106–114.

Jaccard, S.L., Galbraith, E.D., Martínezgarcía, A., Anderson, R.F., 2016. Covariation of deep Southern Ocean oxygenation and atmospheric CO_2 through the last ice age. Nature 530, 207.

Jacobsen, S.B., Wasserburg, G., 1980. Sm–Nd isotopic evolution of chondrites. Earth Planet. Sci. Lett. 50, 139–155.

Joussain, R., Colin, C., Liu, Z.F., Meynadier, L., Fournier, L., Fauquembergue, K., Zaragosi, S., Schmidt, F., Rojas, V., Bassinot, F., 2016. Climatic control of sediment transport from the Himalayas to the proximal NE Bengal Fan during the last glacial–interglacial cycle. Quat. Sci. Rev. 148, 1–16.

Joussain, R., Liu, Z.F., Colin, C., Duchamp-Alphonse, S., Yu, Z.J., Moreno, E., Fournier, L., Zaragosi, S., Dapoigny, A., Meynadier, L., Bassinot, F., 2017. Link between Indian monsoon rainfall and physical erosion in the Himalayan system during the Holocene. Geochem. Geophys. Geosyst. 18, 3452–3469.

Kudrass, H.R., Hofmann, A., Doose, H., Emeis, K., Erlenkeuser, H., 2001. Modulation and amplification of climatic changes in the Northern Hemisphere by the Indian summer monsoon during the past 80 ky. Geology 29, 63–66.

Lugmair, G., Shimamura, T., Lewis, R., Anders, E., 1983. Samarium-146 in the early solar system: evidence from neodymium in the Allende meteorite. Science 222, 1015–1018.

Lynch-Stieglitz, J., Fairbanks, R.G., Charles, C.D., 1994. Glacial–interglacial history of Antarctic Intermediate Water: relative strengths of Antarctic versus Indian Ocean sources. Paleoceanography 9, 7–29.

Mahowald, N.M., Muhs, D.R., Levis, S., Rasch, P.J., Yoshioka, M., Zender, C.S., Luo, C., 2006. Change in atmospheric mineral aerosols in response to climate: last glacial period, preindustrial, modern, and doubled carbon dioxide climates. J. Geophys. Res., Atmos. 111.

Mangini, A., Godoy, J.M., Godoy, M.L., Kowsmann, R., Santos, G.M., Ruckelshausen, M., Schroeder-Ritzrau, A., Wacker, L., 2010. Deep sea corals off Brazil verify a poorly ventilated Southern Pacific Ocean during H2, H1 and the Younger Dryas. Earth Planet. Sci. Lett. 293, 269–276.

Marchitto, T.M., Lehman, S.J., Ortiz, J.D., Flückiger, J., Van, G.A., 2007. Marine radiocarbon evidence for the mechanism of deglacial atmospheric CO_2 rise. Science 316, 1456.

Marzin, C., Kallel, N., Kageyama, M., Duplessy, J.C., Braconnot, P., 2013. Glacial fluctuations of the Indian monsoon and their relationship with North Atlantic climate: new data and modelling experiments. Clim. Past 9, 2135–2151.

Monnin, E., Barnola, J.M., 2001. Atmospheric CO_2 concentrations over the last glacial termination. Science 291, 112.

Pahnke, K., Goldstein, S.L., Hemming, S.R., 2008. Abrupt changes in Antarctic Intermediate Water circulation over the past 25,000 years. Nat. Geosci. 1, 870–874.

Appendix

Piepgras, D.J., Wasserburg, G.J., 1982. Isotopic composition of neodymium in waters from the drake passage. Science 217, 207–214.

Piotrowski, A., Galy, A., Nicholl, J., Roberts, N., Wilson, D., Clegg, J., Yu, J., 2012. Reconstructing deglacial North and South Atlantic deep water sourcing using foraminiferal Nd isotopes. Earth Planet. Sci. Lett. 357, 289–297.

Ribbe, J., 2001. Intermediate water mass production controlled by southern hemisphere winds. Geophys. Res. Lett. 28, 535–538.

Roberts, N.L., Piotrowski, A.M., McManus, J.F., Keigwin, L.D., 2010. Synchronous deglacial overturning and water mass source changes. Science 327, 75–78.

Robinson, L.F., van de Flierdt, T., 2009. Southern Ocean evidence for reduced export of North Atlantic Deep Water during Heinrich event 1. Geology 37, 195–198.

Scheuvens, D., Schütz, L., Kandler, K., Ebert, M., Weinbruch, S., 2013. Bulk composition of northern African dust and its source sediments — a compilation. Earth-Sci. Rev. 116, 170–194.

Schlitzer, R., 2015. Ocean Data View. odv.awi.de.

Shankar, D., Vinayachandran, P., Unnikrishnan, A., 2002. The monsoon currents in the north Indian Ocean. Prog. Oceanogr. 52, 63–120.

Sigman, D.M., Boyle, E.A., 2000. Glacial/interglacial variations in atmospheric carbon dioxide. Nature 407, 859–869.

Singh, S.P., Singh, S.K., Goswami, V., Bhushan, R., Rai, V.K., 2012. Spatial distribution of dissolved neodymium and ε_{Nd} in the Bay of Bengal: role of particulate matter and mixing of water masses. Geochim. Cosmochim. Acta 94, 38–56.

Skinner, L.C., Fallon, S., Waelbroeck, C., Michel, E., Barker, S., 2010. Ventilation of the Deep Southern Ocean and deglacial CO_2 rise. Science 328, 1147–1151.

Skinner, L.C., Waelbroeck, C., Scrivner, A.E., Fallon, S.J., 2014. Radiocarbon evidence for alternating northern and southern sources of ventilation of the deep Atlantic carbon pool during the last deglaciation. Proc. Natl. Acad. Sci. USA 111, 5480.

Spero, H.J., Lea, D.W., 2002. The cause of carbon isotope minimum events on glacial terminations. Science 296, 522–525.

Stichel, T., Frank, M., Rickli, J., Haley, B.A., 2012. The hafnium and neodymium isotope composition of seawater in the Atlantic sector of the Southern Ocean. Earth Planet. Sci. Lett. 317, 282–294.

Stoll, H.M., Vance, D., Arevalos, A., 2007. Records of the Nd isotope composition of seawater from the Bay of Bengal: implications for the impact of Northern Hemisphere cooling on ITCZ movement. Earth Planet. Sci. Lett. 255, 213–228.

Stott, L., Southon, J., Timmermann, A., Koutavas, A., 2009. Radiocarbon age anomaly at intermediate water depth in the Pacific Ocean during the last deglaciation. Paleoceanography 24.

Stuiver, M., Reimer, P.J., 1993. Extended ^{14}C data base and revised calib 3.0 ^{14}C age calibration program. Radiocarbon 35, 215–230.

Stuiver, M.K., Reimer, P.J., Braziunas, T.F., 1998. High-precision radiocarbon age calibration for terrestrial and marine samples. Radiocarbon 40, 580–589.

Tachikawa, K., Athias, V., Jeandel, C., 2003. Neodymium budget in the modern ocean and paleo-oceanographic implications. J. Geophys. Res., Oceans 108.

Tachikawa, K., Jeandel, C., Roy-Barman, M., 1999. A new approach to the Nd residence time in the ocean: the role of atmospheric inputs. Earth Planet. Sci. Lett. 170, 433–446.

Tachikawa, K., Piotrowski, A.M., Bayon, G., 2014. Neodymium associated with foraminiferal carbonate as a recorder of seawater isotopic signatures. Quat. Sci. Rev. 88, 1–13.

Tanaka, T., Togashi, S., Kamioka, H., Amakawa, H., Kagami, H., Hamamoto, T., Yuhara, M., Orihashi, Y., Yoneda, S., Shimizu, H., 2000. JNdi-1: a neodymium isotopic reference in consistency with LaJolla neodymium. Chem. Geol. 168, 279–281.

Wilson, D.J., Piotrowski, A.M., Galy, A., Banakar, V.K., 2015. Interhemispheric controls on deep ocean circulation and carbon chemistry during the last two glacial cycles. Paleoceanography 30, 621–641.

Yu, Z., Colin, C., Meynadier, L., Douville, E., Dapoigny, A., Reverdin, G., Wu, Q., Wan, S., Song, L., Xu, Z., 2017a. Seasonal variations in dissolved neodymium isotope composition in the Bay of Bengal. Earth Planet. Sci. Lett. 479, 310–321.

Yu, Z.J., Colin, C., Douville, E., Meynadier, L., Duchamp-Alphonse, S., Sepulcre, S., Wan, S.M., Song, L.N., Wu, Q., Xu, Z.K., Bassinot, F., 2017b. Yttrium and rare earth element partitioning in seawaters from the Bay of Bengal. Geochem. Geophys. Geosyst. 18, 1388–1403.

Appendix 2

Variations à l'échelle millénaire de la circulation intermédiaire dans l'océan Indien depuis la dernière période glaciaire reconstruites d'après les assemblages et la géochimie des foraminifères benthiques

Les principaux objectifs de cette étude étaient de reconstituer l'évolution de la circulation des eaux intermédiaires dans l'océan Indien aux échelles de temps glaciaire-interglaciaire et millénaire, et de mieux comprendre les relations entre la circulation océanique (en particulier le rôle de l'eau intermédiaire antarctique AAIW), l'intensité de la remontée d'eau (upwelling) dans l'océan Austral et les modifications du CO_2 atmosphérique via le cycle global du Carbone. Pour ce faire, nous avons étudié les assemblages de foraminifères benthiques ainsi que les isotopes stables ($\delta^{13}C$, $\delta^{18}O$), la géochimie élémentaire (rapports Mg/Ca, Sr/Ca, Cd/Ca, Li/Ca, Ba/Ca et U/Ca) et les âges ^{14}C de foraminifères benthiques de carottes marines prélevées à profondeur intermédiaire dans le nord de l'océan Indien (Baie du Bengale et Mer d'Oman) et dans l'est de l'océan Indien équatorial. Cette approche multi-traceurs sur plusieurs archives a ainsi permis de reconstituer les modifications hydrologiques des masses d'eau intermédiaires à haute résolution temporelle depuis le dernier maximum glaciaire, mais également sur plusieurs cycles climatiques. Les analyses des rapports élémentaires de foraminifères benthiques ont été effectuées pour reconstituer les propriétés chimiques de masses d'eau intermédiaires telles que la concentration en ions carbonate CO_3^{2-} (Mg/Ca, Sr/Ca, Li/Ca et U/Ca), la température de l'eau de fond (Mg/Li) ou les changements paléo-nutritifs (Cd/Ca et Ba/Ca). Cette stratégie a permis de mieux comprendre l'évolution temporelle de la source et de la ventilation des masses d'eau intermédiaires dans le nord de l'océan Indien et, en particulier, les variations à l'échelle du millénaire au cours de la dernière déglaciation dans le nord de l'océan Indien, ainsi que des changements de tendance à plus long terme.

Dans le nord-est de la baie du Bengale, les assemblages de foraminifères benthiques couplés aux enregistrements du $\delta^{13}C$, du $\delta^{18}O$ et du ^{14}C ont été réalisés sur la carotte MD77-176 (14°30'5N-93°07'6E) à profondeur intermédiaire (1375 m) pour reconstituer l'évolution des masses d'eau intermédiaires depuis le dernier maximum glaciaire (LGM). Nos résultats semblent indiquer que le LGM était principalement influencé par les eaux provenant du sud (Océan Austral). Une abondance relative élevée d'espèces endofaunales intermédiaires et profondes associées à des valeurs de $\delta^{13}C$ benthiques appauvries au cours de la LGM traduisent une faible concentration en oxygène et/ou des conditions d'eaux profondes méso- à eutrophes. Au cours de l'Holocène, les assemblages de foraminifères benthiques indiquent un environnement oligo- à mésotrophe avec des conditions de fond bien ventilées par rapport au LGM, en accord avec l'augmentation du $\delta^{13}C$. Des événements à

l'échelle millénaire (intervalles de 17-14 et 13-10.6 kyr BP) ont ponctué la dernière déglaciation, affichant une augmentation des valeurs du $\delta^{13}C$ et de l'εNd (Yu et al., 2018) coïncidant avec des décalages d'âge appauvris en B-P ^{14}C (i.e., les écarts d'âge ^{14}C entre foraminifères benthiques et planctoniques). De plus, le $\delta^{13}C$ benthique pourrait également augmenter via une forte remontée durant la formation de AAIW/SAMW en raison de l'influence des échanges air-mer (Lynch-Stieglitz et al., 1994). Ainsi, ces enregistrements indiquent une augmentation de la contribution de l'AAIW sur le site étudié, accompagnée d'une remontée accrue dans l'océan Austral. Cela pourrait être associé à un fort échange de CO_2 depuis l'océan vers l'atmosphère via la ventilation de l'océan Austral au cours de la dernière déglaciation. Cette étude a fait l'objet d'une publication dans la revue *Geochemistry, Geophysics, Geosystems* (Ma et al., 2019).

Dans le nord de l'océan Indien, les enregistrements du $\delta^{13}C$ et du $\delta^{18}O$ des foraminifères benthiques associés aux rapports élémentaires de l'espèce *Hoeglundina elegans* (Mg/Ca, Sr/Ca, Li/Ca et U/Ca) ont été analysés sur les carottes MD77-191 (07°30'N-76°43'E) situé à 1254 m de profondeur à l'extrémité sud de l'Inde et MD77-176 collectée dans le nord de la Baie du Bengale (BoB). Nous avons mis en évidence que les rapports élémentaires benthiques (Mg/Ca, Sr/Ca, Li/Ca et U/Ca) semblent être principalement influencés par les changements de concentration en ions carbonate [CO_3^{2-}] et que la température de l'eau de fond ne semble pas influencer fortement ces ratios. Nous avons reconstitué la concentration [CO_3^{2-}] de l'eau de mer en convertissant le rapport Sr/Ca de *H. elegans* en [CO_3^{2-}], en construisant une relation empirique basée sur les données de la littérature reliant le Δ[CO_3^{2-}] de l'aragonite au Sr/Ca de *H. elegans* à profondeur d'eau intermédiaire (500-1500 m) dans l'océan moderne (Rosenthal et al., 2006; Yu et al., 2014). Nous avons ensuite comparé les enregistrements du [CO_3^{2-}] de l'eau de mer des carottes MD77-191 (mer d'Arabie) et MD77-176 (nord-est de la BoB) avec des enregistrements du [CO_3^{2-}] à différentes profondeurs de l'océan Atlantique (BOFS 17K, 1150 m) et de l'océan Indien (WIND 28K, 4147 m de profondeur) (Yu et al., 2008, 2010). Tous les enregistrements de [CO_3^{2-}] à des profondeurs d'eau intermédiaires affichent des valeurs faibles pendant les intervalles de temps 17-15.2 et 12.6-10.5 kyr durant la dernière déglaciation, indiquant un transfert de CO_2 de l'océan profond vers les eaux supérieures. En outre, la diminution des valeurs de [CO_3^{2-}] correspond également à une augmentation du $\delta^{13}C$ benthique au cours de la dernière déglaciation, également observée sur le $\delta^{13}C$ benthique d'études précédentes dans le nord-est de la baie du Bengale, de la Mer d'Arabie et de l'Océan Pacifique (par exemple, Duplessy et al., 1984; Curry et al., 1988; Naqvi et al., 1994; Jung et al., 2009; Ma et al., 2019). De plus, cette diminution du [CO_3^{2-}] couplée à l'augmentation du $\delta^{13}C$ benthique est également associée à une diminution des décalages d'âge du B-P du golfe du Bengale survenue aux intervalles de temps compris entre 17-15.2 et 12.6-10.5 kyr BP (Ma et al., 2019). Tous ces résultats

suggèrent le lien étroit qui existe entre la ventilation accrue de l'océan Austral observée via les AAIW et le dégazage de CO_2 au cours de la dernière déglaciation. Au cours de l'Holocène, la diminution de $[CO_3^{2-}]$ dans les masses d'eau intermédiaires témoigne également de l'importance de la variation des stocks mondiaux d'alcalinité, qui correspond à l'augmentation du CO_2 atmosphérique depuis 8 cal kyr BP et/ou à une productivité accrue pendant l'Holocène (du moins pour la carotte MD77-191). En effet, la reminéralisation de la matière organique peut également entraîner une diminution de $[CO_3^{2-}]$ (Holligan et Robertson, 1996). Ce travail fait l'objet d'un manuscrit qui sera soumis pour publication avant la fin de l'année 2019.

Nous avons également effectué des analyses des rapports élémentaires Cd/Ca et Ba/Ca de différentes espèces de foraminifères benthiques sur les carottes MD77-176 et MD77-191, afin de reconstituer l'évolution de la circulation intermédiaire de l'eau et des modifications paléo-nutritives dans le nord de l'océan Indien depuis la dernière déglaciation. En effet, les rapports benthiques Cd/Ca et Ba/Ca semblent principalement influencés par les changements de productivité en surface et/ou par la ventilation des masses d'eau de fond. La concentration Cd_w de l'eau de mer à profondeur intermédiaire a été calculée à partir du Cd/Ca de *H. elegans* d'après l'équation de Boyle (1992). Au cours de l'Holocène tardif (de 5.2 à 2.4 kP cal cal), les concentrations accrues en Cd_w des deux carottes MD77-191 et MD77-176 indiquent une augmentation de la productivité de surface. En revanche, dans le nord-est de la baie du Bengale, les valeurs plus faibles de Cd_w intermédiaire au début de l'Holocène (de 10 à 6 kP BP) indiquent une faible productivité en surface. Cette grande variation de la Cd_w intermédiaire durant l'Holocène est en accord avec les changements dans les précipitations de mousson observés dans le BoB et sur le continent indien (Marzin et al., 2013 ; Contreras-Rosales et al., 2014 ; Sarkar et al., 2015). Ces enregistrements permettent d'appuyer l'hypothèse de la relation de bascule entre les pluies de mousson intenses et la productivité en surface dans la BoB et la pointe sud de la mer d'Arabie pendant l'Holocène. De plus, au cours de la dernière déglaciation, une diminution de la concentration en Cd_w et des rapports Ba/Ca benthiques dans les eaux intermédiaires pourrait être liée à une diminution de la productivité de surface et/ou à une meilleure ventilation aux intervalles 16-15.2 et 12.6-11 kyr BP. L'amélioration de la ventilation des masses d'eau intermédiaires est associée à l'augmentation du $\delta^{13}C$ benthique, à l'épuisement de la $[CO_3^{2-}]$ et à la diminution des décalages d'âge B-P obtenus à partir des mêmes carottes et se produit pendant les mêmes intervalles. Tous ces changements pourraient également fournir des preuves solides de l'augmentation du flux d'AAIW vers le nord au cours d'intervalles compris entre 16-15.2 kal BP et 12.6-11 kyr BP. En outre, l'étude d'assemblages de foraminifères benthiques de la carotte MD77-191 a permis d'établir deux assemblages principaux caractérisés principalement par *Bulimina aculeata*, C*ibicidoides pachyderma*, *Pullenia bulloides* et *Ehrenbergina trigona* pour l'assemblage 1 et *H. elegans*, *Bulimina marginata*, *C. wuellerstorfi* et *Globocassidulina subglobosa*

pour l'assemblage 2. Les assemblages de foramnifères benthiques sont globalement en accord avec les enregistrements de l'abondance relative de *G. bulloides* (Bassinot et al., 2011) et du Cd_w intermédiaire obtenu à partir de la même carotte, ce qui pourrait refléter des changements dans la productivité de surface depuis 17 kyr BP. L'analyse de l'assemblage de foraminifères benthiques indique que l'assemblage 2 (au cours d'un intervalle de 17 à 6 kyr BP) reflète des conditions d'oxygène dans l'eau de fond élevées et un faible flux de matière organique, correspondant à une faible productivité. L'assemblage de l'Holocène tardif indique une teneur en oxygène relativement basse et des conditions d'eaux profondes méso- à eutrophiques par rapport à l'assemblage 2 au cours de l'intervalle de 17-6 kyr BP et associé à une productivité de surface élevée au cours de l'Holocène tardif.

Dans l'est de l'océan Indien équatorial, la carotte SHI9001 couvre les 685 derniers kyr, atteignant le stade isotopique marin (MIS) 17, permettant d'appréhender des variations hydrologiques sur plusieurs cycles climatiques. La température de l'eau de fond calculée à partir du Mg/Li de l'espèce *Uvigerina peregrina* est en bon accord avec les calculs du rapport Mg/Ca de *H. elegans*, allant de de 4.29 à 9.9 °C. Les tendances de la température des eaux de fond sont en accord avec la variabilité glaciaire-interglaciaire, suggérant des masses d'eau plus froides pendant les périodes glaciaires par rapport aux masses interglaciaires. Les rapports Sr/Ca, Cd/Ca et Ba/Ca de *U. peregrina*, ainsi que les rapports Cd/Ba et Ba/Ca de *H. elegans* ont tendance à présenter des variations opposées à l'enregistrement de $\delta^{13}C$ obtenu sur *C. wuellerstorfi*, ce qui peut indiquer des changements dans la source d'eau, avec une contribution variable des masses d'eau de l'océan Austral. En outre, les enregistrements de Li/Ca et U/Ca de *H. elegans* présentent une variation opposée abrupte autour de 400 kyr, qui ne semble pas refléter la variabilité glaciaire-interglaciaire ni les tendances à long terme décrites dans l'enregistrement $\delta^{13}C$. Tous ces enregistrements pourraient indiquer un fort changement dans le cycle du carbone océanique à des profondeurs d'eau intermédiaires, ce qui pourrait être en relation avec le changement global de C enregistré dans le $\delta^{13}C$. Des travaux ultérieurs aideront à déchiffrer ces différents mécanismes.

Tous les enregistrements obtenus au cours de cette étude permettent de mieux comprendre l'évolution temporelle de la source et de la ventilation des masses d'eau intermédiaires dans l'océan Indien nord et leurs relations avec les autres bassins océaniques et le cycle global du C. Les principaux résultats sont:

(1). Au cours du LGM, les masses d'eau provenant du sud étaient dominantes dans le nord de l'océan Indien et se caractérisaient par une faible concentration en oxygène et / ou des conditions d'eaux profondes méso à eutrophes.

(2). Au cours de la dernière déglaciation, on a mis en évidence un flux accru d'AAIW vers le nord dans le nord de l'océan Indien, associé à un upwelling renforcé dans l'océan Austral. En outre,

les enregistrements géochimiques fournissent également des preuves solides que la ventilation améliorée de l'océan Austral pourrait jouer un rôle important dans une augmentation rapide en deux étapes du CO_2 atmosphérique pendant les intervalles de temps de 18-14.7 et de 12.8 à 11.7 kP BP.

(3). Au cours de l'Holocène, l'hydrologie du nord de l'océan Indien est caractérisée par une augmentation progressive de l'influence de la NADW. En outre, l'augmentation de la productivité de surface a eu lieu au cours de l'Holocène supérieur (5.2-2.4 kyr BP), tandis que l'Holocène précoce-moyen (10-6 kyr BP) affiche une productivité de surface plus faible, induite par une plus grande stratification de la colonne d'eau associée à l'intensification de la mousson estivale indienne induisant une augmentation du débit d'eau douce des rivières asiatiques.

(4). À plus long terme, la connexion entre l'océan Indien et l'océan Austral, avec ses conséquences sur le cycle global du carbone, a également été soulignée, bien que des recherches supplémentaires doivent être menées pour mieux comprendre ces processus.

université PARIS-SACLAY
ÉCOLE DOCTORALE
Sciences mécaniques et énergétiques, matériaux et géosciences (SMEMAG)

Titre: Variations à l'échelle millénaire de la circulation intermédiaire dans l'océan Indien depuis la dernière période glaciaire reconstruites d'après les assemblages et la géochimie des foraminifères benthiques.

Mots clés : circulation d'eau intermédiaire, foraminifères benthiques, géochimie, assemblages, dernier maximum glaciaire, Océan Indien septentrional.

Résumé : L'objectif principal de cette thèse était de reconstituer l'évolution de la circulation intermédiaire depuis la dernière période glaciaire à partir de carottes de sédiments marins prélevées dans le golfe du Bengale GB, la Mer d'Arabie MA et l'océan Indien équatorial oriental OIEO. La stratégie scientifique mise en œuvre inclut l'étude des assemblages et de la géochimie des foraminifères benthiques ($\delta^{13}C$, $\delta^{18}O$, ^{14}C et rapports élémentaires), afin de reconstruire les changements de source et de ventilation des masses d'eau. Les résultats obtenus dans le GB ont permis de restituer les changements hydrologiques à profondeur intermédiaire à haute résolution temporelle au cours des derniers 40 ka. Les enregistrements témoignent de changements dans la source des masses d'eau, entre l'Océan austral avec les eaux antarctiques intermédiaires AAIW et les eaux Nord Atlantique NADW, à l'échelle glaciaire-interglaciaire mais aussi lors des événements millénaires. Ce travail a aussi permis de fournir les premiers enregistrements à haute résolution temporelle des rapports élémentaires des foraminifères benthiques (Mg/Ca, Sr/Ca, U/Ca et Li/Ca) dans le GB et en MA. Ces résultats permettent notamment de mieux contraindre la pénétration des AAIW vers le nord depuis la dernière période glaciaire. La reconstruction de la concentration en ion carbonate permet également de discuter des relations entre les variations de la circulation intermédiaire et les changements profonds du cycle du Carbone à l'échelle globale, notamment via les échanges se produisant dans l'Océan Austral. Nous avons également fourni dans ce travail les premiers enregistrements de Cd/Ca et de Ba/Ca continus et à haute résolution dans le nord de l'océan Indien, pour reconstituer les modifications passées de la teneur en éléments nutritifs. Les enregistrements géochimiques dans l'OIEO témoignent de profonds changements des propriétés des masses d'eau intermédiaires, associées aux changements de circulation.

Title: Millennial-scale variations of the intermediate water circulation in the Indian Ocean since the last glacial period inferred from assemblages and geochemistry of benthic foraminifera.

Keywords: intermediate water circulation, benthic foraminifera, geochemistry, assemblages, Bay of Bengal, Arabian Sea, eastern Equatorial Indian Ocean.

Abstract: The main objective of this study was to reconstruct the evolution of the intermediate water circulation since the last glacial period by the investigation of marine cores collected from the Bay of Bengal (BoB), Arabian Sea (AS) and Eastern Equatorial Indian Ocean (EEIO). The scientific strategy involves benthic foraminiferal assemblages and geochemical proxies ($\delta^{13}C$, $\delta^{18}O$, ^{14}C and elemental ratios analysis) to better constrain past changes in the source and ventilation of water masses. Records from the BoB allowed reconstructing hydrological changes at intermediate depth over the last 40 cal kyr. The records highlight changes in the source of water masses, with a balance between the contribution of southern Antarctic Intermediate Water (AAIW) versus North Atlantic Deep Water (NADW) at glacial-interglacial timescale as well as during millennial events. This work also provided the first high-resolution benthic foraminifera elemental ratio records (Mg/Ca, Sr/Ca, U/Ca and Li/Ca) from the BoB and the AS. These records especially help to better constrain the northward penetration of AAIW over the last glacial period. The reconstruction of the carbonate ion concentration allowed to discuss the relationships between the intermediate water circulation and deep changes in the global Carbon cycle, with a special interest for the Southern Ocean. This work also provides the first continuous and high-resolution benthic Cd/Ca and Ba/Ca records in the northern Indian Ocean, could reconstruct past changes in the nutrient content. Geochemical records from the EEIO exhibit strong changes in the chemical properties of the intermediate water masses, related to global circulation changes in the area.

Université Paris-Saclay
Espace Technologique / Immeuble Discovery
Route de l'Orme aux Merisiers RD 128 / 91190 Saint-Aubin, France